Integrating remotely sensed information into the APSIM Wheat model to improve crop yield prediction

Von der Fakultät für Georessourcen und Materialtechnik der
Rheinisch-Westfälischen Technischen Hochschule Aachen

zur Erlangung des akademischen Grades einer

Doktorin der Naturwissenschaften

genehmigte Dissertation

vorgelegt von

Shirui Hao, M.Sc.

Berichtende: **Univ.-Prof. Dr. Harrie-Jan Hendricks-Franssen**
Univ.-Prof. Dr. Dongryeol Ryu
Univ.-Prof. Dr. Andrew Western

Tag der mündlichen Prüfung: 30.04.2024

Abstract

In agriculture, monitoring crop growth, and predicting crop yield in a timely manner are of great importance. Crop yield modelling and forecasting provide information to test various crop management options, guide crop breeding, understand and explore mitigation of environmental impacts, and optimise production. Process-based crop models, such as the Agricultural Production Systems sIMulator (APSIM), have been widely applied to simulate crop growth and predict yield because they incorporate the current understanding of complex crop-environment dynamics. However, models simplify complex processes and predict yield with uncertainty. Remote sensing technology provides spatially distributed and reliable quantitative estimation of crop status near real-time, which can be integrated with crop models by using data assimilation methods to mitigate prediction uncertainties and improve predictive performance. This thesis (1) reviews the performance of the APSIM-Wheat model and identifies the important factors that influence yield prediction uncertainty; (2) undertakes sensitivity analyses using the Sobol' method to examine the sensitivity of crop yield prediction to six influential parameters identified in part (1); (3) determines the most suitable APSIM-wheat state variables for data assimilation and develops an observation operator to facilitate model updating with remote sensing observations; and (4) develops a data assimilation scheme to integrate remotely sensed crop information into the APSIM-Wheat model. The proposed scheme improves the wheat yield estimation performance and enables the model to better simulate spatial variability in yield.

Chapter 2 reviews the performance of APSIM-Wheat, one of the most popular crop modules in APSIM, and identifies the factors that influence yield prediction uncertainty. Model evaluation results from 76 published studies across thirteen countries on four continents were analysed. In addition, a meta-database of modelled and observed yields was established from 30 papers within these studies. The analysis indicates that with site-specific calibration, APSIM predicts yield with an RMSE typically smaller than 1 t/ha under a wide range of environments. For rainfed wheat, the review and meta-analysis found that estimated soil hydraulic characteristics, soil water conditions, nitrogen availability, heat and frost events, and some other abiotic stresses (lodging and root disease) lead to larger yield prediction residuals and uncertainty.

Integrating satellite observations into APSIM-Wheat is hypothesised to improve the yield prediction accuracy and robustness. As an important steppingstone towards the satellite-APSIM integration, a global sensitivity analysis (using the Sobol' method) was conducted to rank the sensitivity of influential parameters affecting yield prediction (Chapter 3). Results indicate that precipitation, initial soil nitrogen content, and soil parameters have the largest influence on yield variability. APSIM's yield prediction becomes more sensitive to a factor when that factor becomes more limiting. These results are used to guide the design of data assimilation schemes for crop models.

Green leaf area index (GLAI) was selected as the variable to assimilate into the APSIM-Wheat model. Sentinel-2 was chosen to produce the observations due to its high spatial (10-20 m) and temporal (5 days) resolutions and its relevance to estimating GLAI. An observation operator, which provides the mathematical mapping from model state to observation space (or vice versa), was developed to link several vegetation indices with APSIM GLAI in Chapter 4. The results show that Sentinel-2 derived chlorophyll index (CI) calculated using red edge bands have the closest relationship with APSIM simulated GLAI. The uncertainty of the observation operator was also determined and used to represent the background prediction uncertainty in the observation space.

Data assimilation (DA) is a set of statistical techniques that can be employed to combine external information (such as *in situ* measurements or remotely sensed observations) with a model to improve model prediction performance. It enables the updating of model time-step state variables using available information. In Chapter 5, a synthetic data assimilation experiment was conducted to test the updated state variables, the updating periods, the updating intervals, and the uncertainties added to the model and observations. It was found that updating all biomass components in the wheat module (grain, leaf, stem, spike, and root) from the whole duration of sowing-harvest at a daily frequency resulted in the best yield prediction performance. A more realistic 5-day updating interval still resulted in noticeable improvement. The designed data assimilation strategy was validated for eight scenarios representing high-, medium-, and low-yield cases. The results show that updating all biomass states every 5 days across the whole growing season effectively corrected yield prediction *residual* by 51% - 85%, with the *residual* decreasing from 230 – 2134 kg/ha to 93 – 533 kg/ha. The standard deviation was also decreased by 41.7% – 66.7%.

After the synthetic experiment, the data assimilation scheme was applied to a rainfed winter wheat field located in north-western Victoria, Australia using Sentinel-2 and Planet Scope observations (Chapter 6). The field was segmented into 58 patches characterising yield spatial variability. Two open loop cases were used to assess the robustness of the data assimilation performance. The results show that for the high-yield open loop case, data assimilation corrected yield prediction *residual* by 37% – 97%, with a median correction efficiency of 73%. The uncertainty was decreased from 0.71 t/ha to a range of 0.52 – 0.60 t/ha. For the low yield open loop case, the *residual* was corrected by 18% – 94%, and a more significant uncertainty reduction was achieved, decreasing from 0.76 t/ha to between 0.29 and 0.40 t/ha.

The developed data assimilation framework for the APSIM-Wheat model shows efficiency and robustness for improving model yield estimation. The improvement provides the potential to deliver quality yield predictions with credibility, enabling better planning of management practices and optimisation of food production. This work also provides a pipeline for the design process of a crop model data assimilation framework, which can serve as a guide for estimating model uncertainty, choosing appropriate observations, estimating their errors, and determining the state updating strategy.

Zusammenfassung

In der Landwirtschaft ist das Monitoring des Pflanzenwachstums und die rechtzeitige Vorhersage des Ernteertrags von großer Bedeutung. Die Modellierung und Vorhersage des Ernteertrags liefern Informationen zur Prüfung verschiedener Möglichkeiten zur Bewirtschaftung von Kulturen, zur Lenkung der Pflanzenzüchtung, zur Erkenntnis und Erforschung der Minderung von Umweltauswirkungen und zur Optimierung der Produktion. Prozessbasierte Ertragsmodelle, wie der Agricultural Production Systems sIMulator (APSIM), wurden weit verbreitet eingesetzt, um das Pflanzenwachstum zu simulieren und den Ertrag vorherzusagen, da sie das aktuelle Verständnis komplexer Zusammenhänge zwischen Pflanzen und Umwelt integrieren. Modelle vereinfachen jedoch komplexe Prozesse und es gibt Unsicherheiten in den prognostizieren Erträgen. Die Fernerkundungstechnologie bietet eine räumlich verteilte und zuverlässige quantitative Schätzung des Pflanzenzustands in Echtzeit, die durch die Verwendung von Datenassimilationsmethoden mit Ertragsmodellen integriert werden kann, um Vorhersageunsicherheiten zu reduzieren und damit die Vorhersagequalität zu verbessern. Diese Dissertation (1) überprüft die Leistung des APSIM-Wheat-Modells und identifiziert wichtige Faktoren, die die Unsicherheit der Ertragsvorhersage beeinflussen; (2) führt Sensitivitätsanalysen mit der Sobol'-Methode durch, um die Empfindlichkeit der Ertragsvorhersage gegenüber sechs einflussreichen Parametern zu untersuchen, die in Teil (1) identifiziert wurden; (3) bestimmt die geeignetsten Zustandsvariablen des APSIM-Wheat für die Datenassimilation und entwickelt einen Beobachtungsoperator, um die Modellanpassung mit Fernerkundungsbeobachtungen zu erleichtern; und (4) entwickelt ein Datenassimilationsschema, um fernerkundliche Informationen zur Pflanzenentwicklung in das APSIM-Wheat-Modell zu integrieren. Dieses neue Datenassimilationsschema soll die Simulation der Weizenerträge sowie deren räumliche Variabilität mit dem APSIM-Wheat-Modell verbessern.

Kapitel 2 überprüft die Vorhersagequalität von APSIM-Wheat, einem der gängigsten Getreide-Module von APSIM, und identifiziert die Faktoren, die die Unsicherheit der Ertragsvorhersage beeinflussen. Die Ergebnisse der Modellbewertung aus 76 veröffentlichten Studien in dreizehn Ländern auf vier Kontinenten wurden analysiert. Darüber hinaus wurde eine Metadatenbank aus modellierten und beobachteten Erträgen aus 30 Arbeiten innerhalb dieser Studien erstellt. Die Analyse zeigt, dass APSIM mit standortspezifischer Kalibrierung den Ertrag unter einer breiten Palette von Umgebungen in der Regel mit einem RMSE kleiner als 1 t/ha vorhersagt. Für regenwassergespeisten Weizen ergab die Überprüfung und Metaanalyse, dass geschätzte bodenhydraulische Eigenschaften, Bodenfeuchtebedingungen, Stickstoffverfügbarkeit, Hitze- und Frostereignisse sowie einige andere abiotische Stressfaktoren (Lagerung und

Wurzelerkrankungen) zu größeren Abweichungen und Unsicherheiten in der Ertragsvorhersage führen.

Kapitel 3 beschäftigt sich mich der Integration von Satellitenbeobachtungen in APSIM-Wheat, um die Genauigkeit und Robustheit der Ertragsvorhersage zu verbessern. Als wichtiger Schritt hin zur Integration von Satelliten und APSIM wurde in Kapitel 3 eine globale Sensitivitätsanalyse (unter Verwendung der Sobol'-Methode) durchgeführt, um die Empfindlichkeit von Einflussparametern auf die Ertragsvorhersage zu bewerten. Die Ergebnisse zeigen, dass der Niederschlag, der Anfangsgehalt an Bodenstickstoff und die Bodenparameter den größten Einfluss auf die Ertragsvariabilität haben. Die Vorhersage des Ertrags durch APSIM reagiert empfindlicher auf einen bestimmten Faktor, wenn dieser Faktor limitierend wirkt. Diese Ergebnisse werden im Folgenden verwendet, um ein Datenassimilationsschemata für Ertragsmodelle zu entwickeln.

Der Index der grünen Blattfläche (GLAI) wurde als die Variable ausgewählt, die in das APSIM-Wheat-Modell integriert werden sollte. Sentinel-2 wurde aufgrund seiner hohen räumlichen (10-20 m) und zeitlichen (5 Tage) Auflösung und seiner Relevanz für die Schätzung des GLAI für die Erstellung der Beobachtungen ausgewählt. Ein Beobachtungsoperator, der die mathematische Zuordnung vom Modellzustand in den Beobachtungsraum (oder umgekehrt) liefert, wurde entwickelt, um verschiedene Vegetationsindizes mit dem APSIM GLAI in Kapitel 4 zu verknüpfen. Die Ergebnisse zeigen, dass der aus Sentinel-2 abgeleitete Chlorophyllindex (CI) unter Verwendung von Red-Edge-Bändern die engste Beziehung zum APSIM-simulierten GLAI aufweist. Die Unsicherheit des Beobachtungsoperators wurde ebenfalls ermittelt und zur Darstellung der Hintergrundvorhersageunsicherheit im Beobachtungsraum verwendet.

Datenassimilation (DA) ist eine Reihe von statistischen Techniken, die eingesetzt werden können, um externe Informationen (wie In-situ-Messungen oder fernerkundliche Beobachtungen) mit einem Modell zu kombinieren, um die Vorhersageleistung des Modells zu verbessern. Sie ermöglicht die Aktualisierung der Modellzeitschritt-Zustandsvariablen mithilfe verfügbarer Informationen. In Kapitel 5 wurde ein synthetisches Datenassimilationsexperiment durchgeführt, um die aktualisierten Zustandsvariablen, die Aktualisierungszeiträume, die Aktualisierungsintervalle und die Unsicherheiten im Modell und in den Beobachtungen zu testen. Es wurde festgestellt, dass die Aktualisierung aller Biomassekomponenten im Weizenmodul (Korn, Blatt, Stängel, Ähre und Wurzel) über die gesamte Aussaat-Ernte-Dauer in täglicher Häufigkeit zu den besten Ergebnissen in der Ertragsvorhersage führt. Ein realistischerer Aktualisierungsintervall von 5 Tagen führte dennoch zu einer deutlichen Verbesserung. Die entwickelte Datenassimilationsstrategie wurde für acht Szenarien validiert, die hohe, mittlere und niedrige Ertragsfälle repräsentieren. Die Ergebnisse zeigen, dass die Aktualisierung aller Biomassezustände alle 5 Tage über die gesamte Wachstumsperiode hinweg die Vorhersageabweichung des Ertrags um 51% - 85% korrigierte, wobei die Abweichung von 230 - 2134 kg/ha auf 93 - 533 kg/ha reduziert wurde. Die Standardabweichung wurde ebenfalls um 41,7% - 66,7% reduziert.

Nach dem synthetischen Experiment wurde das Datenassimilationsschema auf ein regenwassergespeisten Weizenfeld im Nordwesten von Victoria, Australien, angewendet, wobei Sentinel-2- und Planet-Scope-Beobachtungen verwendet wurden (Kapitel 6). Das Feld wurde hierzu in 58 Patches unterteilt, die die räumliche Variabilität des Ertrags charakterisieren. Zwei Fälle von offenem Kreislauf wurden verwendet, um die Robustheit der Datenassimilationsleistung zu bewerten. Die Ergebnisse zeigen, dass für den Hochertragsfall die Datenassimilation die Abweichung der Ertragsvorhersage um 37% - 97% korrigierte, mit einer mittleren Korrekturleistung von 73%. Die Unsicherheit wurde von 0,71 t/ha auf einen Bereich von 0,52 - 0,60 t/ha reduziert. Für den Niederertragsfall wurde die Abweichung um 18% - 94% korrigiert, und es wurde eine signifikante Unsicherheitsreduktion erreicht, die von 0,76 t/ha auf einen Bereich von 0,29 - 0,40 t/ha reduziert wurde.

Es konnte die Effizienz und Robustheit des entwickelten Datenassimilationsschema für das APSIM-Wheat-Modell bei der Verbesserung der Ertragsabschätzung des Modells bezeigt werden. Diese Verbesserung bietet das Potenzial, qualitativ hochwertige Ertragsvorhersagen mit Glaubwürdigkeit zu liefern, um eine bessere Planung von Bewirtschaftungspraktiken und die Optimierung der Lebensmittelproduktion zu ermöglichen. Diese Arbeit bietet auch einen Leitfaden für den Designprozess eines Datenassimilationsframeworks für Ertragsmodelle, der als Anleitung zur Schätzung von Modellunsicherheit, zur Auswahl geeigneter Beobachtungen, zur Schätzung ihrer Fehler und zur Bestimmung der Zustandsaktualisierungsstrategie dienen kann.

Preface

The research presented in this thesis is primarily my own work completed during my PhD candidature from 2018 to 2023. The main chapters (Chapters 2 to 6) have either been published, submitted, or will be submitted for publication. They are co-authored with my supervisors, who assisted in framing research questions and editing the manuscripts. I conducted the core tasks, including the development of methods, modelling, data analysis, creating figures and tables, and writing the manuscripts. No work was performed outside of my candidature, no content was submitted for other qualifications, and no external editorial assistance was received for this thesis.

Chapter 2 has been published as Hao, S., Ryu, D., Western, A., Perry, E., Bogena, H., & Franssen, H. J. H. (2021). Performance of a wheat yield prediction model and factors influencing the performance: A review and meta-analysis. *Agricultural Systems*, 194, 103278.

Chapter 3 has been published as Hao, S., Ryu, D., Western, A. W., Perry, E., Bogena, H., & Franssen, H. J. H. (2024). Global sensitivity analysis of APSIM-wheat yield predictions to model parameters and inputs. *Ecological Modelling*, 487, 110551.

Chapter 4 will be submitted as Hao, S., Ryu, D., Western, A., Perry, E., Bogena, H., & Franssen, H. J. H. Remotely sensed wheat GLAI model at field scale for assimilating Sentinel-2 imagery into a crop yield prediction model. Will be submitted to *MethodsX* and is currently under internal review.

Chapter 5 has been submitted as Hao, S., Ryu, D., Western, A., Perry, E., Bogena, H., & Franssen, H. J. H. Assimilating remotely sensed vegetation observations for wheat yield estimates: a synthetic experiment. Submitted to *European Journal of Agronomy* and is currently under peer review.

Chapter 6 will be submitted as Hao, S., Ryu, D., Western, A., Perry, E., Bogena, H., & Franssen, H. J. H. Assimilating remotely sensed vegetation observations for wheat yield estimates: a case study using satellite data. Will be submitted to *Remote Sensing* and is currently under internal review.

Acknowledgments

Over the past four years, I have been striving to understand and reduce the uncertainty in crop model simulation and have come to realise just how much this work mirrors the uncertainty and unpredictability of life itself. The unexpected events of the pandemic, bushfires, and earthquakes made this PhD candidature a challenging journey, but I was fortunate to have support. I am deeply grateful for the support and encouragement of those who have accompanied me, whose unwavering belief in me and constant encouragement have been a source of strength and inspiration. I would like to express my profound gratitude to my supervisors: Professor Dongryeol Ryu, Professor Andrew Western, Dr. Eileen Perry, Dr. Heye Bogena, and Professor Harrie-Jan Hendricks Franssen. Your support and guidance have been instrumental in helping me navigate the complexities and uncertainties of both my research and personal life. Without your unconditional and patient assistance, I would have been adrift in the research jungle. It is through your constant guidance that a clear path was paved. I also want to extend my thanks to Professor Pablo Zarco-Tejada, for being my committee chair and for always cheering me up whenever I felt lost or stressed during my candidature.

I would like to express my gratitude to all members of the Water group, especially Professor Rory Nathan, Dr. Wenyan Wu, Dr. Danlu Guo, Professor QJ Wang, Dr. Conrad Wasko, and Dr. Murray Peel, for sharing your academic and career advice and for providing invaluable suggestions. Thanks to Emma Payne, for your efficient and considerate assistance with administrative and logistical arrangements. I am also grateful to my close friends Jie Jian, Zitian Gao, and Yawen Shao, who have contributed to many interesting discussions, activities, and have provided me with mental support. I would also like to thank Yiliang Du, Anne Wang, Huazhen Li, Wen Wang, Arash Parehkar, Manish Kumar Patel, Lilangi Wijesinghe, Jia Xu, Zhiyuan Yang, Peiye Li, Shuci Liu, Chihchung Chou, Naveen Joseph, Pengcheng Zhao, Suwash Acharya, Seema Karki, and Zahra Riazi for your friendship, support, and encouragement for my life and research.

To The University of Melbourne, which has provided me the opportunity to study here and fully funded me with the Melbourne Research Scholarship. I truly appreciate the

chance and financial support. To all the collaborators, including the Birchip Cropping Group and crop grower Rodney Pohlner. Thank you for providing the data that supported this research.

I am grateful to have a supportive family, particularly my parents, aunt, and grandparents, who have been role models in my life. You have encouraged me to persist in exploring science and have shown your unconditional support for all my decisions. Finally, my deepest love and appreciation go to Yuerong Zhou. Together, we have shared countless joyful moments and triumphed over difficulties. Your intelligence, bravery, perseverance, and love have inspired me to strive to be a better person. Thank you for always being by my side.

Table of Contents

Abstract ..... **ii**

Zusammenfassung ..... **v**

Preface ..... **viii**

Acknowledgments ..... **ix**

Table of Contents ..... **xi**

List of tables ..... **xvi**

List of figures ..... **xix**

Chapter 1 Thesis introduction **1**

1.1 Crop yield predictions by process-based crop models 1

1.2 Crop model yield prediction uncertainty 3

1.3 Improving crop model yield prediction 5

1.4 Crop model data assimilation 6

1.5 Assimilating observations into crop models using EnKF 9

1.6 Research questions and objectives 14

1.6.1 Research question 1 (Chapter 2) 15

1.6.2 Research question 2 (Chapter 3) 15

1.6.3 Research question 3 (Chapter 4) 16

1.6.4 Research question 4 (Chapters 5 and 6) 16

1.7 Thesis structure and publications 16

Chapter 2 Performance of APSIM-Wheat and factors influencing the performance: A review and meta-analysis **18**

2.1 Abstract 18

2.2 Introduction 19

2.3 Methods and materials 22

2.3.1 Overview of the APSIM Classic and Wheat module 22
2.3.2 Literature search and selection criteria 24
2.3.3 APSIM-Wheat calibration and evaluation metrics 25
2.3.4 Description of reviewed datasets 28
2.3.5 Building database for meta-analysis and performance metrics 32
2.4 Factors affecting APSIM yield prediction 33
2.4.1 Model calibration 34
2.4.2 Water availability 37
2.4.3 Nitrogen availability 40
2.4.4 Other stresses 41
2.4.5 Implications of the influential factors in changing climate 45
2.5 Summary and conclusion 46
Chapter 3 Sensitivity of APSIM-Wheat yield predictions to model parameters and inputs 50
3.1 Abstract 50
3.2 Introduction 51
3.3 Materials and methodology 54
3.3.1 The study area 54
3.3.2 APSIM and wheat module 54
3.3.3 The Sobol' sensitivity analysis and resampling by bootstrap 55
3.3.4 Weather, soil, and nitrogen fertilisation scenarios 57
3.3.5 Perturbation of weather inputs, soil texture and nitrogen parameters 58
3.4 Results 61
3.4.1 Effect of sample size 61
3.4.2 Ranking of the influential input parameters 62
3.4.3 Fertilisation amount effects on sensitivity 64
3.4.4 Weather condition effects on sensitivity 64

3.4.5 Interactions between factors 65
3.4.6 Yield prediction variability 67
3.5 Discussion 68
3.5.1 Effects of water and nitrogen availability 68
3.5.2 Implications for modellers 70
3.5.3 Implications for crop managers 70
3.5.4 Limitation and future work 72
3.6 Conclusion 73
Chapter 4 Remote sensing observations for updatable state variables in APSIM-Wheat model 75
4.1 Abstract 75
4.2 Introduction 75
4.3 Methods 77
4.3.1 Study area 77
4.3.2 Vegetation indices 78
4.3.3 Observation operator development 79
4.4 Results 81
4.4.1 The selection of ideal observation candidate 81
4.4.2 Operator uncertainty 83
4.4.3 Method validation 83
4.5 Conclusion 84
Chapter 5 Assimilating remotely sensed green leaf area index for wheat yield estimates: a synthetic experiment 85
5.1 Abstract 85
5.2 Introduction 86
5.3 Materials and methods 90
5.3.1 Study site 90
5.3.2 APSIM-Wheat and input datasets 91

5.3.3 Synthetic twin experiment 94
5.3.4 APSIM-Wheat data assimilation 99
5.3.5 Evaluation of data assimilation performance 101
5.4 Results 102
5.4.1 Performance of different data assimilation strategies 102
5.4.2 Performance of the designed data assimilation 104
5.5 Discussion 106
5.5.1 The influence of updating different biomass components in the APSIM-Wheat 106
5.5.2 The influence of updating APSIM-Wheat biomass states at different growth stages 109
5.5.3 The updating interval and observation availability 110
5.5.4 Adequacy of uncertainty estimation 111
5.6 Conclusion 112
Chapter 6 Real case study and spatial yield prediction based on satellite data ... 114
6.1 Abstract 114
6.2 Introduction 115
6.3 Methods and materials 116
6.3.1 Study site 116
6.3.2 APSIM-Wheat data assimilation framework 117
6.3.3 Evaluation of data assimilation performance 122
6.4 Results and discussion 122
6.4.1 Observation uncertainty experiments 122
6.4.2 Data assimilation performance 125
6.5 Conclusion 128
Chapter 7 Discussions and conclusions 130
7.1 Research findings 130
7.2 Research limitations and extension opportunities 133

Reference **136**

Appendix A Supplementary material for Chapter 1 ..... **181**

Appendix B Supplementary material for Chapter 2 ..... **182**

Appendix C Supplementary material for Chapter 3 ..... **199**

Appendix D Supplementary material for Chapter 5 ..... **207**

Appendix E Supplementary material for Chapter 6 ..... **207**

List of tables

Table 1-1. Summary of studies assimilating observations into crop models with EnKF 9
Table 2-1. Calibration methods defined in this paper 26
Table 2-2. Definition of the genetic parameters 26
Table 2-3. List of validation datasets from the literature used in this study (* Data were used to compose the meta-database for further analysis in Chapter 2.4) 29
Table 3-1. The perturbation sampling parameters of uncertain sources (e: Euler's number, was used as the base of natural logarithm, approximately equals to 2.71828) 59
Table 4-1. Multispectral vegetation indices investigated in this study (S: Sentinel-2, α, a, b, c used in calculating WDRVI and GLAI follow values proposed by Nguy-Robertson et al. (2014) 78
Table 4-2. The fitted curve slope for all candidate vegetation indices during the pre- and post-GLAI peak period 82
Table 5-1. The perturbation of uncertain input variables 96
Table 5-2. The DA performance of different assimilation strategies (TRUE: the TRUE model simulation; OL: the open loop model simulation; DA: data assimilation; std: standard deviation; RMSE: root mean squared error; LAI: leaf area index) 103
Table 5-3. The performance of the selected representative ensemble members to assess the designed DA strategy (TRUE: the TRUE model simulation; OL: the open loop model simulation; DA: data assimilation; std: standard deviation; RMSE: root mean squared error; LAI: leaf area index) 105
Table 6-1. The perturbation of uncertain input variables 118

Table B. 1. Calibrated cultivar parameters of APSIM-Wheat 182
Table B. 2. Detailed Information of validation datasets 183

Table C. 1. The selected weather scenarios 199

Table C. 2. The historic weather data of Nhill, Victoria, Australia (Station 078040 for precipitation and Station 078031 for temperatures, Tmax: maximum temperature, Tmin: minimum temperature) 199
Table C. 3. The selected soil textures and the proportion of sand, silt, and clay sized particles 199
Table C. 4. Mean and standard deviation values of the soil textures used for the soil layers of the three soil types used in this study 199
Table C. 5. The first order and total index variability with changing sample size for all parameters 200
Table C. 6. First order and total sensitivity index with bootstrap confidence intervals for Scenario Norm _Lm_100 200
Table C. 7. First order and total indices of uncertain factors at 50 kg N/ha nitrogen fertilisation amount 202
Table C. 8. First order and total indices of uncertain factors at 100 kg N/ha nitrogen fertilisation amount 203
Table C. 9. The ensemble yield mean and standard deviation (kg/ha) 205

Table D. 1. The mean and standard deviation (std) of the lower limit of 15 bar (LL15), drained upper limit (DUL), saturation (SAT), crop lower limit (CLL), and plant available water capacity (PAWC) for the selected soil profile. 207

Table E. 1. The mean and standard deviation (std) of the lower limit of 15 bar (LL15), drained upper limit (DUL), saturation (SAT), crop lower limit (CLL), and plant available water capacity (PAWC) for the low-yield open loop selected soil profile. Soil information was obtained by selecting a suitable soil profile from the APSoil database (Oliver and Robertson, 2009) 207
Table E. 2. The mean and standard deviation (std) of the lower limit of 15 bar (LL15), drained upper limit (DUL), saturation (SAT), crop lower limit (CLL), and plant available water capacity (PAWC) for the high-yield open loop selected soil profile. Soil information was obtained by selecting a suitable soil profile from the APSoil database (Oliver and Robertson, 2009) 208

Table E. 3. The specific dates for the 15 cloud-free Sentinel-2 and 13 cloud-free PlanetScope images. 208
Table E. 4. The performance of low-yield and high-yield open loop cases with different observation errors (DA: data assimilation, A: additive, M: multiplicative). 208
Table E. 5. The performance data assimilation for all 58 patches with the low-yield open loop case using 20% multiplicative observation error (DA: data assimilation) 209
Table E. 6. The performance data assimilation for all 58 patches with the high-yield open loop case using 20% multiplicative observation error (DA: data assimilation) 211

List of figures

Figure 2-1. Number of articles for each country (the dataset of United States of America is in the conterminous United States)..... 25
Figure 2-2. Comparison between observed and APSIM-Wheat simulated grain yields (black dashed line: 1:1 line; grey dashed line: regression line) 34
Figure 2-3. Comparison between observed and APSIM-Wheat simulated grain yields when cultivar parameters were manually tuned, and/or soil parameters were specified with ground observations (green circle: both cultivar and soil parameters were calibrated, R^2=0.87, RMSE=0.44 t/ha, NRMSE=10.15%, EF=0.85; blue dot: only cultivar parameters were tuned, R^2=0.82, RMSE=0.7 t/ha, NRMSE=12.93%, EF=0.8; orange square: only soil parameters were specified using field measurements, R^2=0.77, RMSE=0.51 t/ha, NRMSE=20.82%, EF=0.77) 36
Figure 2-4. Comparison between observed and APSIM-Wheat simulated grain yields when soil parameters specified using APSoil or estimated data (blue dot: estimated soil characteristics, R^2=0.45, RMSE=1.37 t/ha, NRMSE=40.45%, EF=-0.27; orange square: soil parameters were specified using APSoil, R^2=0.78, RMSE=0.7 t/ha, NRMSE=13.0%, EF=0.76) 37
Figure 2-5. Boxplot of APSIM predicted yield residuals under different irrigation practices..... 40
Figure 2-6. Boxplot of APSIM predicted yield residuals under different nitrogen application rates (* fertiliser amount was not specified) 41
Figure 2-7. Comparison between predicted yield residuals and observed yield under irrigated and fertilised condition 44
Figure 3-1. The 18 simulation scenarios used in this study, the key model inputs, and the main outcomes of the sensitivity analysis. The scenarios are a combination of three weather conditions, three soil types, and two nitrogen fertiliser applications. 58
Figure 3-2. Evolution of (a) the first order index and (b) total index values for uncertain factors under Scenario Norm _Lm_100 (normal weather, loamy soil, 100 kg N/ha) when the sample size increased from 10 to 10,000. Different colours represent different

uncertain factors. Blue: Precipitation; orange: Tmax; green: Tmin; red: Fertilisation Amount; purple: Initial Nitrogen Content; brown: Soil Parameters. 62
Figure 3-3. The first order index ranks (left panel) and the total index ranks (right panel) of the six influencing factors in terms of yield sensitivity under eighteen scenarios. The six parameters are listed on the horizontal axis; the eighteen scenarios are ordered along the vertical axis depending on their weather conditions, soil properties, and fertilisation amount; each grid cell shows the output sensitivity via a colour scale, where white denotes the largest influence in affecting the yield prediction and dark blue represents the minimum influence. 63
Figure 3-4. Comparison of first order and total sensitivity indices under low and high nitrogen fertilisation scenarios for six soil and weather combinations. The three subplots in the left column show first order sensitivity indices, the three subplots in the right column are for the total sensitivity indices. Plots are grouped horizontally by soil type and vertically by weather conditions as indicated by the headings. Each sub-plot shows a pair of columns the values of the sensitivity indices for the six factors as indicated in the legend under nitrogen fertilisation levels of 50 kg N/ha and 100 kg N/ha. 66
Figure 3-5. The mean estimated yield (bars) with $\pm$ standard deviation (whiskers) under all scenarios. The horizontal axis shows nine different scenario groups, each of which contains the nitrogen fertilisation level of 50 kg N/ha (blue) and 100 kg N/ha (orange). The first three groups are for the wet weather condition and each of the three soil types, the middle three groups are for normal weather conditions, and the last three for dry weather conditions. 68
Figure 4-1. The geographical location of the study area and selected ROIs (blue rectangle: selected ROIs) 77
Figure 4-2. The LOWESS function and the different trends at the pre- and post-GLAI peak growth periods (a: pre-GLAI peak period; b: post-GLAI peak period) 80
Figure 4-3. The comparison of curve slope among red edge CI, GLAI, WDRVI, and NDVI (with positive slope values). Only the slope of the fitted curves during the pre-GLAI peak period is displayed. The vertical line of rescaled GLAI=0.58 m^2/m^2 (corresponding to GLAI value=4 m^2/m^2) served as the baseline reference for estimating the curve slope..... 82
Figure 5-1. The study site location, (a) the paddock is located in north-western Victoria, Australia, (b) a satellite image of the paddock, and (c) ground measured yield data shown in tonnes per hectare (t/ha). 91

Figure 5-2. The (a) biomass amount and (b) proportion of each biomass organ in total biomass predicted by APSIM-Wheat. 93
Figure 5-3. Comparison between leaf biomass and GLAI simulated by APSIM-Wheat (different point colour represent different month). 94
Figure 5-4. Schematic diagram of the synthetic twin experiment 95
Figure 5-5. Daily yield from the open loop (OL) simulation, perturbed ensemble members, and the chosen TRUE simulations. 98
Figure 5-6. Time-series of aboveground biomass (a) and root biomass (b) variations for the high yield case when all biomass components were updated across the whole growth season at in an interval of five days. 106
Figure 5-7. Time-series of aboveground biomass (a) and root biomass (b) variations for the high yield case when only leaf biomass was updated across the whole growth season at in an interval of five days. 107
Figure 5-8. Time series of ensemble correlations between GLAI and (a) spike, (b) stem, (c) root, and (d) grain biomass components (vertical dashed lines indicate updating time points). 108
Figure 5-9. The ensemble of biomass amounts for the different plant organs before (pink lines) and after data assimilation (blue lines). 109
Figure 5-10. Time-series of leaf biomass variations for the low yield case when updating the model states at a (a) 5-day interval and a (b) 1-day interval. 110
Figure 6-1. The study site location. The paddock was segmented into 58 patches (indicated by the black lines) and also separated into two parts (indicated by the dark blue line). Four patches covering a range of low to high harvest yields were selected as test scenarios to evaluate the performance of data assimilation with varying observation errors (highlighted by light blue rectangles). The left part of the paddock consists of 31 patches, while the right part contains 27 patches. (a) shows the patch number and (b) shows the ground measured yield data for each patch (t/ha). 117
Figure 6-2. Cloud-free Sentinel-2 red edge chlorophyll index (RECI) plotted against cloud-free PlanetScope normalised difference vegetation index (NDVI). The solid red line indicates the exponential fitted equation. The R^2 for the fitted curve is 0.98. 120
Figure 6-3. The time series averaged RECI values for the whole paddock from 2019. PlanetScope was used to fill in the Sentinel-2 data gap. Orange points represent Sentinel-2 data, blue points represent PlanetScope data. 121

Figure 6-4. Performance of data assimilation for different types and magnitudes of observation error with (a) the low-yield open loop case and (b) the high-yield open loop case. The grey points represent the open loop model estimated yields. Different colours of plus signs and cross marks represent the data assimilation results with different levels of additive and multiplicative observation error, respectively. The specific colours for the varying levels of error are indicated in the legend (DA: data assimilation; obs error: observation error). 124
Figure 6-5. Performance of data assimilation for all 58 patches in the paddock with (a) the low-yield open loop case and (b) the high-yield open loop case. The multiplicative observation error with an error level of 20% was used to perturb the observations. The grey points represent the open loop model estimated yields. The blue points represent the data assimilation results (DA: data assimilation). 127
Figure 6-6. The comparison between the residual (= open loop – ground truth yield) and increment obtained through data assimilation for (a) the low-yield open loop and (b) the high-yield open loop results. The blue points represent the results from the 58 patches (DA: data assimilation). 127
Figure 6-7. The comparison between the observation variance and model forecasted states equivalent observations variance for (a) the low-yield open loop and (b) the high-yield open loop results. The specific point colours for the growth stages are indicated in the legend. 128

Figure A. 1. Schematic of the APSIM model's main processes used in this study 181

Figure C. 1. The distribution of (a) first order index and (b) total index ranks for each parameter under all eighteen scenarios. The six parameters are listed on the horizontal axis; the ranks are ordered along the vertical axis. The cross mark represents the median value, the box denotes the interquartile range, the whisker shows the maximum and minimum ranks. 205
Figure C. 2. The first order sensitivity index, total sensitivity index, and total interaction of each of the six factors for all scenarios. The different columns of plots are results for different soil types; the upper three rows are for the 50 kg N/ha fertilisation level under wet, normal, and dry weather scenarios, the lower three rows are for the 100 kg N/ha;

The first order sensitivity index, total sensitivity index, and total interaction for each of the six parameters are indicated in the legend. 206

Chapter 1 Thesis introduction

1.1 Crop yield predictions by process-based crop models

Agriculture is an important contributor to Australia's economy (Hunt et al., 2014). In agriculture, monitoring crop growth and accurately predicting yield are important for optimising management decisions regarding crop inputs, climate variability and other environmental factors (Fritz et al., 2019). One example is matching fertiliser application to the crop requirements under the prevailing conditions (Smith et al., 1997). This helps improve both economic and environmental outcomes. Yield prediction also assists governments and policy-makers in reforming import/export plans and addressing food security issues (Resnick, 2020), among other applications.

There are three main methods used for yield forecasting – field measurements and analysis of standing crops, the utilisation of remote-sensing technologies, and the implementation of crop models (Horie et al., 1992a). Field measurements assess crop conditions, such as tiller and spikelet numbers, damages due to diseases, pests and/or environmental stress impacts. Yield forecasts are subsequently made using rules of thumb or informal models based on local experience (Wisiol, 1987). Remote sensing data capture various measurements, including spectral reflectance, thermal radiation, and other electromagnetic spectra from crops. Empirical regression models can be developed by applying statistical methods to analyse the relationship between crop yield and the remote sensing-captured data. Additionally, both field measurements and remote sensing observations can be utilised to train machine learning-based models. The observations are divided into training and testing datasets, enabling the model to accurately predict crop yield by tuning hyperparameters. The trained models can subsequently be employed to forecast crop yield (Čorňák and Delina, 2022; Muruganantham et al., 2022). Among all three methods, process-based crop models, which simulate the biophysical processes linking environmental and management factors to crop yield outcomes (Roberts et al., 2017), have been widely used to understand the complex interactions between crops and their environment (Horie et al., 1992b). These models estimate crop growth, water balance, and nutrient cycling on a daily basis, providing not only predictions but also

insights into the environmental impacts on crops, enhancing resource use efficiency and ensuring food production.

Widely used process-based crop models include Simulateur mulTIdisciplinaire pour les Cultures Standard (STICS) (Brission et al., 2002; Brisson et al., 1998b; N. Brisson et al., 2003), Environmental Policy Integrated Climate (EPIC) (Williams et al., 1989), Decision Support System for Agrotechnology Transfer (DSSAT) (Jones et al., 2003), WOrld FOod Studies (WOFOST) (Supit et al., 1994), Soil Water Atmosphere Plant (SWAP) (Van Dam et al., 1997), AquaCrop (Hsiao et al., 2009; Raes et al., 2009a; Steduto et al., 2009a), and Agricultural Production System SIMulator (APSIM) (Brown et al., 2018; Holzworth et al., 2006, 2014a; Keating et al., 2003).

The APSIM model, developed in Australia, has been widely used across the globe for research and practical purposes. It comprises modules that are interconnected and simulate the complex biophysical interactions between soil water, nutrients, organic matter, crops, weather, and management. APSIM is capable of simulating a wide range of crops and pastures, including wheat (Asseng et al., 2000, 1998a), sorghum (Carberry and Abrecht, 1991; Hammer and Muchow, 1991), maize (Archontoulis et al., 2014; Shamudzarira and Robertson, 2002), cotton (Hearn, 1994), canola (Robertson and Lilley, 2016), rice (Oryza2000) (Bouman, 2001; Li et al., 2017), and various legumes (Robertson et al., 2002). Given its relevance to Australian agriculture and international application, this study will use APSIM-Wheat as an example to represent process-based crop models.

The main APSIM modules used in this study include Wheat, Weather, SoilN, SoilWat, Surface organic matters (OM), and Management. Schematic depicting the main processes accounted for by APSIM are shown in Figure A. 1. These modules have their own processes and also interact with each other to account for the interaction of wheat with the environment and management.

The Wheat module (Brown et al., 2014; Zheng et al., 2014) simulates crop growth by modelling states such as phenological development, leaf development and senescence, radiation interception, plant morphology, biomass, and nitrogen accumulation in different wheat components. This is based on state variables and parameters including thermal time, available water and nutrient content, radiation use efficiency, stress factors, and carbon dioxide factor. The state variables are provided by other modules.

The SoilWat module (Jones and Kiniry, 1986; Littleboy et al., 1992) calculates soil water movement using a cascading water balance model. Key parameters describing soil water holding characteristics include the lower limit of 15 bar (LL15, the wilting point), drained upper limit (DUL, the field capacity), crop lower limit (CLL), and saturation (SAT). It provides available water and nutrient content across the soil profile for each soil layer to the Wheat module, allowing it to determine the amount of water and nutrient uptake.

The SoilN module considers three organic matter pools (fresh, biom, and hum) to simulate the conversion of nitrogen and carbon in each soil layer through processes including nitrification, denitrification, mineralisation, and immobilisation. This module thereby calculates the available nitrogen in soils based on the crop residuals and fertiliser inputs. The available nitrogen content is provided to SoilWat to determine the distribution and movement of nitrogen content for each soil layer.

The Surface OM module (Probert et al., 1998; Thorburn et al., 2001) simulates the dynamics of organic materials, such as crop residues and other plant debris, on the soil surface. It calculates the decomposition and incorporation of organic matter into the soil, providing information to the three organic matter pools in SoilN.

The Weather module provides daily meteorological information such as precipitation, global radiation, maximum and minimum temperature. The Management module uses user-defined scripts for activities such as sowing, fertilisation, and irrigation to specify the amount and timing of these management measures.

1.2 Crop model yield prediction uncertainty

Although the APSIM-Wheat is a process-based crop model, it is subject to uncertainties that arise from widely known sources such as the model structure, climate forcing, parameters, and observations (Vrugt et al., 2008). It is crucial to have a comprehensive understanding of these uncertainties as they can negatively impact the performance of crop system yield predictions and introduce risk to cropping decisions (Challinor and Wheeler, 2008; Ramirez-Villegas et al., 2017; Seidel et al., 2018).

Crop model structural uncertainties are mainly due to an inadequate understanding of the biophysical processes and the varying levels of detail that modellers attempt to represent. Model algorithms may also be oversimplified or mischaracterise the complex interactions between climate, soil, and crops. Concern about structural uncertainty has

increased in the last decade (Asseng et al., 2015, 2013; Martre et al., 2015b; Palosuo et al., 2011; Rötter et al., 2011). Parameter uncertainties stem from a lack of high-quality experimental measurements under sufficiently diverse conditions and from unmapped heterogeneities in various properties, especially soils. Many studies have investigated the impact of parameter uncertainty on model performance (Dzotsi et al., 2015; Iizumi et al., 2009; Post et al., 2008; Ran et al., 2022; Wallach et al., 2002). Calibration, which iteratively adjusts parameter values to bring model predictions closer to observations, can reduce parameter uncertainties. However, calibration efficacy depends on the uncertainties in the observations and the identifiability of individual parameters, which can be impacted by parameter interactions, for example. Observation uncertainty refers to errors in measurements that are used for model calibration and validation. It is often ignored in crop modelling studies, but has received increasing attention in recent years (Confalonieri et al., 2016; Kersebaum et al., 2015; Zhao et al., 2015). The uncertainty associated with climate forcing data, such as measurement and estimation errors of weather conditions, has been shown to significantly affect model prediction (Ojeda et al., 2021; Rötter et al., 2012; Tao and Zhang, 2013). The impact of future climate change on crop models has also gained attention from researchers. Chapagain et al. (2022) reviewed 277 published articles and reported that a majority of the studies (52%) were focused on assessing uncertainty related to model inputs. Among these studies, the projected changing climate was found to be the most frequently considered source. In contrast, only 28% and 20% of the articles focused on uncertainties arising from model parameters and model structure, respectively.

APSIM-Wheat yield prediction accuracy has been extensively evaluated for research purposes and as a decision support tool for providing advice to policymakers and stakeholders. A large dataset for validating model yield predictions under a wide range of environmental and management conditions is available on the APSIM website (https://www. apsim.info/). Multiple studies have also evaluated the model's accuracy before it was applied in various regions, including Australia (Asseng et al., 1998b; Bryan et al., 2014; Hunt et al., 2006; O'Leary et al., 2016; Phelan et al., 2018), New Zealand (Asseng et al., 2004; Bell et al., 2009), Asia (Chen et al., 2010a; Gaydon et al., 2017; Liu et al., 2016a; Wang et al., 2014; Zhang et al., 2013; Zhao et al., 2017), Africa (Araya et al., 2020, 2017), Europe, and America (Asseng et al., 2000; Brown et al., 2018, 2014; Holzworth et al., 2018, 2014a). The details of the literature review on APSIM yield

prediction accuracy are presented in Chapter 2. The APSIM yield prediction exhibited varying levels of performance when validated under different environmental and management conditions and for various cultivars. Despite extensive work has been done to evaluate the accuracy of the model's yield prediction, each evaluation was limited to a few sites. Therefore, a more comprehensive understanding of the model's behaviour under various conditions is necessary to improve the understanding of the model's prediction uncertainty and the factors that affect its performance. This highlights the need to find effective methods for diagnosing uncertainties in crop models.

1.3 Improving crop model yield prediction

Researchers have been actively seeking approaches to identify and quantify the modelling uncertainties from various sources (Asseng et al., 2013; Dokoohaki et al., 2021; Rosenzweig et al., 2013; Rötter et al., 2011; Tao et al., 2018) to improve model yield prediction performance.

Comparison of multi-model ensembles is a common approach to understanding model structural uncertainty. It involves analysing the variability between predictions from different models (Asseng et al., 2015; Bai et al., 2022; Iizumi et al., 2018; Maiorano et al., 2017a; Osman et al., 2022; Rettie et al., 2022; Wallach et al., 2017; Wallach and Thorburn, 2017). It has been found that the ensemble mean or median predictions are more accurate than individual model results (Martre et al., 2015b). Ensemble intercomparison information can also assist in incorporating and/or modifying the functions describing biophysical processes in crop models to reduce prediction uncertainty and improve performance (Wang et al., 2017). However, this approach requires extensive collaboration from multiple crop modelling teams and can be time-consuming to implement (Asseng et al., 2013; Rötter et al., 2011). Another option is to directly improve inadequate simulations of the biophysical processes by developing new modules or modifying relevant existing functions. These methods require extensive field work and laboratory experiments, which can be costly and long-term solutions.

Uncertainty analysis and sensitivity analysis are used to evaluate the influence of uncertain parameters and inputs on model outcomes and to guide model improvement. Uncertainty analysis examines how the uncertainty from possible parameter and input values propagates through the model and produces results with a probability of

occurrence. Sensitivity analysis aims to identify the factors that significantly affect crop model predictions (Jain and Singh, 2003). In prior research, this approach has been utilised to identify the primary influential factors across multiple crop models (Laluet et al., 2023; Liang et al., 2017; Lu et al., 2021a; Ma et al., 2023; Makowski et al., 2006; Richter et al., 2010; Varella et al., 2010; Wang et al., 2013a; Xing et al., 2017; Yu et al., 2023). Existing uncertainty and sensitivity analyses on APSIM mostly focused on analysing the impacts of crop genetics (Casadebaig et al., 2016; Collins et al., 2021; He et al., 2015; Zhao et al., 2014), soil parameters (Dokoohaki et al., 2018; Vogeler et al., 2022; Wu et al., 2019), and climate conditions (Luo and Kathuria, 2013) on key model outputs such as yield, biomass, phenological stage, soil moisture, drainage, and nitrogen leaching. A detailed literature review on sensitivity analysis of the APSIM model can be found in Chapter 3.

Once the influential factors are identified, a calibration can be performed to adjust their values and improve the fit of model simulations to observations. However, it is important to note that calibration can only improve the accuracy of model predictions and does not reduce the model's structural uncertainty. The influential factors can also be useful for targeting algorithm improvements by identifying the parts of the model that are most critical for prediction accuracy.

1.4 Crop model data assimilation

Data assimilation is a technique that combines model simulations with observations to improve the accuracy of predictions. This technique involves adjusting the model's initial conditions, parameters, and/or state variables, based on the available observations, to enhance the agreement between the model's output and the *in situ* data. There are several approaches to integrating observations with crop model simulations, as categorised by Dorigo et al. (2007) and Jin et al. (2018) as "calibration", "forcing", and "updating" methods.

The "calibration" method, also referred to as model calibration, is regarded as a data integration technique by several authors (Dorigo et al., 2007; Eicker et al., 2014; Jin et al., 2018) because it serves the same purpose. Model calibration adjusts model parameters and/or initial states to find the optimal set of parameter values that minimise the difference between the model simulations and observations. It effectively combines the observed data and models to improve the model prediction performance. This aligns

with the aim and practice of data assimilation. Various algorithms have been applied to optimise simulations, such as Genetic Algorithms (GA) (Ines et al., 2006), the Simplex Search Algorithm (SRA) (Claverie et al., 2009; Guérif and Duke, 2000; Jégo et al., 2012; Launay and Guérif, 2005), Shuffled Complex Evolution (SCE-UA) (Huang et al., 2019b, 2015b, 2015a; Jin et al., 2022; Ma et al., 2013; Ren et al., 2010, 2009; Tian et al., 2013), Annealing Algorithms (AA) (Dong et al., 2013; Jin et al., 2016; Morel et al., 2014), and Particle Swarm Optimization Algorithms (PSO) (Guo et al., 2018; Jin et al., 2015, 2022, 2020, 2017; Z. Li et al., 2015b, 2015a; Liu et al., 2015; Silvestro et al., 2017; Wagner et al., 2020).

The "forcing" method, also known as direct insertion (Bernard et al., 1981; Jackson et al., 1981; Manivasagam et al., 2021; Ramos et al., 2018; Robinson and Lermusiaux, 2000; Walker and Houser, 2005) or Newtonian nudging (Houser et al., 1998; Paniconi et al., 2003) method, involves the direct substitution of model-simulated state variables with corresponding observations at each time step of the model. Remotely sensed vegetation indices are commonly used as observations to update corresponding variables in crop models. Bouman (1995), Schneider (2003), Hadria et al. (2006), Jongschaap (2006), Tripathy et al. (2013), Thorp et al. (2010), Morel et al. (2014), Yao et al. (2015), Ban et al. (2019), and Abi Saab et al. (2021) estimated indices such as normalised difference vegetation index (NDVI), leaf area index (LAI), fraction of absorbed photosynthetically active radiation (fAPAR), aboveground nitrogen accumulation (AGN), and water stress factor from various satellite sensors and directly replaced the corresponding model value with the observation during simulations. This improved predicted LAI, aboveground biomass (AGB), and yield. The "forcing" method is easy to implement. However, its efficacy largely depends on the accuracy of the observations.

Both "calibration" and "forcing" methods provide ways to blend model simulations and observations. However, these two techniques tend to over-correct the model simulations due to its inherent assumption that observations are error-free. In contrast, statistical or stochastic updating methods consider uncertainties in both observations and simulations to continuously update model state variables in an optimal manner. The Kalman Filter (KF) is a widely used statistical updating data assimilation technique (Kalman, 1960; Welch et al., 1995) with variants such as the Extended Kalman Filter (EKF) (Julier and Uhlmann, 2004), Ensemble Kalman Filter (EnKF) (Evensen, 2003, 1994), Particle Filter (PF) (Del Moral, 1997; Liu and Chen, 1998), Three-Dimensional Variational Data

Assimilation (3DVar) (Lorenc, 1986; Sasaki, 1970), and Four-Dimensional Variational Data Assimilation (4DVar) (Le Dimet and Talagrand, 1986; Talagrand and Courtier, 1987).

Variational methods, such as 3DVar and 4DVar, have been successfully applied in weather forecasting (Lorenc, 1986; Lorenc et al., 2000). 3DVar assimilates observations into models at a single analysis time, while 4DVar assimilates observations over a time window that typically extends throughout the forecast period, providing a more accurate representation of the model outputs' temporal evolution. (Le Dimet and Talagrand, 1986; Talagrand and Courtier, 1987). However, these methods require the use of all observations within the data assimilation time window to adjust model predictions by minimising the error between observations and model analysis, as measured by constructed cost functions. Furthermore, the adjoint method is required to compute the gradient of the cost function with respect to the model states, which can be challenging to construct and modify for changes in the model (Altaf et al., 2013; Courtier et al., 1994; Elbern et al., 1997). These methods can be computationally demanding and may not be suitable for applications that require rapid assimilation of large volumes of data, such as predicting harvest yield during the growing season.

The KF equations are only applicable to linear simulation models and linear observation operators, with an assumption that all statistics follow a Gaussian distribution (Aubert et al., 2003; Huang et al., 2019a). The strict requirements of the KF limit its applicability in crop model data assimilation as most dynamic crop models are nonlinear. To address the limitations, the EKF was developed. EKFs use a local linear approximation to propagate the model error covariance matrix based on Taylor series expansion (Jazwinski, 2007). A challenge with this method is that it can lead to instabilities or divergences due to the linear approximation of nonlinear processes (Clark et al., 2008). The EnKF was developed to deal with high-dimensional non-linear model systems and is widely used in environmental models. Essentially, the EnKF is a stochastic version of the KF, which enables explicit error representations to be propagated through the non-linear model using a Monte Carlo approach. It utilises an ensemble of model simulations to effectively capture both model nonlinearity and interdependence between model multiple states. The PF allows for the propagation of non-Gaussian distributed observations and model simulations by representing the model state's probability distribution with a set of

weighted particles, the weights of the particles are adjusted at each time step based on how well they match the observations (Hartig et al., 2011; Huang et al., 2019a).

1.5 Assimilating observations into crop models using EnKF

The EnKF is one of the most popular sequential data assimilation techniques used with non-linear models due to its computational efficiency and ease of implementation (Luo et al., 2023; Zhang et al., 2021a). It has been widely used in land surface models and hydrological models, including for the assimilation of microwave-derived soil moisture (SM), thermal infrared image-based evapotranspiration retrievals, and remote sensing-based soil moisture proxy into land surface models (Crow and Ryu, 2009; Draper and Reichle, 2015; Hain et al., 2012; Pipunic et al., 2008; Reichle et al., 2002; Reichle and Koster, 2005), and the assimilation of stream discharge and/or soil moisture into hydrological models (Alvarez-Garreton et al., 2014; Li et al., 2015, 2013; Y. Li et al., 2014; Massari et al., 2014; Vrugt et al., 2006). These studies have demonstrated the efficacy of EnKF in improving model simulation and prediction capability by integrating remote sensing observations. EnKF is also broadly applied in crop model data assimilation. Table 1-1 summarises the studies that have used EnKF to assimilate observations into various crop models.

Table 1-1. Summary of studies assimilating observations into crop models with EnKF

Crop models	Crops	Observations	Updated state variables	References
DSSAT	Wheat	LAI, SM	Biomass weights, canopy height, leaf area	Nearing et al. (2012)
	Maize	LAI, SM	LAI, SM	Ines et al. (2013)
	Soybean	SM	SM	Chakrabarti et al. (2014)
	Maize	SM	SM	Mishra et al. (2021)
WOFOST	Wheat, Maize	SM	SM	De Wit and van Diepen (2007)
	Wheat	LAI, SM	LAI, SM	Pauwels et al. (2007)
	Wheat	LAI	LAI	Curnel et al. (2011)
	Maize	LAI	LAI	Wang et al. (2013a)

	Maize	LAI	LAI	Zhao et al. (2013)
	Wheat	LAI	LAI	Huang et al. (2016)
	Wheat	Gross primary production (GPP)	GPP	Zhuo et al. (2022)
	Wheat	LAI	LAI	Huang et al. (2023)
AquaCrop	Maize	Evapotranspiration (converted from latent heat flux), SM, canopy cover (converted from LAI)	Canopy cover, SM	Lu et al. (2021)
	Rice	Canopy cover (CC), biomass, phenological observations	CC, biomass, growing degree day (GDD), parameters related to canopy development, water transformation, and phenology development	Yang et al. (2023)
SAFY	Wheat	LAI	LAI	Silvestro et al. (2017)
	Maize	LAI	LAI	Silvestro et al. (2021)
	Maize	LAI	LAI	Kang and Özdoğan (2019)
	Wheat	LAI	LAI	Zhang et al. (2021a)
APSIM	Wheat	LAI, leaf biomass, stem biomass, aboveground biomass, phenology, SM, soil nitrate-nitrogen	LAI, leaf biomass, stem biomass, aboveground biomass, phenology, SM, soil nitrate-nitrogen	Zhang et al. (2021)
	Wheat	LAI, leaf weight and nitrogen, stem weight and nitrogen, spike nitrogen, SM, soil nitrate-nitrogen, soil ammonium-nitrogen	LAI, leaf weight and nitrogen, stem weight and nitrogen, spike nitrogen, SM, soil nitrate-nitrogen, soil ammonium-nitrogen	Zhang et al. (2022)
	Maize, Soybean	SM	SM	Kivi et al. (2022)

LAI: leaf area index, SM: soil moisture

1

The application of EnKF in crop model data assimilation has shown mixed outcomes. Some studies found that integrating observations and models using an EnKF has improved model yield prediction performance. Ines et al. (2013) used an EnKF to incorporate AMSR-E soil moisture and Moderate Resolution Imaging Spectroradiometer (MODIS) LAI data, both independently and simultaneously, into the DSSAT-CSM-Maize model to develop an effective DA framework for improving crop yield prediction at the county-level in Story County, Iowa, USA. The results showed that the correlation between observed and simulated yields improved more when both SM and LAI were assimilated into the model, compared to assimilating either variable. However, the assimilation of LAI alone may be more suitable in extremely wet conditions, while the simultaneous assimilation of both SM and LAI is recommended under more nominal conditions. Chakrabarti et al. (2014) used EnKF to assimilate downscaled 1 km Soil Moisture and Ocean Salinity (SMOS) soil moisture observations into the DSSAT-Soybean model to improve model yield prediction in a rain-fed agricultural region of the lower La Plata Basin in Brazil during two growing seasons. The yields obtained after assimilation were improved in both seasons, with a larger improvement during the drought-affected season. Mishra et al. (2021) assimilated coupled microwave and thermal infrared SM profiles into the DSSAT-Maize model over the Southeast United States. In both irrigated and non-irrigated scenarios, the EnKF was demonstrated to significantly reduce the model's yield prediction errors. Zhao et al. (2013), Wang et al. (2013a), Huang et al. (2016), and Huang et al. (2023) used an EnKF to integrate satellite-derived LAI observations from PROBA/CHRIS, MODIS, Landsat, and Global LAnd Surface Satellite (GLASS) into the WOFOST model using the EnKF to improve maize and wheat yield predictions at the regional scale in north-western and north-eastern China. The results showed that the EnKF can provide accurate regional estimates of crop growth and final yield. Zhuo et al. (2022) assimilated accumulative GPP from a satellite-based vegetation photosynthesis model into the WOFOST model at both site and regional scales in the south-central United States. The results highlighted the data assimilation's capacity to enhance the model's accuracy in estimating wheat yields at both scales. Lu et al. (2021) introduced an EnKF-based framework that assimilates separate and combined in situ SM and canopy cover observations into the AquaCrop model. To evaluate the effectiveness of the approach, the researchers applied it to a rain-fed maize field in Nebraska, USA over six growing seasons. The study found that the joint assimilation of both variables outperformed assimilation of a single variable, and the

system was able to predict yield around three months prior to harvest with improved accuracy (RMSE = 1.7 t/ha, nRMSE = 15.74%) compared to the no-assimilation case (RMSE = 2.01 t/ha, nRMSE = 18.61%). Silvestro et al. (2021, 2017) and Zhang et al. (2021a) used an EnKF to assimilate LAI observations into the SAFY model across central Italy, central China, and north-western China. These LAI observations were derived from field spectral measurements and various satellite images, including Landsat 8 Operational Land Imager (OLI), Huan Jing (HJ) HJ1A/B, and Sentinel-2. The assimilation results demonstrated the ability of EnKF to improve wheat and maize yield predictions at both the field and district levels.

Some other studies found limited improvements in prediction performance when using EnKF. Nearing et al. (2012) used an EnKF to assimilate MODIS LAI and SMOS SM observations into the DSSAT wheat model in energy-limited and water-limited environments in the UK and Canada. The results indicated that the potential for data assimilation to improve yield estimates was low, due to a lack of correlation between leaf and grain growth. The correction in LAI state values did not translate into improved yield estimates. Pauwels et al. (2007), Zhang et al. (2022, 2021), and Kivi et al. (2022) also found that the lack of correlation between different state variables limited the effectiveness of data assimilation. The updating of wheat state variables, such as LAI, leaf or stem biomass, did not improve soil moisture estimation or nitrogen cycle simulation using the WOFOST or APSIM models, and vice versa.

To improve the accuracy of yield prediction through data assimilation, it is important to consider the simulation of grain development, as simulated yield typically refers to the simulation of harvested grain. Simulated grain development is controlled by multiple factors such as cultivar characteristics, resource availability, weather conditions, and soil parameters. Updating limited state variables is inadequate for correcting yield estimates. Nearing et al. (2012) reported that the assimilation of LAI observations into the DSSAT model had low potential for improving wheat yield estimation due to the lack of root-zone soil moisture data. Insufficient information about available water content failed to inform the model about water stress situations. Curnel et al. (2011) found that the WOFOST model simulated phenological development disagreed with observed development, so updating only LAI in WOFOST led to poor results. To address the mismatch between simulated and observed phenological development, Chen et al. (2018) adjusted the MCWLA-Wheat simulated phenology using remote sensing data retrieved

phenology information before implementing data assimilation. This assimilation scheme substantially improved model yield prediction. Zhang et al. (2022, 2021) corrected the phenology estimates simulated by APSIM-Wheat with *in situ* phenological development information. With this phenology constraint, data assimilation showed improved results in estimating final yield. Yang et al. (2023) developed an EnKF-based data assimilation method to incorporate phenological observations into the AquaCrop model, subsequently adjusting model parameters to maintain phenological consistency. The proposed strategy significantly improved yield estimation, particularly in cases with high phenological heterogeneity among plots, thereby highlighting the potential of assimilating phenological observations for enhancing in-season yield forecasting.

Accurately quantifying model and observation errors is crucial for the effectiveness of an EnKF (Kivi et al., 2022; Tandeo et al., 2020). De Wit and van Diepen (2007) found that underestimating errors in the WOFOST model and satellite SM observation resulted in insignificant improvements in wheat and maize yield predictions. Nearing et al. (2012) conducted an experiment where they examined how observation uncertainty affected assimilation results by testing eight sets of satellite LAI and SM observation errors. The study found that assimilating LAI into the DSSAT model was successful in water-limited situations when the standard deviation of LAI observation errors ranged from 0.05 to 0.30 m^2/m^2. Silvestro et al. (2021) tested six LAI observation errors ranging from 0.05 to 0.30. The results showed that data assimilation performed best when the observation error was 0.05, and filter performance decreased with increasing error. Zhang et al. (2022) confirmed that reducing observation uncertainty led to greater improvements in yield estimation. It is essential to consider and incorporate model and observation errors in designing an effective EnKF-based data assimilation strategy.

A variety of data sources, including field measurements and remote sensing data, can provide observations and be assimilated into crop models. Remote sensing data have been widely used in recent decades to improve model predictions due to their ability to provide spatially distributed and regular (under favourable atmospheric conditions) observations of land surface characteristics. Satellite imagery provides repeated observations to estimate crop growth attributes and soil properties. Current practices in crop model data assimilation use a variety of observations to adjust model simulations, including LAI (Baret et al., 2007; Bouman, 1995; Dente et al., 2008; Dong et al., 2013; Fang et al., 2011, 2008; Hadria et al., 2006; Huang et al., 2015b, 2015a; Jiang et al.,

2014b, 2014a; Li et al., 2014; Ma et al., 2013; Pagani et al., 2018; Prévot et al., 2003; Ren et al., 2010), FAPAR (Clevers, 1997; Gobron et al., 2000; Morel et al., 2014), AGB (Claverie et al., 2009; Jin et al., 2015), phenological stage (Chen et al., 2018; Xu et al., 2021; Zhang et al., 2021), evapotranspiration (ET) (Bastiaanssen and Ali, 2003; Huang et al., 2015a; Hurtado et al., 1994), and SM (Bach and Mauser, 2003; Chakrabarti et al., 2014; Dente et al., 2008). Vegetation observations are mainly from open-access satellite products such as the Advanced Very High Resolution Radiometer (AVHRR), MODIS, MEdium-spectral Resolution Imaging Spectrometer (MERIS), Landsat EM, ETM+, OLI, Sentinel-2 MSI, RapidEye, and PlanetScope. These products have spatial resolutions ranging from 2 km to 3 m. Soil moisture observations come from sources such as ENVISAT Advanced Synthetic Aperture Radar (ASAR), SMOS, and Soil Moisture Active Passive (SMAP). The selection of data sources is based on the scale of the study area and the required observation revisit time. With the multiple options of easily accessible satellite observations, the integration of crop models and remote sensing observations provides valuable spatial information on crop yields for both crop management and market strategy adjustment (Lobell, 2013a).

1.6 Research questions and objectives

Accurate crop model yield predictions provide reliable information to stakeholders and policymakers to manage crops, maximise crop productivity, and reform import/export plans to ensure food security. Data assimilation is a promising approach for improving model yield prediction performance. However, accurately predicting crop yield by integrating remotely sensed observations still presents challenges. Most studies assimilated multiple sources of observations into crop models, such as soil moisture, soil nutrient content, biomass, and indices representing leaf growth. Some studies also used field-measured yield data, soil hydraulic parameters, or observed phenological stages to calibrate the model and ensure the performance of data assimilation. However, obtaining multiple sources of information can be time-consuming and labour-intensive, making it challenging to implement in a real-world application. The efficacy of incorporating a single-source and simply obtained observation from satellite into APSIM has not been thoroughly assessed. Additionally, current studies have indicated that accurately quantifying model and observation errors is crucial for the performance of data assimilation. However, knowledge about APSIM-Wheat yield prediction uncertainty and the factors that affect the model's performance is limited. The appropriate satellite

observation to be fused into the model also need to be investigated. Lastly, an effective data assimilation strategy for varying updating intervals, phenological stages, and updated biomass state variables needs to be explored and designed under controlled conditions.

The goal of this thesis is to design, implement, and evaluate an effective data assimilation strategy for improving field-level yield prediction performance and providing spatial variability information of crop yield by integrating simply obtained remotely sensed observations into APSIM-Wheat using EnKF. Therefore, the following research questions are proposed to achieve the overarching research objective.

1.6.1 Research question 1 (Chapter 2)

How accurate is the APSIM-Wheat yield prediction, and what are the more influential factors that affect the model's yield prediction accuracy and uncertainty?

Previous studies have primarily focused on evaluating the accuracy of APSIM-Wheat yield predictions at a limited number of sites, with limited research investigating the uncertainty of these predictions. Therefore, research question 1 aims to assess the accuracy and uncertainty of APSIM-Wheat yield predictions, as well as to explore the underlying factors that affect the model's performance and estimate their contributions to the prediction uncertainty. This question is addressed by conducting an extensive literature review and meta-analysis on the performance of APSIM-Wheat under various environmental conditions, fertilisations, and model calibrations to provide a more comprehensive understanding of the model's behaviour.

1.6.2 Research question 2 (Chapter 3)

How sensitive are APSIM-Wheat yield predictions to the influential factors identified in research question 1? How do changing environment and management conditions affect the sensitivity of yield variability to these influential factors?

Previous studies have examined the sensitivity of APSIM crop yield to cultivar parameters, soil hydraulic parameters, and forcing inputs. Studies focusing on the interplay of water availability, nitrogen fertilisation, weather conditions, and soils on crop growth and yield has not yet been thoroughly analysed. To address research question 2, a sensitivity analysis was conducted to measure the contribution of uncertain input

variations to the variability of APSIM-Wheat yield predictions under various climate conditions, soil types, and nitrogen fertilisation rates.

1.6.3 Research question 3 (Chapter 4)

What satellite observation is most suitable for updating the APSIM-Wheat model, and how should it be converted through an observation operator for use in data assimilation?

There are multiple satellite sources and observations available for crop model data assimilation, but the selected observation should be both accessible and closely related to the state variable in the APSIM-Wheat model. It is also necessary to establish the connection between the observation and the state variable, so that the state can be converted to be comparable with the observation.

1.6.4 Research question 4 (Chapters 5 and 6)

How can crop biomass information from satellite be integrated into APSIM-Wheat to effectively improve yield prediction? More specific questions are:

1. Which model state variables should be updated, and how can the non-leaf biomass of wheat be effectively updated by assimilating leaf biomass information?
2. What is the influence of the timing and frequency of updates?
3. How uncertain is the satellite observation? Will data assimilation with real satellite data improve the model's yield prediction performance?

The first two sub-questions are answered through a synthetic experiment. By testing and comparing the efficacy of updating various state variables at different frequencies and growth stages, the most efficient data assimilation strategy can be determined. The third sub-question is addressed by conducting data assimilation with real satellite observations and comparing the results to within-field yield measurements to assess the data assimilation performance.

1.7 Thesis structure and publications

This thesis consists of five main chapters (Chapter 2 to Chapter 6). Chapter 2 to 4 correspond to research question 1 to 3, while Chapter 5 and 6 correspond to research question 4. Chapter 2 to 6 are presented in a journal article style, including an abstract, introduction, methods and materials, results, discussions, and conclusions. Chapter 7 is

a conclusion chapter, which integrates the main methods and findings, acknowledges the limitations, identifies future opportunities, and concludes the thesis.

Chapter 2 Performance of APSIM-Wheat and factors influencing the performance: A review and meta-analysis

2.1 Abstract

Process-based crop models provide ways to predict crop growth, evaluate environmental impacts on crops, test various crop management options, and guide crop breeding. They can be used to explore options for mitigating climate change impacts when combined with climate projections and explore mitigation of environmental impacts of production. The Agricultural Production Systems SIMulator (APSIM) is a widely adopted crop model that offers modules for simulation of various crops, soil processes, climate, and grazing within a modelling system that enables robust addition of new components. This study uses APSIM Classic-Wheat as an example to examine yield prediction accuracy of biophysically based crop yield modelling and to analyse the factors influencing the model performance. We analysed yield prediction results of APSIM Classic-Wheat from 76 published studies across thirteen countries on four continents. In addition, a meta-database of modelled and observed yields from 30 studies was established and used to identify factors that influence yield prediction uncertainty. Our analysis indicates that, with site-specific calibration, APSIM predicts yield with a root mean squared error (*RMSE*) smaller than 1 t/ha and a normalised RMSE (*NRMSE*) of about 28%, across a wide range of environmental conditions for independent evaluation periods. The results show increasing errors in yield with limited modelling information and adverse environmental conditions. Using soil hydraulic parameters derived from site-specific measurements and/or tuning cultivar parameters improves yield prediction accuracy: *RMSE* decreases from 1.25 t/ha to 0.64 t/ha and *NRMSE* from 32% to 14%. Lower model accuracy was found where APSIM overestimates yield under high water deficit condition and when it underestimates yield under nitrogen limitation. APSIM severely over-predicts yield when some abiotic stresses such as heatwaves and frost affect the crop growth. This paper uses APSIM-Wheat as an example to provide perspectives on crop

model yield prediction performance under different conditions covering a wide spectrum of management practices, and environments. The findings deepen the understanding of model uncertainty associated with different calibration processes or under various stressed conditions. The results also indicate the need to improve the model's predictive skill by filling functional gaps in the wheat simulations and by assimilating external observations (e.g., biomass information estimated by remote sensing) to adjust the model simulation for stressed crops.

2.2 Introduction

Biophysical models, as agricultural simulation systems, are widely used to simulate crop growth, test management options, assess environmental trade-offs, and explore ways to cope with climate change impacts. The key strength of process-based biophysical models is their embodiment of our understanding of the dynamic interactions among crop, soil, water, atmosphere, and solar radiation within the agricultural system (Horie et al., 1992a). In essence, they simulate the biological and physical processes linking environmental effects to crop yield outcomes (Roberts et al., 2017). These models can assist in quantifying the impacts of changing climate on crop yield, designing efficient management practices, and informing crop breeding (Bustos-Korts et al., 2019; Chapman et al., 2003; Luo et al., 2009) to secure food production. But deficiencies in the models and their implementations (e.g., calibration and weather inputs) can introduce random or systematic errors leading to uncertain yield predictions. While current efforts are underway to improve biophysical schemes, model inputs and implementation, understanding the current state of process-based model performance and sources of uncertainty can guide us to more effective strategies.

There exist several widely used process-based crop models that include Agricultural Production System SIMulator (APSIM) (Brown et al., 2018; Holzworth et al., 2014b; Keating et al., 2003; McCown et al., 1996, 1995), Simulateur mulTIdisciplinaire pour les Cultures Standard (STICS) (Brisson et al., 2002, 1998a; Nadine Brisson et al., 2003), Environmental Policy Integrated Climate (EPIC) (Williams et al., 1989), The Soil & Water Assessment Tool (SWAT) (Neitsch et al., 2011), Decision Support System for Agrotechnology Transfer (DSSAT) (Jones et al., 2003), World Food Studies (WOFOST) (Van Diepen et al., 1989; van Ittersum et al., 2003), Soil Water Atmosphere Plant (SWAP) (Van Dam et al., 1997), and AquaCrop (Hsiao et al., 2009; Raes et al., 2009b; Steduto et

al., 2009b). This work focuses on APSIM Classic as an example to explore a biophysical model's performance in predicting yield and the factors influencing the performance.

APSIM has been used for research and practical applications globally for over 25 years. It is also available as an online commercial agricultural decision-support tool, named Yield Prophet®, to serve Australian growers (Carberry et al., 2009; Hochman et al., 2009b). APSIM consists of interconnected modules describing the biophysical roles of soil water, soil nutrients, organic matter, crops, weather, and management. It can simulate various crop types and pastures. Simulated crops include wheat (Asseng et al., 2000, 1998a), maize (Archontoulis et al., 2014; Shamudzarira and Robertson, 2002), canola (Robertson and Lilley, 2016), and various legumes (Robertson et al., 2002). Previous studies have used it as a tool to reproduce the biophysical processes of the cropping system from paddock to regional level (Araya et al., 2020; Gaydon et al., 2006; Keating et al., 2002), including representing the role of soils (Connolly et al., 2002; Probert and Dimes, 2004; Thorburn et al., 2001), the influence of climate (Asseng et al., 2015; Bahri et al., 2019), and animal grazing (Bosi et al., 2020; Holzworth et al., 2014b). It has also been used to guide genotype design of future cultivars (Rötter et al., 2015) and to understand genotype, environment and management interactions (Casadebaig et al., 2016; Hammer et al., 2010; Manschadi et al., 2006; Martre et al., 2015a; Zheng et al., 2015). Researchers have also combined APSIM with various climate projection models to investigate future food security challenges and explore solutions to mitigate environmental impacts on production (Akinseye et al., 2020; Anwar et al., 2020; Asseng et al., 2011, 2004; Liu et al., 2016a; Ludwig and Asseng, 2006). It has been coupled with economic models to develop profit maximisation strategies and to study the effectiveness of crop insurance (Hansen et al., 2009; Van Wijk et al., 2014). As a cropping system tool, the accuracy and uncertainty of APSIM simulations under different environmental and input resources conditions are important to model users, as they need to be aware of the uncertainty in model outputs under the circumstances of their interest.

Globally, wheat is the fourth most-produced crop and provides 20% of the calories consumed by people (FAO, 2020; Shiferaw et al., 2013). APSIM-Wheat yield prediction accuracy has been extensively evaluated for research applications and as a decision support tool for farmers. In addition to evaluations of APSIM-Wheat at field or regional scales with particular management practices or wheat cultivars, several APSIM

developers and researchers have also collected assessment datasets covering a broader spectrum of management practices, environments, and cultivars to analyse model strengths, weaknesses, and identify aspects for further development. An extensive set of the model validation data and descriptions are available on the APSIM website (https://www.apsim.info/). Holzworth et al. (2011) presented part of the wheat final yield validation results from those datasets, reporting a coefficient of determination (R^2) of 0.93 and root mean squared error (*RMSE*) of 0.46 t/ha. Brown et al. (2014) compared the predicted against observed yields for 164 simulations under a wide range of environments and treatments, resulting in an R^2 =0.92. Gaydon et al. (2017) reviewed APSIM performance across various cropping systems in Asia and identified its strengths and weaknesses with 43 experimental datasets from 12 countries. They concluded that the model could be further improved in aspects related to harsh environments, conservation agriculture, and low input systems. Brown et al. (2018) validated the model with experimental datasets from 8 countries covering a broad range of crop treatments. The results demonstrated that the model performed well overall with an $R^2 \geq 0.84$ and Nash-Sutcliffe Efficiency (*NSE*)≥0.81.

While extensive work has been done to evaluate the model yield prediction accuracy, factors that affect the model's yield prediction uncertainty remain to be investigated comprehensively. In general, model prediction uncertainty originates from deficient/inaccurate model structure, input forcing data, parameter specification, and observations used for model calibration/validation (Vrugt et al., 2008). In this paper, we review and quantify APSIM Classic (which hereafter is referred to as "APSIM")-Wheat yield prediction accuracy by compiling existing evaluation datasets from the literature and analysing the contribution of environmental and input resource factors to the model prediction uncertainty. The objective of the study is to review the performance of process-based crop model yield prediction and identify influential factors affecting prediction accuracy, with APSIM-Wheat used as an example. Firstly, an overview of the APSIM-Wheat yield prediction accuracy and uncertainty is provided by collating the model evaluation results from published studies. Next, a meta-analysis based on existing literature is performed to identify the factors influencing uncertain yield prediction, which include model specification and calibration, heat and frost stresses, water, and nitrogen availability. The uncertainties in yield prediction associated with the above-mentioned factors are discussed. Finally, suggestions are provided for improving the

accuracy of crop models such as APSIM-Wheat prediction under circumstances of high prediction uncertainty.

2.3 Methods and materials

2.3.1 Overview of the APSIM Classic and Wheat module

APSIM is an agricultural modelling platform equipped with various biophysical and management modules to simulate cropping systems (Holzworth et al., 2014b; Keating et al., 2003). The model is composed of multiple modules that simulate soil water, nutrients (carbon, nitrogen, and phosphorus), and crop growth processes under different environmental and management conditions. For example, the SoilWat (Jones and Kiniry, 1986; Littleboy et al., 1992) calculates soil water movement using a cascading water balance model, and it is used by most APSIM users (all studies reviewed in this work used SoilWat). Soil Water Infiltration and Movement (SWIM) is another option to simulate the soil-water-solute balance based on Richards' equation and the advection-dispersion equation but is not adopted by most model users. This is likely because SoilWat was developed earlier than SWIM within the APSIM framework. It has been traditionally favoured by the APSIM user community due to its familiarity and the availability of extensive historical data. Its alignment with widely used soil measurement guidelines for APSIM (Dalgliesh et al., 2016) and the APSoil database enhances its compatibility and ease of use. SoilWat's capacity for calibration across a wide range of soil types enables flexible parameterisation, allowing customisation for specific soil and climatic conditions. This adaptability makes SoilWat highly versatile for various agricultural systems and environmental contexts. The SoilN module simulates the transformations of carbon and nitrogen in the soil. SoilWat and SoilN interact with each other and together provide plant available soil water and nitrogen information to the Wheat module (Zheng et al., 2014) for simulating crop growth. The Wheat module simulates phenological development, plant morphology, biomass, and nitrogen concentration of different wheat components, grain number and grain size on a daily basis (Keating et al., 2001). Here we use APSIM-Wheat to collectively represent the wheat growth simulation model which consists of the required APSIM modules including SoilWat, SoilN, and Wheat. A detailed description of the Wheat module is provided by Zheng et al. (2014). We only provide an overview of the stress factors

considered in Wheat since they are used to better understand the factors influencing yield prediction performance.

Water stress: The Wheat module accounts for water stress impacts in simulating photosynthesis and leaf expansion. The water stress factors affecting photosynthesis (f_{W_photo}) and leaf expansion (f_{W_expan}) is calculated as follows:

$$f_{W\_photo} = \frac{W_u}{W_d} \tag{2-1}$$

$$f_{W\_expan} = h_{w\_expan}(\frac{W_u}{W_d}) \tag{2-2}$$

where W_u and W_d are crop water uptake and water demand, respectively. f_{w_photo} is a water stress factor ranging from 0 (complete stress) to 1 (no stress). This factor is then directly multiplied by the daily potential biomass accumulation to determine the actual biomass accumulation. h_{w_expan} is a water stress factor piecewise linearly related to $\frac{W_u}{W_d}$. At $\frac{W_u}{W_d} = 0.1$, the water stress factor f_{W_expan} is 0, indicating complete stress on leaf expansion, the water stress factor increases linearly to 1 (no stress) as $\frac{W_u}{W_d}$ approaches 1. Equations (2-1) and (2-2) indicate that both biomass accumulation and leaf expansion are scaled by the ratio of total daily water uptake to crop water demand, with leaf expansion more sensitive to the water stress.

Nitrogen stress: The Wheat module accounts for nitrogen stress on phenology (not applied), biomass accumulation, leaf appearance and expansion, and grain filling. The stress for these aspects is determined by the difference between organ nitrogen concentration and minimum and critical nitrogen concentration.

Heat stress: The Wheat module takes temperature as a factor affecting the crop into account in many ways (Zheng et al., 2014). The daily maximum temperature is considered as the temperature stress in calculating LAI senescence. The daily mean temperature $(T_{max} + T_{min})/2$ is considered as the stress factor affecting wheat growth in (1) crop phenology via the thermal time; (2) root depth growth; (3) biomass accumulation; (4) biomass demand of grain and the rate of grain filling.

Frost stress: The Wheat module incorporates the leaf area senescence effect using a frost stress function; however, the default parameterisation of the stress factor results in zero impact during the whole simulation, which means it is not in application.

2.3.2 Literature search and selection criteria

We performed a literature search for peer-reviewed journal articles focused on APSIM-Wheat performance evaluation using Scopus, ISI Web of Science, and Google Scholar. The following keywords in English were employed to search the literature: APSIM, wheat, Triticum aestivum, yield prediction, validation, evaluation, verification, and performance. A total of 108 articles published between September 1997 and February 2020 are reviewed. Among these, only the 76 articles that included independent validation datasets (independent growing seasons/fields from calibration) of APSIM-Wheat grain yield prediction using *in situ* yield data at field scale are used for the meta-analysis of APSIM-Wheat yield uncertainty. The APSIM-Wheat validation datasets from these papers are across thirteen countries in four continents, including Australia (41 studies), New Zealand (2 studies), United States of America (1 study), Belgium (1 study), The Netherlands (1 study), Turkey (1 study), China (20 studies), India (3 studies), Pakistan (2 studies), Syria (1 study), Iran (2 studies), Ethiopia (3 studies), Tunisia (1 study) (some papers include locations from several countries, Figure 2-1). It has to be noted that the studies and collated data sets used in our meta-analysis are not representative of the full range of climates and management practices worldwide due to the limited spatial application of the model. Nevertheless, ninety-five percent of these studies cover arid and temperate Köppen-Geiger climate types while the other five percent are located in tropical and cold climates (Peel et al., 2007). The dataset we compiled covers mainly Australia, China, and North Africa, five papers also feature global data collections that include North American and European sites. The number of studies reflects the level of acceptance and popularity of APSIM in the respective countries. Although the wheat regions of Europe and North America are underrepresented in our data, wheat production in Australia and China accounts for a significant proportion (approx. 22% according to FAOSTAT Statistical Database, 2017) of global wheat production. In addition, situations such as extreme temperatures,

different water and nitrogen availability, various soil types, and hydraulic conditions are well covered by our dataset.

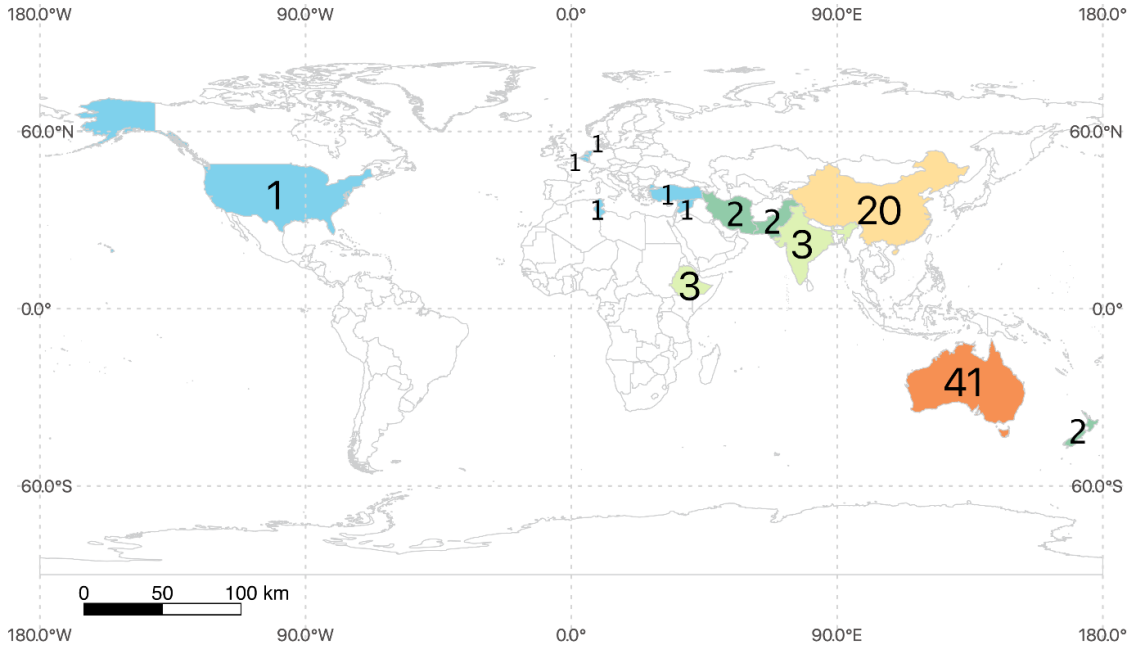

Figure 2-1. Number of articles for each country (the dataset of United States of America is in the conterminous United States)

2.3.3 APSIM-Wheat calibration and evaluation metrics

The model evaluation datasets in reviewed papers contain calibration and validation processes. Here calibration refers to all processes to improve the model fit to data, while validation refers to testing models against independent data not used in calibration to ensure the rigour of the model evaluation. In model calibration, variables that are related to crop growth, such as physiological dates, leaf area index (LAI), biomass, yield, soil water content, and evapotranspiration are typically considered as the benchmarks for calibration and validation. Based on different data sources used, three calibration (or parameter setting) methods were defined in this paper: (1) Manual/automatic tuning of parameters to make the model simulations better fit the observations; (2) Direct specification of parameters using field measurements of these parameters; (3) Parameter specification using available databases (e.g., APSoil) or estimated data such as estimating lower limits from soil texture. The first two methods are collectively referred to as a fully site-specific calibration. If only one of them is adopted, it is partially site-specific calibration. The third method is classified as non-site-specific calibration (Table 2-1).

Table 2-1. Calibration methods defined in this paper

Manual tuning of parameters	Site-specific calibration
Parameter specification using ground observations.	
Parameter specification using APSoil or estimated data.	Non-site-specific calibration

Many researchers specify the specific cultivar used in the simulation or manually adjust genetic parameters, especially those controlling wheat phenology and yield development by trial-and-error to improve the model predictions against field observations. The genetic parameters used to characterise the cultivar and their calibrated value ranges are summarised in Table 2-2. The details of reported calibrated values of these parameters are summarised in Table B. 1. Some coefficients listed in Table B. 1 were derived from results for multiple soil types, sowing dates, sites, and growing seasons, which should help ensure the model robustness.

Table 2-2. Definition of the genetic parameters

Generic parameter name	Unit	Definition	Value range
tt_end_of_juverile	°C	The thermal time from end of juvenile to terminal spikelet stage	590 – 680 (North China Plain, China) 380 (North-eastern Iran)
tt_floral_initiation	°C	The thermal time target for floral initiation	500 (North-eastern Iran)
tt_start_grain_fill	°C	The thermal time target to start grain filling stage	545, 707 (Iran)
tt_startgf_to_mat	°C	The thermal time target from beginning of grain filling to maturity	420 – 650 (North China Plain, China, Iran) 750 (India)
potential_grain_filling_rate	g/(grain °Cd)	Potential grain filling rate	0.002 – 0.003 (North China Plain, China) 0.00129 (Iran)
grain_per_gram_stem	grain	Numbers of grain per gram stem	22 – 33 (North China Plain, China, Iran)
max_grain_size	g	Maximum grain size	0.038 – 0.05 (North China Plain, China)

vern_sens	N/A	Sensitivities to vernalisation	1.0 – 3.1 (North China Plain, China, India, Iran)
photop_sens	N/A	Sensitivities to photoperiod	1.8 – 3.5 (North China Plain, China) 3.8 (India) 3.5, 4.7 (Iran)
phyllochron	°Cd	Phyllochron interval	85 (North China Plain, China) 95 (India, Iran)

Soil parameters such as soil texture, soil hydraulic, and chemical parameters were usually specified in studies using laboratory test data (soil samples were taken from study fields), APSoil soil database (Dalgliesh et al., 2012, 2009), semblable objects or estimated data, such as estimating lower limits from soil texture (Sadras et al., 2003).

Several statistical criteria are commonly selected to evaluate model performance: the coefficient of determination (R^2), root mean square error (*RMSE*, also referred to as root mean square difference, *RMSD*), normalised *RMSE* (*NRMSE*), model efficiency (*EF*), and/or index of agreement (*d*) defined as:

$$RMSE = \sqrt{\frac{1}{N}\sum_{i=1}^{N}(P_i - O_i)^2} \tag{2-3}$$

$$NRMSE = RMSE/\overline{O} \tag{2-4}$$

$$EF = 1 - \frac{\sum_{i=1}^{N}(P_i - O_i)^2}{\sum_{i=1}^{N}\left(O_i - \overline{O}\right)^2} \tag{2-5}$$

$$d = 1 - \frac{\sum_{i=1}^{N}(P_i - O_i)^2}{\sum_{i=1}^{N}\left(\left|P_i - \overline{O}\right| + \left|O_i - \overline{O}\right|\right)^2} \tag{2-6}$$

where P_i and O_i represent *i*th predicted and observed values, respectively, $\overline{O}$ the mean observed values, and N the sample size. R^2 measures the goodness-of-fit of a linear relationship between simulated and observed values, and hence ignores model bias. R^2 is also sensitive to the variance of the samples. *RMSE* and *NRMSE* represent the mean difference of predictions and observations, and they include measures of both bias and

random errors. *EF* and *d* assess the degree of model prediction and are similar to R^2, except they are influenced by both bias and random errors. The index of agreement *d* is normalised by a measure of combined spread in observations and predictions, while *EF* (and R^2) are normalised by the spread in observations. The model reproduces experimental data perfectly when R^2=1, *RMSE*=0, *NRMSE*=0, *EF*=1 and *d*=1.

2.3.4 Description of reviewed datasets

Table 2-3 presents basic information on each paper validation datasets – location, reference, APSIM version, APSIM performance, and influential factors affecting the model performance. All reviewed works used APSIM Classic (version 1.X – version 7.9). The model has been applied mostly at plot or paddock, and sometimes regional, scales as a cropping system tool solely to assess the environmental impacts on food production, or combined with other models (e.g., climate projection models, economic models) to investigate future food security challenges and explore solutions or to develop profit maximisation strategies and study the effectiveness of crop insurance. A full version of Table 2-3 with detailed information is shown in Table B. 2.

Table 2-3. List of validation datasets from the literature used in this study (* Data were used to compose the meta-database for further analysis in Chapter 2.4)

Country	Region	Reference	APSIM version	APSIM performance	Influential factor
Australia	Western Australia	(Asseng et al., 2004, 2002, 2001, 1998b, 1998a; Bell et al., 2009*; Bryan et al., 2014*; Fisher et al., 2001; Fletcher et al., 2020*; Lawes et al., 2009; Oliver et al., 2006*, 2009; Oliver and Robertson, 2009; Wang et al., 2003*; Wong and Asseng, 2006)	NWheat, 5.2, 5.4, 7.3, 7.8, N/A	Yield-RMSE=0.31 to 1.2 t/ha Yield-R^2=0.69 to 0.86 Biomass-RMSE=0.8 to 2.8 t/ha Biomass-R^2=0.80 to 0.94 LAI-RMSE=0.6 to 1.3 LAI-R^2=0.53 to 0.73	Model calibration (Hunt et al., 2006; Lilley et al., 2003; Sadras et al., 2003) Soil cracking (Paydar et al., 2005) Water stress (Fletcher et al., 2020; Peake et al., 2014; Zeleke and Nendel, 2016) Nitrogen stress (Peake et al., 2014) Heat stress (Hochman et al., 2009a; Peake et al., 2014) Lodging (Peake et al., 2014) Root-lesion nematode (O'Leary et al., 2016; Probert et al., 1995) Subsoil constraints (Hochman et al., 2007)
	Queensland	(Bell et al., 2009*; Hochman et al., 2007; Mielenz et al., 2016*; O'Leary et al., 2016*; Peake et al., 2014*; Probert et al., 1998, 1995; Wang et al., 2003*)	1.X, 5.0, 5.4, 7.4, 7.5, 7.6, N/A	Yield-RMSE=0.50 to 1.62 t/ha Yield-R^2=0.30 to 0.92	
	New South Wales	(Bryan et al., 2014*; Hochman et al., 2007; Innes et al., 2015; Lilley et al., 2003; Lilley and Kirkegaard, 2008*; O'Leary et al., 2016*; Paydar et al., 2005*; Zeleke and Nendel, 2016*)	2.1, 5.0, 7.3, 7.5, 7.6, N/A	Yield-RMSE=0.40 to 1.39 t/ha Yield-NRMSE=18.9% (Innes et al., 2015) Yield-R^2=0.69 to 0.92	
	Victoria	(Anwar et al., 2009; Bryan et al., 2014*; Hochman et al., 2013; O'Leary et al., 2015; Sadras et al., 2003*)	5.3, 7.3, 7.4, N/A	Yield-RMSE=0.19 to 1.29 t/ha Yyield-R^2=0.6 to 0.96	
	South Australia	(Bryan et al., 2014*; Luo et al., 2005; Yunusa et al., 2004)	1.4 Patch 2, 2.0, 7.3	Yield-RMSE=0.45 t/ha Yield-R^2=0.69 Yield-residuals=~0.4 t/ha	
	Tasmania	(Acuña et al., 2015; Phelan et al., 2018*)	7.1, 7.8	Yield-RMSE=1 t/ha Yield-R^2=0.83 to 0.84 Yield-EF=0.82	
Australia assembled data		(Carberry et al., 2013, 2009; Hochman et al., 2009a; Hunt et al., 2006*)	Yield Prophet	Yield-RMSE=0.19 to 0.80 t/ha Yield-R^2=0.52 to 0.89	
New Zealand	Lincoln	(Asseng et al., 2004; Bell et al., 2009*)	NWheat, 5.4	Yield-RMSE=0.5 to 1.2 t/ha Yield-NRMSE=~18% Yield-R^2=0.72 to 0.77 Biomass-RMSE=1.1 to 2.8 t/ha Biomass-NRMSE=~17%	

				Biomass-R^2=0.86 to 0.94 LAI-RMSE=0.9 to 1.3 LAI-R^2=0.53 to 0.73	
China	North China Plain, Loess Plateau, Gongzhuling, Ürümqi, Zhengzhou, Xuzhou, Inner Mongolia	(Bai et al., 2020; Chen et al., 2010c*, 2010b*, 2010a*; He et al., 2014; Li et al., 2016, 2014; Liu et al., 2016a*; Sun et al., 2015; Van Oort et al., 2016; Wang et al., 2009*, 2014*, 2013*; Xiao and Tao, 2014*; Yan et al., 2020*; Zhang et al., 2013*, 2012*; Zhao et al., 2017*, 2015*, 2014a, 2014b*)	5.1, 5.3, 6.1, 7.0, 7.4, 7.5, N/A	Yield-RMSE=0.29 to 1.26 t/ha Yield-NRMSE=7% to 22% Yield-R^2=0.46 to 0.97 Yield-d=0.85 to 0.97 Biomass-RMSE=0.88 to 1.4 t/ha Biomass-R^2=0.62 to 0.91	Model calibration (Zhao et al., 2014b) Water stress (Balwinder-Singh et al., 2011; Deihimfard et al., 2015) Nitrogen stress (Zhao et al., 2014a) Heat stress (Hussain et al., 2018; Liu et al., 2016a; Lobell et al., 2012; Zhang et al., 2012) Frost stress (Chen et al., 2010a, 2010c; Wang et al., 2009; Zhang et al., 2013, 2012) Soil cracking (Moeller et al., 2007; Mohanty et al., 2012)
India	Punjab, Indo-Gangetic Plains, Bhopal	(Balwinder-Singh et al., 2011*; Lobell et al., 2012; Mohanty et al., 2012)	5.1, 6.0, N/A	Yield-RMSE=0.44 to 0.55 t/ha Yield-NRMSE=12.4% to 16.5% Yield-R^2=0.86 to 0.91 Biomass-RMSE=0.3 to 0.8 t/ha Biomass-NRMSE=3.6% to 10.8% Biomass-R^2=0.92 to 0.99 (Balwinder-Singh et al., 2011)	
Iran	Grogan region and Khorasan province	(Deihimfard et al., 2015*; Soltani and Sinclair, 2015)	7.X, 7.2	Yield-RMSE=0.62 to 0.71 t/ha Yield-R^2=0.81 to 0.83	
Syria	Dry areas at Tel Hadya, north-western Syria	(Moeller et al., 2007)	4.2	At pre-anthesis stage, the model overestimated leaf-area, nitrogen uptake and biomass accumulation (Moeller et al., 2007).	
Pakistan	Islamabad; Faisalabad and Layyah in Punjab-Pakistan	(Ahmed et al., 2016; Hussain et al., 2018)	7.8, N/A	Phenology-RMSE=2.0 to 5.1 days Phenology-R^2=0.8 LAI-RMSE=0.14 to 0.32 LAI-R^2=0.83 Biomass-RMSE=0.15 to 0.40 t/ha Biomass-R^2=0.92 Yield-RMSE=0.12 to 0.31 t/ha	

				Yield- R^2=0.82 (Ahmed et al., 2016) The model overestimated yield with late planting dates (Hussain et al., 2018).	
Asia assembled data (Twelve Asian countries, total of 43 experimental datasets, 966 crops, 326 of them were wheat)		(Gaydon et al., 2017)*	Multiple versions	Yield-RMSE=0.845 t/ha Yield-R^2=0.79 Yield-standard deviation=1.794 t/ha APSIM underestimated LAI, biomass, and yield in NCP, China due to incorrect temperature response of physiological processes.	
Ethiopia	Northern Ethiopia	(Araya et al., 2020*, 2017)	7.4, 7.7	Yield-NRMSE=7.7% to 22.8% Yield-R^2=0.63 Days of flowering-NRMSE=3.1% to 4.3% Days of flowering-R^2=0.91 Days of maturity-NRMSE=7.5% to 8.3% Days of maturity-R^2=0.81	
Tunisia	semiarid (Kef) and sub-humid (Bizerte)	(Bahri et al., 2019)	N/A	Yield-RMSE=1.647 t/ha Yield-d=0.83 (Bahri et al., 2019)	
The Netherlands, Australia, Belgium, China, Ethiopia, Iran, New Zealand, Turkey, United States of America		(Asseng et al., 2000; Brown et al., 2018, 2014; Holzworth et al., 2018, 2014b)	Multiple versions	Yield-RMSE=0.46 to 1 t/ha Yield-R^2=0.84 to 0.93 More validation results can be found in the model fields.	

Overall, researchers report that site-specifically calibrated APSIM-Wheat provides a useful yield prediction tool for a wide range of environments. Nevertheless, while the model incorporates stress functions to account for limitations of water, nitrogen, heat, and frost (Zheng et al., 2014), it sometimes fails to capture these stress effects sufficiently (Barlow et al., 2015). Each of the stress effects will be discussed in more detail in Chapter 2.4.

2.3.5 Building database for meta-analysis and performance metrics

All papers listed in Chapter 2.3.4 that had data that were extractable from tables, figures, text, or provided by the authors were included in the meta-database. In total, data from 30 studies were used to compose the meta-database for further analysis. These 30 studies are marked with asterisks in Table 2-3. Digitising the data from published scatter plots in the literature was performed with the WebPlotDigitizer tool (https://automeris.io/WebPlotDigitizer/). The database includes 1895 pairs of observed and simulated grain yields expressed in tons per ha. All these points were for validation simulations. The data originated from seven countries and included 51 wheat cultivars (see Table 2-3). These data were assembled and categorised according to different crop stresses and model initialisations. The conditions captured were:

- Crop stresses: water availability, nitrogen availability, heat stress, lodging, disease.
- Model initialisations: fully site-specific calibration, partially site-specific calibration, non-site-specific calibration.

APSIM Classic (model version please refer to Table 2-3) performance was evaluated for the whole dataset and subsets corresponding to various conditions using the performance metrics in Chapter 2.3.3. To obtain R^2, a linear regression was fitted to the observed and simulated grain yield pairs. Residuals (simulated – observed yield) were also calculated and box plots drawn for different conditions. Comparisons between predicted yield residuals and observed yields were also plotted to visually investigate model capability and limitations. Statistics of coefficient of determination (R^2), *RMSE* (equation (2-3)), *NRMSE* (equation (2-4)), and *EF* (equation (2-5)) were utilised to quantify the model performance.

2.4 Factors affecting APSIM yield prediction

Several factors affecting APSIM-Wheat yield prediction were distilled and presented in the following chapter after all papers in Table 2-3 were reviewed and the meta-database composed with 30 papers was analysed (Chapter 2.3.5). Identified influencing factors include model calibration, crop resources (water, nitrogen), temperature, and other biotic or abiotic stresses.

Overall, the model performed well. Figure 2-2 compares the predicted yield with the observed yield from the meta-database. APSIM-Wheat predicted grain yield with R^2=0.68, *RMSE*=1.06 t/ha, *NRMSE*=28.89%, *EF*=0.63. This result is consistent with the findings from most papers reviewed in Chapter 2.3. To put these results in context of practical cropping decisions, Yield Prophet® users reported that discrepancies between the predicted and observed yields exceeding 0.5 t/ha reduced their confidence in using the model for decision support (Hochman et al., 2009a), indicating that factors contributing to the uncertainty and potential solutions should be explored. The deviation of observed vs. simulated yields scatters from the 1:1 line in Figure 2-2 (black dashed line) denotes model simulation deficiencies. The discrepancy between the regression line (grey dashed line) and the 1:1 line indicates existence of bias that varies from positive to negative values with yield. Potential causes of this bias include not fully site-specific calibration, water stress, nitrogen stress, heat stress, lodging, root-lesion nematode. The variation of yield prediction error and uncertainty under different environments, treatments, and model initialisations will be analysed in the following chapters separately.

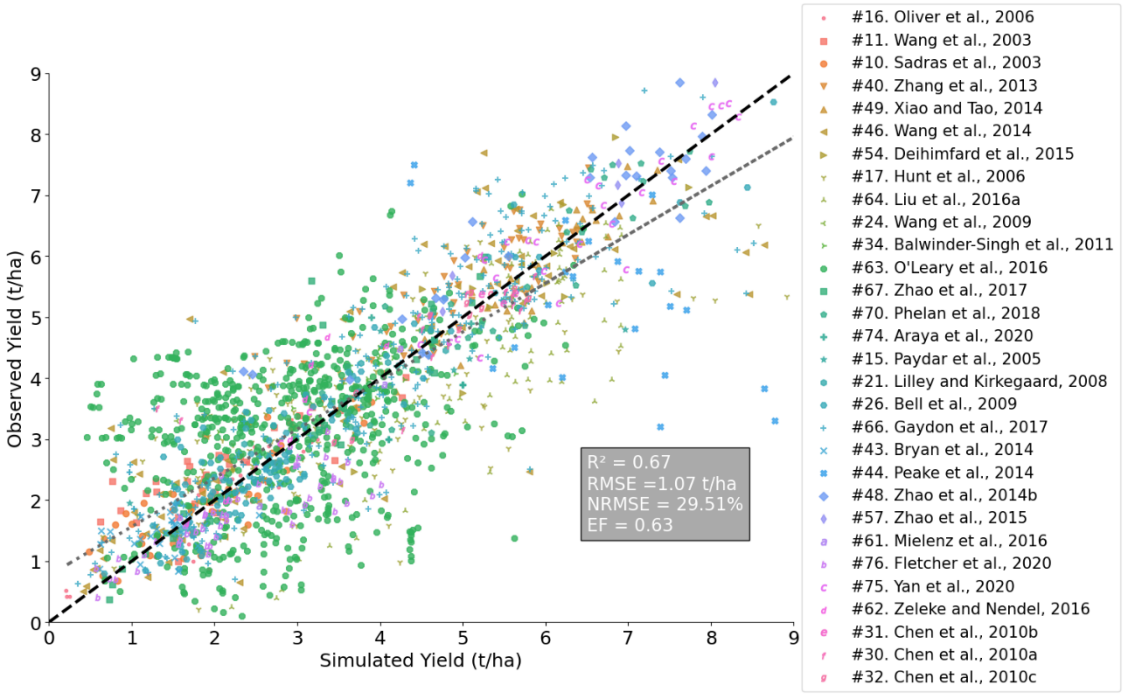

Figure 2-2. Comparison between observed and APSIM-Wheat simulated grain yields (black dashed line: 1:1 line; grey dashed line: regression line)

2.4.1 Model calibration

APSIM-Wheat performs optimally when reliable and accurate soil information is available and biotic/abiotic stresses are absent (Dalgliesh et al., 2012). Accurate specification of soil water holding characteristics affects APSIM-Wheat prediction performance (Lilley et al., 2003; Sadras et al., 2003). Specifying lower limits of plant available water with field measurements rather than using estimations from soil texture can improve simulation accuracy. In one study, the R^2 of the relationship between simulated and observed yields increased from 0.60 to 0.74, and the *RMSE* decreased from 0.31 t/ha to 0.19 t/ha when using lower limits of extractable water derived from field gravimetric soil water measurements , compared with texture based estimates (Sadras et al., 2003). Hunt et al. (2006) indicated that when the model was initialised with appropriate soil water holding characteristics and input data, 68% of the yield predictions were within ±0.5 t/ha of the observed yields.

Figure 2-3 shows APSIM-Wheat validation results of the studies that used site-specific calibration. As described in Chapter 2.3.3, site-specific calibration is done by (1) manually tuning parameters to make the simulations correspond well with the observations or (2) specifying parameters with field measurements (usually soil texture,

soil hydraulic, and/or chemical parameters. The results indicated that the model, once site-specifically calibrated ((1), (2) individually or simultaneously), was able to estimate the harvest yield with an R^2 of 0.90, *RMSE*=0.64 t/ha, and a *NRMSE* of 14.08%. The model performance improved when model cultivar parameters were manually tuned and soil parameters were initialised with ground observations simultaneously (fully site-specific calibration), resulting in *RMSE* smaller than 0.5 t/ha, *NRMSE* of 10.15%, and an *EF* of 0.85, indicating that the model is performing well. When only the cultivar parameters were calibrated, the model maintained the *EF* of 0.8, with *RMSE* and *NRMSE* slightly increased to 0.7 t/ha and 12.93%, and an R^2 of 0.82. The yield prediction performance began to decline when only the soil parameters were specified with field measurements without adjusting other model parameters, both R^2 and *EF* decreased to 0.77, with an *NRMSE*=20.82%. The *RMSE* was only 0.51 t/ha since the yield range in this case were lower than in other cases.

Across the Australian dryland cropping area, the crucial challenge for predicting commercial wheat yield is to accurately describe the soil characteristics, soil water, and nitrogen sources (Carberry et al., 2009). This requirement motivated the development of the APSoil soil database (Dalgliesh et al., 2012, 2009), which provides representative soil parameters for major Australian soils. For Australian paddocks, if field measured soil parameters are not available, APSoil can provide soil information such as the Plant Available Water Capacity (PAWC) based on approximate soil type information (Innes et al., 2015; Phelan et al., 2018).

Figure 2-4 shows results when soil parameters were specified using a soil database – APSoil or estimated soil hydraulic characteristics. Model default genotype parameters were utilised for specific cultivars. Compared to cases in Figure 2-3, these initialisation methods led to decrease the model accuracy and uncertainty, resulting in *RMSE* increasing from 0.64 to 1.25 t/ha and *NRMSE* increasing from 14.0% to 32.46%. When estimated soil hydraulic parameters were used, the *RMSE* of yield prediction was 1.37 t/ha and the *NRMSE* was 40.45%. Performance improved using the APSoil database to specify soil parameters resulting in model predictions with lower *RMSE* and *NRMSE* of 0.7 t/ha and 13.0%, compared with the model performance when using soil texture-derived soil parameters.

Results in Figure 2-3 and Figure 2-4 indicate that manually tuning cultivar parameters, and/or specifying the soil characteristics with ground observations can substantially improve the model performance. Convincing evidence is presented to demonstrate that APSIM-Wheat is able to simulate wheat grain yield within 0.5 t/ha when fully site-specific calibration implemented. When field measured data is not available, using a look-up-table approach that uses APSoil to specify the soil hydraulic properties can achieve yield prediction accuracy of *RMSE*=0.7 t/ha. Setting soil parameters with estimated data is still acceptable, but not ideal. The estimated soil parameters largely affect the yield prediction accuracy and uncertainty since they cannot appropriately describe the soil properties.

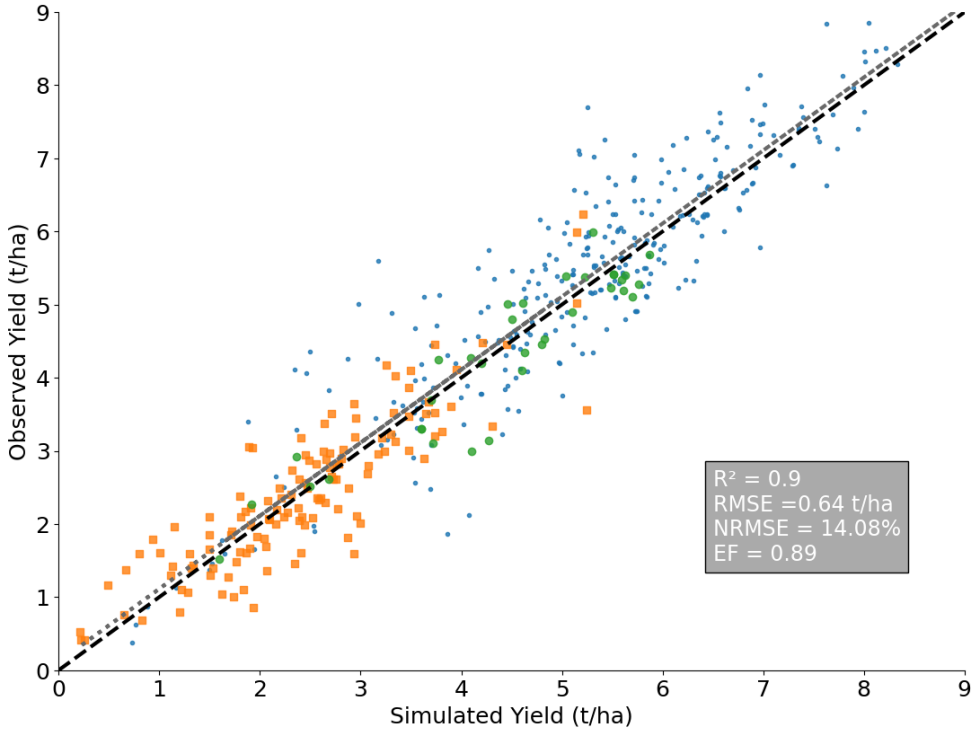

Figure 2-3. Comparison between observed and APSIM-Wheat simulated grain yields when cultivar parameters were manually tuned, and/or soil parameters were specified with ground observations (green circle: both cultivar and soil parameters were calibrated, R^2=0.87, RMSE=0.44 t/ha, NRMSE=10.15%, EF=0.85; blue dot: only cultivar parameters were tuned, R^2=0.82, RMSE=0.7 t/ha, NRMSE=12.93%, EF=0.8; orange square: only soil parameters were specified using field measurements, R^2=0.77, RMSE=0.51 t/ha, NRMSE=20.82%, EF=0.77)

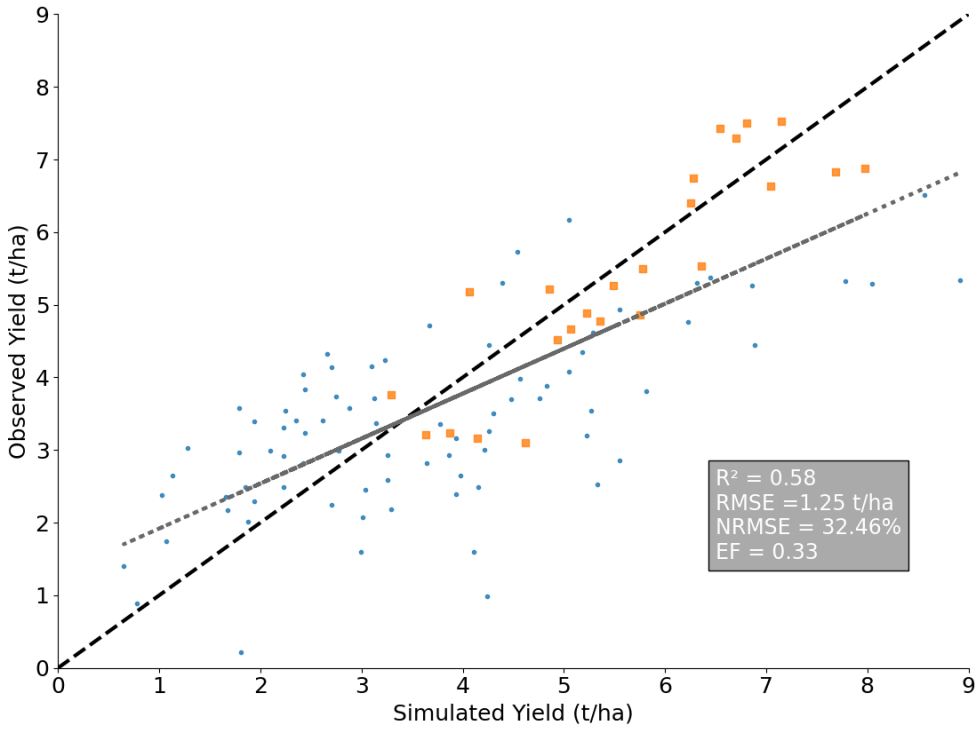

Figure 2-4. Comparison between observed and APSIM-Wheat simulated grain yields when soil parameters specified using APSoil or estimated data (blue dot: estimated soil characteristics, R^2=0.45, RMSE=1.37 t/ha, NRMSE=40.45%, EF=-0.27; orange square: soil parameters were specified using APSoil, R^2=0.78, RMSE=0.7 t/ha, NRMSE=13.0%, EF=0.76)

Some other parameters and functions in APSIM have been modified by authors to achieve better performance. The maximum and critical nitrogen concentration in leaves used in the APSIM-Wheat model was too low when compared to the observed data collected from North China Plain (NCP) fields. Adjustment of these two parameters can improve the model simulation, especially under low nitrogen input (Zhao et al., 2014a). Root growth parameters were modified to better simulate the root biomass and its distribution (Zhao et al., 2015, 2014b). The soil moisture factor used for the denitrification rate calculation was modified by Mielenz et al. (2016), instead of using drained upper limit (DUL) as the threshold, the authors modified it to be decided by the water-filled pore space and saturation (SAT). Brown et al. (2018) pointed out that the phenology model needs careful parametrisation for different cultivars.

2.4.2 Water availability

To assess the impacts of water availability on APSIM yield prediction, only site-specifically calibrated datasets from irrigated or water limited fields have been selected. Figure 2-5 shows box plots of prediction residuals. The cases are presented in the order

of water stress, from highest (1) to lowest (3). Case 1 shows datasets for crops under water limited conditions. Datasets from two papers were included (Fletcher et al., 2020; Peake et al., 2014). Wheat from Case 2 was irrigated at critical growth stages with different amounts of water (Balwinder-Singh et al., 2011; Chen et al., 2010a; Deihimfard et al., 2015; Wang et al., 2013c; Xiao and Tao, 2014; Yan et al., 2020; Zhang et al., 2013; Zhao et al., 2014b). Wheat from Case 3 was also irrigated, but not at specific growth stages. The irrigation amount and scheduling were adapted to the actual water demand (Gaydon et al., 2017; Mielenz et al., 2016; Yan et al., 2020).

Wheat in Case 1 suffered from water stress. Peake et al. (2014) observed mild water stress during the pre- and post-anthesis, while the model was also used to predict water-limited yield (Fletcher et al., 2020). 50% of the predicted yield residuals were within the range of 0.2–1 t/ha, 99.3% of them were within the range -0.4–2.4 t/ha, while the median was approximately 0.33 t/ha. From the datasets we analysed, yield overestimation was more obvious than underestimation under water stressed conditions. In Case 2, the fields were mainly from Punjab, India, NCP, China, and North-eastern Iran. They were irrigated at critical growth stages, e.g., sowing, jointing, flowering, and grain filling, with total irrigation amounts between 75 and 450 mm. The accuracy of modelled yields was acceptable with *RMSE* around 0.65 t/ha. The median of residuals of modelled yields did not exceed -0.5 t/ha. Approximately 50% of the predicted yield residuals were within the range of -0.65–0.15 t/ha, and 99.3% of them were within the range of -1.7–1.25 t/ha. Underestimation was more obvious than overestimation. The model was examined by Balwinder-Singh et al. (2011) in India for six irrigation scheduling treatments. The results indicated that it underpredicted grain yield by 0.6–1 t/ha when crops were subject to water deficit. Case 3 shows crops irrigated according to their water demand. Irrigation scheduling and amount were adjusted according to rainfall amount, soil water content, and crop requirement. Crops in this case barely experienced water limitation and the model performance was more accurate and stable. The residual medians were less than 0.2 t/ha, and 99.3% of the residuals were within ±0.7 t/ha.

Case 1 demonstrated that APSIM-Wheat tend to overestimate yield with more significant uncertainty under water-limited conditions. It seems that the constraint on wheat growth by limited water is not well accounted for by APSIM-Wheat, leading to overly optimistic grain yield prediction. The mechanism that APSIM-Wheat uses to handle water stress

was described in Chapter 2.3.1. The model only accounts for water deficit impacts on biomass production and leaf expansion. It does include a function intended to account for water stress on phenology, but the default parameterisation results in no effect on phenology. Consequently, proper parametrisation to correctly estimate drought impact on phenology under water-limited condition is needed. For example, Chauchan et al. (2019) accounted for soil water effect to modulate APSIM Classic (version 7.10) predicted flowering time. But the proposed method can only reduce the daily thermal time and delay the flowering time when the soil water is sufficient (fractional available soil water>0.65). A proper scheme to directly simulate the impact of soil water stress on flowering time is yet to be developed. Greater water limitations result in higher canopy temperatures, which reduce the duration of biomass accumulation. The increased canopy temperatures under water deficit conditions should be considered to improve the performance of yield prediction (Asseng et al., 2004). Asseng et al. (1998b) also attributed the underpredicted yield to insufficient re-translocation of stored pre-anthesis carbohydrates to the grain by APSIM. They suggested the model can be improved by including functions to remobilise additional carbohydrates of stem into the grain when crops experience severe drought conditions. Case 2 showed that with critical-stage irrigation the model can predict yield with acceptable accuracy (*RMSE*=0.65 t/ha), while the uncertainty is still obvious. These datasets demonstrated that once extra water was supplied (in addition to rainfall), APSIM-Wheat could capture the additional water resource. Case 3 showed that supplying irrigation water according to crop demand to avoid water limitation was associated with better modelling performance.

Users operating APSIM in a water-limited situation should be aware of uncertainty and possible yield overestimation. Most researchers validate the model using real-world datasets to create confidence in its performance before using it in combination with climate projections for predicting food production under climate change scenarios. The frequency and intensity of droughts are projected to increase (Zhou et al., 2019) and the water availability for rain-fed agriculture is decreasing, and the crop model will probably underestimate yields under those conditions. Larger prediction uncertainty should be considered when utilising cropping system as a tool to assess future food production and security.

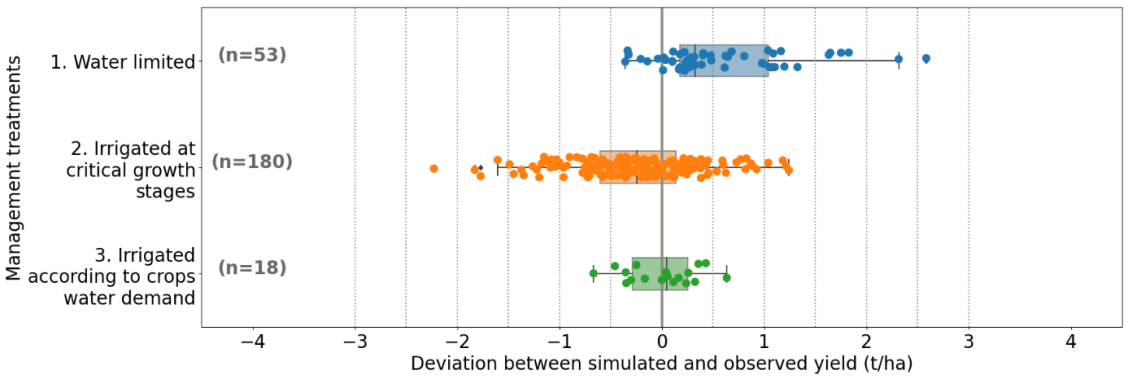

Figure 2-5. Boxplot of APSIM predicted yield residuals under different irrigation practices

2.4.3 Nitrogen availability

We selected site-specific calibrated datasets to assess the impacts of nitrogen availability on APSIM yield prediction, in the absence of other stresses. Figure 2-6 shows box plots of prediction residuals of six cases, which were ordered from the largest to the smallest nitrogen stress. Case 1 shows datasets when crops experience nitrogen limitation. Datasets from two papers were included (Peake et al., 2014; Wang et al., 2014). Case 2 was also composed of datasets from two papers (Sadras et al., 2003; Zhao et al., 2014b). The authors did not specify the nitrogen rate in these datasets but declared no nitrogen stress was observed. Wheat from Cases 3–6 was fertilised with different rates of nitrogen. The application amount increased from 64 kg N/ha to 195 kg N/ha. Data for Case 3 were collected from three papers (Araya et al., 2020; Paydar et al., 2005; Phelan et al., 2018), while Cases 4–6 used datasets from Xiao and Tao (2014) and Yan et al. (2020).

Case 1 reported nitrogen stress symptoms (leaf yellowing) at DC31 (early stem elongation) (Peake et al., 2014), while the model was also used to predict yield when no fertiliser was applied in fields (Wang et al., 2014). Both overestimation and underestimation were observed with the median of residuals approximately -0.3 t/ha. In some cases, the underestimation was even more than 3 t/ha. Case 2 collected datasets with not specified fertilisation amounts, but no nitrogen stress was observed in the fields. The model predicted yield with acceptable accuracy and uncertainty. The median of residuals was close to zero. 50% of the predicted yield residuals were within the range of -0.5–0.2 t/ha, and 99.3% of them were within the range of -1.25–1 t/ha. Case 3 contained datasets with nitrogen rates of 64, 75, 100, and 128 kg N/ha. The distribution of the prediction residuals was similar to those in Case 2. With the increasing nitrogen application rate, the predicted yield residuals were less scattered, ranging within ±1.0

t/ha to ±0.5 t/ha while the medians tended towards 0 t/ha. The model was well-performed to catch the fertilisation differences.

Under nitrogen limited conditions (Case 1), APSIM-Wheat showed the largest uncertainties and more severe yield underestimation and the model tended to underestimate yield when crops suffered from nitrogen limitation. The reason as indicated by Peake et al. (2014) is that APSIM-Wheat overrated the nitrogen stress duration by two weeks longer compared to observed nitrogen stress in the paddocks. Cases 2–6 showed that once extra nitrogen was supplied, the model captured the increasing trend and tended to predict yield with better accuracy and lower uncertainty. The residuals were contained within ±1.0 t/ha when sufficient nitrogen was applied.

An additional parametrisation of the nitrogen impacts on phenology would be able to better address potential simulation problems. Zhao et al. (2014a) assessed the nitrogen concentration parameters used in the model, the results indicated that the higher leaf maximum and critical nitrogen concentrations led the model to overrate the nitrogen stress impacts on biomass accumulation and underrate the impacts on leaf expansion. They suggested to adjust and verify these parameters to increase the prediction accuracy of the model for grain yield.

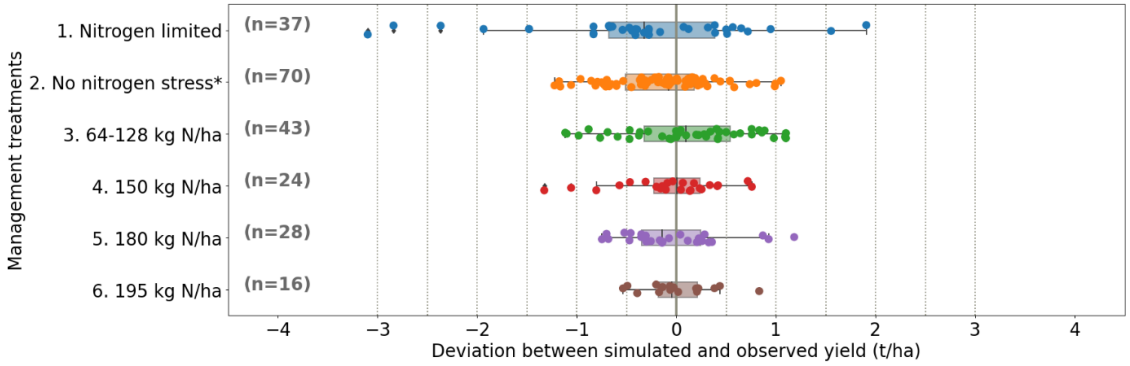

Figure 2-6. Boxplot of APSIM predicted yield residuals under different nitrogen application rates (* fertiliser amount was not specified)

2.4.4 Other stresses

Figure 2-7 illustrates the model predicted yield residuals against the observed yield for datasets under irrigated and fertilised conditions. We intentionally included datasets for wheat without stress and under some abiotic stresses such as heat and lodging, to compare the model performance under stressed and stress-free situations (Deihimfard et al., 2015;

Liu et al., 2016b; Mielenz et al., 2016; Peake et al., 2014; Xiao and Tao, 2014; Yan et al., 2020; Zeleke and Nendel, 2016; Zhao et al., 2015, 2014b). The model showed a good performance for all stress-free cases, with *RMSE*=0.66 t/ha and *NRMSE*=12.49%. However, when the stressed cases are included, *RMSE* increased to around 1.03 t/ha and *NRMSE* to 20.26%, respectively. The mean residual is 0.3 t/ha and standard deviation is 0.99 t/ha. Most of the residuals are between the range of $\pm$ 1.96 times of the standard deviation around the mean. The outliers are from the cases where the crops were under heat stress and impacted by lodging.

Heat stress. Heat stress during wheat growth, especially at anthesis and grain filling stages, affects APSIM yield prediction significantly (Liu et al., 2016a). Hochman et al. (2009) reported that a widespread unseasonal heatwave, followed by a frost in the Wimmera and Mallee regions of Victoria, Australia in 2004 caused the model to overestimate yields by 0.9 t/ha with a mean simulated yield of 1.8 t/ha. Lobell et al. (2012) found that the shortening of the green season (by +2°C warming) was underrated by APSIM by up to eight days, and yield losses were underestimated by up to 50% after comparing the model simulation with a regression model based on nine years of wheat phenology (from satellite observations) and daily temperature data. Liu et al. (2016a) conducted environment-controlled chamber experiments to test the model response when heat stress happened at anthesis and grain filling stages. Wheat is more sensitive to heat at anthesis (orange squares in Figure 2-7) with *RMSE*=1.5 t/ha and *NRMSE*=35.47% since both grain number and size are affected, while heat during grain filling (green circles in Figure 2-7) only decreased the grain size, due to a shorter grain filling duration, resulting in *RMSE*=1.14 t/ha and *NRMSE*=22.75%. Barlow et al. (2015) also emphasised the need to define response functions for calculating extreme temperatures impacts, with a priority on the response during anthesis and grain filling stages. Hussain et al. (2018) evaluated performance of APSIM simulations of winter wheat sown at different times, from early to extremely late. The model poorly predicted yield for late planting dates due to high temperature during grain filling. Even a short-term exposure of wheat to extreme high temperatures at early grain filling can reduce the duration of grain filling and hence the cumulative degree days and resulting in smaller harvest yield (Stone and Nicolas, 1995). Lobell et al. (2012) also detected greater senescence from extreme heat, beyond the impacts of increased average temperatures.

In summary, the quality of grain number and size simulation exerts a critical influence on the accuracy of yield prediction. Only using the daily mean temperature to apply heat stress is not effective in accounting for heat wave impacts. In addition, short periods (1–3 days) of extremely high temperatures (> 33˚C) can also affect the crop growth and ultimately result in a significant reduction in grain yield (Barlow et al., 2015). Accounting for high daily maximum temperatures as another variable to determine the heat stress impact would help the model better respond to heat waves.

Frost damage. Barlow et al. (2015) summarised three crucial physiological damages that have impacts on yield production in response to a frost event: seedling death during the vegetative stage, sterility at anthesis and death of formed grains during grain filling. Frost during the vegetative stage has smaller impact on harvest yield than during later stages as it mainly affects seedling survival (Fuller et al., 2007) and causes leaf senescence (Shroyer et al., 1995). The greatest yield production impacts resulting from frost are at the reproductive stage, and this frost sensitivity increases from heading to the end of anthesis (Frederiks et al., 2012).

Hochman et al. (2013) found that the APSIM-Wheat (with the model default frost parameters) could not account for extreme events such as severe frosts and might overestimate harvest yields under those conditions, based on an assessment of the model with data collected from the Wimmera region of Victoria, Australia. In 1998 the crops on one farm of this region were severely damaged by stem frost and the model overestimated the harvest yield by more than 5 t/ha. Hochman et al. (2009) also reported an occurrence of both frost and heat damages in October 2004, late anthesis or early grain filling stages (the period when the crops are sensitive to extreme temperatures) in the Wimmera and Mallee regions of Victoria that caused the model to over-predict yield. For varieties with strong cold tolerance in the North China Plain, the minimum temperature threshold to cause leaf senescence was changed from -15°C to -20°C to eliminate the underestimation of LAI, biomass, and yield (Chen et al., 2010a; Wang et al., 2009; Zhang et al., 2013, 2012). The modified temperature response of thermal time calculation and the temperature response of radiation use efficiency (RUE) led to further improve model simulations (Chen et al., 2010a, 2010c).

Lodging. The brown triangular points from Figure 2-7 represent the model predicted residuals against the observed yield when crops were impacted by lodging (the data is

from Peake et al. (2014)). Yield is severely over-estimated with *RMSE*=3.26 t/ha, *NRMSE*=76.77%. The reviewed APSIM-Wheat version does not consider effects of crop lodging, while lodging can be caused by many factors, e.g., excessive nitrogen fertilisation and irrigation, heavy rain, wind, or hailstorm. The development of functions in APSIM-Wheat that accounts for the effects of lodging would be desirable although it would require collection of extensive databases of crops affected by lodging.

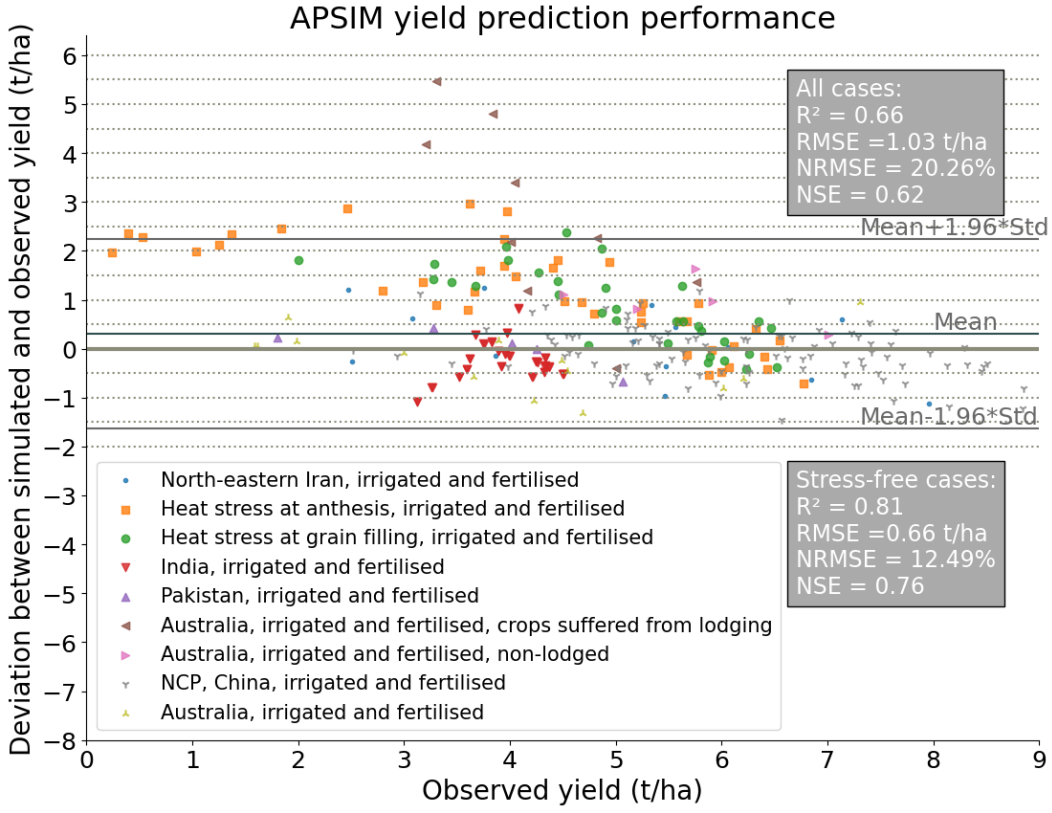

Figure 2-7. Comparison between predicted yield residuals and observed yield under irrigated and fertilised condition

Other abiotic stresses. Some other factors APSIM-Wheat fails to simulate have been identified in model validation. The effect of soil cracking on soil evaporation is not taken into account in the reviewed model version, which leads the model to incorrectly simulate the water movement and further decreases yield prediction accuracy (Moeller et al., 2007; Mohanty et al., 2012; Paydar et al., 2005). Hochman et al. (2007) mentioned there was potential to improve yield prediction if a suitable function could be developed to describe the effects of subsoil constraints. When crops suffered hail damage in 1997 on one farm in the Wimmera region of Victoria, Australia, the model totally missed the hail storm damage and still predicted grain yield over 7 t/ha (Hochman et al., 2013). O'Leary et al.

(2015) tested the APSIM-Wheat under two water regimes (irrigation and rain-fed), two nitrogen fertilisation regimes (0 and 53 – 138 kg N/ha), and two sowing dates for daytime ambient (365 μmol/mol) and elevated (550 μmol/mol) CO_2 environments at Horsham, Australia. The results indicated that the model showed a tendency to overestimate early biomass (DC31, stem elongation) (Zadoks et al., 1974), biomass at DC65 (anthesis), LAI at DC65, and grain yield under the normal CO_2 conditions; the resulting *RMSE* values were 1.592 t/ha, 1.542 t/ha, 0.70 m^2/m^2, and 1.294 t/ha, respectively. Under the elevated CO_2 condition, the model overcompensated the CO_2 effect and over predicted early biomass and harvest yields.

Biotic Stress. Crops in most of the reviewed papers were well managed, with no significant insects, weeds, pests, or plant diseases observed. O'Leary et al. (2016) examined the performance of the APSIM-Wheat model under different stubble, tillage, and nitrogen application management scenarios. Some large predictive errors were found when the model predicted yields for fields of Warwick, Australia, where the wheat was heavily infected with the root-lesion nematode. Biotic stress such as root disease load can have major impacts that are not represented in APSIM-Wheat yet. The simulated yield deviated more from the observed (*RMSE*=1.54 t/ha) when high nitrogen fertiliser was applied.

2.4.5 Implications of the influential factors in changing climate

Under future climate scenarios, both mean and variance of temperatures are projected to increase, along with precipitation variability. This will lead to increased heat waves, frost risk, and changing risk of drought and flood (Kundzewicz et al., 2014; Meehl et al., 2000; Perkins et al., 2012; Rigby and Porporato, 2008; Trenberth, 2011; Zeppel et al., 2014). The changing climate may also be favourable to certain wheat diseases, e.g. stripe rust (Luck et al., 2011) which have not been represented in the model yet. APSIM-Wheat, as a major cropping system tool used to study climate change impacts and seek solutions to address them (Deihimfard et al., 2018; Yang et al., 2014), needs improvement in the representation of heat stress, frost stress, water deficit, and the effects of pests, particularly when it is adopted to predict wheat production under the projected climate scenarios.

In addition to daily mean temperature, maximum temperature could be included as a variable to determine heat stress impact. The underestimation of heat stress impacts will

lead to over-optimistic simulations of the future wheat production. Meanwhile, increasing mean temperatures accelerate crop growth and shorten the growing season, resulting in crops reaching the frost-sensitive anthesis stage more rapidly (Zheng et al., 2015). The absence of parameter values for functions to account for frosts can potentially lead to overestimation of harvest yields. Parameterising the frost damages of leaf senescence, seedling death, or death of formed grains will improve the model simulation capability. The variable precipitation intensity and probability may reduce users' confidence in simulation accuracy since the model showed uncertainty in predicting water-limited yield. Improved functioning and parametrisation to correctly estimate water deficit impacts on wheat growth is warranted. Apart from using the model to study future climate impacts on production, when users apply the model to a new study area or cultivar, accurate soil parameters and site-specifically calibrated cultivar parameters improve the model performance.

2.5 Summary and conclusion

In this work, we have reviewed 76 articles and conducted a meta-analysis of 30 applications of the APSIM model (APSIM Classic, version 1.X – version 7.9) to obtain detailed information on the process-based model's performance in predicting wheat yields. Our study shows that the model provides reasonably accurate wheat grain yields across a wide range of varieties, environments, and management practices around the world with an overall uncertainty of about 1 t/ha. However, we found a large variation in uncertainties within the modelling studies considered, especially between studies with site-specific calibration and non-site-specific calibration.

Furthermore, we found that factors such as heat and frost stress, water and nitrogen availability, soil parameterisation, calibration of genotype parameters, soil cracking, lodging, increased atmospheric CO_2 concentration and plant diseases are important factors affecting model performance. Heat and frost stresses, in particular, caused large discrepancies in the prediction of grain yield. One reason for this is that the reviewed model versions use only daily mean temperature as a heat factor to calculate the effects on biomass accumulation, although wheat is particularly sensitive to shorter-term heat stress during the anthesis and grain filling phases. Therefore, APSIM tended to overestimate crop yield that experienced heat wave conditions. Frost stress functions are already implemented in the reviewed model but without default parametrisation which

negates their effect (impact factor = 0), so APSIM overestimates yield in crops subject to frost damage. The applications of APSIM to situations with water stress and nitrogen limitation led to greater uncertainties (overestimation for water stress and underestimation for nitrogen stress). Like the frost stress function, the effects of water and nitrogen stress on phenology are not yet parameterised. Therefore, suggestions to improve the model include: (1) incorporating daily maximum and minimum temperatures as impact factors to account for their effects on crop growth, (2) parameterising frost stress, water stress, and nitrogen stress functions in relation to phenology.

A fully or partial site-specific calibration resulted in crop yields being predicted with higher accuracy (on average, *RMSE* and *NRMSE* were 0.64 t/ha and 14.08%, respectively). A fully site-specific calibration, including the determination of soil hydraulic parameters, initial soil conditions from field measurements and adjustment of other parameters (such as crop parameters), resulted in the lowest uncertainty in crop prediction (*RMSE*=0.44 t/ha, *NRMSE*=10.15%). If only soil parameters, and not cultivar parameters, are calibrated, the yield prediction accuracy slightly decreases, resulting in RMSE=0.51 t/ha and NRMSE=20.8%. This paper has summarised tuned cultivar parameters where available, with Table 2-2 lists the parameters and their calibrated value ranges and Table B. 1 provides detailed parameter values reported by individual studies. These calibrated values reflect the effect of genetic differences under differing management or environmental scenarios. Future model users could start setting the parameters using values from Table B. 1 when calibrating identical cultivars and running the model under similar conditions. If soil parameters are not available, using a soil database such as APSoil to specify soil hydraulic properties is a good alternative, leading to yield predictions on average with *RMSE*=0.7 t/ha and *NRMSE*=13.0%. Soil texture-derived soil parameterisation is also acceptable but with comparatively lower accuracy and uncertainty with an *RMSE*=1.37 t/ha and an *NRMSE*=40.45%.

The reviewed APSIM-Wheat version is not equipped with functions that account for other abiotic and biotic influences like soil cracking, lodging, or crop disease. Improving the model functionally to consider all these factors could lead to better crop predictions; however, a major challenge is that there is often a significant stochastic component to these influences. The most practical suggestions to reduce the errors in predicting would

be (1) fully calibrating the model to local conditions by tuning soil and cultivar parameters; (2) developing a database sharing cultivar parameter sets which could help in specifying the genetic characteristics under various conditions, similar to the APSOIL database; and (3) applying frost-heat damage functions like Bell et al. (2015) developed to adjust grain yields when encountering temperature stresses. An alternative would be to pursue methods such as assimilating external observations into the model to continuously adjust certain model state variables and properties to improve model performance. Remote sensing data can provide timely information on the crop or environment status and could be used to update the model simulation regularly during the simulation. Another option is to use multi-model ensembles to account for model uncertainty in describing the impact of climate change on agricultural productivity (Asseng et al., 2015, 2013; Iizumi et al., 2018; Maiorano et al., 2017b; Martre et al., 2015b; Wang et al., 2017).

This work did not assess the model's ability of simulating other crop states such as biomass, leaf area, water use, or fertility dynamics. The simulation quality of these dynamics is still largely unknown and worth further investigation.

The meta-database in this paper was composed of datasets from separate papers. In our meta-analysis, datasets from existing papers were compiled to analyse the impact of certain factors, while other factors could not be held constant, which may have led to some bias. The model validations considered in our study were all point-based, the plant models are usually used at the plot, field scales or even larger. However, the effects of spatial heterogeneity were not considered in our study. Finally, we did not consider the uncertainties embedded in the forcing inputs. According to Tao et al. (2018), when coupling climate models with crop models, the uncertainty from downscaled climate projections could be larger than those from crop models.

Crop models like APSIM are not just predictive tools, but also exploratory tools in conjunction with future scenarios. The vision for agricultural systems models is to accelerate progress of finding ways to address the global food security challenges. This paper aims to provide the perspectives on the model outputs credibility and uncertainty under various conditions covering a wide spectrum of management practices, environments, and wheat varieties. We expect that our analysis of APSIM-Wheat model

performance will assist users to have appropriate interpretations and avoid misuse of the model.

Chapter 3 Sensitivity of APSIM-Wheat yield predictions to model parameters and inputs

3.1 Abstract

The performance of cropping system models is often limited by uncertainties in model parameters and inputs. This study aims to explore how model yield prediction responds to these uncertainties under various environmental and management conditions. The Sobol' method was used to investigate the sensitivity of the Agricultural Production Systems SIMulator (APSIM)-Wheat yield prediction to the following factors: air temperature (maximum and minimum), precipitation, initial soil nitrogen content, nitrogen fertilisation amount, and soil hydraulic parameters. Eighteen scenarios were defined to consider a combination of three weather conditions (wet, normal, and dry growing season, based on the historical climatology of the Wimmera district of Victoria, Australia), three soil types (sandy, loamy, and clayey soils), and two nitrogen fertilisation applications (50 and 100 kg N/ha). Eight thousand APSIM simulations were used to calculate the first order and total sensitivity indices for each scenario. The effects of weather, soil water characteristics, and nitrogen availability were estimated by measuring their impacts on sensitivity indices. Our results show that yield was more sensitive either to variables that control water availability (precipitation and soil type) or variables that control nitrogen availability, depending on which was more limiting to wheat growth under the scenario. For example, in case of low nitrogen fertilisation scenario, the initial nitrogen content sensitivity ranked first. Variation of this factor contributed 64% to 79% to the variance in simulated yield for clayey soils, nearly four times higher than the second-ranked factor (nitrogen fertilisation amount). Soil hydraulic parameters and precipitation were most important when the crop growth was more constrained by water availability than by nitrogen availability. In the case of sandy soils in dry years with high nitrogen fertilisation level, soil parameters and precipitation accounted for 83% of the yield variability. Maximum and minimum temperatures were consistently ranked as the least important factors under all scenarios. This work will help researchers better understand the model inputs' impacts on the simulated yield variability under various

soil, management, and weather conditions. The results also support agronomists and practitioners in the optimal use of the APSIM-Wheat model as a management tool.

3.2 Introduction

Process-based biophysical models are widely used to simulate crop growth, test management practices, and explore the impacts of environmental conditions on yields due to their simulation of the dynamic interactions among crop, soil, water, nutrient, and weather variables. They can assist in mitigating climate change impacts on crop yield by designing efficient management practices and improving food production by guiding crop breeding. The Agricultural Production Systems sIMulator (APSIM) (Holzworth et al., 2014b), as one of the popular process-based crop models, has been utilised for research and practical applications for over 25 years. It is also available as an online commercial tool – Yield Prophet®, to support crop growers with management decisions (Hunt et al., 2006). APSIM model consists of modules describing weather, management, soil hydrology and soil nutrient impact, and growth of various crops. APSIM-Wheat is one of the most utilised modules within APSIM due to the fundamental role of wheat in global food security (Shiferaw et al., 2013).

APSIM-Wheat yield predictions contain errors that vary with, for example, available soil water, heat, fertilisation, and model calibration (Ahmed et al., 2017; Asseng et al., 2015, 2013; Collins et al., 2021; Hao et al., 2021; Hussain et al., 2020; Kawakita et al., 2020; Wang et al., 2020; Zhao et al., 2014). Hao et al. (2021) investigated APSIM-Wheat yield prediction uncertainties by analysing model evaluation results from the extensive APSIM-Wheat literature. They found that, on average, APSIM-Wheat predicted yield with a root mean squared error (RMSE) of approximately 1 t/ha. Prediction uncertainty increased with limited soil information and adverse environmental conditions, such as water and/or nitrogen deficit, heatwave, and frost conditions. Zhao et al. (2014) showed that the grain yield uncertainty derived from the variation of the cultivar parameters was large. Their results emphasised the importance of well-calibrated cultivar parameter values.

Understanding the sources of uncertainty in yield prediction and their influences is important to estimate and reduce yield prediction uncertainty under diverse conditions. Sensitivity analysis is usually applied to evaluate the importance of uncertain information

such as model inputs and parameters on the target model outputs. Previous studies employed the method to determine the key influential parameters in a variety of crop models (Laluet et al., 2023; Liang et al., 2017; Lu et al., 2021a; Ma et al., 2023; Makowski et al., 2006; Richter et al., 2010; Varella et al., 2010; Wang et al., 2013a; Xing et al., 2017; Yu et al., 2023). Most existing studies investigating APSIM-Wheat yield prediction sensitivity to model parameters have focused on crop genetics, soil hydraulic parameters, and climate (Casadebaig et al., 2016; Collins et al., 2021; He et al., 2015; Luo and Kathuria, 2013; Wu et al., 2019; Zhao et al., 2014).

For crop genetics, Zhao et al. (2014), He et al. (2015), Casadebaig et al. (2016), and Collins et al. (2021) examined the sensitivity of several APSIM-Wheat outputs, including yield, to cultivar and phenological parameters under different fertilisation rates or climate-soil conditions. They found that yield is mainly influenced by parameters controlling thermal time, photoperiod, grain formation, and the duration of crucial reproductive stages.

In terms of soil hydraulic parameters, Dokoohaki et al. (2018) investigated the sensitivity of model simulated soil water content to soil hydraulic parameters using the APSIM-SOILWAT module at a farm near Lewis, Iowa, USA. The results indicated that under the tested conditions, field capacity and saturated hydraulic conductivity were the most crucial parameters in determining total soil water content. Wu et al. (2019) conducted a sensitivity analysis of the water-limited potential yield (*Yw*) to the variation of soil hydraulic parameters at two contrasting sites with high and low rainfall and for two soil types (shallow sandy duplex and clay). Among the soil properties, change in plant available water capacity (PAWC) was the main source of variation in *Yw*. The impact of PAWC estimation error was marginal when the error was within 20 mm, while yield predictions were more sensitive to underestimation than overestimation of PAWC outside this range. Vogeler et al. (2022) carried out a sensitivity analysis using the APSIM-SWIM3 module to determine the impact of soil hydraulic properties on various model outputs, including soil moisture, drainage, nitrogen leaching, and pasture productions. The results revealed that for well-drained soils under high precipitation conditions with no water limitation, the model shows low sensitivity to soil hydraulic parameters. However, the authors emphasised the need for further analysis to consider different soil types and weather conditions.

APSIM-Wheat yield prediction sensitivity to changing climate conditions has also been studied by Luo and Kathuria (2013). They used correlation and regression analysis to test the yield sensitivity to temperature, rainfall, and atmospheric carbon dioxide concentration under two different soil types at six locations. The results showed that the median yield was positively related with rainfall and atmospheric CO_2, but negatively correlated with temperature. The yield response to changes in meteorology was affected by soil types and locations. Soil type was the most influential factor among all these environmental factors, followed by climate, changes in atmospheric CO_2 concentration, amount of rainfall, and temperature.

The abovementioned studies investigated APSIM-Wheat yield sensitivity to key variables and parameters including cultivar parameters, soil hydraulic parameters, and changing climate under different management or environmental conditions. Our recent review work revealed that the model's yield predictions exhibit an overall root mean square error (RMSE) of about 1 t/ha (Hao et al., 2021). Prediction uncertainties tend to increase under circumstances characterised by limited soil information and challenging environmental conditions, including water and/or nitrogen deficits, heatwaves, and frost events. This observation is grounded in a comprehensive overview of 76 published studies spanning thirteen countries across four continents. To gain a deeper understanding of how these factors influence the model and to obtain clear insights into reducing uncertainties during model calibration, we need to focus on studying the interplay of water availability, nitrogen fertilization, weather conditions, and soils on crop growth and yield, which is currently lacking. This also underscores the need to quantify and differentiate the contribution of variables related to weather conditions (precipitation, temperature) and nutrient supply to crop growth, as modulated by soil conditions. In light of this context, our study aims to investigate the sensitivity of the APSIM wheat yield to the variabilities in these crop growth factors. We examined the model response of rain-fed winter wheat yield to six input variables with the Sobol' method: daily maximum and minimum temperature (Tmax and Tmin), precipitation, initial nitrogen content, nitrogen fertilisation amount, and soil parameters. These sensitivities were evaluated for a broad range of conditions in eighteen scenarios comprising three representative weather conditions (wet, normal, dry growing seasons), three soil types (sandy, loamy, and clayey soils), and two fertilisation applications (50 and 100 kg N/ha over the cropping cycle) to assess their impact on yield variability. The

results of the Sobol' analysis were analysed and discussed to quantify the yield prediction sensitivity to the factors. The yield prediction variability was quantified using the outputs from the sensitivity analysis. Main finding of this work will enable a more realistic representation of APSIM-Wheat yield uncertainty via a Monte-Carlo-based ensemble simulation approach and to provide insights for putting calibration efforts to the key parameters most influential to yield under various soil-nutrient-weather conditions.

3.3 Materials and methodology

3.3.1 The study area

The Wimmera district of Victoria, Australia was selected to study the sensitivity of the APSIM-Wheat yield prediction. From 2015 to 2019, the Wimmera region accounted for approximately 30 percent of the total wheat production in Victoria (ABS, 2020). The soils in the region show large variability in plant available water capacity (PAWC), ranging from 50 mm to 170 mm (Hochman et al., 2013). To match the variable soil characteristics, especially with respect to its water holding capacity, three soil types were specified (Chapter 3.3.4). Peel et al. (2002) found that Australia has relatively higher variability in precipitation other than other continents due to ENSO. Therefore, it is also important to consider the effect of climatic variability on model sensitivity. The climate type of the Wimmera region is temperate with warm summers and cool, wet winters (Nuttall et al., 2010; Peel et al., 2007). Over the past 120 years the annual rainfall decreased in the region while the temperature increased with frost and heatwave occurring more often (Bureau of Meteorology, 2020). To account for the inter-annual variability in weather impacts on the rainfed cropping lands, three weather scenarios based on the historic weather data are selected to perform the sensitivity analysis (Chapter 3.3.4).

3.3.2 APSIM and wheat module

The APSIM model (Holzworth et al., 2018, 2014b) is a modular modelling platform to simulate biophysical processes in agricultural systems. In this work, the most recent version of the model, called APSIM Next Generation, is used. Processes such as crop growth, soil hydrology, nutrient cycling, the effects of weather conditions, and management practices are represented by various modules. Five main modules, namely Wheat, SoilWat, SoilN, Met, and Fertilisation (a self-defined script to specify the amount and timing of nitrogen fertiliser) were linked within APSIM for simulations in this paper.

The Wheat module in APSIM (APSIM-Wheat) simulates wheat growth on a daily basis (Keating et al., 2001). The SoilWat module is used to calculate the soil water dynamics based on a multi-layer, cascading water balance model (Jones and Kiniry, 1986; Littleboy et al., 1992). The water holding characteristics of the soil are specified with several soil parameters: lower limit of 15 bar (*LL15* or wilting point), drained upper limit (*DUL* or field capacity), crop lower limit (*CLL*), and saturation (*SAT*). The SoilN module simulates the conversion of nitrogen and carbon in each soil layer and thereby calculates the nitrogen supply available to crops based on the previous residual nitrogen situation and fertiliser inputs (Probert et al., 1998). The Met module is used to specify daily meteorological information such as precipitation, global radiation, daily maximum and minimum temperature, and to calculate potential evapotranspiration. All these modules interact with each other within an APSIM simulation to update the water and nitrogen status and to determine the wheat growth. The model yield prediction is well-validated around the world with an overall RMSE of 1 t/ha (Hao et al., 2021).

Six variables representing weather conditions, soil conditions, and nitrogen conditions are considered for the Sobol' sensitivity analysis of the APSIM-Wheat model for yield simulations. The selection of the six variables was based on the important factors affecting APSIM wheat yield prediction performance identified in Hao et al. (2021). Please note that the maximum and minimum temperatures were considered as two separate variables since we intended to distinguish the possible effects of heat stress and frost respectively. Precipitation, initial nitrogen content, and nitrogen fertilisation amount were also considered individually. Due to strong cross-correlation between individual soil parameters, key soil parameters (porosity (*PO*), *DUL*, and *LL15*) were treated as one group of variables to produce varied soil water holding capacity. Saltelli (2002) described this as a closed sensitivity measure within a subset of factors. We measured the model yield's sensitivity to the soil parameters group by calculating the closed effects of porosity, *DUL*, and *LL15*.

3.3.3 The Sobol' sensitivity analysis and resampling by bootstrap

The Sobol' method (Sobol', 1990) is a global sensitivity analysis method that is based on variance decomposition. The method decomposes the variance of the model output to estimate the importance of individual input factors or the interaction between those factors. Here "factors" is used to encompass all model inputs and parameters that are

included in the Sobol' analysis. The resulting sensitivity indices represent an average sensitivity across the joint domain of all the factors (Pianosi et al., 2016). First order sensitivity index (S_i) and total sensitivity index (S_{Ti}) are computed to represent the importance fractions:

$$S_i = \frac{V_i}{V} = \frac{V[E(Y|X_i)]}{V} \tag{3-1}$$

$$S_{Ti} = S_i + \sum_{j \neq i} S_{ij} + \sum_{j \neq k \neq i} S_{ijk} + \cdots = 1 - \frac{V_{\sim i}}{V} = 1 - \frac{V[E(Y|X_{\sim i})]}{V} \tag{3-2}$$

The first order index S_i, which is also called the 'main effect' of the individual input factor X_i on a model output Y, measures the contribution of X_i to the model output variance V. V_i is the partial variance associated with the main effect of the input X_i. S_{Ti} quantifies the overall contribution of X_i on the model output. It estimates the effect involving X_i and all its interactions with the other input factors. S_{ij} denotes the impact on the model output variance from the second order interaction between X_i and X_j, S_{ijk} represents the third order interaction between X_i, X_j, and X_k, etc. The calculation of S_{Ti} can be based on the variance $V_{\sim i}$ that results from the variation of all factors, except X_i ($X_{\sim i}$ indicates all the other factors except factor X_i.). Higher S_i values mean that the variation of that factor directly affects the output variance more. Higher S_{Ti} values mean that the combined direct and indirect impacts of that factor are greater. The total interactions between X_i and other factors can be determined by calculating the difference between S_{Ti} and S_i, with larger values denoting greater effects of that factor in combination with variations in other factors on the model outputs. Glen and Isaacs (2012) pointed out that the sum of S_i and the sum of S_{Ti} from all input factors equal one only if there is no interaction among these factors. Interactions lead main effects summing to less than one as interactions are omitted, while total indices sum to more than one as individual interactions are considered multiple times (see equation (3-2)).

Sobol' original method to estimate S_i and S_{Ti} requires $n \cdot (2k + 1)$ model simulations to calculate the high-order interactions between factors, where k is the number of input factors and n is the sample size. We used a method proposed by Saltelli (2002) that reduces the model runs to $n \cdot (k + 2)$ instead.

Bootstrapping was used to estimate confidence intervals for the sensitivity indices. The n samples were used to estimate the sensitivity index. Each bootstrap sample was created by selecting n points from the n model runs with replacement, and then calculating S_i and S_{Ti}. This was repeated 5000 times and the 95% confidence intervals for S_i and S_{Ti} were calculated by finding the 2.5 and 97.5 percentiles. A narrow range between the 2.5 percentile and 97.5 percentile represents a high level of confidence in getting a stable result.

In this work, k is the number of tested factors and equals six, which is the number of the tested factors as described in Chapter 3.3.2. The evolution of S_i and S_{Ti} with increasing sample size ($10<n<10{,}000$) was investigated, to assess the convergence of results. The perturbed input factors were used to initialise the ensemble APSIM-Wheat model simulations, and the output yield variance was analysed to estimate each input factor's contribution.

3.3.4 Weather, soil, and nitrogen fertilisation scenarios

Sensitivity analyses was performed for eighteen scenarios selected based on rainfed conditions in the Wimmera district of Victoria, Australia. These scenarios considered combinations of three climatic conditions, three soil types, and two fertilisation amounts, resulting in 18 scenarios (Figure 3-1). The key model inputs, tested output, and their units are also specified in Figure 3-1. The values of the perturbed parameters are reported in Chapter 3.3.4. Using these scenarios enabled us to assess the sensitivity of APSIM wheat yield prediction to within season variations across a broader range of weather, soil, and fertilisation conditions.

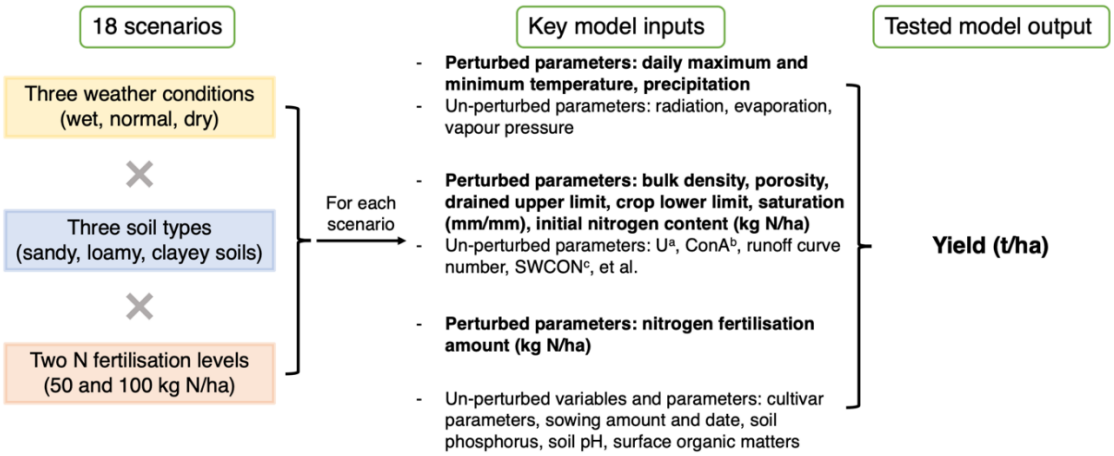

[a] U: first stage evaporation-amount of cumulative evaporation before soil supply falls below atmospheric demand
[b] ConA: second stage evaporation-coefficient of cumulative second stage evaporation against the square root of time

[c] SWCON: saturated Flow- proportional daily drainage of water from above DUL into adjacent soil layers

Figure 3-1. The 18 simulation scenarios used in this study, the key model inputs, and the main outcomes of the sensitivity analysis. The scenarios are a combination of three weather conditions, three soil types, and two nitrogen fertiliser applications.

The scenarios were chosen based on the historic daily weather data from the meteorological station Nhill (station number: 078040) in Woorak (Bureau of Meteorology, 2020): wet, normal, and dry growing season (Table C. 1). The average values of maximum, minimum temperatures, and precipitation of chosen weather scenarios represented approximately the 10^{th} percentile, median, and 90^{th} percentile of 120-year historic weather data (Table C. 2). From the wet to the dry growing season, the average maximum and minimum temperatures increased from 20.5 °C to 22.7 °C, and from 7.4 °C to 8.6 °C, respectively, while precipitation decreased from 546.2 mm to 253.4 mm.

To account for the variable soil hydraulic properties, three soil types were selected based on different soil textures: sandy soils, loamy soils, and clayey soils. See Table C. 3 for more details. For all soil types we assumed six layers (from the top layer, three layers with a thickness of 10 cm, one layer with a thickness of 30 cm, and two layers with a thickness of 40 cm), resulting in a total soil depth of 140 cm. Please note that the first layer of each soil type is allocated with a different soil texture than the deeper soil layers (Table C. 3).

The most common nitrogen application amount for wheat in Australia is between 50 and 80 kg N/ha (ABARE-BRS, 2003). Accordingly, two fertilisation levels were set in this work: a normal level of 50 kg N/ha, and a high level of 100 kg N/ha. The fertiliser was applied around the start of seedling growth described by Zadoks growth stages (GS11 – GS13) (Zadoks et al., 1974).

3.3.5 Perturbation of weather inputs, soil texture and nitrogen parameters

To run Sobol' analysis, perturbations were applied to all six variables representing weather conditions, soil conditions, and nitrogen conditions. The perturbations led to variations in air temperature, water availability and nitrogen availability. Perturbation methods are described below, and key values are summarised in Table 3-1.

Table 3-1. The perturbation sampling parameters of uncertain sources (*e*: Euler's number, was used as the base of natural logarithm, approximately equals to 2.71828)

Uncertain sources	Error distribution type	Error magnitude	Autocorrelation coefficient[a]
Precipitation	Log-normal distributed (mean=1, additive error)	Std=40%	1/*e*
Daily maximum air temperature (Tmax)	Normal distributed (mean=0, multiplicative error)	Std=3℃	1/*e*
Daily minimum air temperature (Tmin)	Normal distributed (mean=0, multiplicative error)	Std=3℃	1/*e*
Soil textures	Normal distributed (mean=0, multiplicative error)	Specific std values are listed in Table C. 4	/
Initial nitrogen content (61 kg N/ha)	Normal distributed (mean=0, multiplicative error)	Std=20 kg N/ha	/
Nitrogen fertilisation amount (50/100 kg N/ha)	Normal distributed (mean=0, multiplicative error)	Std=8.5 kg N/ha	/

[a]First-order autocorrelation coefficient assumes a daily time series.

3.3.5.1 Perturbation of weather inputs

Like all measured values, weather data are subject to inaccuracies, which is an important component of the crop model uncertainty (Lobell, 2013b; Nonhebel, 1994). Weather input uncertainty was stochastically simulated by adding error to daily measured weather data. Perturbation of precipitation was assumed to follow a lognormal distribution with a mean of 1 and standard deviation of 40%. Perturbations of maximum and minimum temperatures were generated as additive errors using Gaussian random numbers with zero mean and a standard deviation of 3 ℃. Perturbing the temperatures consequently led to perturbations in evapotranspiration. To account for the temporal correlation of the weather input errors, a first-order autoregressive process, AR(1), with a correlation coefficient of 1/*e* was implemented on a daily basis to each weather factor, following Reichle et al. (2007) and Li et al. (2014). The perturbations for the different meteorological variables were assumed to be independent from each other.

3.3.5.2 Perturbation of soil information

Soil parameters were perturbed by adding cross-correlated (correlation coefficient=0.5 between each pair of variables) and normally distributed errors to *PO*, *DUL*, and *LL15*. Table C. 4 specifies the mean and standard deviation of each soil texture for each soil type (Ratliff et al., 1983). These values were used to perturb the soil parameters. The main purpose of soil parameter perturbation was to generate difference in plant available water capacity so that the model simulated soil moisture would show uncertainty. Other parameters including *SAT*, *CLL*, and bulk density (*BD*) were then calculated using the following equations (Dalgliesh et al., 2016). These soil hydraulic parameters were used to specify the soil water holding properties:

$$SAT = PO - EA \tag{3-3}$$

$$CLL = DUL \times f_{CLL} \tag{3-4}$$

$$BD = 2.65 \times (1 - PO) \tag{3-5}$$

where the *SAT* is the soil saturation value and *EA* is the entrapped air. *EA* depends on soil texture: clay: 3%, loam: 5%, and sand: 7%. *CLL* defines the crop lower limit. The estimation of it relates to the *DUL* and the soil depth. f_{CLL} is soil depth dependent and was assumed to be: layers 1 – 3: 50%, layer 4: 60%, layer 5, 70%, and layer 6: 80%. The assumed particle density used in calculating *BD* is 2.65 g/cm^3, the value is suggested by Dalgliesh et al. (2016).

Initial nitrogen content of 61 kg N/ha was set from a 100-year model spin up (1918 – 2018) with fertilisation of 80 kg N/ha across all growing seasons. Considering that the most common nitrogen application amount rate for wheat in Australia is between 50 and 80 kg N/ha (ABARE-BRS, 2003), fertilisation of 35 kg N/ha and 95 kg N/ha across all growing seasons for spin-ups were also tested. The resulting soil nitrogen contents were approximately between 10 kg N/ha and 117 kg N/ha. Therefore, an additive Gaussian error with a mean of 0 and standard deviation of 20 kg N/ha was added to the 61 kg N/ha base value to represent the uncertainty, which resulted in initial soil nitrogen content enveloped approximately between 0 and 121 kg N/ha.

3.3.5.3 Perturbation of fertilisation amount

For a given fertilisation level, the actual application of nitrogen fertiliser can be spatially variable due to machinery variations. However, the APSIM model is one-dimensional. Therefore, an additive error was added to nitrogen fertilisation to represent the spatial heterogeneity in fertilisation. The error was assumed to be Gaussian with a standard deviation of 8.5 kg N/ha. For fertilisation level of 50 kg N/ha, 99.7% of perturbed fertilisation amounts were therefore within the range of 24.5 to 75.5 kg N/ha, and this range was between 74.5 and 125.5 kg N/ha for 100 kg N/ha fertilisation level. The perturbation of these two fertilisation levels can provide uncertainties at both normal and excessive levels of fertilisation.

3.4 Results

3.4.1 Effect of sample size

Figure 3-2 shows the evolution of the first order index S_i and total index S_{Ti} with increasing sample size, selected from the Scenario of normal weather, loamy soil, 100 kg N/ha fertilisation amount as an example. Confidence intervals (CI) for the Sobol' indices were also calculated via bootstrapping. In general, the S_i and S_{Ti} for each factor reach stable values within a sample size of 10,000. The S_i values of the various factors featured small fluctuations for sample sizes greater than 7000. The evolution of the Sobol' sensitivity indices with increasing sample size suggests that the total sensitivity indices may require a larger sample size to reach stable values. The standard deviation of the S_i and S_{Ti} across all parameters were calculated for sample sizes between 30 and 3000, 30 and 6000, 30 and 9000, and 30 and 10,000 (Table C. 5). For precipitation, Tmax, Tmin, and soil parameters, the total index showed relatively noticeable fluctuations since the standard deviation in the total index is twice as large as the standard deviation in the first order index. Factors with larger S_i and S_{Ti} values usually required a larger sample to converge to their final values. The 95% confidence intervals for all factors' S_i and S_{Ti} were calculated. Table C. 6 shows that the 95% CI widths of S_{Ti} values for precipitation and soil parameters are suitably narrow at 0.0012 and 0.0017. The CI widths for all coefficients in Table C. 6 are between 0.2% and 0.8% relative to their absolute sensitivity index values, indicating acceptably low levels of sampling uncertainty.

For this research, a sample size of 10,000 (n) was used for each of eighteen scenarios. The Sobol' method requires $n\cdot(k+2)$ runs for each scenario, where k = 6 in this case,

resulting in 80,000 model realisations for one scenario to calculate the first order and total sensitivity indices. Therefore, a total of 18*80,000 = 1,440,000 model simulations were required for all scenarios.

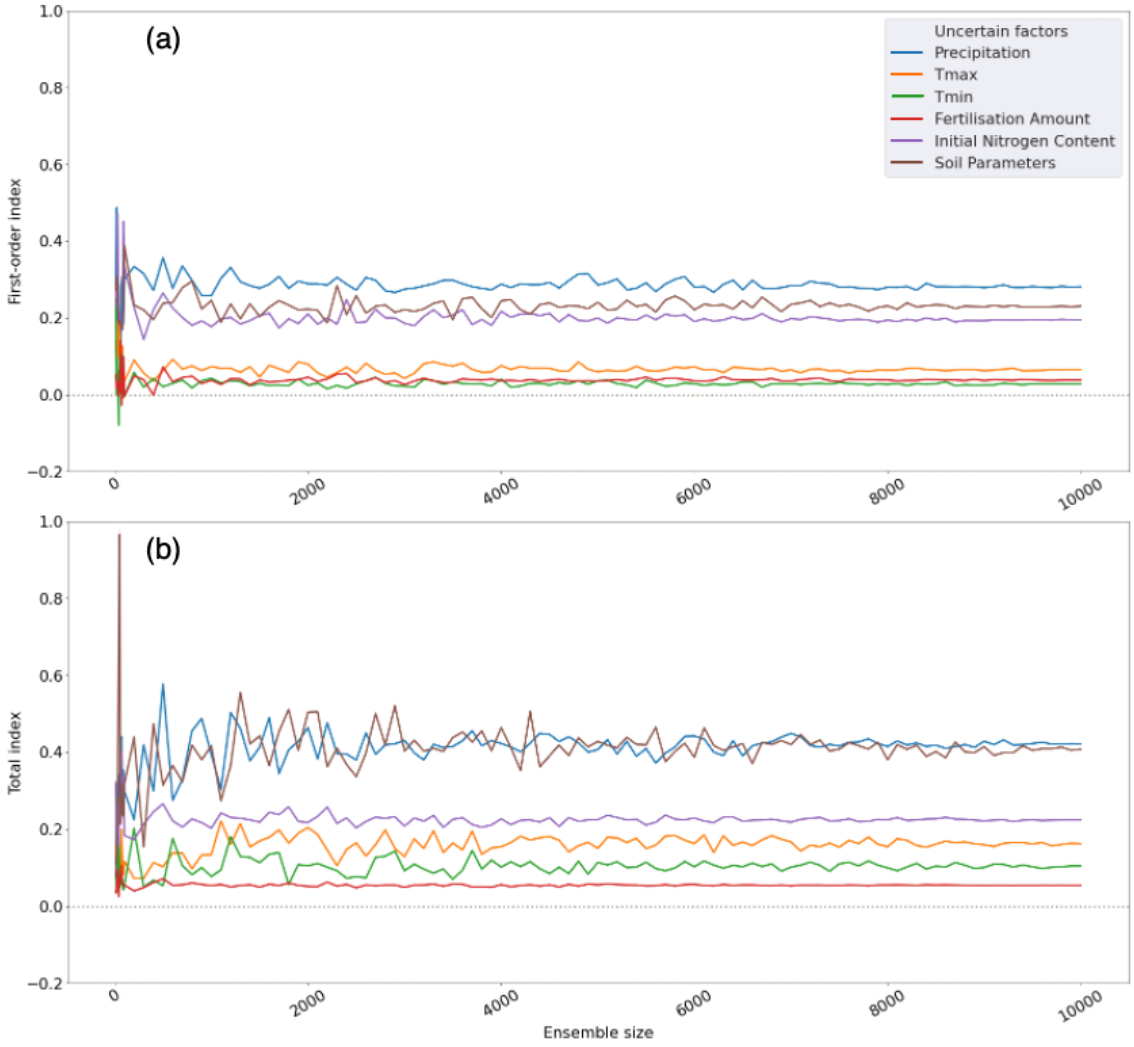

Figure 3-2. Evolution of (a) the first order index and (b) total index values for uncertain factors under Scenario Norm _Lm_100 (normal weather, loamy soil, 100 kg N/ha) when the sample size increased from 10 to 10,000. Different colours represent different uncertain factors. Blue: Precipitation; orange: Tmax; green: Tmin; red: Fertilisation Amount; purple: Initial Nitrogen Content; brown: Soil Parameters.

3.4.2 Ranking of the influential input parameters

Figure 3-3 shows the first order index (S_i) and the total index (S_{Ti}) ranks of the six factors in terms of yield sensitivity. The S_i show similar clusters in ranks to the corresponding ranks in the S_{Ti} across the factors and scenarios. The specific S_i and S_{Ti} values for all eighteen scenarios are listed in Table C. 7 and Table C. 8. Figure C. 1 shows the

distribution of ranks for each parameter under all eighteen scenarios. From both main effect and total effect perspectives, initial nitrogen content, soil parameters, and precipitation were the most influential factors. Temperatures were typically the least important factors, although Tmax ranked second or third when the weather turned warmer and drier, and fertilisation was higher. Tmin was always in the last two ranks. The low ranks of the temperature values may be due to the relatively small range of temperature variation between warm and cold years in the experimental region.

Sensitivity to initial nitrogen content and fertilisation amount tended to be higher when the fertilisation amount was 50 kg N/ha instead of 100 kg N/ha, especially under wet and normal weather conditions, implying stronger control of nitrogen stress on yield under limited soil nitrogen availability. In contrast, the water availability-related factors (soil parameters and precipitation) are more important for high fertilisation applications or under drier weather conditions.

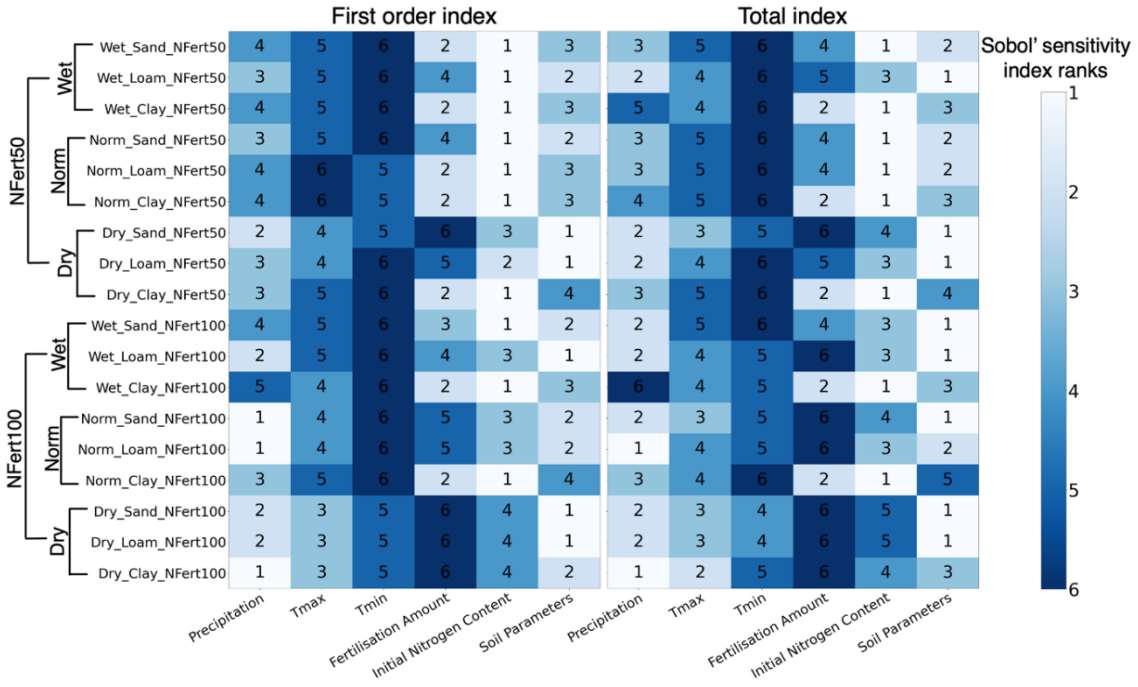

Figure 3-3. The first order index ranks (left panel) and the total index ranks (right panel) of the six influencing factors in terms of yield sensitivity under eighteen scenarios. The six parameters are listed on the horizontal axis; the eighteen scenarios are ordered along the vertical axis depending on their weather conditions, soil properties, and fertilisation amount; each grid cell shows the output sensitivity via a colour scale, where white denotes the largest influence in affecting the yield prediction and dark blue represents the minimum influence.

3.4.3 Fertilisation amount effects on sensitivity

Figure 3-4, Table C. 7, and Table C. 8 show the first order index (S_i) and total index (S_{Ti}) values of all six factors for all eighteen scenarios. Considering S_i under a nitrogen fertilisation of 50 kg N/ha, the prediction of wheat yield was most sensitive to initial nitrogen content, with the S_i of this factor ranking first in 7 out of 9 scenarios (Table C. 7). By comparing the S_i values for initial nitrogen content in Figure 3-4, we can see that for given weather and soil conditions, crop growth relies more on the initial soil nitrogen amount when nitrogen provision by fertilisation is limited. Its importance was greatest for clay soil for which S_i ranged from 0.62 to 0.79 (Figure 3-4), nearly four times more than the fertilisation amount. Figure 3-4 also shows that wheat yield was more sensitive to nitrogen factors at low fertilisation levels, as nitrogen has a stronger limiting effect here than soil water supply.

With a nitrogen fertilisation of 100 kg N/ha, the importance of initial nitrogen content and fertilisation amount decreased. Instead, soil parameters and precipitation became the predominant influences, especially for sandy soils and under dry weather conditions, both featuring limited plant available water content via fast drainage (sandy soil) or reduced input (dry weather), with these factors occupying the first two places for 6 out of 9 scenarios in case of S_i (Table C. 8). Figure 3-4(g) show that S_i for soil parameters was highest under dry conditions and for sandy soils, while the S_i for precipitation was highest for the normal year with sandy soils (Figure 3-4(d)). Soil parameters and precipitation were the most important factors affecting yield in terms of total effect. S_{Ti} was largest for sandy and loam soils under all three weather conditions with precipitation S_{Ti} = 0.41 to 0.67, and soil parameter S_{Ti} = 0.41 to 0.73 (Figure 3-4(j, k, m, n, p, and q)). An exception to this pattern for high nitrogen applications (100 kg/ha) was under wet and normal weather conditions and clay soils when the wheat was more sensitive to initial nitrogen content and fertilisation amount, as under those conditions water supply was sufficient due in part to high water holding capacity (enabling the soil to store the higher precipitation more effectively) (Figure 3-4(l and o)).

3.4.4 Weather condition effects on sensitivity

We compared the S_i and S_{Ti} values in Figure 3-4 for both 50 kg N/ha and 100 kg N/ha fertilisation level groups, we found that the main and total effects of initial nitrogen content decreased dramatically when under dry conditions, especially for sandy soils.

The S_i dropped to 0.079 and 0.029 for both fertilisation levels under this specific weather and soil conditions (Table C. 7). At the same time, soil parameters and precipitation replaced the nitrogen availability-related factors as the most important, with S_i = 0.40 and 0.21 for these two factors and S_i < 0.08 for the other factors when the fertilisation level is 50 kg N/ha. This is because water becomes more limiting on yield under a dry weather, especially for sandy soils with low water holding capacity. Reduced soil water also influences the amount of dissolved soil nitrogen consumed by the crop. The same tendency was observed for the total effect. Overall, the impact of soil parameters and precipitation was higher for the 100 kg N/ha case as crop growth was constrained more by water availability than nitrogen availability. Under the most extreme scenario – high fertilisation level, dry weather, and sandy soils (Figure 3-4(g)) – the soil parameters and precipitation showed their largest contribution to the yield variability with S_i = 0.41 and 0.26 respectively.

Unlike the factors controlling available soil nitrogen and water, temperature is generally the least important factor, with Tmin always ranked among the two least important factors. Exceptions occur for Tmax under 100 kg N/ha fertilisation in the dry year, when it ranked number three (Figure 3-4(g, h, and I for S_i), Figure 3-4(p, q, and r for S_{Ti})). The dry weather scenario selected in this study not only had lower precipitation but also had higher temperatures, and the perturbed Tmax in this case could exceed 40 °C in October and November, during the anthesis and grain filling stages. Wheat is sensitive to high temperatures at these stages and the final yield is reduced (Liu et al., 2016a; Stone and Nicolas, 1995).

3.4.5 Interactions between factors

The orange bars in Figure C. 2 show the total interactions for all factors. Results show that soil parameters and precipitation have the largest interactions. The largest total interactions for these two factors occurred under the 100 kg N/ha, wet weather and loamy soil scenario, the increments from S_i to S_{Ti} were 0.53 and 0.56 (Figure C. 2). Under higher fertilisation availability, wheat growth was more sensitive to the water supply. Wet weather and loamy soils retain more water which is more accessible to the plants. The interactions between soil parameters and precipitation reduced dramatically for all clay soils scenarios since the large water holding capacity reduced drainage and provided a higher reserve of water to supply plants between rainfall events.

In contrast to the soil and precipitation factors, the total interactions for the initial nitrogen content and fertilisation factors were marginal under all scenarios, being less than 0.07 and 0.04 (Figure C. 2). S_{Ti} for Tmax and Tmin increased, implying interactions between the two temperature factors and other factors. The total interactions for Tmax were always larger than those for Tmin. We suspect that this was due to the interaction between Tmax and water-related factors. Higher daily maximum temperature increases the wheat water demand, reducing soil water, and causing a stronger interaction. Tmax even ranked number two (after precipitation) for 100 kg N/ha fertilisation, dry weather conditions and clayey soils.

It is also worth noting that the sum of all first order indices from Figure 3-4 is less than one, while the sum of total indices for all scenarios is larger than one. It is clear that the sum of S_i and the sum of S_{Ti} deviate most from one for the precipitation and soil parameter factors and that these sums for other factors are with 0.9 to 1.1 (Table C. 7 and Table C. 8). This implies that most of the interactions occur between the precipitation and soils factors.

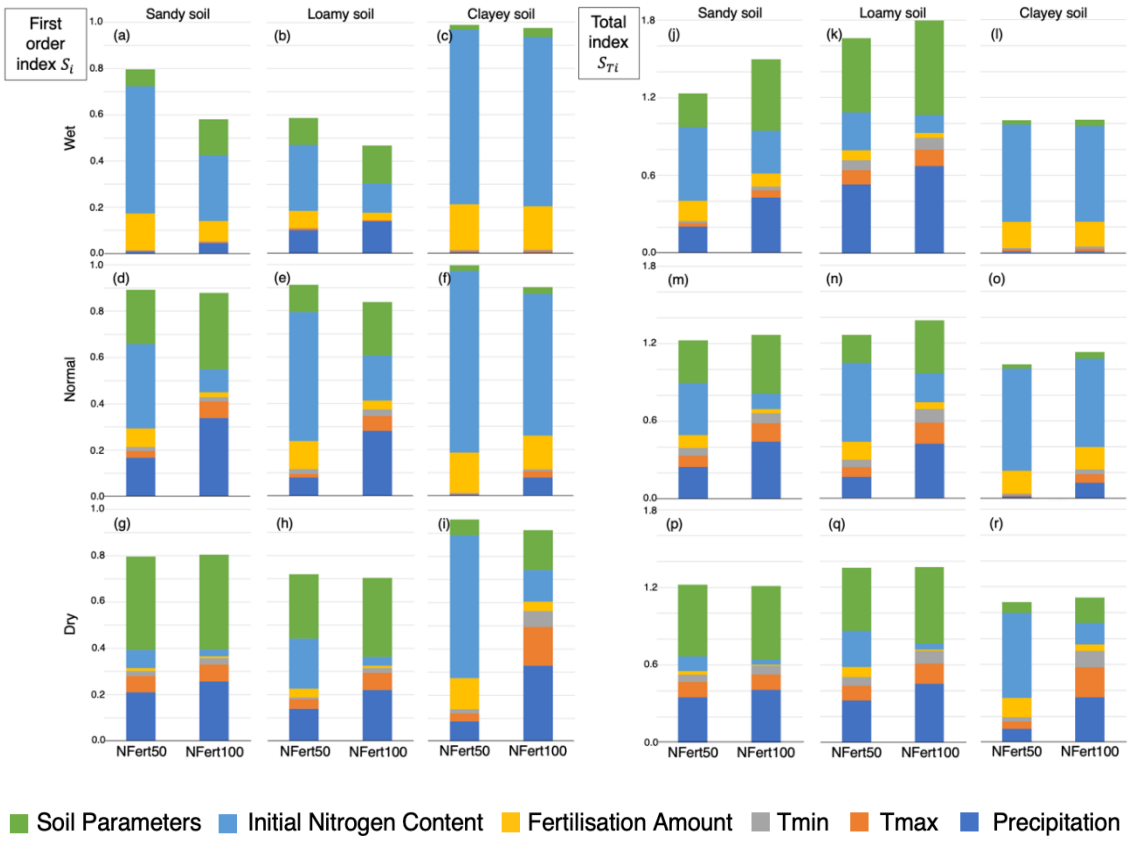

Figure 3-4. Comparison of first order and total sensitivity indices under low and high nitrogen fertilisation scenarios for six soil and weather combinations. The three subplots in the left column

show first order sensitivity indices, the three subplots in the right column are for the total sensitivity indices. Plots are grouped horizontally by soil type and vertically by weather conditions as indicated by the headings. Each sub-plot shows a pair of columns the values of the sensitivity indices for the six factors as indicated in the legend under nitrogen fertilisation levels of 50 kg N/ha and 100 kg N/ha.

3.4.6 Yield prediction variability

The sensitivity analysis above gives insight into the contribution to yield variance of the factors considered. This chapter investigates the simulated yield variability under different environmental and management conditions. The ensemble mean yield (μ) and standard deviation (σ) under all eighteen scenarios are shown in Figure 3-5 and Table C. 9.

The mean estimated yield increased when fertilisation increased from 50 kg N/ha to 100 kg N/ha. This increase in mean yield was more pronounced under wetter weather conditions and for the loamy and clayey soils. With more fertiliser, yield increased by 38% on average for the wet year on loamy and clayey soils and the normal year for clayey soils, while it increased by only 6 % for the dry year and sandy soils. It means that higher fertilisation is more effective with sufficient water supply, moderate air temperatures, and soils with higher water holding capacity. This matches our findings from the Sobol' sensitivity analysis.

The mean yield declined when the weather conditions were drier, with the yield reduction being greater for lighter soils. For the two fertilisation amounts, yield decreased by 44% and 56% for the sandy soils, while it decreased by 22% and 34% for the clayey soils. Thus, yields from light soils with lower water holding capacity were more susceptible to declining precipitation. The effect of soil on mean yield varied with weather conditions (Figure 3-5). For the wet year, the yield barely changed with soil type for either fertiliser amount. For the normal year, yield increased from sandy to clay soils for the 100 kg N/ha fertilisation level, while for the dry year, the mean yield increased markedly from sandy to clayey soils for both fertilisation amounts. For the 100 kg N/ha level, yield increased by 0%, 28 %, and 51 %, from sandy to clayey soils. Thus, soil texture had little impact on yield under favourable weather conditions, but yield was more sensitive to the soil texture under dry weather, matching our sensitivity results.

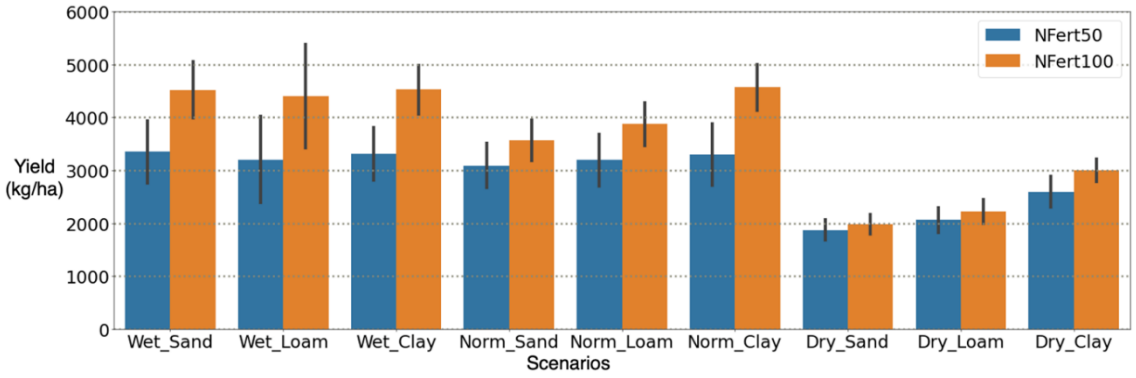

Figure 3-5. The mean estimated yield (bars) with ± standard deviation (whiskers) under all scenarios. The horizontal axis shows nine different scenario groups, each of which contains the nitrogen fertilisation level of 50 kg N/ha (blue) and 100 kg N/ha (orange). The first three groups are for the wet weather condition and each of the three soil types, the middle three groups are for normal weather conditions, and the last three for dry weather conditions.

3.5 Discussion

In Chapter 3.4, we presented the Sobol' sensitivity indices under different environmental and management conditions. We also quantified the yield prediction variability resulting from the variation of the tested factors. This chapter discusses the effects of nitrogen, water availability, and weather conditions on yield sensitivity. In addition, the implications of these results for modellers and crop managers are discussed.

3.5.1 Effects of water and nitrogen availability

APSIM-Wheat yield prediction performance was affected by factors including water and nitrogen deficit, temperature stress, and the quality of soil information. To improve confidence in our results and offer robust information for decision making under these circumstances, the model requires a site-specific calibration process to reduce uncertainty. Prioritising smaller subsets of influential parameters should reduce the model calibration workload. This sensitivity analysis tries to understand which key parameters contribute the most to uncertainties in yield under various weather, soil, and fertilisation scenarios.

Nitrogen-related factors were more important than other factors under conditions of low nitrogen supply with yield variability being more sensitive to variations in initial nitrogen content and fertilisation amount. Furthermore, the importance of these two factors decreased with high nitrogen application. The high sensitivity to nitrogen when nitrogen

supply is low is likely attributed to the fact that when water supply is sufficient, nutrients such as nitrogen become more important in affecting photosynthesis. Inadequate nitrogen availability can reduce chlorophyll content in leaves, thereby hindering the plant's ability to capture light energy and convert it into carbohydrates through photosynthesis. Consequently, limited nitrogen can directly limit a plant's capacity for energy production and biomass accumulation. Additionally, during the reproductive growth stage, inadequate nitrogen can also result in a decrease in grain number, smaller grain size, and therefore lower crop yields. The increasing importance of nitrogen-related factors in low nitrogen conditions resonates with previous research, such as the work of Pardon et al. (2017) and Zhao et al. (2014), which emphasise the dynamic nature of model parameters in response to changing conditions. Specifically, nitrogen fertilisation becomes increasingly influential, exhibiting more pronounced interactions with groundcover vegetation and legume fraction in nitrogen-deficient scenarios (Pardon et al., 2017). Conversely, under conditions of high fertilisation levels, the location (climate-soil condition), takes on greater importance in determining the sensitivities of APSIM-Wheat cultivar parameters (Zhao et al., 2014).

Conversely, the influence of water-related factors gains prominence under high water stress conditions, a similar trend was also identified by Sexton et al. (2017), Pardon et al. (2017), and Ojeda et al. (2021). Notably, parameters such as transpiration efficiency, root conductance, maximum root depth, and soil water lower limit exhibit increased interactions and importance in water-stressed environments. This can be attributed to crops undergoing critical physiological alterations when faced with a deficit in water supply. These changes encompass reduced water uptake by the roots, reduced rates of photosynthesis and transpiration, and constrained leaf expansion, which collectively exert substantial and detrimental effects on crop growth and overall production. Irrigation strategies can mitigate the impact of water-related factors, as seen in the study by Ojeda et al. (2021), where the availability of irrigation altered the influential variables from water-related parameters to non-water-related ones.

3.5.2 Implications for modellers

The results of this study indicate that the factors that most limit crop yield are the primary sources of model sensitivity. Thus, calibration or improvement efforts should focus on different subsets of parameters under different conditions. For water-limited and high-temperature conditions, accurate characterisation of precipitation, maximum temperature, and soil hydraulic parameters is crucial for accurate yield predictions, while factors affecting nitrogen content should be carefully calibrated in other conditions. Prioritising smaller subsets of influential parameters could effectively reduce the model calibration workload.

With the growing interest in assimilating ground-based and remotely sensed observations into crop growth models (Jin et al., 2018; Machwitz et al., 2014; Zhang et al., 2021), understanding the key sensitivities will assist in the optimal choice of observations to be assimilated and the design of data assimilation schemes. The detailed insights gained from this sensitivity analysis will also inform the selection and perturbation of model inputs and parameters, enabling us to effectively implement "stochastic" data assimilation techniques. By understanding the sensitivity of the model outputs to the selected parameters, we can more accurately introduce perturbations that reflect the inherent uncertainties in the system, thereby enhancing the reliability and robustness of the data assimilation process. In the case of rainfed conditions that considered, with sufficient water and nitrogen resources, among the factors included in our study (rainfall, temperature, soil properties, nitrogen), the main driver of yield variance are the factors controlling water availability. This implies that the data assimilation scheme design should focus on addressing the uncertainty in the water supply to reduce yield prediction uncertainty. However, when soils have a higher water holding capacity or nitrogen becomes more limiting to crop growth, the uncertainty in nitrogen availability should be addressed to decrease prediction uncertainty.

3.5.3 Implications for crop managers

The simulated yields in this study are similar to those observed overall in the region. This gives some confidence that the findings of this Sobol' sensitivity analysis are transferable to real-world applications. According to the Australian Bureau of Agricultural and Resource Economics and Sciences (ABARES, 2022), the state-wide average wheat yield in Victoria, Australia, was approximately 3.5 t/ha in 2022, which is consistent with the

average yield of 3.3 t/ha (from all eighteen scenarios shown in Table C. 9) reported in this study. Hochman et al. (2013) collected data on water-limited wheat fields from Yield Prophet subscribers in the Wimmera region of Victoria, Australia and reported an average yield of 1.98 t/ha. This data corresponds with our yield prediction results under dry weather condition, where the average yield is 1.93 t/ha for sandy soils and 2.14 t/ha for loamy soils (Table C. 9).

The analysis of the variability of yield prediction confirm that agricultural production is particularly sensitive to decreasing precipitation and increasing temperature trends potentially induced by changing climate. The dry weather condition restricted the final yield to less than 3 t/ha, even with clay soils and/or high fertilisation levels. Light soils are particularly susceptible to low yields under drier and warmer weather conditions. The resulting yield is likely to be lower than 2 t/ha, regardless of nitrogen fertilisation amount.

Conversely, under wet weather conditions, grain yield appears to be less influenced by soil types. When under wet or normal weather conditions, the expected yield is approximately 3.2 t/ha, regardless of soil type. Instead, crop production becomes more dependent on nitrogen availability. The sensitivity analysis found that yield is more sensitive to nitrogen availability-related factors under a fertilisation level of 50 kg N/ha, compared with 100 kg N/ha. Since 50 – 80 kg N/ha is the most common nitrogen application amount in Australia (ABARE-BRS, 2003), the amount of nitrogen fertilisation should be adjusted more carefully in management practice. Given the interplay between weather and nitrogen suggesting greater nitrogen fertilisation is more valuable under wetter conditions, while reduced fertilisation could be considered under dry weather conditions.

The initial soil nitrogen content is another important factor affecting yield variance, which also requires careful estimation. This study estimated the value based on a 100-year model spin up (1918 – 2018) as a substitute for the field measurements. Soil parameters always show a large total effect on the yield variability, and the accuracy of the estimated soil parameters will materially affect the yield prediction performance, especially under dry weather conditions and/or for light soils. Thus, good soil parameter estimation is needed prior to model usage. Hao et al. (2021) found that soil databases such as APSoil provide a reasonable alternative for specifying soil parameters if field measurements are not available.

3.5.4 Limitation and future work

One limitation of the research is the input factors' variation ranges, as the results of the sensitivity test can change depending on the magnitude and error model for perturbation. Wang et al. (2013) found that the parameter sensitivity in the WOFOST model showed significant differences depending on whether the parameter variation ranges were determined using a fixed ±10% perturbation or they were based on observations, the literature, and statistical crop data. The sensitivity of crop yield to perturbations added to key meteorological input data and parameters can guide the realistic representation of yield prediction errors when assimilating ground-based or remotely sensed observations into the model (e.g., Li et al., 2015, 2014; Nearing et al., 2012; Reichle et al., 2010, 2007). This research determined the parameter and input variation ranges based on south-eastern Australian dryland cropping conditions. Factor perturbation ranges may change under different environmental conditions. Comparing sensitivity results determined for different ranges of factor perturbation could further improve the understanding of the model behaviour.

Another limitation of this study lies in the use of single years to represent different weather conditions (wet, normal, and dry years). This does not account for variations in rainfall patterns between years with similar rainfalls. While historical wheat yields indicate total rainfall is a strong driver of interannual yield variation (French and Schultz, 1984), future studies could extend this analysis to more years to account for scenarios involving long-term variations in rainfall patterns.

The selection of the six factors considered in this paper was based on a recent review (Hao et al., 2021). Our study was specifically designed to focus on a scenario within the Wimmera district of Victoria, Australia. In the context of sensitivity analysis conducted in different scenarios, it is important to consider other influential factors affecting APSIM-Wheat yield prediction (Liu et al., 2023). For example, factors such as water logging and root disease identified as detrimental to crop yield and associated uncertainty were not considered in this work since the current version of the model does not account for their impacts. Cultivar parameters have not been tested here since Zhao et al. (2014) and Casadebaig et al. (2016) have already conducted thorough investigations of the sensitivity of APSIM-Wheat outputs (including yield) to cultivar parameters under various environmental conditions in Australia. When evaluating model prediction

sensitivity in alternative scenarios, such as different weather regimes and/or wheat cultivars, the model's sensitivity analysis should be reperformed to capture the differences in model behaviour brought about by different cultivars. Additionally, the influence of other factors, including global radiation, organic matter content, organic N, mineralization, and nitrification rate need to be further investigated.

The Sobol' method, utilising Saltelli's (2002) efficient numerical approach, was used to evaluate the sensitivity of yield predictions due to its ability to handle non-linear and non-monotonic systems. Although the Sobol' method requires a large sample size to achieve convergence of results, in our case, we used 10,000 samples for each parameter to obtain reliable outputs. It provides a more detailed and comprehensive sensitivity analysis, including main effects and higher-order interactions. Methods such as Fourier Amplitude Sensitivity Test (FAST) or extended FAST may be used to reduce the sample size and optimise computational efficiency, as they generally converge faster than Sobol' (Pianosi et al., 2016; Zhao et al., 2014). However, these methods provide a less detailed understanding of the contributions of individual input variables and their interactions to the output variance.

3.6 Conclusion

This paper presented the results of a Sobol' sensitivity analysis for APSIM-Wheat yield prediction for rainfed conditions in the Wimmera district of Victoria, Australia. The sensitivity of predicted yield was analysed for six factors based on the review by Hao et al. (2021). These were: daily precipitation, maximum and minimum temperature, initial nitrogen content, nitrogen fertilisation amount, and soil water parameters. Sensitivity was analysed for eighteen scenarios which were combinations of three weather conditions (wet, normal, and dry years), three soil types (sandy, loamy, and clayey soils), and two fertilisation levels (50 and 100 kg N/ha). Convergence checks and bootstrap-based confidence intervals showed that estimated sensitivity indices were very reliable.

The Sobol' sensitivity indices revealed that the ranking of factors was significantly affected by environmental and management conditions. APSIM-Wheat yield prediction tended to be more sensitive to the variability of limiting factors. Under dry weather conditions, the water deficit and high temperatures affected yield more, with precipitation and soil parameters having the highest sensitivity indices. When the weather

1 became wetter, the stress gradually transferred to nitrogen availability, particularly in the
2 lower fertilisation cases and the sensitivity of nitrogen factors increased. Precipitation
3 and soil parameters have larger total interactions for sandy and loamy soils. The
4 interactions are more noticeable under 100 kg N/ha. Tmax and Tmin also showed
5 interaction effects but of a smaller magnitude, while the total interactions of initial
6 nitrogen content and fertilisation amount were marginal. The larger total interactions of
7 the two water-related factors increased their influences on the yield variability. The
8 analysis of ensemble mean yield showed that clay soils were less affected by changes
9 between wet and dry conditions. Yield also showed less variability under dry weather
10 and higher fertilisation levels. In contrast, more humid weather conditions resulted in
11 higher yields, but with greater yield variability, regardless of soil type. We anticipate that
12 our results can help to reduce uncertainty in the application of the APSIM crop model as
13 well as other crop models.
14
15

Chapter 4 Remote sensing observations for updatable state variables in APSIM-Wheat model

4.1 Abstract

The relationship between satellite observations and model state variables is crucial within the data assimilation framework. To facilitate this, an observation operator is needed to map predicted state variables to equivalent remote sensing observations. In this study, various vegetation indices with different band combinations derived from Sentinel-2 were evaluated for suitability in developing an observation operator for the APSIM-Wheat model data assimilation. Indices such as the green leaf area index (GLAI), wide dynamic range vegetation index (WDRVI), chlorophyll index (CI), and normalised difference vegetation index (NDVI) were linked with APSIM-Wheat simulated GLAI by using the LOWESS curve-fitting method for a rainfed winter-wheat field located in north-western Victoria, Australia. The linearity of the fitted curves was evaluated to determine the most suitable index. RMSE of the developed model was computed as the observation uncertainty. The results indicated that distinct observation operators are necessary for the pre- and post-GLAI peak periods, as the trends observed during these growth stages differed. The most appropriate candidate for an observation operator is the CI calculated using the red edge and near-infrared bands, as the corresponding models exhibited the closest approximation to linearity. The NDVI exhibited saturation at moderate to high GLAI values. However, if only developing an observation operator for the post-GLAI peak period, it is recommended to use green NDVI due to its minimal uncertainty and the most linear curve.

4.2 Introduction

Process-based crop models, such as APSIM, are widely used as predictive tools to provide information for crop management to optimise sources utilisation and improve productivity. However, as reported by Hao et al. (2021), poor calibration and stresses

related to water, nitrogen, heat, and frost, can negatively impact the performance of APSIM-Wheat yield predictions. Remote sensing data has the potential to provide insights into crop growth status in response to spatial and temporal variability. Integrating crop model simulations and remote sensing observations through data assimilation can enhance in-season crop growth modelling and ultimately lead to improved yield estimates. However, satellite observations are not directly comparable to model states as they characterise surface reflectance measurements. Therefore, an observation operator, which translates model state variables into equivalent remotely sensed observations, is needed as a crucial component of the data assimilation system.

When assimilating satellite observations into crop models, the observation operator can be presented in various forms, such as empirical relationships or radiative transfer models. De Wit and van Diepen (2007) assimilated volumetric soil moisture estimated from the soil water index data into the WOrld FOod STudies (WOFOST) model, updating the soil moisture state by using an identity matrix as the observation operator, since the model state is observed directly. Jiang et al. (2014) used a leaf area index (LAI) function as the observation operator to assimilate LAI into the Crop Environment Resource Synthesis (CERES)-Wheat model. The function calculated LAI with model state variables including plant leaf area, senesced leaf area, growth plant area, and reduced leaf area. Thorp et al. (2012), Wu et al. (2013), Machwitz et al. (2014), and Huang et al. (2019) applied the combined PROSPECT leaf optical properties model and SAIL canopy bidirectional reflectance model (PROSAIL) as an observation operator to associate spectral reflectance with model state variables. Surface reflectance measurements from a portable field spectroradiometer (Thorp et al., 2012), a portable chlorophyll meter (Wu et al., 2013), RapidEye (Machwitz et al., 2014), and MODIS (Huang et al., 2019b) were assimilated into crop models such as Decision Support System for Agrotechnology Transfer (DSSAT), WOFOST, and Agricultural Production Systems sIMulator (APSIM).

In this work, we develop empirical models to link Sentinel-2 retrieved vegetation indices (VIs) with the green leaf area index (GLAI) simulated by the APSIM-Wheat model (Holzworth et al., 2018). The suitability of various vegetation indices is evaluated based on the model's linearity. Additionally, uncertainty is calculated for the developed models. The methodology of this study enables the assimilation of satellite-derived vegetation observations into crop models.

4.3 Methods

4.3.1 Study area

Figure 4-1 shows the geographic location and yield map of a 2019 winter wheat (*Triticum aestivum L.*) paddock in north-western Victoria, Australia. The field was rainfed and managed with nitrogen fertilisation, with urea applied at 50 kg N/ha and 60 kg N/ha on July 1st and 31st, respectively. Wheat was sown on May 12th and harvested in mid-December. The climate in the study area is semiarid, with an average annual rainfall of 240-520 mm in the past 30 years, most of which falls between May and October. The paddock had an average yield of 5.9 t/ha for the 2019 season. The blue rectangles in Figure 4-1 represent seven selected regions of interest (ROIs) with yields ranging from 3 to 8 t/ha and an average yield of 5.5 t/ha. These ROIs were chosen to represent the within-field yield variability and the overall paddock yield level. The APSIM-Wheat model was calibrated for each ROI to ensure that the predicted yields matched the observed yields.

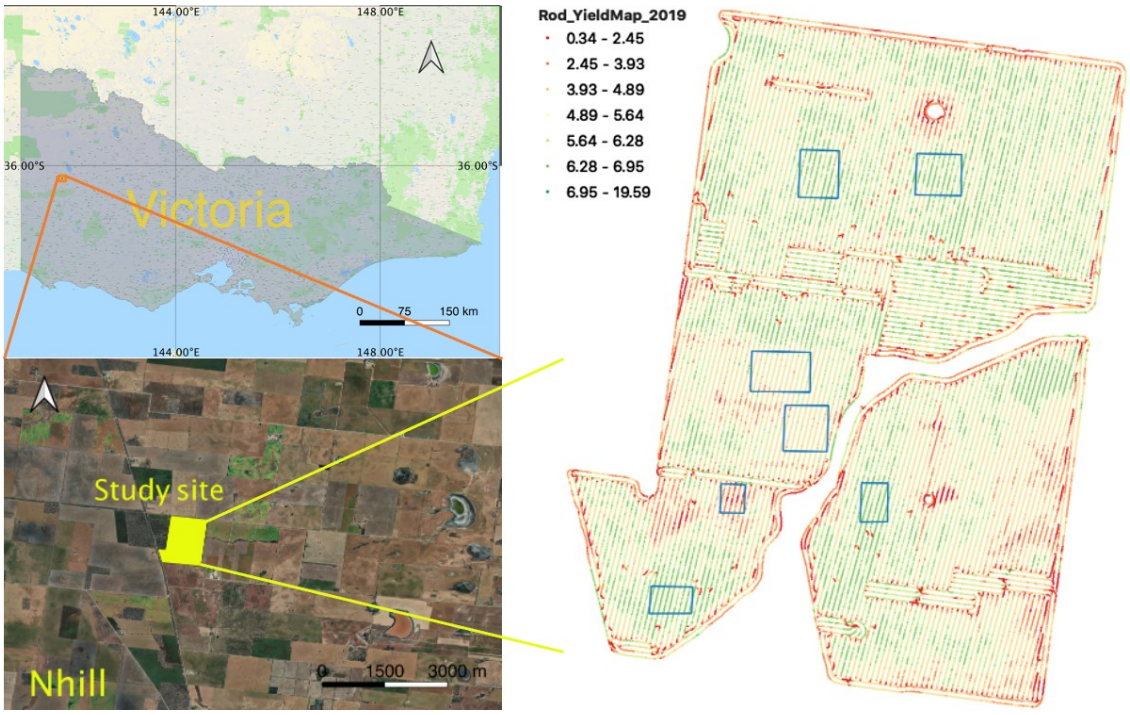

Figure 4-1. The geographical location of the study area and selected ROIs (blue rectangle: selected ROIs)

4.3.2 Vegetation indices

APSIM-Wheat simulated green leaf area index (GLAI) was chosen as the state variable to be mapped to the observation space. Sentinel-2 was selected as the observation source due to its high spatial resolution of 10/20 m and temporal resolution of 5 days, which is sufficient to capture within-field variability and provide timely observations of crop status.

Four Sentinel-2 derived vegetation indices (VIs) with different band combinations were nominated for the development of the observation operator: GLAI, wide dynamic range vegetation index (WDRVI), chlorophyll index (CI), and normalised difference vegetation index (NDVI). The band settings and calculations for these VIs are listed in Table 4-1. These indices were selected based on their close relationship to chlorophyll content (Gitelson et al., 2003a, 2003b) and the fact that chlorophyll content has been shown to be closely related to GLAI (Boegh et al., 2013). Therefore, the nominated VIs are potentially closely related to APSIM-Wheat simulated GLAI.

Table 4-1. Multispectral vegetation indices investigated in this study (S: Sentinel-2, α, a, b, c used in calculating WDRVI and GLAI follow values proposed by Nguy-Robertson et al. (2014)

Index category	Vegetation index	Equations (for Sentinel-2)	Resolution	Reference
WDRVI	Red WDRVI	$(\alpha \cdot NIR_{S8} - Red_{S4})/(\alpha \cdot NIR_{S8} + Red_{S4}) + (1 - \alpha)/(1 + \alpha)$	10 m	Gitelson (2004), Peng and Gitelson (2011)
	Green WDRVI	$(\alpha \cdot NIR_{S8} - Green_{S3})/(\alpha \cdot NIR_{S8} + Green_{S3}) + (1 - \alpha)/(1 + \alpha)$	10 m	
	Red edge WDRVI	$(\alpha \cdot Red\ edge_{S7} - Red\ edge_{S5})/(\alpha \cdot Red\ edge_{S7} + Red\ edge_{S5}) + (1 - \alpha)/(1 + \alpha)$	20 m	
GLAI	Green GLAI	$a \cdot Green\ WDRVI^2 + b \cdot Green\ WDRVI + c$	10 m	Nguy-Robertson et al. (2014)
	Red edge GLAI	$a \cdot Red\ edge\ WDRVI^2 + b \cdot Red\ edge\ WDRVI + c$	20 m	
CI	Green CI	$(NIR_{S8A}/Green_{S3}) - 1$	20 m	Gitelson et al. (2005, 2003)
	Red edge CI	$(Red\ edge_{S7}/Red\ edge_{S5}) - 1$	20 m	
NDVI	Red NDVI	$(NIR_{S8A} - Red_{S4})/(NIR_{S8A} + Red_{S4})$	20 m	Rouse et al. (1973)
	Green NDVI	$(NIR_{S8A} - Green_{S3})/(NIR_{S8A} + Green_{S3})$	20 m	Gitelson and Merzlyak (1994)
	Red edge NDVI	$(Red\ edge_{S7} - Red\ edge_{S5})/(Red\ edge_{S7} + Red\ edge_{S5})$	20 m	

4.3.3 Observation operator development

The APSIM model was first calibrated for each ROI to ensure that the simulated yields matched the observed yields, and the APSIM GLAI curve was derived. The atmospherically corrected Sentinel-2 satellite imagery was used to generate VI time series at each ROI. The APSIM GLAI curve and Sentinel-2 VI time series were then compared. The LOcally WEighted Scatterplot Smoothing (LOWESS) method was used to establish a model connecting APSIM GLAI and Sentinel-2 VIs over the growing season. The root mean squared error (*RMSE*) between LOWESS-predicted VIs and Sentinel-2 VIs were calculated to assess the fit of the LOWESS curves. The *RMSE* value was also treated as the observation operator uncertainty. APSIM GLAI and VI values were normalised to calculate the slope, which was used as a measure of the curve linearity to select the ideal VI candidate.

4.3.3.1 Calibration of APSIM

To match the APSIM simulation with satellite observations, the APSIM model needs to be calibrated at each ROI. Model calibration involves adjusting soil hydraulic parameters and fertilisation amounts due to their variability within the field. The lower limit of 15 bar (*LL15*), drained upper limit (*DUL*), crop lower limit (*CLL*), and saturation (*SAT*) were tuned to determine the soil water holding capacity. The total fertilisation amount was adjusted from 90 to 120 kg N/ha. Daily weather data was obtained from the nearest climate station, Nhill (Woorak) (Bureau of Meteorology). The base initial nitrogen content was initialised from a 100-year model spin up (1918 – 2018) with a fertilisation rate of 80 kg N/ha during every growing season. The APSIM simulated yield and *in situ* yield measurements were used as benchmarks for calibration.

4.3.3.2 Processing of Sentinel-2 VIs data

All available and cloud-free surface reflectance data from Sentinel-2A and -2B for 2019 were used to calculate pixel-scale vegetation indices for each ROI on the Google Earth Engine cloud platform (Gorelick et al., 2017). The VIs baseline for each pixel was then calculated and subtracted from each VI value to ensure the reflectance properties from objects other than crops are excluded. The baseline was defined as the minimum VI value throughout 2019 that was larger than zero (Perry et al., 2014). The adjusted VIs (= Original VIs - Baseline VIs) of all pixels within each ROI were averaged to obtain VI time series data.

4.3.3.3 Consideration of growing periods

The LOWESS regression lines between APSIM GLAI and Sentinel-2 VIs showed different trends at the increasing and decreasing sides of the growth cycle, which were defined as the pre- and post-APSIM GLAI peak periods (Figure 4-2). Therefore, the observation operator should be developed separately for these two growing periods. September 21st was identified as the GLAI peak time based on calibrated APSIM simulations for all seven ROIs.

The LOWESS curve-fitting method was used to develop the model. At each point in the data set, a polynomial is fit to a subset of the data using weighted least squares, with more weight assigned to points near the point whose response is being estimated and less weight to points further away. There were 163 and 96 data points at the pre- and post-APSIM GLAI peak growing periods, respectively. The number of points used as the subset of the data to fit the polynomial was 27 and 16, respectively. Figure 4-2 shows the fitted LOWESS curves, which will be considered as the developed observation operators.

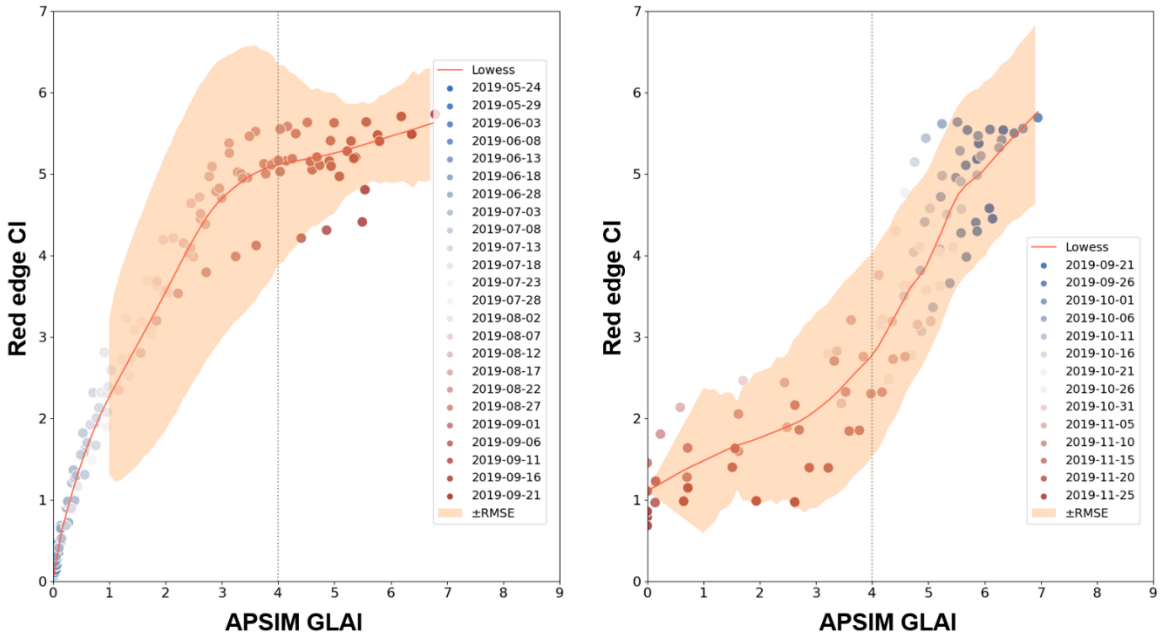

Figure 4-2. The LOWESS function and the different trends at the pre- and post-GLAI peak growth periods (a: pre-GLAI peak period; b: post-GLAI peak period)

4.3.3.4 Uncertainty assessment

Properly accounting for observation uncertainty in data assimilation is important. In our case, the observation uncertainty can be estimated by calculating *RMSE* between the APSIM GLAI simulation and satellite VI observations along the LOWESS fitting curves

to assess the average difference between them. *RMSE* will be used as the measure of the observation uncertainty in the following data assimilation.

The orange shaded areas along the LOWESS curves in Figure 4-2 denote the ±*RMSE*. The *RMSE* calculation started from where the APSIM GLAI value was equal to one. A window of size two was set, and all points within the window were used to calculate the *RMSE* value for the centre point. The window moved forward with a step of 0.1 to calculate the *RMSE* along the entire LOWESS curve.

4.3.3.5 Curve linearity

To find a suitable vegetation index for use as an observation, the slope of the LOWESS curve between APSIM GLAI and each VI candidate was evaluated as a measure of the curve linearity. Researchers have found that normalised difference VIs are sensitive to low to moderate GLAI values but tend to saturate at moderate to high GLAI values (Gitelson et al., 2003b; Huete et al., 2002). This insensitivity can cause VIs to show minimal variation with varying APSIM GLAI values, with almost the same value of VIs corresponding to GLAI values ranging from 4 to over 6 m^2/m^2 (Nguy-Robertson et al., 2012). Therefore, it is necessary to calculate the curve slope at the GLAI=4 m^2/m^2 point and find the VI candidate with the most linear fitted curve (the curve slope most proximate to one). To ensure that VIs with different value ranges can be compared with each other, the normalised APSIM GLAI and VI values were calculated for the comparison.

4.4 Results

4.4.1 The selection of ideal observation candidate

The selection of a suitable vegetation index was based on the slope of the fitted curve between APSIM GLAI and VI candidates. Figure 4-3 shows the fitted curves and their slopes between the rescaled APSIM GLAI and rescaled red edge-based vegetation indices during the pre-GLAI peak period. The values were rescaled using the equation $x' = \frac{x - x_{min}}{x_{max} - x_{min}}$. The turning point, a vertical line of GLAI=4 m^2/m^2 (corresponding to a rescaled GLAI value of 0.58 m^2/m^2), served as the baseline reference for estimating the curve slope. This slope represents the change in satellite VI observations with respect to the variations in APSIM GLAI. We only evaluated the linearity of the fitted curves during the pre-GLAI peak period since all fitted curves developed during the post-GLAI peak

period exhibited more linear tendencies, with slopes ranging from 0.95 to 1.41 (Table 4-2).

The red edge-based indices were found to have the most linear curves among all three band combinations during the pre-GLAI peak period, and the red edge CI was the most suitable candidate for developing an observation operator with a slope value of 0.21 (Table 4-2). Some VIs exhibit a negative slope with APSIM GLAI due to a temporal shift between the APSIM GLAI and VI curves. When the VI values are increasing, the APSIM GLAI has already peaked and started to decrease. This likely results from using only yield data to calibrate the model. APSIM was calibrated to match the simulated yield with the observed yield. However, this approach does not ensure alignment between the APSIM GLAI and the observed GLAI. NDVI with all three different band combinations exhibited saturation at moderate to high APSIM GLAI values, making it the least suitable candidate. This saturation has also been reported by Gitelson et al. (2003b) and Huete et al. (2002).

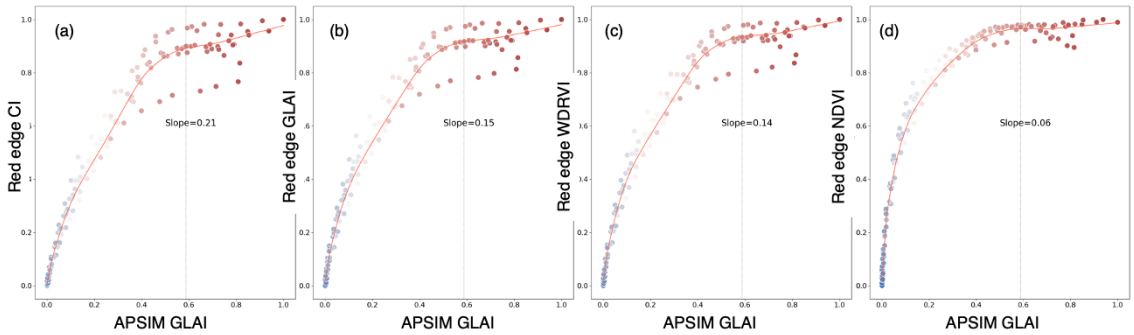

Figure 4-3. The comparison of curve slope among red edge CI, GLAI, WDRVI, and NDVI (with positive slope values). Only the slope of the fitted curves during the pre-GLAI peak period is displayed. The vertical line of rescaled GLAI=0.58 m^2/m^2 (corresponding to GLAI value=4 m^2/m^2) served as the baseline reference for estimating the curve slope.

Table 4-2. The fitted curve slope for all candidate vegetation indices during the pre- and post-GLAI peak period

Vegetation index	The slope at pre-GLAI peak period	The slope at post-GLAI peak period
Red WDRVI	-0.13	1.16
Green WDRVI	-0.11	1.13
Red edge WDRVI	0.14	1.36
Green GLAI	-0.06	1.17

Red edge GLAI	0.15	1.41
Green CI	-0.02	1.22
Red edge CI	0.21	1.41
Red NDVI	-0.14	0.95
Green NDVI	-0.12	0.98
Red edge NDVI	0.06	1.37

4.4.2 Operator uncertainty

Red edge CI was selected as the observation to develop an observation operator for data assimilation. The *RMSE* of the fitted curve was used as the measure of the observation uncertainty. Equations (4-1) – (4-7) list the observation uncertainty during the pre- and post-GLAI peak periods. The uncertainty was represented by piecewise functions for both periods.

(1) Observation uncertainty for the pre-GLAI peak period:

$$y = 0.69x + 0.32 \quad (0 \le x < 2) \tag{4-1}$$
$$y = 1.7 \quad (2 \le x < 3) \tag{4-2}$$
$$y = -0.49x + 3.16 \quad (3 \le x < 5.6) \tag{4-3}$$
$$y = 0.25x - 0.93 \quad (5.6 \le x) \tag{4-4}$$

(2) Observation uncertainty for the post-GLAI peak period:

$$y = 0.29x + 0.28 \quad (0 \le x < 3.53) \tag{4-5}$$
$$y = -0.09x + 1.62 \quad (3.53 \le x < 6.41) \tag{4-6}$$
$$y = 0.15x + 0.05 \quad (6.41 \le x) \tag{4-7}$$

4.4.3 Method validation

The method for developing the observation operator is validated within the data assimilation framework to enhance yield prediction using APSIM-Wheat and satellite vegetation observations. The LOWESS curves fitting results for red edge CI from Sentinel-2 and PlanetScope, compared against APSIM-simulated GLAI, are utilised in a synthetic experiment (Chapter 5) to demonstrate its efficacy in improving model yield estimates. Furthermore, this observation operator development method is applied in real case data assimilation (Chapter 6) and confirms its reliability in establishing the relationship between observations and model states, leading to improved model yield estimates.

4.5 Conclusion

This work developed an approach for establishing observation operators that connect satellite observations to model simulated states for use in a data assimilation framework. Ten vegetation indices with different band combinations were tested. The LOWESS curve-fitting method was used to develop the model and the *RMSE* was computed along the curve as the observation operator uncertainty. We found that individual observation operators should be developed for the pre- and post-GLAI peak periods, as the curves showed different trends during these two growth stages. The red edge CI was demonstrated to be the most suitable candidate, as the curve fitted between it and the APSIM GLAI was closest to linear during the pre-GLAI peak period. Therefore, it was selected as the observation in the following data assimilation work. In contrast, NDVI-based vegetation indices tend to saturate at moderate to high GLAI values. If only developing an observation operator during the post-GLAI peak period, green NDVI is recommended to be the observation as it has the least uncertainty and the most linear curve.

Chapter 5 Assimilating remotely sensed green leaf area index for wheat yield estimates: a synthetic experiment

5.1 Abstract

Accurate crop yield prediction is crucial for adapting farm management, especially given an increase in extreme weather conditions related with climate change and other environmental influences. While crop growth models or remote sensing methods can be used to predict yield, their respective yield prediction skills can be improved by integrating them via data assimilation. In this study, a synthetic experiment was designed using the Ensemble Kalman filter (EnKF) method to investigate the potential improvement in wheat yield estimation by assimilating green leaf area index (GLAI) observations into crop growth model, APSIM-Wheat. The experiment compared the results from (1) updating only the leaf biomass and all biomass components; (2) updating at a 5-day and 1-day frequency; and (3) updating across the whole season, only prior to the GLAI peak, and only the post-GLAI peak growth stages. The resulting field-level APSIM-Wheat yield prediction performance for a rainfed winter-wheat condition in north-western Victoria, Australia is focussed on. The most effective data assimilation strategy was determined and validated for eight representative cases spanning high, median, and low yield estimates. The results showed that updating all biomass components across the whole growing season at a daily frequency resulted in the best yield prediction performance while a 5-day updating frequency was more realistic considering the availability of currently operational satellite observations. For the eight validation cases, the updating every 5 days for the whole season decreased the yield prediction *residual* from 230-2134 kg/ha to 93-533 kg/ha. The *standard deviation* was also decreased by 41.7-66.7%. This work provides a detailed exploration of the efficacy when assimilating GLAI observations into APSIM-Wheat to improve the model yield prediction performance. The findings provide guidance for crop model data assimilation

practices more generally in choosing suitable observations in connection with model state variables and determining the updating frequency and stage.

5.2 Introduction

Climate changing including the increase of weather extremes as well as a growing population pose threats to food security and socioeconomic stability. Timely prediction of crop yield can contribute to efficient farming practice decisions, optimising resource usage efficiency, and securing food production (Boas et al., 2021; Horie et al., 1992a). Various tools are used to monitor agricultural systems and predict yield, such as biophysical crop models and remote sensing techniques (Bouman, 1995; Jin et al., 2018).

Process-based biophysical models are widely used to provide in-season crop growth simulation and yield estimation (Basso et al., 2013; Basso and Liu, 2019; Boas et al., 2021; Togliatti et al., 2017). In essence, these models simulate the biological and physical processes linking soil, climate conditions, and other factors to crop yield outcomes. However, due to the complexity of climate-soil-crop interactions, prediction uncertainties originate from model structure, forcing inputs, parameters, and observations (Vrugt et al., 2008). These modelling uncertainties limit cropping system predictability (Challinor and Wheeler, 2008; Ramirez-Villegas et al., 2017; Seidel et al., 2018). On the other hand, remote sensing data allows for large-scale crop monitoring and yield forecasting. The empirical method is widely used for this purpose. It is based on the correlation between remote sensing measurements and field-measured yield data, which is utilised to train statistical models or machine learning models (Čorňák and Delina, 2022; Muruganantham et al., 2022). However, these developed models also have inherent uncertainties (Foody and Atkinson, 2002; Povey and Grainger, 2015). Integrating remote sensing data into crop models can reduce the uncertainties from both sources and provides a way to simulate crops and predict yields with spatial variability. Remote sensing observations can be integrated into crop modelling in different ways: “calibration”, “forcing”, and “updating” methods (Jin et al., 2018). The calibration method relies on remote sensing observations to adjust model initial conditions or calibrate parameters to minimise the difference between model simulations and observations (Claverie et al., 2009; Clevers et al., 1994; Jégo et al., 2012; Liu et al., 2014; Ma et al., 2013). The forcing method directly replaces some model state variables with the remote sensing observations (Bouman, 1995; Jongschaap and Schouten, 2005; Thorp

et al., 2010; Yao et al., 2015). One obvious drawback of these two methods is considering remote sensing observations as the truth without accounting for their biases. The updating method, also known as data assimilation, explicitly takes into account uncertainties in both model simulations and observations in order to continuously update the state variables of the model.

Among the available data assimilation algorithms, the Ensemble Kalman Filter (EnKF) (Evensen, 2003) is one of the most popular methods used for improving model performance due to its computational efficiency and ability to deal with non-linear and high-dimensional model systems. It has been widely adopted in other environmental models, such as land surface, hydrological, meteorological, and climate models (Carrassi et al., 2018; Helmert et al., 2018; Lahoz and Schneider, 2014; Moradkhani and Sorooshian, 2009; Sun et al., 2016). The filter weighs the uncertainties from both observations and background predictions to update the values of certain state variables. For crop modelling, the EnKF has already been applied to DSSAT (Chakrabarti et al., 2014; Ines et al., 2013; Nearing et al., 2012), WOFOST (Curnel et al., 2011; de Wit and van Diepen, 2007; Huang et al., 2016; Pauwels et al., 2007; Wang et al., 2013b; Zhao et al., 2013), AquaCrop (Lu et al., 2021b), SAFY (Kang and Özdoğan, 2019; Silvestro et al., 2021, 2017) and Agricultural Production Systems sIMulator (APSIM) (Kivi et al., 2022; Zhang et al., 2021; Zhang et al., 2022) with varying assimilation performance.

Some studies using the EnKF have shown improved accuracy of the final yield estimates by integrating remotely sensed vegetation and/or soil observations with model simulations. Wang et al. (2013) and Zhao et al. (2013) integrated satellite-derived leaf area index (LAI) observations into the WOFOST model using an EnKF to effectively reduce maize yield prediction errors at regional scale in north-western and north-eastern China. Kang and Özdoğan (2019) used satellite LAI observations and yield statistics to calibrate the SAFY maize model at a county level. Then LAI observations were assimilated into the calibrated model using the EnKF to improve the yield prediction at a paddock level. In the abovementioned studies, the ground measured soil parameters, GLAI, and/or yield data were used to calibrate the model prior to data assimilation. These site-specific calibration measures ensured the model to have a smaller uncertainty.

The performance of data assimilation can be inconsistent under different conditions. Lu et al. (2021) found that jointly-assimilating *in situ* canopy cover and soil moisture (SM)

observations into AquaCrop improved maize yield prediction performance at the field-level. Ines et al. (2013) showed that DSSAT-Maize yield predictions were generally improved when both MODIS LAI and AMSR-E SM observations were integrated into the model at a county-level aggregated scale. But the results also suggested that under extremely wet conditions, integrating only LAI might be more effective. Chakrabarti et al. (2014) found that when the rainfed soybean crop was affected by drought, the accuracy of the DSSAT yield prediction was improved more by assimilating the downscaled 1-km SM observations from the SM and Ocean Salinity (SMOS) mission.

Some other studies found limited improvement in prediction performance at times using an EnKF. The lack of correlation between different state variables constrained the efficacy of the filter. Pauwels et al. (2007) and Zhang et al. (2022, 2021) found that updating wheat state variables did not improve the soil water and soil nitrogen state estimation accuracy using WOFOST and APSIM, and vice versa. In a separate study, Kivi et al. (2022) concluded that by assimilating daily *in situ* SM observations into the APSIM, the soil water and the soil nitrogen cycles were better characterised, while the impact on LAI and yield was negligible. Nearing et al. (2012) reported that assimilating LAI observations into the DSSAT model did not transfer into improving the wheat yield estimation.

Grain development is controlled by multiple factors such as weather conditions, cultivar characteristics, and soil parameters, updating only the leaf state variable(s) is inadequate in correcting grain growth. Curnel et al. (2011) found that the assimilation of the LAI in WOFOST led to poor results, as the phenological development simulated by the model and the observed development did not match. Zhang et al. (2022) indicated that correcting the phenological stage simulation could lead to a better yield estimation. However, the phenological stage observations are difficult to obtain.

Various studies have also underlined that accurately quantifying model and observation errors is decisive in the effectiveness of the EnKF (Kivi et al., 2022; Tandeo et al., 2020). De Wit and van Diepen (2007) found that if the errors of the WOFOST model and the SM satellite observations were underestimated, this could lead to an insignificant improvement in the predictions for wheat and maize yields.

Past studies have tested the efficacy of EnKFs or particle filters (PF) to assimilate observations at different growth stages for improving APSIM model estimates. Zhang et al. (2022, 2021) explored the potential improvements due to assimilating wheat and/or soil observations in APSIM during various phenological stages. The results suggested that assimilating only leaf area index, or aboveground biomass, or surface SM could avoid over-correction and resulted in a better yield estimation. The correction of simulated phenological stage led to an improved yield estimation due to the reduced uncertainties caused by temperature and cultivar parameters. Kivi et al. (2022) effectively improved the soil water and soil nitrogen estimates by integrating daily SM measurements into APSIM, which improved the estimated tile drainage flow and annual NO_3 load. However, differing from Zhang et al. (2022), they did not find obvious improvements in LAI or yield estimates. This was likely due to the limited potential of SM updates to improve wheat state variables for a site without water stress. Machwitz et al. (2014), Ziliani et al. (2022), and Lei et al. (2020) all employed PFs to assimilate satellite-derived aboveground biomass, LAI, and surface SM observations into APSIM to effectively improve the yield and soil moisture estimates. The results demonstrated the ability of the PF to handle the nonlinear relationship between model simulations and observations.

To summarise, achieving robust crop yield estimation by integrating crop models and remotely sensed observations using an EnKF still faces challenges. Most studies on data assimilation in crop models evaluated performance by integrating multiple sources of observations, such as soil moisture, and biomass/LAI, into crop models. Some studies used field measurements, including soil hydraulic parameters, yield data, and phenological observations, to calibrate the model prior to or during data assimilation to ensure its efficacy. However, obtaining multiple sources of observations and field-measured data necessitates additional resources. Additionally, the lack of correlation between different state variables limited the efficacy of the filter. The effectiveness of incorporating a single-source vegetation observation from optical satellite imagery into APSIM has not yet been assessed under controlled conditions for varying updating intervals, phenological stages, and updated biomass state variables. A comprehensive synthetic experiment should be conducted to validate the performance of various updating strategies and identify the most effective data assimilation scheme.

In this study, we will explore the efficacy of integrating simply obtained remote sensing vegetation observations into the APSIM model to improve the field-level wheat yield prediction. Considering the importance of accurately quantifying model and observation errors, a comprehensive uncertainty estimation is carried out. Based on a synthetic experiment, we propose to identify which observations are more suitable to update the model states, and to explore different updating strategies in terms of interval, phenological stage, and the wheat biomass components updated. The proposed observations are selected to be easily acquired from satellite sources, with well-developed retrieval algorithms available, and closely related to the wheat biomass state variables. The biophysically determined cross-correlation among all simulated biomass components is discussed in order to analyse if updating all components can achieve a higher efficacy other than updating only the leaf biomass. The developed data assimilation strategy is validated using various cases with high, median, and low yield estimates.

5.3 Materials and methods

5.3.1 Study site

The study site is a rainfed winter-wheat (*Triticum aestivum* L.) field located in north-western Victoria, Australia during 2019 (Figure 5-1). The climate type in this area is semiarid, with an average annual rainfall varying from 240 to 520 mm over the past 30 years, with most rainfall occurring between May and October (Bureau of Meteorology, 2020). The area under cultivation was 106 ha, with an average yield of 5.9 t/ha and large spatial variations due to different soil properties. For example, the clay content in the top 30 cm of the soil decreases from the northeast to the southwest (ASRIS, 2011).

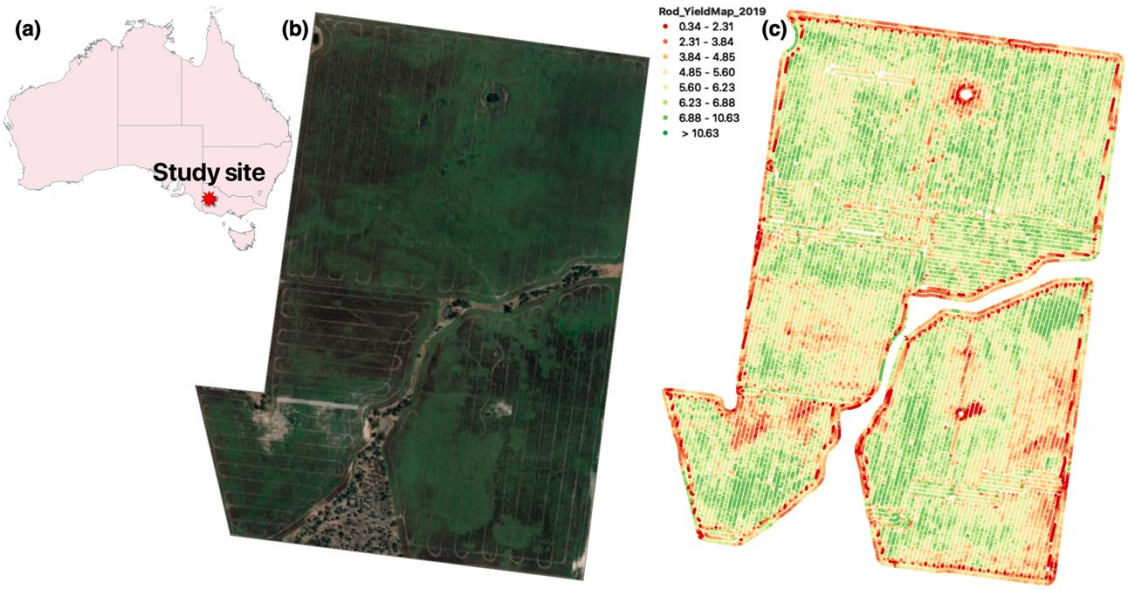

Figure 5-1. The study site location, (a) the paddock is located in north-western Victoria, Australia, (b) a satellite image of the paddock, and (c) ground measured yield data shown in tonnes per hectare (t/ha).

5.3.2 APSIM-Wheat and input datasets

The APSIM-Wheat model (Next Generation) (Holzworth et al., 2018, 2014b) was used to simulate biophysical processes of daily wheat growth. The Wheat, SoilWat, SoilN, Weather, and Fertilisation modules are the main components linked within APSIM to account for the interaction of wheat with the environment and management. The SoilWat module calculates the soil water dynamics based on a multi-layer cascading water balance model. The key parameters describing the soil water holding characteristics include lower limit of 15 bar (LL15, the wilting point), drained upper limit (DUL, the field capacity), crop lower limit (CLL), and saturation (SAT). The SoilN module considers three organic matter pools (fresh, biom, and hum) to simulate the conversion of nitrogen and carbon in each soil layer through processes including nitrification, denitrification, mineralisation, and immobilisation, thereby calculating the available nitrogen in soils based on the crop residuals and fertiliser inputs. The Weather module takes in daily meteorological information, including precipitation, global radiation, maximum and minimum temperature, and feeds the information to other modules, such as Wheat, SoilWat, and SoilN. The Fertilisation module is a self-defined script specifying the amount and timing of nitrogen fertilisation.

The Wheat module accounts for biomass supply from four sources: fixation (photosynthesis), uptake, retranslocation, and reallocation. Fixation is based on a radiation use efficiency model. The income biomass is determined by the leaf area index (LAI), solar radiation, and radiation use efficiency. Water, nitrogen, and temperature stress are considered to affect the actual biomass accumulation. Uptake is mostly relevant to nitrogen (N) and carbon. The root organ absorbs mineral N and carbon substrates from the soil, the leaf organ uptakes foliar-applied N. Retranslocation and reallocation supply biomass from a "live" or a "senescing" organ. The total biomass supply is then allocated to form five wheat organs: leaf, stem, spike, grain, and root biomass (Brown et al., 2019). The allocation to each organ is determined by their relative demands (g g^{-1}) for biomass:

$$RelativeDemand[o] = \frac{Demand[o]}{TotalDemand} \quad (5\text{-}1)$$

where $[o]$ represents the particular organ. $TotalDemand$ is the sum of $Demand[o]$ for all organs. Organs with a greater relative demand receive a greater share of the biomass supply. The $Demand[o]$ for each organ is determined by specific parameters and stress factors that vary with phenological stages and environmental conditions. As a result, biomass allocation changes accordingly.

APSIM requires a range of information to be specified. The management information was collected from the crop grower. Wheat was sown on 12 May 2019 at a rate of 120 plants/m^2, a depth of 30 mm and a row spacing of 300 mm. Urea was applied at the rate of 50 kg N/ha and 60 kg N/ha on 1 July and 31 July, respectively. Soil information was obtained by selecting a suitable soil profile from the APSoil database (Oliver and Robertson, 2009) (Table D. 1). The selection was based on the soil profile's similarities to ground-based soil textures and soil moisture measurements. Seven soil layers were considered, with 10 cm thickness in each of the top five soil layers and 40 cm in the deepest two layers. The rooting depth is 130 cm. Hao et al. (2021) reported that parameters derived from APSoil lead to acceptable performance in APSIM-Wheat yield predictions (RMSE=0.7 t/ha). The amount of initial soil water content in each layer was defined as the value between LL15 and DUL. Other initial model states were specified from a 100-year model spin up (1918 – 2018) with fertilisation of 80 kg N/ha across all growing seasons. The initial nitrogen content after the spin up was 52 kg N/ha. The daily weather data are from the nearest meteorological station to the study site (Nhill station)

(Bureau of Meteorology, 2020). The annual precipitation in 2019 was 268 mm, with about 241 mm of precipitation falling in the growing season (May - November). The information was used to initialise the single-member open loop (OL) model simulation (Chapter 5.3.3.1).

Figure 5-2 shows the time series of biomass amount and proportion of each biomass organ to the total biomass from the open loop simulation. Initially, the leaf organ emerges and continues to grow, along with the roots. The leaf proportion increases until the flag leaf is visible (stage 38) (Zadoks et al., 1974). Root biomass increases together with the leaf organ, but its proportion decreases until the start of the reproductive stage, followed by an increase and stabilisation before the harvest. Stem biomass starts to accumulate after the leaf organ. Its proportion increases gradually, reaching a peak at the middle of the reproductive stage (stage 71) and then declining to zero. The spike organ shows up at the start of the reproductive stage (stage 50), the proportion reaches a peak soon after the onset of the grain organ and decreases to a relatively stable value (approximately 10% of the total biomass). The grain organ is the last organ to begin growing and its proportion to the total biomass increases rapidly during the reproductive stage until the harvest (stage 90).

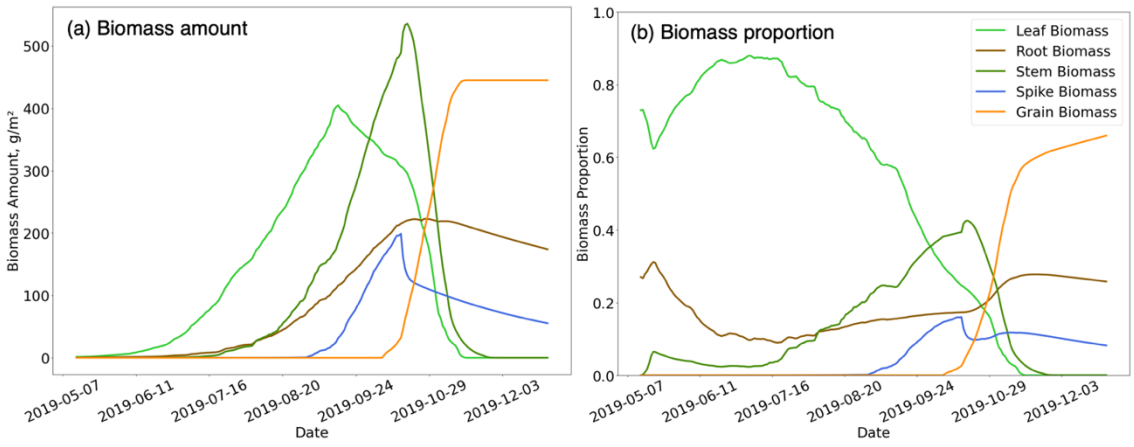

Figure 5-2. The (a) biomass amount and (b) proportion of each biomass organ in total biomass predicted by APSIM-Wheat.

The green leaf area index (GLAI) is used to quantify the ratio of live leaf area per unit ground area in APSIM-Wheat. It is calculated as the sum of the total "live" leaf areas of all leaf cohorts. As a result, it is strongly correlated with the "live" leaf biomass output

from the wheat module. Figure 5-3 compares the leaf biomass with GLAI across the whole crop growth period, as simulated by APSIM-Wheat.

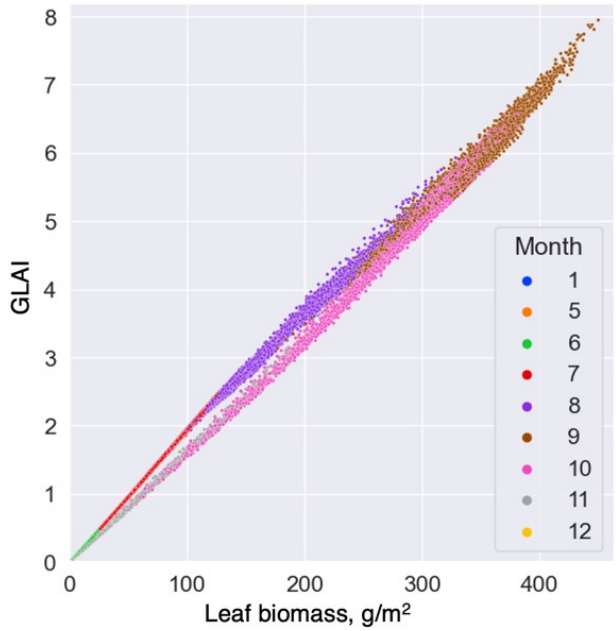

Figure 5-3. Comparison between leaf biomass and GLAI simulated by APSIM-Wheat (different point colour represent different month).

5.3.3 Synthetic twin experiment

The synthetic twin experiments performed here were designed to investigate the influences of updating different model states, updating during different growth stages, and updating at different frequencies. The experiments are based on the 2019 rainfed winter-wheat field described in Chapter 5.3.1. This provides realistic growing conditions for the experiments. The model simulation with ground-based inputs (Chapter 5.3.2) is deployed as the single-member open loop (OL) simulation and is also used for model perturbation to represent modelling uncertainty (Chapter 5.3.3.1). Some specific ensemble member can be assumed to be the "TRUE" simulation and used to generate synthetic observations (Chapter 5.3.3.2 and 5.3.3.3). The synthetic observations were assimilated into the ensemble perturbed simulations (DA) with different experiment configurations for updating the model states (Chapter 5.3.3.4). The OL and DA were then compared to the TRUE simulation to determine each experiment's ability to recover the TRUE scenario. Figure 5-4 is a schematic representation of the used synthetic twin experiment approach.

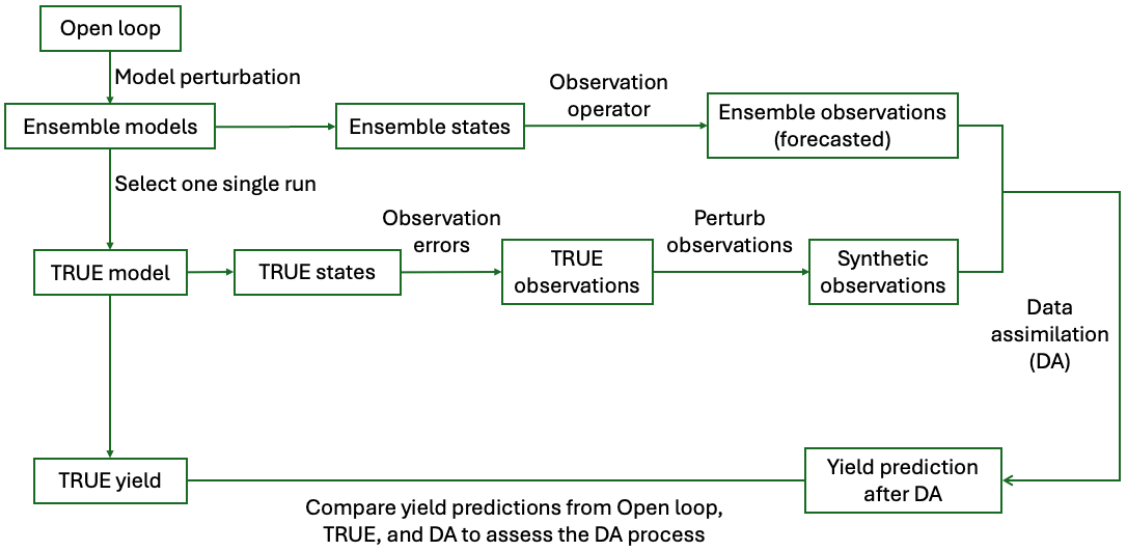

Figure 5-4. Schematic diagram of the synthetic twin experiment

5.3.3.1 Model uncertainties

The open loop simulation can be viewed as a "first guess" of the true parameters and states available and is initialised with information as described in Chapter 5.3.2. Like all models (Vrugt et al., 2008), it should consider uncertainties resulting from deficient/inaccurate model structure, forcing inputs, and parameters. This work considered uncertainties in weather forcing data, soil-related parameters, and soil nitrogen states. We perturbed maximum and minimum air temperature, soil hydraulic parameters, precipitation, fertilisation amount, and initial nitrogen content to emulate the uncertainties in temperature, water, and nitrogen availability. These aspects were identified as important factors contributing to APSIM-Wheat yield uncertainty (Hao et al., 2021). Table 5-1 specifies the perturbation type and error magnitude added to each uncertain input/parameter/state.

Perturbation of precipitation was multiplicative, and lognormally distributed with a mean of 1 and standard deviations of 40%. Perturbations of maximum and minimum temperatures were assumed to be additive and Gaussian with zero mean and a standard deviation of 3 ℃. To include temporal autocorrelation, each weather input error was implemented with a first-order autoregressive process, AR(1), with a correlation coefficient of 1/e on a daily basis, following Reichle et al. (2007) and Li et al. (2014). The perturbations for the different weather inputs were not cross correlated.

Soil parameters were perturbed by adding cross-correlated and normally distributed errors to *LL15*, *DUL*, *SAT*, and *CLL*. A correlation coefficient of 0.5 is assumed between each pair of parameters. The mean and standard deviation of each soil parameter and for each soil layer were obtained from Ratliff et al. (1983) as the selected APSoil profile only provided the base value for soil hydraulic parameters (Table D. 1). The purpose of the perturbation was to realistically represent the uncertainty in soil parameter configuration and also generate difference in water holding capacity.

Nitrogen resources were perturbed in two ways: the initial nitrogen content and the fertilisation amount. For the initial nitrogen content, an additive Gaussian error with a standard deviation of 30% of the base value was added to the base value, which was 52 kg N/ha. The nitrogen fertilisation amounts of 50 kg N/ha and 60 kg N/ha were perturbed to represent the spatial variability of fertiliser application due to machinery variations. The error was assumed to be Gaussian with a standard deviation of 15%. The perturbed fertilisation amounts were between 29 kg N/ha and 70 kg N/ha, and 35 and 88 kg N/ha, respectively.

An ensemble size of 100 was used to represent the model uncertainty. An ensemble size of 50 was recommended for APSIM (Kivi et al., 2022; Zhang et al., 2022) and the WOFOST model (Curnel et al., 2011; de Wit and van Diepen, 2007) after ensemble size tests. A number of 100 ensemble members was recommended by Nearing et al. (2012) for the CERES-Wheat model. Lu et al. (2021) proved that 50 is an adequate ensemble size to achieve stable results in crop model data assimilation. The standard deviation of the resulting ensemble yield predictions was 0.76 t/ha, which is close to the uncertainty of 0.7 t/ha found by Hao et al. (2021) when soil parameters were specified with APSoil and no other stresses was considered.

Table 5-1. The perturbation of uncertain input variables

Uncertain sources	Error type	Error magnitude	Temporal autocorrelation coefficient[a]
Precipitation	Log-normal distributed (mean=1)	Std=40%	1/e
Daily maximum air temperature (Tmax)	Normal distributed (mean=0)	Std=3℃	1/e
Daily minimum air temperature (Tmin)	Normal distributed (mean=0)	Std=3℃	1/e

Soil parameters	Normal distributed (mean=0)	Specific std values are listed in Table D. 1	NA
Initial N content (52 kg N/ha)	Normal distributed (mean=0)	Std=30%	NA
Nitrogen fertilisation amount	Normal distributed (mean=0)	Std=15%	NA

[a]First-order autocorrelation coefficient assumes a daily time series.

5.3.3.2 The selection of TRUE simulations

In the synthetic twin experiment, a TRUE simulation is required to generate synthetic observations and is also used as the benchmark to evaluate the ability of the data assimilation to retrieve the TRUE scenario. After the open loop simulation was perturbed to generate 100 ensemble members with the uncertainties considered above, we first selected two ensemble members as TRUE simulations – those with the highest and the lowest yield predictions and used these to explore and design the DA strategy. Following that, eight representative ensemble members spanning high, median, and low yields were chosen to assess and analyse the efficacy of the designed DA strategy. These were the highest, 95^{th}, 90^{th}, the larger 50^{th}, the smaller 50^{th}, 10^{th}, 5^{th} percentiles, and the lowest yield cases. The ensemble size of 100 is an even number so we show two realisations for the median (smaller and larger) instead of averaging them. Figure 5-5 shows the daily grain biomass from the OL simulation, all perturbed ensemble members, and the chosen TRUE simulations. The yield predictions for the OL simulation, mean of perturbed ensembles, and standard deviation of perturbed ensembles are 4451.6 kg/ha, 4182.7 kg/ha, and 756.7 kg/ha, respectively.

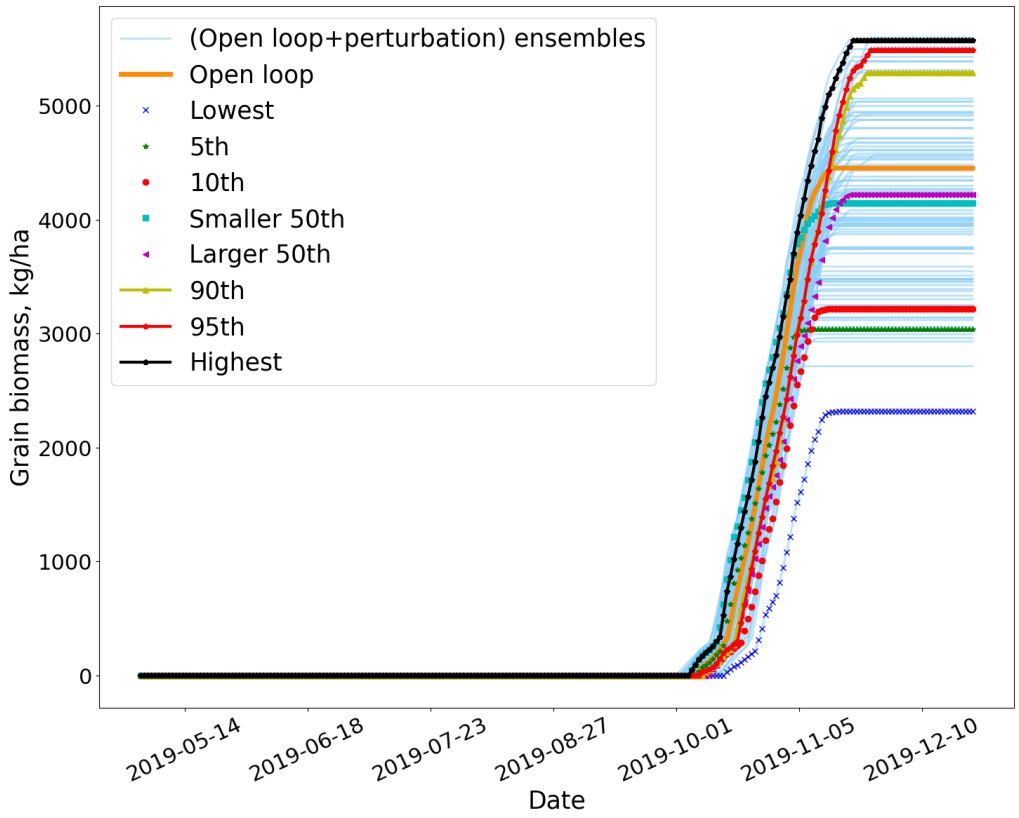

Figure 5-5. Daily yield from the open loop (OL) simulation, perturbed ensemble members, and the chosen TRUE simulations.

5.3.3.3 Synthetic observations

GLAI was selected as the observation to update biomass states in the APSIM-Wheat due to its stable relationship with the leaf biomass and its observability via remote sensing techniques. Figure 5-3 shows that the correlation between them was always close to 1. The synthetic observations were generated based on the synthetic TURE simulations with observation errors. The observation error was randomly generated based on the RMSE between APSIM GLAI and satellite VIs (Chapter 5.3.4.3). At each state update timestep, we generated a single synthetic observation by adding the observation error to the GLAI extracted from the TRUE simulation. The observation error added represents random errors embedded in typical real observations.

5.3.3.4 Experimental design

The efficacy of the data assimilation may be influenced by the updated state variables, the assimilation interval, as well as the specific phenological stages where observations are assimilated. Therefore, this work explored and designed three aspects of a DA strategy:

(1) Choice of state variables: Two different sets of model state variables were updated. One approach updated leaf biomass only, the other one updated all biomass components (leaf, stem, spike, grain, and root biomass). The leaf biomass shows a direct connect with GLAI in the APSIM-Wheat (Figure 5-3), which implies that leaf biomass has the potential to be effectively updated by assimilating GLAI. The efficacy of updating other biomass parts relies on their correlations with leaf biomass. If the embedded correlations approximate those in reality, updating all biomass components should improve performance more than updating leaf biomass only.

(2) Phenological stages: Assimilation of observations over three periods has been tested: (1) Full Season - the whole growing season from sowing to harvest; (2) pre-GLAI peak - from sowing to the GLAI peak time; and (3) post-GLAI peak - from GLAI peak time to harvest.

(3) Assimilation frequency: Assimilation intervals of 5 days and 1-day were investigated. The 5-day interval was chosen to match the temporal resolution of Sentinel-2. The 1-day interval was tested given the APSIM model estimates states on a daily basis.

5.3.4 APSIM-Wheat data assimilation

5.3.4.1 Ensemble Kalman filter

The ensemble Kalman filter (EnKF) is an extension of the Kalman filter, where the forcing data, parameters, and/or model states are perturbed in a Monte Carlo method to generate an ensemble of stochastic model simulations (Evensen, 2003, 1994). The EnKF is implemented in forecast and update steps. The forecast step estimates the ensemble of model state vector X^t at time t from the previous timestep $t-1$. When an observation O^t is available at time t, the *i*th member in state vector ${X_i}^t$ is updated as:

$$ {X_i}^{t+} = {X_i}^{t-} + K^t[O^t + {\varepsilon_i}^t - H({X_i}^{t-})] \quad (5\text{-}2) $$

where ${X_i}^{t+}$ refer to the posterior state vector following the update, ${X_i}^{t-}$ is the prior state vector, ${\varepsilon_i}^t$ represents the observation error, and $H(\cdot)$ is the observation operator that maps the state vector from the model space to the observation space. K^t is the Kalman gain, which weights relative uncertainties of forecast and observation based on the covariance matrices:

$$ K^t = {C_{XY}}^t({C_{YY}}^t + R^t)^{-1} \quad (5\text{-}3) $$

where ${C_{XY}}^t$ is the error cross-covariance between model state vector X^{t-} and the corresponding model forecasted observation $H(X^{t-})$. The model forecasted observations are generated by passing model state vector through the observation operator. ${C_{YY}}^t$ is the error covariance of $H(X^{t-})$, It is to quantify how the observed values vary with respect to their mean across ensemble members. R^t is the observation error covariance.

5.3.4.2 Perturbation bias correction

Due to the nonlinearity of the APSIM-Wheat model (Hao et al., Chapter 3), the state perturbation using mean-zero Gaussian noise can induce biased background predictions in the ensemble model simulations, leading to cumulative errors. To correct this bias, a perturbation bias correction model developed by Ryu et al. (2009) was applied during the state update step. The mean bias of the perturbed state variable is:

$$\delta_t = \frac{1}{n}\sum_{i=1}^{n}({X_i}^{t-} - {X_{OL}}^t) \tag{5-4}$$

where ${X_{OL}}^t$ is a single APSIM-Wheat simulation without any perturbation (the so-called open loop). The mean perturbation bias calculated in equation (5-4) is then subtracted from each perturbed ${X_i}^{t-}$ to produce an unbiased forecast.

5.3.4.3 Observation operator

H in equation (5-2) is the observation operator required in the DA framework. It projects the state vector from the model space to the observation space. In this work, we developed the observation operator based on some sub-field patches from the 2019 rainfed winter-wheat paddock described in Chapter 5.3.1. Sentinel-2 derived time series vegetation indices (VIs) from each patch were compared with the APSIM simulated GLAI. The APSIM simulation for each patch was calibrated against the field measured yield data. The LOcally WEighted Scatterplot Smoothing method (LOWESS) was employed to establish the observation operator connecting APSIM GLAI and Sentinel-2 VIs over the growing season. The *RMSE* between APSIM GLAI and Sentinel-2 VIs was used to represent the prescribed error of the observations, which is the R^t in equation (5-3). The details of the observation operator development are included in the MethodsX article related to this paper (Hao et al., submitted to MethodsX; Chapter 4 in this thesis).

5.3.5 Evaluation of data assimilation performance

The performance of the data assimilation was evaluated in terms of accuracy and uncertainty. The *Residual* indicates the difference between the predicted and observed yield after data assimilation. The *Efficiency* represents the proportional correction due to the data assimilation, compared with the open loop. These two metrics were calculated as:

$$Residual = \overline{Y_{DA}} - Y_{Truth} \tag{5-5}$$

$$Efficiency = 1 - \frac{|\overline{Y_{DA}} - Y_{Truth}|}{|Y_{OL} - Y_{Truth}|} \tag{5-6}$$

where $\overline{Y_{DA}}$ is the ensemble mean of the final yield estimation after data assimilation. Y_{Truth} and Y_{OL} represent the predicted final yield from the truth and the open loop simulations, respectively.

The standard deviation (σ) and the root mean squared error (*RMSE)* were used to evaluate the prediction uncertainty after data assimilation. These were calculated as:

$$\sigma = \sqrt{\frac{1}{n}\sum_{i=1}^{n}(Y_i - \overline{Y_{DA}})^2} \tag{5-7}$$

$$RMSE = \sqrt{\frac{1}{n}\sum_{i=1}^{n}(Y_i - Y_{Truth})^2} \tag{5-8}$$

where n is the number of ensemble members and Y_i is the predicted final yield from the i^{th} ensemble model simulation.

Innovation is a commonly used tool to evaluate filter performance. It can diagnose the appropriateness of the model perturbation and observation uncertainty. The innovation sequence $v^t = O^t - H({X_i}^{t-})$ describes the difference between the observation and the corresponding model forecasted observation at time t. If all assumptions underlying the application of the EnKF are met, including that the system is linear, both model

perturbations and observation errors are uncorrelated and Gaussian distributed. v^t should have a Gaussian distribution with a mean of zero and a variance of ${C_{XY}}^t + R^t$. Therefore, the normalised filter innovation $\widehat{v_t}$ is defined by normalising v^t with its expected variance should have a standard normal distribution:

$$\widehat{v_t} = \frac{\langle O^t - H({X_i}^{t-}) \rangle}{\sqrt{{C_{XY}}^t + R^t}} \sim N(0,1) \tag{5-9}$$

where the angle brackets denote averaging over the ensemble. A biased mean over the time series of $\hat{v}$ can result from observation errors or from the observation operator when the developed operator does not fully represent all scenarios in the experiment. When the variance of the time series of $\hat{v}$ is larger than one, the assumed model error and/or observation error are underestimated, and when it is smaller than one, the assumed errors are overestimated (Crow and Van Loon, 2006; Kumar et al., 2008; Reichle et al., 2002).

5.4 Results

5.4.1 Performance of different data assimilation strategies

The two perturbed open loop ensemble members with the highest (5573.0 kg/ha) and the lowest (2317.3 kg/ha) yield predictions were selected as the TRUE simulations to generate synthetic observations. DA was run for each of these two cases using a variety of DA strategies and the results evaluated. Table 5-2 summarises the performance of the different assimilation strategies for the two TRUE scenarios. All DA strategies listed in Chapter 5.3.3.4 provided improved yield prediction performance. The mean ensemble yield prediction moved towards the TRUE yield predictions after data assimilation. The σ and *RMSE* of ensembles reduced compared to the ensemble uncertainty before assimilation. However, the degree of improvement depended on the DA strategy.

5.4.1.1 Updating different biomass components

Updating all biomass components with an interval of five days across the whole growing season resulted in a greater improvement than updating only leaf biomass. The evaluation metrics values of Table 5-2 show that for the high yield case, when all biomass components were updated, the *residual* between the yield ensemble mean after data assimilation and TRUE yield prediction was only 172.1 kg/ha, producing an *efficiency* of 0.85. The accuracy was substantially improved compared with the difference between

the OL and TRUE yield prediction of 1121.4 kg/ha. The prediction uncertainty also decreased compared with the ensemble spread prior to data assimilation, with the ensemble standard deviation reduced by 43.6%, and *RMSE* reduced by 66.3%.

When only the leaf biomass was updated (Table 5-2), the DA performance was poorer than when updating all the biomass components, in terms of both accuracy and uncertainty. The *residual* between the DA ensemble mean and TRUE was 435.7 kg/ha, with an *efficiency* of 0.61. Data assimilation decreased the ensemble standard deviation by 41.4%, and the *RMSE* by 54.7%.

The low yield case produces similar results in that updating all the biomass components was more effective than updating only leaf biomass (Table 5-2). However, the improved accuracy was lower than the high yield case, with *residual* values of 533.1 and 866.2 kg/ha, and *efficiency* values of 0.75 and 0.59. The uncertainty was decreased by a larger extent, with the reduced percentage of *standard deviation* reaching 74.4% and 66.7%, and for *RMSE* 71.8% and 55.2%, respectively.

Table 5-2. The DA performance of different assimilation strategies (TRUE: the TRUE model simulation; OL: the open loop model simulation; DA: data assimilation; std: standard deviation; RMSE: root mean squared error; LAI: leaf area index)

TRUE member	Yield prediction from the TRUE (kg/ha)	*Residual* between TRUE and OL (kg/ha)	Settings	DA ensemble mean (kg/ha)	*Residual* (kg/ha)	*Efficiency*	DA ensemble std (σ) (kg/ha)	% change of std[a]	*RMSE* before DA (kg/ha)	*RMSE* after DA (kg/ha)
Ensemble member with the highest yield	5573.0	-1121.4	All biomass updated, from sowing to harvest, 5-day	5400.9	-172.1	0.85	426.5	-43.6%	1582.9	534.1
			Leaf biomass updated, from sowing to harvest, 5-day	5137.3	-435.7	0.61	443.3	-41.4%		717.2
			All biomass updated, from sowing to LAI_{peak}, 5-day	4519.6	-1053.4	0.06	568.9	-24.8%		1197
			All biomass update, from LAI_{peak} to harvest, 5-day	5054.4	-518.6	0.54	452.6	-40.2%		701.2
			All biomass updated, from sowing to harvest, 1-day	5402.8	-170.2	0.86	422.3	-44.2%		529.8
Ensemble member with the lowest yield	2317.3	2134.3	All biomass updated, from sowing to harvest, 5-day	2850.3	533.1	0.75	193.4	-74.4%	2013.0	567.1
			Leaf biomass updated, from sowing to harvest, 5-day	3183.4	866.2	0.59	252.6	-66.7%		902.2
			All biomass updated, from sowing to LAI_{peak}, 5-day	3869.6	1552.4	0.27	571.3	-24.5%		1658.3
			All biomass update, from LAI_{peak} to harvest, 5-day	3686.8	1369.5	0.36	298.9	-60.5%		1401.8
			All biomass updated, from sowing to harvest, 1-day	2620.8	303.6	0.86	152.5	-79.9%		339.7

[a] % change of std=$(\sigma_{after-DA} - \sigma_{before-DA})/\sigma_{before-DA}$

5.4.1.2 Updating at different growth stages

For both high and low yield cases, updating through the whole growth season resulted in better model performance than updating only from the $GLAI_{peak}$ time to harvest (late-stage updates), (see evaluation metrics results in Table 5-2, rows 2, 4, 5 and rows 7, 9, 10, respectively). Updating from sowing to the $GLAI_{peak}$ time (early-stage updates) led to even poorer results. The early-stage updates barely shifted the ensemble yield mean towards the TRUE yield prediction, with *efficiency* values of only 0.06 and 0.27 for high and low yield cases. The ensemble uncertainty decreased to a smaller extent. The *standard deviation* reduced by 24.8% and 24.5%, while the *RMSE* reduced by 24.4% and 17.6%. The late-stage updates corrected more than half of the difference between the OL and TRUE simulations for the high yield case and one third of the difference for the low yield case. The reduced ensemble uncertainty was also noticeable for both cases. The late-stage updates are more effective in correcting yield prediction than the early-stage updates, but updating across the whole growth season is best, indicating that assimilation during the early-stage updates was still useful.

5.4.1.3 Update Interval

Updating all biomass components daily across the whole growing season shows improved performance compared with updating with an interval of five days (Table 5-2). The improvement was more noticeable for the low yield case, both in terms of accuracy and uncertainty, with the *efficiency* increased from 0.75 to 0.86, and the *standard deviation* reduction increased from 74.4% to 79.9%. The improvement for the high yield case was minor but still detectable. Updating biomass state variables in APSIM-Wheat at a daily time step is a better strategy. However, due to the satellite optical remote sensing data limitation regarding the revisit frequency and possible cloud contamination, daily observation is challenging in reality. Given the temporal resolution of Sentinel-2 observations, updating at an interval of five days is more realistic.

5.4.2 Performance of the designed data assimilation

The data assimilation strategy presented in Chapter 5.4.1 shows that updating all biomass components at a 5-day assimilation interval across the complete growing season is the more applicable and better performing scheme. Table 5-3 summarises the performance of this data assimilation strategy for the eight representative TRUE cases (Chapter 5.3.3.2). The DA strategy corrected the discrepancies between the OL and TRUE

simulations to varying degrees, as reflected by *residual* values between 93 and 530 kg/ha. Six out of eight cases achieved *efficiency* scores above 0.70. The other two cases have *efficiency* scores of 0.62 and 0.51. The smallest of these (50th larger) had a small residual between the OL and TRUE simulations. The *residual* of these two cases was acceptable, with 320 and 110 kg/ha, respectively. The reduction in ensemble uncertainty increased as TRUE yield decreased. The lowest yield case showed the largest reduction in standard deviation (66.7%), while the 95%ile yield case had the smallest reduction (41.7%). This was likely due to the smaller observation uncertainty for the lower yield cases, as the uncertainty is proportional to the synthetic truth observation. APSIM-Wheat simulations with smaller yield predictions usually show smaller GLAI values during crop growth, which results in smaller observation uncertainties (Chapter 5.3.4.3). The reduction in *RMSE* increased as *efficiency* increased. The highest and 5%ile yield cases had the highest efficiency and largest decreases in *RMSE*, which were greater than 65%. This is because *RMSE* captures both bias and ensemble spread.

The final data assimilation scheme had a consistent outcome for all cases as seven out of eight schemes showed the variance of time series innovations smaller than one, indicating that the assumed model error and/or observation error were overestimated. All innovations mean deviated from zero, the absolute deviation ranged from 0.04 to 0.49. The biased mean values were caused by the model's non-linearity. The highest yield case has the mean and variance of innovations of 0.18 and 1.06, fairly close to 0 and 1, suggesting that this case approaches the theoretically optimal condition for the EnKF with the best performance.

Table 5-3. The performance of the selected representative ensemble members to assess the designed DA strategy (TRUE: the TRUE model simulation; OL: the open loop model simulation; DA: data assimilation; std: standard deviation; RMSE: root mean squared error; LAI: leaf area index)

Case	Yield prediction from the TRUE (kg/ha)	*Residual* between TRUE and OL (kg/ha)	DA ensemble mean (kg/ha)	*Residual* (kg/ha)	*efficiency*	DA ensemble std (σ) (kg/ha)	% change of std	*RMSE* before DA (kg/ha)	*RMSE* after DA (kg/ha)	Innovations mean	Innovations variance
highest	5573.0	-1121.4	5400.9	-172.1	0.85	426.5	-43.6%	1582.9	534.1	0.18	1.06
95th	5486.5	-1035.0	5175.9	-310.7	0.70	441.3	-41.7%	1507.6	603.8	0.04	0.66
90th	5289.8	-838.2	4973.2	-316.6	0.62	422.2	-44.2%	1341.0	585.0	-0.14	0.86
50th-larger	4221.3	230.3	4333.1	111.8	0.51	335.4	-55.7%	757.7	353.6	-0.28	0.88
50th-smaller	4146.1	305.5	4239.3	93.2	0.70	291.7	-61.5%	757.6	306.2	-0.09	0.51
10th	3208.2	1243.4	3524.8	316.7	0.75	275.7	-63.6%	1233.8	485.6	-0.33	0.81
5th	3034.2	1417.4	3263.6	229.4	0.84	261.2	-65.5%	1375.3	347.6	-0.45	0.77

Lowest	2317.3	2134.3	2850.3	533.1	0.75	193.4	-66.7%	2013.0	902.2	-0.49	0.77

5.5 Discussion

5.5.1 The influence of updating different biomass components in the APSIM-Wheat

Updating all biomass components shows better performance than updating leaf biomass. Figure 5-6 is an example from the highest yield case when all biomass components were updated across the whole growth season at an interval of five days. Aboveground biomass is the sum of leaf, grain, spike, and stem biomass organs. The results of the updating with GLAI synthetic observations are that both aboveground and belowground biomass (root biomass) approach the true biomass. Updating resulted in a grain biomass (yield) of 5400.9 kg/ha, with only 172.1 kg/ha compared with the TRUE yield at harvest. Figure 5-7 shows the same yield case but where only the leaf biomass was updated. In this case, leaf biomass still approached the true value, while aboveground biomass moved only halfway and belowground biomass just shifted slightly towards the truth. The difference between grain biomass and the TRUE yield was 435.65 kg/ha, obviously larger than the difference when updating all biomass components.

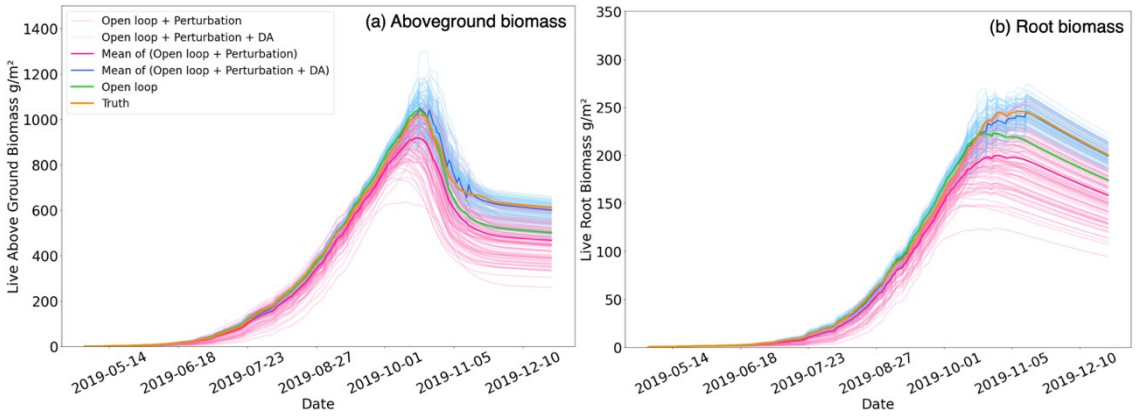

Figure 5-6. Time-series of aboveground biomass (a) and root biomass (b) variations for the high yield case when all biomass components were updated across the whole growth season at in an interval of five days.

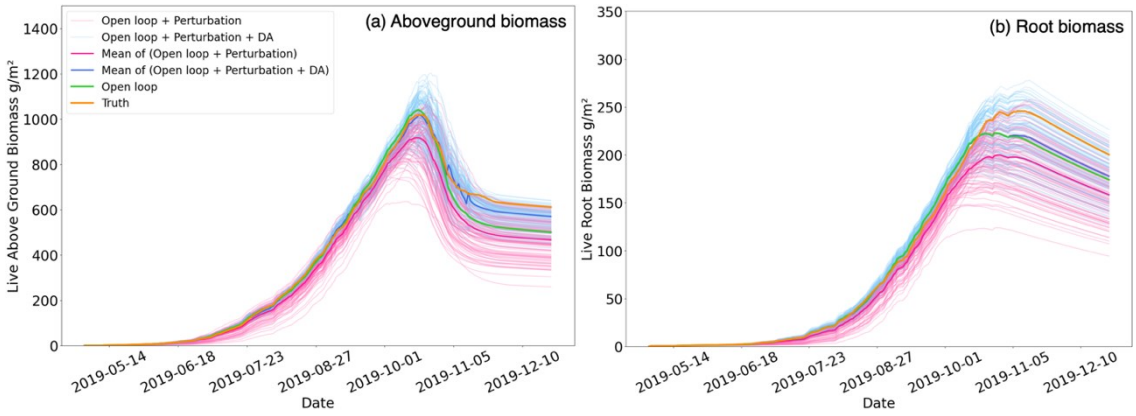

Figure 5-7. Time-series of aboveground biomass (a) and root biomass (b) variations for the high yield case when only leaf biomass was updated across the whole growth season at in an interval of five days.

Updating all biomass components contributed to a better yield prediction, which implies that the model correctly simulated the correlations between GLAI and stem, spike, root, and grain biomass components. The assimilation weighed the corrective impact of the GLAI observation by calculating the error covariance, which effectively avoided any internal inconsistency that may be induced by updating multiple biomass components. Figure 5-8 presents the time series of correlations between GLAI and the other biomass component, as estimated from the ensemble. Before the start of booting (stage 37), spike, stem and root biomass showed positive correlations with GLAI of over 0.8, followed by negative correlations until the middle of flowering (stage 65), and then positive correlations until harvest. Grain biomass began to develop at the start of the reproductive stage (stage 50), and its correlation with GLAI increased from -0.2 to nearly 0.6 in the middle of the dough development stage (stage 84), then quickly dropped to zero at harvest.

The correlations between GLAI and the biomass components can also be demonstrated by the time series of the amount of the different biomass components (Figure 5-9). Figure 5-3 demonstrates that GLAI is highly correlated with leaf biomass. Therefore, the correlations between leaf biomass and other biomass components are almost the same as the correlations between GLAI and those biomass components. Figure 5-9 shows that leaf, stem, and root organs emerged first, followed by the spike organ. They continued to increase until the leaf biomass reached its peak value. From emergence to this stage (37), leaf maintained a positive relationship with stem, root, and spike (Figure 5-8 a-c). After peak leaf biomass, leaf started to senesce while stem, spike, and root continued to

grow. This resulted in a negative relationship between leaf and stem/spike/root biomass until the latter three reached their peak amounts (around stage 65). Then their correlation with leaf became positive again until the harvest. Grain biomass developed continuously from the reproductive stage while leaf biomass amount decreased. Theoretically, the relationship between leaf and grain biomass should stay negative; however, Figure 5-8(d) shows a short period of positive correlation before harvest time. A likely explanation is that when approaching harvest time, ensemble members with a larger leaf biomass usually developed a larger grain biomass, and vice versa. This positive correlation lasted until leaf biomass decreased to zero or the simulation ended at harvest time.

The integration of GLAI into the APSIM-Wheat was shown to be effective in improving yield estimation by updating all biomass components. Zhang et al. (2022) also confirmed the ability of assimilating aboveground biomass in yield prediction. Future research could examine the feasibility of incorporating remotely sensed biomass estimates into the APSIM-Wheat model. However, acquiring biomass observations remains a challenge as remote sensing biomass retrieval still requires the development of statistical regression models between *in situ* biomass measurements and vegetation indices (Asrar et al., 1985; Perry et al., 2014).

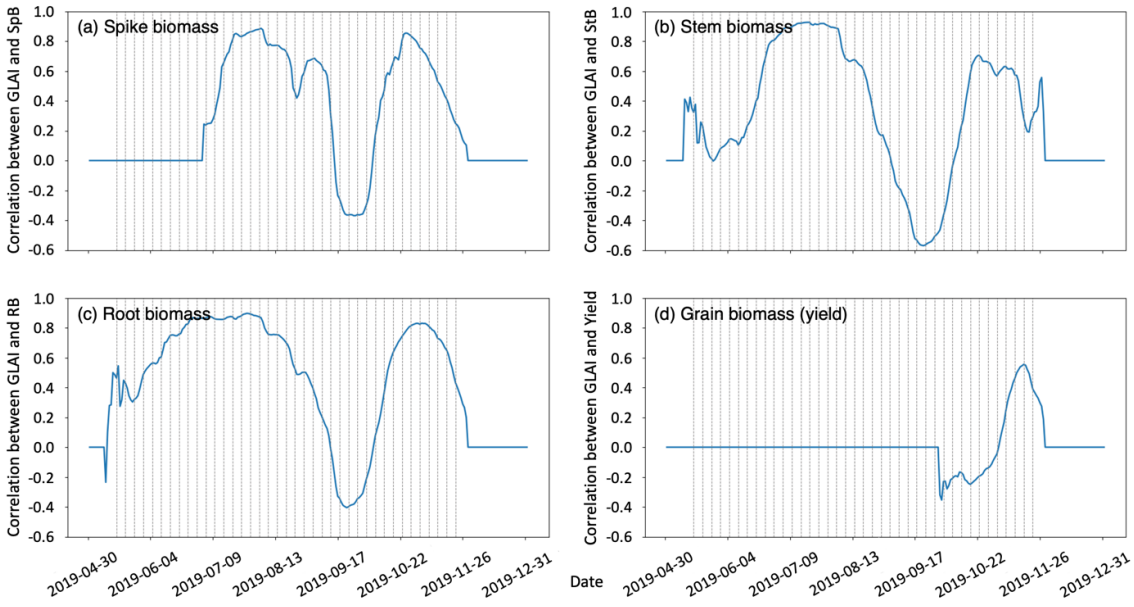

Figure 5-8. Time series of ensemble correlations between GLAI and (a) spike, (b) stem, (c) root, and (d) grain biomass components (vertical dashed lines indicate updating time points).

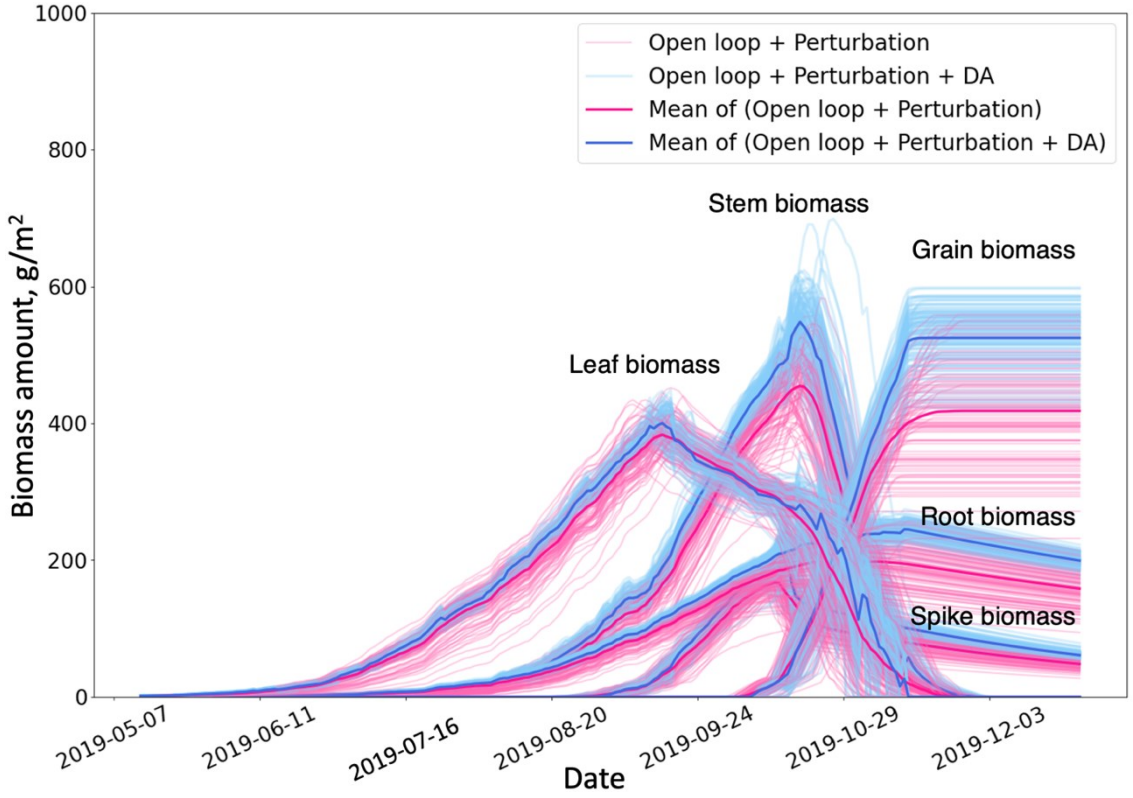

Figure 5-9. The ensemble of biomass amounts for the different plant organs before (pink lines) and after data assimilation (blue lines).

5.5.2 The influence of updating APSIM-Wheat biomass states at different growth stages

The period of data assimilation is important. Updating all biomass components from sowing to harvest outperforms updating from the $GLAI_{peak}$ time to harvest (late-stage updates), and they showed significant improvements compared to updating from sowing to the $GLAI_{peak}$ time (early-stage updates). The greater impact of late-stage updates can be attributed to several factors: (1) The effects of early-stage updates are likely to gradually diminish over time, with the state values trending back towards the simulations without data assimilation. (2) The late-stage state update was applied to the grain biomass, whereas early-stage updates were not because no grain biomass exists early in the simulations (Figure 5-9). Nevertheless, early-stage updates still improved the yield estimation, as shown by updating across the full season outperforming updates only after peak GLAI.

5.5.3 The updating interval and observation availability

The synthetic experiments only considered the updating intervals of 5 days and 1 day. This was motivated by the temporal resolution of Sentinel-2 datasets. The daily frequency was tested to investigate the largest potential of the designed data assimilation scheme. The evaluation metrics (Table 5-2) show that, daily assimilation improves the yield estimate compared to the 5-day updates, with *efficiency* scores increased to 0.86 both for the high and low yield cases. The performance improvement was larger for the low yield case. The greater improvement for the low yield case was likely due to the larger difference between it and the OL, compared with the high yield case. Figure 5-10 compares the differences of the leaf biomass variations for the low yield case when updating the state variables at a 5-day and a 1-day interval. The state variables trended back towards their original simulated values after each assimilation for the 5-day interval, while the daily updates kept the state values closer to the TRUE simulation. The issue of state variables trending back towards their original simulated values can be improved by (1) elaborating model calibration to ensure that the model parameters more accurately represent the real-world system, which can reduce model systematic biases; (2) ensuring that the perturbations of the model and observations reflect realistic uncertainties in the system, by applying perturbations consistent with the statistical properties of the observed data; and (3) monitoring innovation statistics to detect and avoid excessive biases.

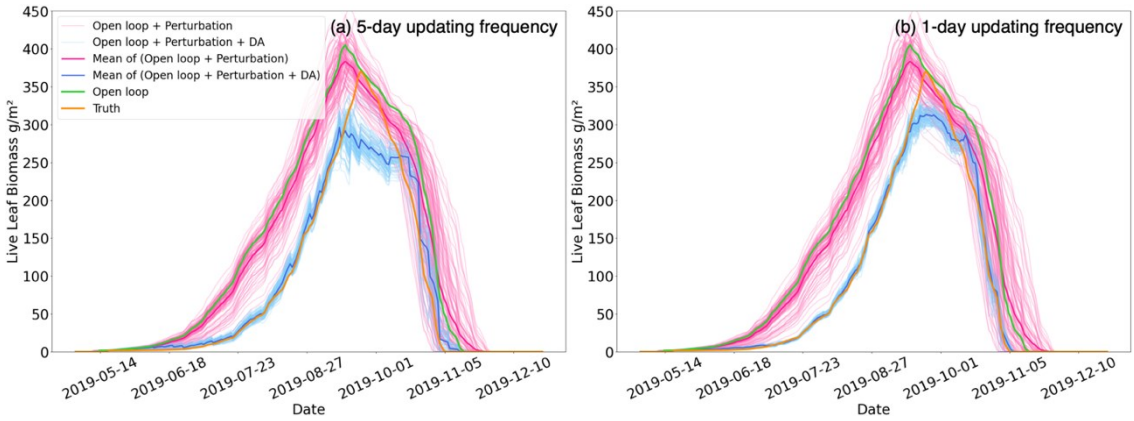

Figure 5-10. Time-series of leaf biomass variations for the low yield case when updating the model states at a (a) 5-day interval and a (b) 1-day interval.

The synthetic experiments demonstrated that the largest potential of assimilating GLAI could be achieved by updating all biomass states in the APSIM-Wheat at a daily time

step. However, at present, assuming application with satellite data, the acquisition of daily remote sensing observations is difficult. For paddock-level work, Sentinel-2 is an obvious potential data source, as it provides up to 10 m spatial resolution spectral reflectance data with sufficient revisit frequency and spectral coverage. PlanetScope is another option, with a daily temporal resolution and approximately 3 m spatial resolution, but the equipped DOVE-R sensor only has four spectral bands (blue, green, red, and near infrared) which limits the retrieval of vegetation indices. For larger spatial scale application, MODIS could be used as the observation source, with its 500 m spatial resolution and daily acquisition intervals. However, significant spatial heterogeneity exists within MODIS pixels, which often contain a mixture of crops and other surfaces. Further investigation is necessary to assess the impact of these issues on assimilating MODIS. Another issue in realistic situations is the availability of the observations, which are subject to cloud contamination leading to missing imagery during critical stages of the crop development.

5.5.4 Adequacy of uncertainty estimation

Table 5-3 summarises the mean and variance of the innovation time series for all eight cases. All mean values of the normalised innovations deviated from zero, implying APSIM-Wheat is a non-linear dynamic simulation system. The finding is consistent with sensitivity analyses of the APSIM model (Casadebaig et al., 2016; Zhao et al., 2014). Six out of eight cases showed negative mean values while the other two had mean values close to zero, indicating that on average the GLAI was overestimated by the model. From the 90%ile to the lowest yield case, the absolute deviation of mean values showed an increasing trend from 0.14 to 0.49, indicating greater GLAI overestimation for lower yield cases.

The variance values of the normalised innovations were generally smaller than one, with a range of 0.51 to 0.88, suggesting that the actual difference between the background prediction (prior to update) and observation is smaller than the assumed errors (perturbations) for them. After incorporating the assumed uncertainty in daily temperature, water, and nitrogen availability (Chapter 5.3.3.1) into the APSIM-Wheat model, the standard deviation of the perturbed ensemble model simulations was approximately 0.75 t/ha. This spread was smaller than the 1 t/ha model yield prediction uncertainty when compared to field-measured yield data (Hao et al., 2021). The

observation operator developed in Chapter 5.3.4.3 used a LOWESS fitting curve between the calibrated APSIM GLAI simulation and the Sentinel-2 derived vegetation index. The observation uncertainty was calculated as the *RMSE* for windows along the curve. The difference between the APSIM GLAI simulation and the remotely sensed vegetation index defined the observation error, which was estimated based on reality but may have been overstated for the synthetic experiment. These factors may cause the actual difference between model prediction and observation to be overestimated.

The innovation-based diagnostics have been widely applied in land surface model data assimilation (Crow and den Berg, 2010; Crow and Van Loon, 2006; Kumar et al., 2008) and crop model data assimilation (de Wit and van Diepen, 2007; Kivi et al., 2022), with the performance successfully improved. In future real-world applications with satellite data, we could use the innovation statistics to modulate the model and observation error covariances and maximise the performance of the EnKF.

5.6 Conclusion

This paper presented an effective and robust data assimilation scheme that helps to improve APSIM-Wheat yield prediction. Using a comprehensive synthetic experiment, we evaluated the potential of integrating GLAI observations to update various biomass state variables during different growth stages and at various assimilation intervals.

The synthetic experiment showed that the selection of updated model states, updating periods and intervals is crucial for the performance of data assimilation. Assimilating synthetic GLAI observations into the APSIM-Wheat model demonstrated its greatest potential for improving yield prediction when all five wheat biomass components (leaf, stem, spike, grain, and root organs) were updated daily from sowing to harvest. In contrast, limiting updates to only leaf biomass or reducing updating periods to only before or after the GLAI peak time resulted in weaker data assimilation performance. Given the availability of satellite observations, a 5-day update interval was recommended for data assimilation in real-world applications, and its performance was found to not be significantly impacted. The proposed data assimilation scheme effectively reduced the *residuals* of yield predictions in eight representative cases to a range of 93-533 kg/ha, compared to *residuals* without data assimilation of 230-2134 kg/ha. However, the non-Gaussian distribution of the normalised filter innovations suggests that the EnKF did not

perform optimally because the assumptions underlying its use were not fully fulfilled. Additionally, the variance values of the normalised innovations were generally smaller than one, suggesting that the imposed model error and/or observation error may have been overestimated.

Future work could focus on better estimating the model and/or observation uncertainty to improve the EnKF performance. It would also be interesting to apply a particle filter (PF) since it does not require a linearity assumption in the data assimilation process. Machwitz et al. (2014) and Lei et al. (2020) demonstrated the efficacy of PF when assimilating satellite data into APSIM coupled with a radiative transfer model to update biomass simulations of maize, and assimilating thermal and radar remote sensing retrievals into APSIM for soil moisture monitoring. We anticipate that our data assimilation framework can also be extended to real case applications with satellite observations to improve yield estimation and produce yield maps displaying detailed spatial variability at a paddock scale. Furthermore, another potential direction for future work is the application of data assimilation to a larger spatial scale, where satellite sources such as Landsat or MODIS can be utilised. However, the mixed reflectance from crops and other surfaces within each pixel requires the incorporation of spatial heterogeneity into the estimation of observation uncertainty.

Chapter 6 Real case study and spatial yield prediction based on satellite data

6.1 Abstract

Accurate prediction of within-field crop yield variations is crucial for farm management to enhance food production and optimise resource utilisation. The use of high spatiotemporal resolution remote sensing data to gain insight into crop growth status allows for the integration of crop models with remote sensing observations, thereby improving crop yield predictions. In this study, the performance of a data assimilation framework based on Ensemble Kalman filter (EnKF) was evaluated by assimilating Sentinel-2 and PlanetScope derived vegetation observations into the APSIM-Wheat model. The appropriate observational uncertainty was determined by tuning the relative uncertainties between model forecasts and satellite observations based on the innovation indicator. A rainfed winter-wheat field located in north-western Victoria, Australia was segmented into 58 patches characterising different levels of harvest yield. Two open loop cases were used to examine the robustness of the data assimilation strategy: a high yield and a low yield scenario. The results from the patch-based evaluation showed that data assimilation effectively improved yield estimates by increasing accuracy and reducing uncertainty. For the high-yield open loop case, the *residuals* between ground measurements and model simulations decreased to a range of 0.01 to 1.24 t/ha with a median value of 0.09 t/ha. The *efficiency* scores for this case ranged between 0.37 and 0.97, with a median value of 0.73. The uncertainty decreased from 0.71 t/ha to a range of 0.52 – 0.60 t/ha. The accuracy improvement for the low-yield open loop case was less significant, with the *efficiency* scores ranging between 0.18 and 0.94 and a median value of 0.24. The uncertainty reduction in this case was more significant, decreasing from 0.76 t/ha to between 0.29 and 0.40 t/ha. The different performances for both cases are likely due to their different model uncertainties. To improve performance in the low-yield case, the observation uncertainty should be adaptively increased. This study provides insights into the importance of accurate estimation of the relative uncertainties of model forecasts

and observations, and it also provides guidance for future agricultural modelling data assimilation practices.

6.2 Introduction

Process-based biophysical models, such as the Agricultural Production Systems sIMulator (APSIM), require careful calibration and initialisation to achieve accurate crop growth simulation and yield estimation (Basso and Liu, 2019). Otherwise, uncertainties arising from model structure, forcing inputs, and parameters limit the predictive ability of crop models (Seidel et al., 2018; Vrugt et al., 2008). Remote sensing data provide repeated monitoring of crop growth and environmental conditions over large spatial and regular temporal scales, enabling yield estimates, such as through remote sensing-based models (Donohue et al., 2018). However, they also carry uncertainties due to instrument inaccuracy and imperfect data retrieval (Povey and Grainger, 2015).

Data assimilation provides an opportunity to address the uncertainty challenges by combining the model simulations and remote sensing observations to produce better crop yield predictions. The potential for improving wheat yield predictions with vegetation observations assimilation has been demonstrated through synthetic experiments in Chapter 5. The designed data assimilation strategy showed its efficacy by assimilating synthetic Green Leaf Area Index (GLAI) observations into the APSIM-Wheat model. However, synthetic observations were generated by adding pre-defined observation errors to the GLAI observations, which were extracted from the assumed "TRUE" model simulations. Two assumptions were made during this procedure: (1) the pre-defined observation errors were estimated from the observation operator developed in Chapter 4. The estimated errors cannot represent the real remote sensing observational uncertainties from imperfect instrument and data retrievals; (2) the "TRUE" simulation was attained by running an assumed "perfect" APSIM-Wheat model, where the extracted synthetic vegetation observations are likely not consistent with the real satellite observations. Therefore, a real case study utilising remote sensing data was performed to further investigate the complexity of data assimilation systems in real-world applications and understand the effects brought by satellite observations.

Various satellite-derived vegetation observations were assimilated into crop models to improve APSIM yield predictions. Machwitz et al. (2014) assimilated RapidEye spectral reflectance data (with a spatial resolution of 6.5 m and up to daily temporal resolution)

(RapidEye, 2016) into the coupled APSIM-Maize and PROSPECT and SAIL (PROSAIL) models to increase the accuracy of maize biomass predictions and enable the production of biomass maps displaying spatial variability in central Luxembourg. The results highlighted the suitability of incorporating RapidEye data into crop models to enhance model prediction abilities. Zhang et al. (2022, 2021) presented a data assimilation framework for integrating both ground measured and remotely sensed data into the APSIM-Wheat model at a farm near Cora Lynn in Victoria, Australia. The remote sensing data included (1) 3 m leaf area index (LAI) images produced by fusing Sentinel-2 LAI and PlanetScope surface reflectance (Sadeh et al., 2021), and (2) surface soil moisture retrieved from tower-based microwave brightness temperature. The results found that the assimilation of remotely sensed LAI effectively corrected the model's underestimation of wheat grain yield by improving the relative difference (RD) from -38.8% to -7.6%. Ziliani et al. (2022) integrated daily 3 m CubeSat-based LAI (Johansen et al., 2022) into the APSIM-Maize model to provide end-of-season yield maps for a rainfed maize field located in Nebraska, USA. The proposed framework demonstrated its ability by reducing yield prediction error from 1 t/ha to 0.2 t/ha.

The challenges faced by this study include accurately estimating the real remote sensing observational uncertainties and modulating the designed data assimilation framework to work with spatially and temporally limited optical satellite observations. This chapter extends the synthetic experiments of Chapter 5 by using satellite and field datasets collected during the 2019 winter wheat growing season. The relative uncertainties between model forecasts and observations were tuned based on the innovation indicator. Successively, the patch-based assimilation of Sentinel-2 and PlanetScope data into the APSIM-Wheat model was performed to evaluate the efficacy of the designed data assimilation strategy.

6.3 Methods and materials

6.3.1 Study site

This work used the same study site as in Chapter 5 – a rainfed winter-wheat (*Triticum aestivum* L.) field located in north-western Victoria, Australia. The area under cultivation was 106 ha, with an average yield of 5.9 t/ha and large spatial variations. The paddock was segmented into 58 patches to characterise different levels of harvest yield. The yield

of each patch varies from 4.67 t/ha to 6.60 t/ha (Figure 6-1). The data assimilation strategy designed in Chapter 5 will be applied on a patch basis to examine its performance.

Observation operators were determined following the method described in Chapter 4. As indicated by the dark blue line in Figure 6-1, the paddock was evenly separated into two parts. The left-part developed observation operator will be applied to the patches in the right part and vice versa to ensure independent model evaluation.

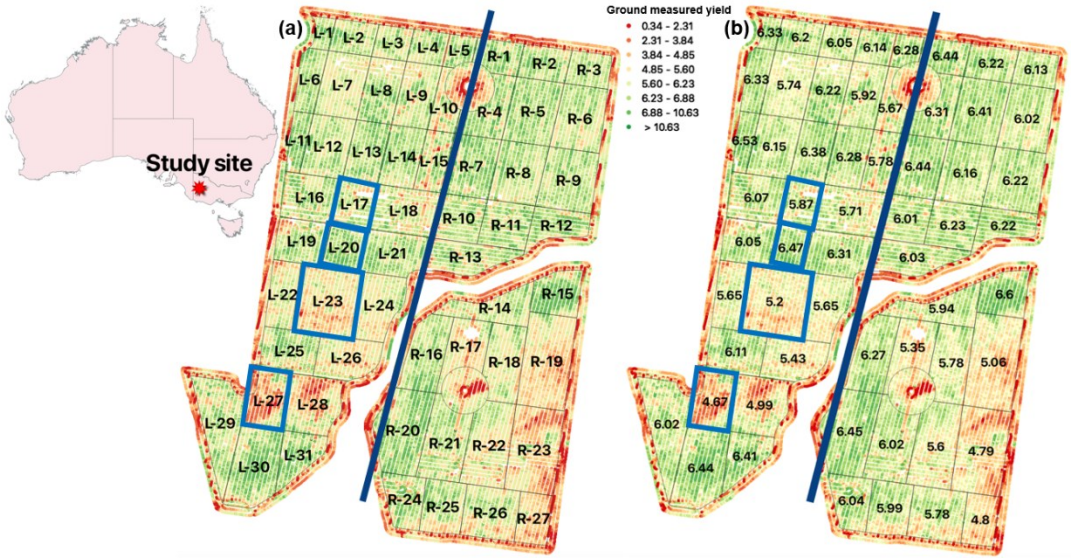

Figure 6-1. The study site location. The paddock was segmented into 58 patches (indicated by the black lines) and also separated into two parts (indicated by the dark blue line). Four patches covering a range of low to high harvest yields were selected as test scenarios to evaluate the performance of data assimilation with varying observation errors (highlighted by light blue rectangles). The left part of the paddock consists of 31 patches, while the right part contains 27 patches. (a) shows the patch number and (b) shows the ground measured yield data for each patch (t/ha).

6.3.2 APSIM-Wheat data assimilation framework

The APSIM-Wheat data assimilation framework applied in this case study was developed and described in Chapter 5. We explored data assimilation strategy in three aspects and concluded that the most applicable and best-performed strategy is updating all biomass components (leaf, stem, spike, grain, and root biomass) at a 5-day time step across the complete growing season. The details of APSIM-Wheat model and its input datasets, ensemble Kalman filter (EnKF), and the perturbation bias correction can be found in Chapters 5.3.2, 5.3.4.1, and 5.3.4.2.

6.3.2.1 The open loop simulations and model uncertainties

To examine the robustness of the developed data assimilation strategy applying with satellite observations, two open loop simulations were used: a low-yield open loop with the predicted yield of 4.45 t/ha and a high-yield open loop with the yield prediction of 6.85 t/ha. The measured yield of the 58 patches varied from 4.67 t/ha to 6.60 t/ha, and the residuals between the two open loop simulations and the field measurements are between 0.22 and 2.15 t/ha and between -0.25 and -2.18 t/ha respectively. Both open loop scenarios were used as the benchmark to evaluate to which degree the data assimilation can improve the open loop predictions to approach the field measurements.

The open loop simulation is seen as a "first guess" of the true parameters and initial states. Ideally, open loop simulation considers uncertainties from deficient/inaccurate model structure, forcing inputs, and parameters (Vrugt et al., 2008). This work considered the same sources of uncertainty as described in Chapter 5.3.3.1 to emulate the uncertainties in temperature, water, and nitrogen availability. We perturbed maximum and minimum air temperature, precipitation, soil hydraulic parameters, initial nitrogen content, and fertilisation amount. Table 6-1 specifies each uncertain source's perturbation type and error magnitude for the low-yield and high-yield open loop simulations. The perturbation details can be found in Chapter 5.3.3.1.

An ensemble size of 100 was used to represent the model uncertainty. After the perturbation, the standard deviation of the resulting ensemble yield prediction for the low-yield open loop was 0.76 t/ha, and the ensemble standard deviation for the high-yield open loop was 0.71 t/ha. Both ensemble uncertainties are close to the uncertainty of 0.7 t/ha found by Hao et al. (2021) when soil parameters were specified with APSoil (Oliver and Robertson, 2009) and no other stresses was considered.

Table 6-1. The perturbation of uncertain input variables

Uncertain sources	Error type	Error magnitude		Temporal autocorrelation coefficient[a]
		Low-yield open loop	High-yield open loop	
Precipitation	Log-normal distributed (mean=1)	Std=40%		1/e
Daily maximum air temperature (Tmax)	Normal distributed (mean=0)	Std=3℃		1/e
Daily minimum air temperature (Tmin)	Normal distributed (mean=0)	Std=3℃		1/e

Soil parameters	Normal distributed (mean=0)	Specific mean and std values are listed in Table E. 1	Specific mean and std values are listed in Table E. 2	NA
Initial N content	Normal distributed (mean=0)	Base value=52 kg N/ha Std=30%	Base value=61 kg N/ha Std=30%	NA
Nitrogen fertilisation amount (two-time fertilisation)	Normal distributed (mean=0)	Base value=50+60 kg N/ha Std=15%	Base value=60+65 kg N/ha Std=15%	NA

[a]First-order autocorrelation coefficient assumes a daily time series.

6.3.2.2 Satellite observation data

Chapter 4 nominated four Sentinel-2 derived vegetation indices with different spectral band combinations to develop the observation operator connecting APSIM-Wheat simulated green leaf area index (GLAI) and satellite observations. We analysed the linearity of the developed operators and found that the red edge chlorophyll index (RECI) is the most suitable candidate to be assimilated into APSIM-Wheat model.

In this study, satellite-based remote sensing observations were derived from Sentinel-2 and PlanetScope. Sentinel-2 is a constellation of two satellites carrying optical sensors that provide images with high spatial resolution (10/20 m) and temporal resolution (5 days). However, cloud contamination limited the availability of Sentinel-2 imagery, and only 15 cloud-free Sentinel-2 RECI images were acquired and processed on the Google Earth Engine platform (Gorelick et al., 2017), with a resolution of 20 m. These images covered the period from sowing (May 12th, 2019) to harvest (November 15th, 2019).

To fill the gaps caused by cloud contamination, PlanetScope data was used. The PlanetScope constellation, consisting of 130+ satellites with imaging radiometers, is able to image nearly all of Earth's land every day with a spatial resolution of 3 m. PlanetScope imagery includes four spectral bands: read, green, blue, and near infrared. Due to the lack of red edge bands, it is not able to retrieve RECI for assimilation into APSIM-Wheat model. Therefore, we calculated the normalised difference vegetation index (NDVI) for PlanetScope as a surrogate and rescaled it to be comparable with Sentinel-2 RECI. The 3 m PlanetScope NDVI images were resampled to 20 m to match the spatial resolution of Sentinel-2 RECI. All cloud-free Sentinel-2 RECI and PlanetScope NDVI from 2019 were compared against each other at a pixel-scale, as shown in Figure 6-2. The fitted curve shown in Equation (6-1) was used to rescale PlanetScope NDVI to be equivalent to Sentinel-2 RECI. The coefficient of determination (R^2) for the fitted curve was 0.98.

The rescaling equation was developed using cloud-free images from both data sources and applied only to retrieve equivalent Sentinel-2 RECI when it was cloud contaminated. The rescaling and application datasets were independent.

$$RECI_{Sentinel-2} = 0.05 * e^{5.6*NDVI_{PlanetScope}} + 0.05 \quad (6\text{-}1)$$

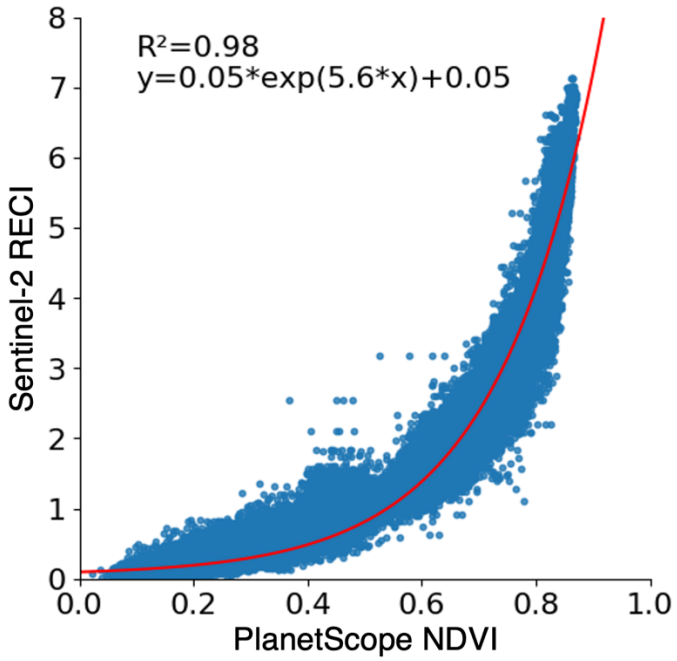

Figure 6-2. Cloud-free Sentinel-2 red edge chlorophyll index (RECI) plotted against cloud-free PlanetScope normalised difference vegetation index (NDVI). The solid red line indicates the exponential fitted equation. The R^2 for the fitted curve is 0.98.

In this study, 13 cloud-free PlanetScope surface reflectance data were acquired from Planet Labs (Planet Labs Inc, 2021) and processed to create equivalent Sentinel-2 RECI images to fill in the Sentinel-2 cloud gap from 2019. With the 15 Sentinel-2 images, a total of 28 RECI observations for the entire growing season were used. Figure 6-3 shows the time series averaged RECI values for the whole paddock as an example to illustrate the dates for both data sources. The specific dates are listed in Table E. 3.

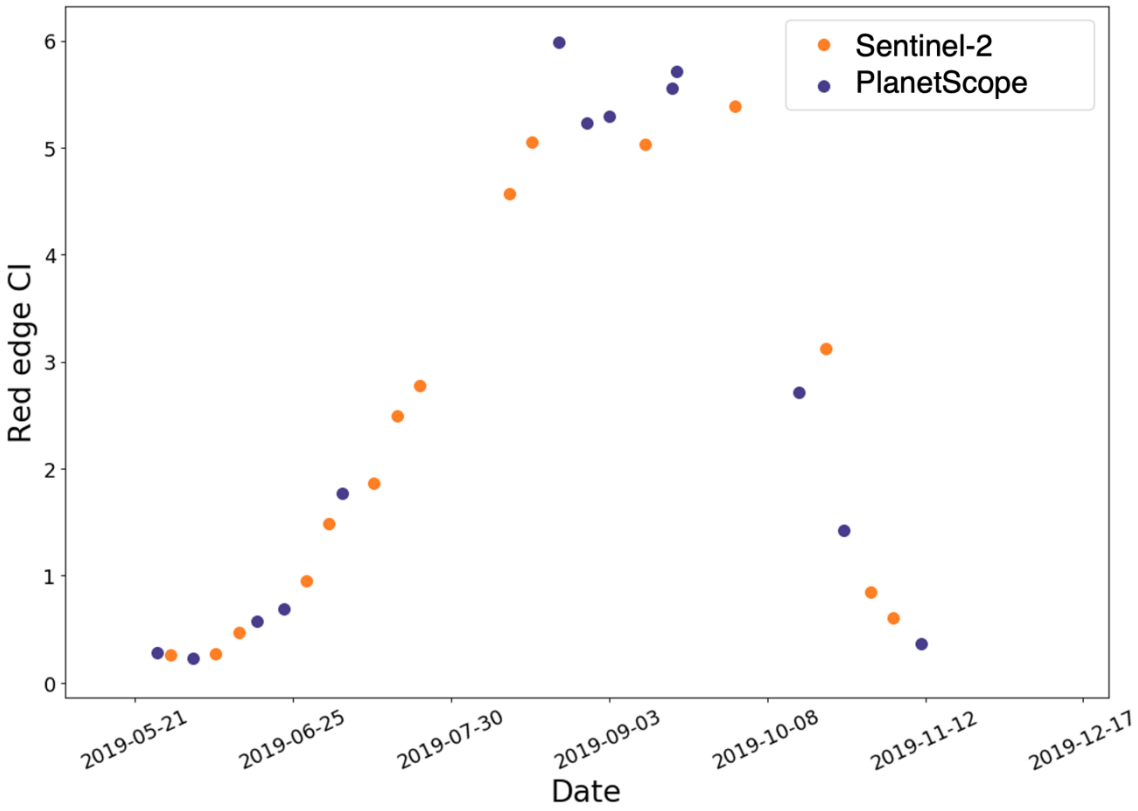

Figure 6-3. The time series averaged RECI values for the whole paddock from 2019. PlanetScope was used to fill in the Sentinel-2 data gap. Orange points represent Sentinel-2 data, blue points represent PlanetScope data.

6.3.2.3 Observation operator

The EnKF requires an observation operator that projects model states to equivalent observations. Chapter 4 presented the detailed steps for developing the observation operator. In this study, we used the same methods to develop two observation operators for the left and right parts of the paddock respectively (Figure 6-1) and applied them to the other part to ensure independence. Specifically, the APSIM simulation was calibrated on a patch-by-patch basis to align its yield prediction with the field-measured yield data obtained from the 31 patches in the left part of the paddock. The comparison between the calibrated APSIM GLAI simulations and the satellite-based time series RECI observations for each patch contributed to the formulation of the observation operator used in data assimilation for the right part of the paddock. Similarly, an observation operator was independently established utilising field-measured yield data from each patch in the right part of the paddock. This operator was subsequently employed in the data assimilation process for the left part of the paddock. Figure 6-1 provides a visual

representation of the field-measured yield data for each patch. The LOcally WEighted Scatterplot Smoothing method (LOWESS) was used to establish the observation operator.

6.3.2.4 Observation uncertainty experiments

Accurate estimation of observation uncertainty is important for the efficacy of data assimilation. Satellite-based observation uncertainty mainly inherits from instrument inaccuracy and imperfect data retrieval. In this work, we investigated the effects of different types and magnitudes of observation uncertainty on data assimilation results. The perturbed observations were generated by adding Gaussian-distributed errors with certain standard deviation values. The evaluated magnitudes include 0.2, 0.5, 0.8, and 1.1 for additive observation error, and 10%, 20%, and 30% for multiplicative observation error.

6.3.3 Evaluation of data assimilation performance

Following the diagnostic indicator and evaluation metrics used in Chapter 5, we continued to use the normalised innovation v^t as an indicator to diagnose and determine the appropriate observation uncertainty. Once the type and magnitude of observation uncertainty were tuned, the *Increment*, *Residual*, and *Efficiency* were used to assess the improvement of yield prediction by data assimilation. The standard deviation (σ) was used to evaluate the uncertainty of yield prediction. Detailed descriptions of the *Residual*, *Efficiency*, and standard deviation (σ) can be found in Chapter 5.3.5. The *Increment* measures the difference between the predicted yield after data assimilation and the open loop simulation. The metric was calculated as:

$$Increment = \overline{Y_{DA}} - Y_{Open\ loop} \tag{6-2}$$

where $\overline{Y_{DA}}$ is the ensemble mean of the final yield estimation after data assimilation. $Y_{Open\ loop}$ represents the open loop simulated yield.

6.4 Results and discussion

6.4.1 Observation uncertainty experiments

We used four patches from the paddock (highlighted by light blue rectangles in Figure 6-1) as test scenarios to evaluate the performance of data assimilation with varying observation errors. The patches covered a range of low to high harvest yields, with ground truth yields of 4.67, 5.2, 5.87, and 6.47 t/ha, respectively. We first tested the low-yield open loop case with four different levels of additive and three levels of

multiplicative observation errors. The results showed that data assimilation with multiplicative observation error outperformed the assimilation with additive observation error.

Figure 6-4(a) and Table E. 4 show the comparison and metric values of data assimilation with different observation errors for the low-yield open loop case. All four levels of additive observation error resulted in lower yield estimates than the open loop, which is the opposite of what data assimilation should achieve. The negative effects of data assimilation when the observation error was additive may be due to the observation uncertainty being comparatively smaller than the model uncertainty during the middle of the growth stage, causing the filter to over-trust the observations. However, the observation error was relatively small compared to the model uncertainty at other stages leading the filter to over-trust the observations. We also observed that the performance of yield estimation deteriorated with decreasing additive observation errors, with the largest *Residual* values found when the error magnitude was 0.2 or 0.5. This also suggests that underestimated observation errors during the middle growth stages caused the filter to mistakenly trust the observations and led to failed yield prediction.

The multiplicative observation error is more appropriate for this data assimilation framework, as the error proportionally changes with the observation values. In the low-yield open loop case, the yield estimation was improved at all three levels of multiplicative observation error, with the greatest improvement observed when the observation uncertainty was 10% or 20%. The largest *Increment* in yield estimates for the four patches were 0.14, 0.23, 0.37, and 0.52 t/ha, respectively (Table E. 4). Overall, the 20% observation error was found to be the most suitable for use in our data assimilation scheme, as it resulted in improving yield estimates by 0.14, 0.21, 0.37, and 0.45 t/ha for the four patches. This improvement was close to the best performance observed among all tested observation errors. In addition to the prediction results, the variance of normalised innovations was also used to decide the observation error magnitude. As described in Chapter 5.3.5, the desired value for the innovation variance is one, as it ensures a correct sum of forecast and observation uncertainty and optimal filter performance. At the 20% error magnitude, the innovation variance for the four patches was within the range of 1.19 to 1.56, approaching the desired value of one. In contrast, the 10% error magnitude resulted in significantly larger innovation variance between 2.79 and 3.07.

In the high-yield open loop case, only the three levels of multiplicative observation error were tested (Figure 6-4(b) and Table E. 4) based on our findings in the low-yield open loop case. Similar to the low-yield open loop case, the best performance was found when the observation error level was 10% or 20%. The largest *Increment* in yield estimates was 0.98, 0.96, 0.74, and 0.39 t/ha, respectively. The patch with a ground truth yield of 6.47 t/ha showed the best performance at the 20% error level, with a *Residual* value of -0.1 t/ha. For patches with ground truth yields of 4.67, 5.2, and 5.87 t/ha, the yield estimates by data assimilation with 10% and 20% error levels were similar, with a better performance observed at the 10% error level. However, the largest difference between the two levels was only 0.07 t/ha, occurring in the patch with a ground truth yield of 5.87 t/ha. Given the marginal performance differences between these two levels, we also included innovation variance as a selection criterion. The innovation variance for the four patches ranged between 1.8 and 2.56 for the 10% error level and between 0.79 and 1.19 for the 20% error level. Therefore, the 20% error magnitude was selected to perturb the observations, as it resulted in normalised innovations with a variance closest to one.

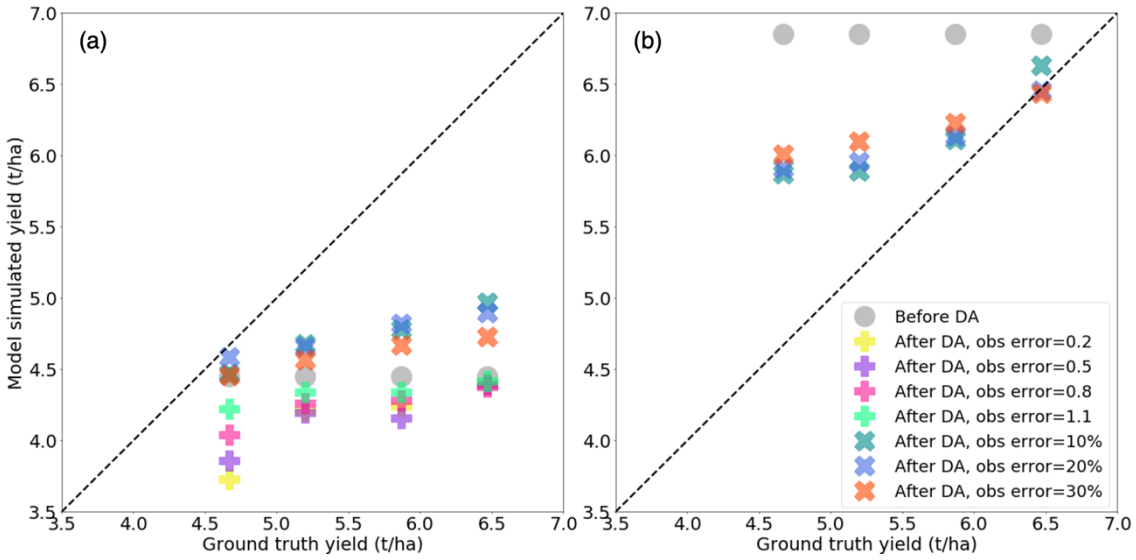

Figure 6-4. Performance of data assimilation for different types and magnitudes of observation error with (a) the low-yield open loop case and (b) the high-yield open loop case. The grey points represent the open loop model estimated yields. Different colours of plus signs and cross marks represent the data assimilation results with different levels of additive and multiplicative observation error, respectively. The specific colours for the varying levels of error are indicated in the legend (DA: data assimilation; obs error: observation error).

6.4.2 Data assimilation performance

A multiplicative observation error with an error level of 20% was applied to perturb the observations and used in the data assimilation. We evaluated the performance of the data assimilation using all 58 patches from the paddock (Figure 6-1) in both low-yield and high-yield open loop cases. The results are presented in Figure 6-5, Table E. 5, and Table E. 6.

Figure 6-5(a) shows that data assimilation slightly improved yield estimates for the low-yield open loop case. For all 58 patches, the *increment* of yield estimates ranged between 0.14 and 0.58 t/ha. The improvement in yield estimates demonstrated an increasing trend as the absolute *residual* between the ground truth yield and open loop simulated yield increased from 0 to 2.5 t/ha (Figure 6-6(a)). However, the *residual* after data assimilation remained large, ranging from 0.02 to 1.63 t/ha, with a median value of 1.26 t/ha. The mediocre performance for the low-yield open loop case was also indicated by the *efficiency* score, which ranged between 0.18 and 0.94, with a median value of 0.24. An improvement in yield estimates uncertainty was observed. The ensemble standard deviation (σ) for all patches decreased from 0.76 t/ha (pre-data assimilation) to between 0.29 and 0.40 t/ha.

Figure 6-5(b) shows an improvement in yield estimates by data assimilation for the high-yield open loop case. The *increment* ranged between 0.22 and 1.22 t/ha, with the magnitude of improvement being more significant than in the low-yield open loop case. This case also displayed the same increasing trend with an increasing absolute *residual* between the ground truth yield and the open loop (Figure 6-6(b)). Data assimilation effectively improved the yield estimates, with the *residual* ranging from 0.01 to 1.24, and a median *residual* value of 0.09 t/ha. Our designed data assimilation strategy showed its best performance for patches with ground truth yields larger than 5.43 t/ha, with all *residual* values smaller than 0.48 t/ha. The *efficiency* score for this case ranged between 0.37 and 0.97, with a median value of 0.73. However, the decrease in yield estimates uncertainty was not as pronounced as in the low-yield open loop case. The standard deviation (σ) decreased from 0.71 t/ha to a range of 0.52 – 0.60 t/ha.

The designed data assimilation strategy performed better for the high-yield open loop case compared to the low-yield open loop case. Both cases used the same observation ensemble throughout the entire model state updating process. The only distinction

between the two cases was the open loop simulations and the perturbations applied to them. Despite using the same type and magnitude of errors in both open loop models, the two model simulations with different configurations behaved differently, resulting in varying model uncertainties. The EnKF weights relative uncertainties of model forecasts and observations based on their covariance matrices and tends to place more trust in the one with lower uncertainty. Therefore, the different performances in both cases are likely attributed to the effects caused by the differing relative uncertainties of the model and observations.

Figure 6-7 compares the variance of observations with the variance of model-predicted states corresponding observations (model forecasts mapped to the observation space via the observation operator) at all updating occasions for both cases. For updates prior to growth stage 50 (reproductive stage) (Zadoks et al., 1974), the relative uncertainties between the model forecasts and observations were similar in both cases, with the variance of observations consistently larger than the variance of model forecasts. This indicates that the filter placed more trust in the model forecasts and performed similarly for both cases at these updating occasions. For updates between growth stage 70 (kernel extending) and stage 82 (early dough development), the variance of model forecasts in the high-yield open loop gradually increased and became larger than observations variance. The largest model forecasts variance was approximately 0.9 and the largest ratio between the variance of model forecasts and that of observations was 4. In contrast, the model forecasts variance in the low-yield open loop increased abruptly during this stage, reaching a maximum value of 2.9 and a ratio of 5.7 with respect to the variance of observations. The increase in model forecasts variance during this stage, particularly in the low-yield open loop case, leading to greater reliance on observations and a higher weight assigned to observations in the low-yield case compared to the high-yield case. The effects of the different assigned observation weights can also be observed in the reduction of uncertainty in yield estimates. The uncertainty of yield estimates in the low-yield case decreased to a range of 0.29 – 0.40 t/ha after data assimilation, whereas the uncertainty in the high-yield case ranged from 0.52 to 0.60 t/ha. The greater trust placed in observations resulted in a decrease in the spread of model forecasts. However, based on the results of yield estimate accuracy, we found that placing excessive trust in observations during the late growth stage may result in less accurate yield estimates, as the data assimilation showed poorer performance for the low-yield open loop case. To

improve the performance in this case, the observation uncertainty should be slightly increased. On the other hand, the promising performance of the filter in the high-yield case highlighted the significance of correctly estimating the uncertainty of model forecasts and observations.

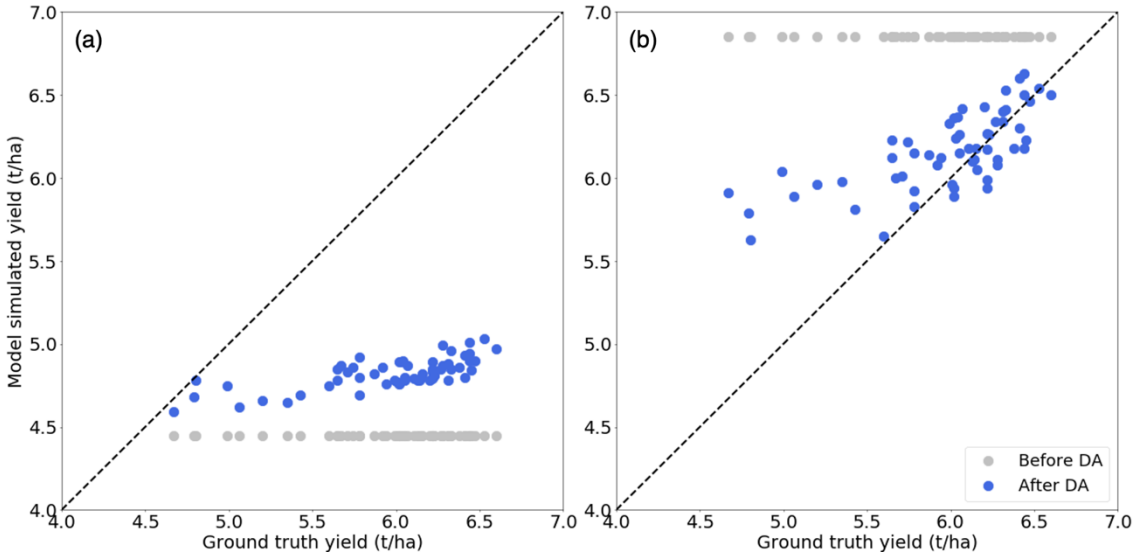

Figure 6-5. Performance of data assimilation for all 58 patches in the paddock with (a) the low-yield open loop case and (b) the high-yield open loop case. The multiplicative observation error with an error level of 20% was used to perturb the observations. The grey points represent the open loop model estimated yields. The blue points represent the data assimilation results (DA: data assimilation).

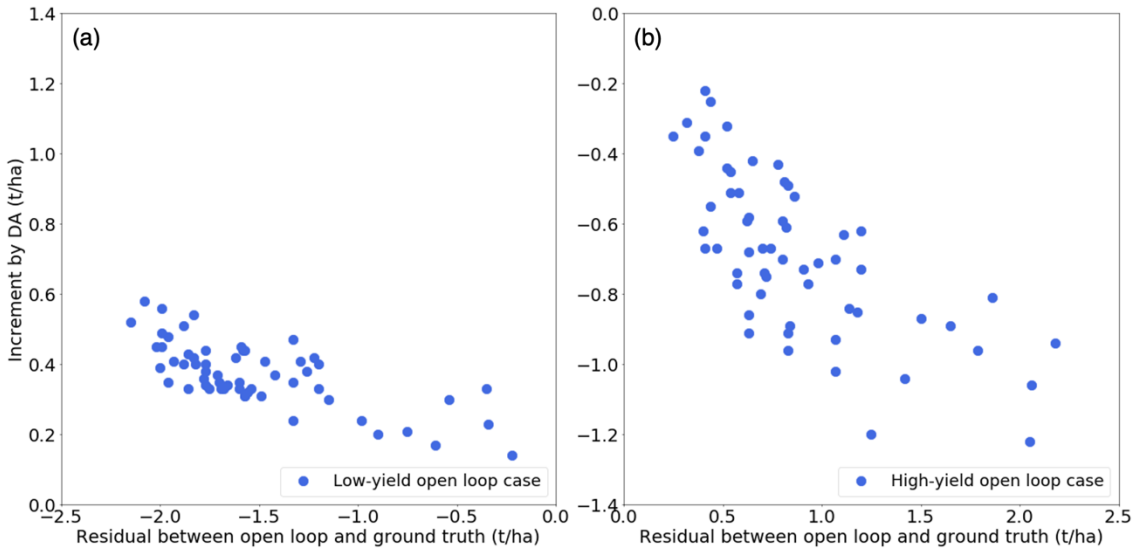

Figure 6-6. The comparison between the residual (= open loop – ground truth yield) and increment obtained through data assimilation for (a) the low-yield open loop and (b) the high-

yield open loop results. The blue points represent the results from the 58 patches (DA: data assimilation).

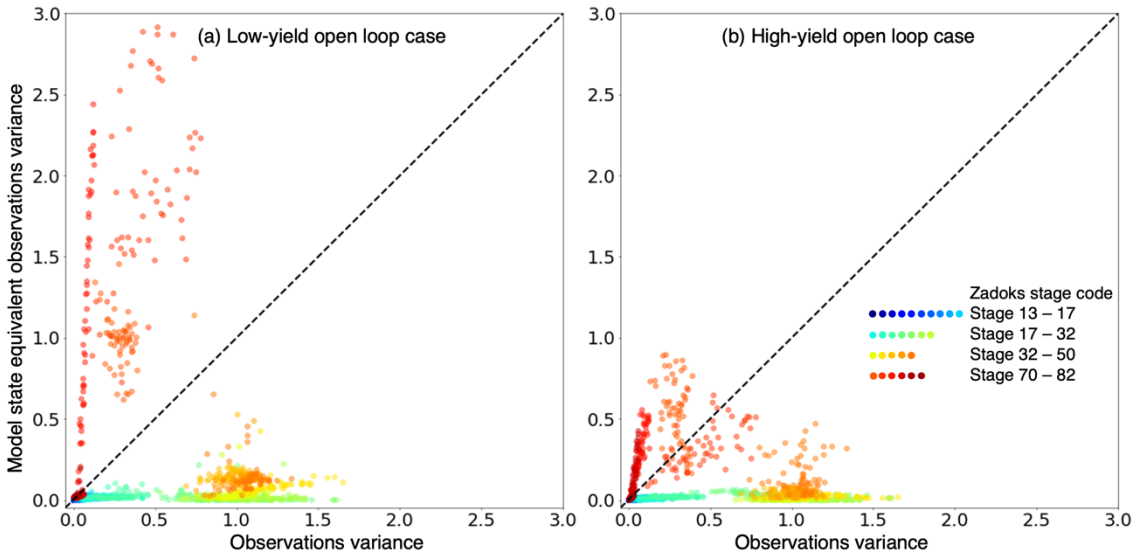

Figure 6-7. The comparison between the observation variance and model forecasted states equivalent observations variance for (a) the low-yield open loop and (b) the high-yield open loop results. The specific point colours for the growth stages are indicated in the legend.

6.5 Conclusion

In this study, satellite-based vegetation observations from Sentienl-2 and PlanetScope during 2019 were assimilated into the APSIM-Wheat model for a rainfed winter-wheat field located in north-western Victoria, Australia. For this, the paddock was segmented into 58 patches with varying levels of harvest yield. A total of 28 red edge chlorophyll index (RECI) imageries were used to represent the wheat growth status throughout the entire growing season. The low-yield and high-yield open loop cases were employed to evaluate the robustness of the designed data assimilation strategy. The results demonstrated that the system can effectively improve the accuracy of yield estimates and constrain uncertainty by integrating vegetation observations and crop models.

Different types and levels of observation errors were evaluated to explore the accurate estimation of observation uncertainty. The Gaussian-distributed multiplicative observation error with a magnitude of 20% was determined to be the most suitable for the data assimilation framework. For the low-yield open loop case, the data assimilation framework improved the accuracy of yield estimates by a less significant *increment* ranged from 0.14 to 0.58 t/ha. The *residual* after data assimilation were between 0.02 and 1.63 t/ha, with a median value of 1.26 t/ha. In contrast, the correction for the high-

yield open loop case was more effective, with the *residual* ranging from 0.01 to 1.24 t/ha and a median value of 0.09 t/ha. However, the reduction of yield estimates uncertainty for the low-yield case was more significant than that for the high-yield case, with a decrease of the standard deviation from 0.76 t/ha to between 0.29 and 0.40 t/ha, compared to a decrease from 0.71 t/ha to a range of 0.52 to 0.60 t/ha.

The different performances for both cases are likely due to the different relative uncertainties of model forecasts and observations. The model uncertainty in the low-yield open loop case was found to be greater than that in the high-yield case, particularly during the late growth stage. The largest ratio of the variance between model forecasts and observations for the low-yield case was 5.7, while it was 4 for the high-yield case. The larger model forecasts uncertainty caused the filter to assign higher weights to observations. From our results, we found that placing excessive trust in observations may lead to poorer yield estimates. To improve performance in the low-yield case, the observation uncertainty should be adaptively increased.

This study only utilised data from a yield monitor in one paddock during a single season as the evaluation dataset. The utilisation of a small dataset for evaluation presented a limitation for the comprehensive assessment of the data assimilation framework. While the results provided useful insights, the analysis could benefit from the inclusion of more data from a greater number of paddocks and seasons to test the robustness of the approach. Furthermore, the use of actual harvest cuts as the “ground truth” may also enhance the accuracy of the evaluation as it could provide a more accurate and reliable reference compared to data from the yield monitor. These measures could lead to a more thorough and reliable evaluation of the data assimilation framework, ultimately contributing to its improvement and broader applicability.

Chapter 7 Discussions and conclusions

The literature review in Chapter 1 identifies the main objective of this thesis as developing an effective data assimilation strategy to improve the performance of within-field crop yield prediction. Several aspects are critical and challenging in designing the data assimilation framework, starting with the accurate estimation of model and observation uncertainty. Estimating model uncertainty involves identifying sources of model uncertainty and quantifying their contributions to yield prediction variability. To address these challenges, Chapter 2 and Chapter 3 present an uncertainty analysis and a sensitivity analysis. The influential factors affecting wheat yield prediction performance were identified through a thorough literature review and meta-analysis. The Sobol' method was then applied to measure the influence of these factors under various environmental and management conditions. Chapter 4 discusses the quantification of observation uncertainty by selecting suitable satellite-based vegetation observations for assimilation and establishing an observation operator. The operator enables direct comparison between observations and model states while allowing for the estimation of observation uncertainty. Chapter 5 designs an effective state updating strategy using a synthetic experiment. The designed framework is then applied in a real case study as presented in Chapter 6, utilising Sentinel-2 and PlanetScope data for a rainfed winter-wheat field located in north-western Victoria, Australia, to evaluate its performance.

7.1 Research findings

1. The APSIM-Wheat yield prediction performance and the factors affecting the performance were investigated. A review of yield prediction results from 76 published studies across four continents was conducted to obtain detailed information about the model's yield prediction performance. A meta-database composed of model evaluation datasets from 30 articles was established to identify influential factors contributing to yield prediction uncertainty. The results showed that the model predicts yield with an uncertainty of approximately 1 t/ha across a wide range of varieties, environments, and management practices worldwide. The calibration of genotype and soil parameters, water and nitrogen

availability, heat and frost stress, lodging, soil cracking, increased atmospheric CO_2 concentration, and plant diseases were identified as influential factors affecting model performance. The most practical suggestions to enhance the model's simulation performance would involve fully calibrating the model to local conditions by fine-tuning soil and cultivar parameters or incorporating observations through data assimilation into the model to continuously adjust specific model state variables and properties. Additionally, suggestions to improve APSIM include: (1) incorporating daily maximum and minimum temperatures as impact factors to account for their effects on crop growth, (2) parameterising frost stress, water stress, and nitrogen stress functions in relation to phenology.

2. In relation to the first contribution, a sensitivity analysis work was conducted to quantify the influential factors' contribution to the final yield prediction variability. The Sobol' method was used to investigate the sensitivity of the APSIM-Wheat yield prediction to factors such as maximum and minimum air temperature, precipitation, initial soil nitrogen content, nitrogen fertilisation amount, and soil hydraulic parameters. Eighteen scenarios were considered to characterise varying environmental and management conditions, including the combination of three weather conditions (wet, moderate, and dry), three soil types (sandy, loamy, and clayey soils), and two nitrogen fertilisation levels (50 kg N/ha and 100 kg N/ha). The results revealed that yield was more sensitive to variables controlling water availability (precipitation and soil hydraulic parameters) or variables controlling nitrogen availability (initial nitrogen content and nitrogen fertilisation amount), depending on which was more limiting to wheat growth under the scenario. Clay soils were less affected by changing weather conditions. Yield exhibited less variability under dry weather and higher fertilisation levels. In contrast, more humid weather conditions resulted in higher yields, but with greater yield variability, regardless of soil type.
3. APSIM-Wheat simulated GLAI was selected as the state variable to be linked with satellite-derived observations during the data assimilation process, as it has strong associations with both observed crop growth status and model-simulated wheat biomass components. An observation operator was developed to map APSIM-Wheat GLAI to equivalent remote sensing observations, enabling direct comparisons between them. Ten vegetation indices derived from Sentinel-2 were

evaluated, and each index was linked with the model-simulated GLAI using the LOWESS curve-fitting method. The linearity of the fitted curves was evaluated to determine the suitability of the index. The results found that individual observation operators were necessary for the pre- and post-GLAI peak periods due to the different trends observed during these two stages. Among the indices evaluated, the chlorophyll index calculated using the red edge and near infrared bands was the most suitable candidate for assimilation into the model, as the corresponding observation operator exhibited the closest approximation to linearity. Additionally, NDVI showed saturation at moderate to high GLAI values.

4. An EnKF-based data assimilation framework was developed by evaluating the efficacy of different state updating strategies, including (1) choice of state variables: updating only the leaf biomass or all biomass components, (2) assimilation interval: updating at a 5-day or 1-day frequency, and (3) phenological stages: updating across the entire growing season, only prior to the GLAI peak time, or only during the post-GLAI peak period. The design of this synthetic experiment was based on the characteristics of the APSIM-Wheat model and Sentinel-2 data. In the APSIM-Wheat model, the leaf biomass is directly linked to the GLAI, suggesting that the leaf biomass can be effectively updated by assimilating vegetation observations. The efficacy of updating other biomass components relies on their correlation with the leaf biomass. The most effective data assimilation strategy was determined and validated through eight representative cases spanning high, median, and low yield estimates. The results indicated that updating all biomass components across the entire growing season at a daily frequency resulted in the greatest improvement in yield prediction. However, giving the temporal resolution of satellite observations, a 5-day frequency was deemed more realistic. For the eight validation cases, updating every 5 days for the entire season effectively decreased the yield prediction *residual* from between 230 and 2134 kg/ha to between 93 and 533 kg/ha. Updating all biomass components outperformed updating only the leaf biomass, suggesting that the model-simulated correlations between the biomass components are reasonably accurate.
5. The designed data assimilation strategy was applied to a real case study for a rainfed winter-wheat field located in north-western Victoria, Australia during

2019. The field was divided into 58 patches with varying levels of harvest yield. PlanetScope data was used to supplement the Sentinel-2 data, which was affected by cloud contamination. A total of 28 red edge chlorophyll index (RECI) images were acquired to track the wheat growth status throughout the growing season. Different types and magnitudes of observation uncertainty were evaluated. The Gaussian-distributed multiplicative observation error with a magnitude of 20% was found to be the most suitable for this data assimilation case. The low-yield and high-yield open loop cases were used to evaluate the robustness of the data assimilation. The results demonstrated that the system is effective in improving the accuracy of yield estimates and limiting uncertainty by integrating vegetation observations and crop models. The proposed data assimilation framework also provides the potential to estimate yield spatially using crop models. Combining spatial continuous remote sensing data with one-dimensional crop models allows for predicting within-field yield variability. The level of spatial detail depends on the spatial resolution of the remote sensing imagery.

7.2 Research limitations and extension opportunities

Chapter 2 through Chapter 6 have presented individual discussions of limitations and recommendations for future work. This Chapter provides an overview of the limitations and future research directions regarding all the research works presented in this thesis.

1. This thesis only focused on the APSIM-Wheat model, the performance of the data assimilation framework when applied to other models and/or crops requires further examination. Different crop models, characterised by distinct parameterisations and configurations, may exhibit varying levels of simulation uncertainty. Various crops, with unique phenological and morphological characteristics, may require the assimilation of observations other than RECI at different updating timings and intervals (Lei et al., 2020; Machwitz et al., 2014; Nearing et al., 2012). Guided by this work, future crop model data assimilation practices can be extended to more models and/or crops by selecting appropriate model states to be updated, determining assimilated observations, developing corresponding observation operators, and designing effective updating strategies.
2. This thesis aimed to improve yield prediction performance by developing a data assimilation framework. Other aspects of model simulation, such as crop

phenology, crop evapotranspiration, and soil-related properties were not explored in this work. The efficacy of assimilating vegetation observations in improving these aspects remains unknown. As reviewed in Chapter 1, researchers have found that the lack of correlations between different state variables can limit the ability of data assimilation (Kivi et al., 2022; Pauwels et al., 2007; Zhang et al., 2021; Zhang et al., 2022). Therefore, to improve the model's prediction ability in other aspects, additional observations may be required.

3. The data assimilation framework developed in this work aims to enhance crop yield predictions by accounting for spatial and temporal variability within fields. It was applied at the field scale. The paddock was segmented into multiple patches, where within each patch, the land surface was considered homogeneous. The weather data was point-based measurements taken at the nearby meteorological station.

   The performance of this framework may vary if it is directly applied at other scales, such as region or global scales, as the heterogeneity of the land surface within each grid may introduce spatial uncertainty into both model simulations and observations (Huang et al., 2015a; Jongschaap and Schouten, 2005; Moulin et al., 1998; Yao et al., 2015). Developing a data assimilation framework at larger scales requires the consideration of additional factors when estimating uncertainties. The development of an observation operator and the characterisation of observation uncertainty necessitate the consideration of topography, land use, and meteorological conditions. The use of geostatistical methods for capturing the spatial autocorrelation of observations can significantly aid in addressing spatial uncertainty. Customisation of observation operators to align with the specific characteristics of the region is necessary. This customisation may entail fine-tuning the observation operators to account for variations in crops, soils, and land use patterns within the region. APSIM, a one-dimensional crop model, requires adaptation to interact with regional climate models or to effectively utilise reanalysis datasets for obtaining more precise meteorological inputs at larger scales.

4. The availability of satellite-based observations is another challenge faced by data assimilation. In Chapter 5, we demonstrated the potential of assimilating synthetic GLAI observations on a 5-day basis in improving yield estimates of the APSIM-Wheat model. Chapter 6 extends the application to a real case study using

remotely sensed observations. Despite supplementing PlanetScope data to fill in the gap of Sentinel-2 due to its cloud contamination, we were only able to find 28 images available during the entire growing season. Observations were missing between growth stage 50 (the start of the reproductive stage) (Zadoks et al., 1974) and 70 (the start of kernel extending), which proved to be a critical period for improving the performance of data assimilation (as discussed in Chapter 5.5.2). In addition, PlanetScope only has four bands available, which required calibration with Sentinel-2 before being applied to data assimilation. In the future, acquiring more frequent and cloud-free remote sensing observations with sufficient spatial resolution and accuracy will further enhance the performance of data assimilation with remotely sensed observations, including synthetic aperture radar (SAR) data, as an observation source to meet the requirements of data assimilation (Arai et al., 2022; Bürgi and Lohman, 2021).

5. This thesis used wheat growth information from a single growing season in one field. The data assimilation framework was evaluated under specific weather and soil conditions. The performance of the framework when applied to other environmental and management conditions remained untested. The sensitivity analysis in Chapter 3 revealed that varying weather, soil, and nitrogen fertilisation conditions affect the sensitivity of the model yield to influential parameters and initial states. Therefore, when applying the framework to other fields with different conditions, it may be necessary to adjust the uncertainty of model forecasts and observations to achieve an appropriate relative uncertainty between them to ensure optimal data assimilation performance. In the future, methods such as adaptive Kalman filtering that can automatically tune the relative uncertainty based on changing conditions can be considered and examined to improve the computational efficiency of the data assimilation process for crop models (Crow and Reichle, 2008; Gruber et al., 2019; Shokri et al., 2019).

Reference

ABARE-BRS, 2003. Australian Farm Survey Report.

ABARES, 2022. Agricultural Commodity Statistics 2022.

Abi Saab, M.T., El Alam, R., Jomaa, I., Skaf, S., Fahed, S., Albrizio, R., Todorovic, M., 2021. Coupling remote sensing data and AquaCrop model for simulation of winter wheat growth under rainfed and irrigated conditions in a Mediterranean environment. Agronomy 11, 2265.

ABS, 2020. Agricultural Commodities, Australia.

Acuña, T.B., Lisson, S., Johnson, P., Dean, G., 2015. Yield and water-use efficiency of wheat in a high-rainfall environment. Crop Pasture Sci. 66, 419–429.

Ahmed, M., Akram, M.N., Asim, M., Aslam, M., ul Hassan, F., Higgins, S., Stöckle, C.O., Hoogenboom, G., 2016. Calibration and validation of APSIM-Wheat and CERES-Wheat for spring wheat under rainfed conditions: Models evaluation and application. Comput. Electron. Agric. 123, 384–401. https://doi.org/10.1016/j.compag.2016.03.015

Ahmed, M., Stöckle, C.O., Nelson, R., Higgins, S., 2017. Assessment of climate change and atmospheric CO2 impact on winter wheat in the Pacific Northwest using a multimodel ensemble. Front. Ecol. Evol. 5, 51.

Akinseye, F.M., Ajeigbe, H.A., Traore, P.C.S., Agele, S.O., Zemadim, B., Whitbread, A., 2020. Improving sorghum productivity under changing climatic conditions: A modelling approach. F. Crop. Res. 246, 107685.

Altaf, M.U., El Gharamti, M., Heemink, A.W., Hoteit, I., 2013. A reduced adjoint approach to variational data assimilation. Comput. Methods Appl. Mech. Eng. 254, 1–13.

Alvarez-Garreton, C., Ryu, D., Western, A.W., Crow, W.T., Robertson, D.E., 2014. The impacts of assimilating satellite soil moisture into a rainfall--runoff model in a semi-arid catchment. J. Hydrol. 519, 2763–2774.

Anwar, M.R., O'Leary, G.J., Rab, M.A., Fisher, P.D., Armstrong, R.D., 2009. Advances in precision agriculture in south-eastern Australia. V. Effect of seasonal conditions on wheat and barley yield response to applied nitrogen across management zones. Crop Pasture Sci. 60, 901–911.

Anwar, M.R., Wang, B., Li Liu, D., Waters, C., 2020. Late planting has great potential to mitigate the effects of future climate change on Australian rain-fed cotton. Sci. Total Environ. 714, 136806.

Arai, H., Le Toan, T., Takeuchi, W., Oyoshi, K., Fumoto, T., Inubushi, K., 2022. Evaluating irrigation status in the Mekong Delta through polarimetric L-band SAR data assimilation. Remote Sens. Environ. 279, 113139.

Araya, A., Kisekka, I., Girma, A., Hadgu, K.M., Tegebu, F.N., Kassa, A.H., Ferreira-Filho, H.R., Beltrao, N.E., Afewerk, A., Abadi, B., others, 2017. The challenges and opportunities for wheat production under future climate in Northern Ethiopia. J. Agric. Sci. 155, 379–393.

Araya, A., Prasad, P.V. V, Gowda, P.H., Djanaguiraman, M., Kassa, A.H., 2020. Potential impacts of climate change factors and agronomic adaptation strategies on wheat yields in central highlands of Ethiopia. Clim. Change 1–19.

Archontoulis, S. V, Miguez, F.E., Moore, K.J., 2014. Evaluating APSIM maize, soil water, soil nitrogen, manure, and soil temperature modules in the Midwestern United States. Agron. J. 106, 1025–1040.

Asrar, G., Kanemasu, E.T., Jackson, R.D., Pinter Jr, P.J., 1985. Estimation of total above-ground phytomass production using remotely sensed data. Remote Sens. Environ. 17, 211–220.

ASRIS, 2011. ASRIS [WWW Document]. Aust. Soil Resour. Inf. Syst. URL http://www.asris.csiro.au (accessed 6.6.22).

Asseng, S., Anderson, G.C., Dunin, F.X., Fillery, I.R.P., Dolling, P.J., Keating, B.A., 1998a. Use of the APSIM wheat model to predict yield, drainage, and NO3-leaching for a deep sand. Aust. J. Agric. Res. 49, 363–378.

Asseng, S., Bar-Tal, A., Bowden, J.W., Keating, B.A., Van Herwaarden, A., Palta, J.A., Huth, N.I., Probert, M.E., 2002. Simulation of grain protein content with APSIM-

Nwheat. Eur. J. Agron. 16, 25–42.

Asseng, S., Ewert, F., Martre, P., Rötter, R.P., Lobell, D.B., Cammarano, D., Kimball, B.A., Ottman, M.J., Wall, G.W., White, J.W., Reynolds, M.P., Alderman, P.D., Prasad, P.V.V., Aggarwal, P.K., Anothai, J., Basso, B., Biernath, C., Challinor, A.J., De Sanctis, G., Doltra, J., Fereres, E., Garcia-Vila, M., Gayler, S., Hoogenboom, G., Hunt, L.A., Izaurralde, R.C., Jabloun, M., Jones, C.D., Kersebaum, K.C., Koehler, A.K., Müller, C., Naresh Kumar, S., Nendel, C., O'leary, G., Olesen, J.E., Palosuo, T., Priesack, E., Eyshi Rezaei, E., Ruane, A.C., Semenov, M.A., Shcherbak, I., Stöckle, C., Stratonovitch, P., Streck, T., Supit, I., Tao, F., Thorburn, P.J., Waha, K., Wang, E., Wallach, D., Wolf, J., Zhao, Z., Zhu, Y., 2015. Rising temperatures reduce global wheat production. Nat. Clim. Chang. 5, 143–147. https://doi.org/10.1038/nclimate2470

Asseng, S., Ewert, F., Rosenzweig, C., Jones, J.W., Hatfield, J.L., Ruane, A.C., Boote, K.J., Thorburn, P.J., Rötter, R.P., Cammarano, D., Brisson, N., Basso, B., Martre, P., Aggarwal, P.K., Angulo, C., Bertuzzi, P., Biernath, C., Challinor, A.J., Doltra, J., Gayler, S., Goldberg, R., Grant, R., Heng, L., Hooker, J., Hunt, L.A., Ingwersen, J., Izaurralde, R.C., Kersebaum, K.C., Müller, C., Naresh Kumar, S., Nendel, C., O'Leary, G., Olesen, J.E., Osborne, T.M., Palosuo, T., Priesack, E., Ripoche, D., Semenov, M.A., Shcherbak, I., Steduto, P., Stöckle, C., Stratonovitch, P., Streck, T., Supit, I., Tao, F., Travasso, M., Waha, K., Wallach, D., White, J.W., Williams, J.R., Wolf, J., 2013. Uncertainty in simulating wheat yields under climate change. Nat. Clim. Chang. 3, 827–832. https://doi.org/10.1038/nclimate1916

Asseng, S., Foster, I.A.N., Turner, N.C., 2011. The impact of temperature variability on wheat yields. Glob. Chang. Biol. 17, 997–1012.

Asseng, S., Jamieson, P.D., Kimball, B., Pinter, P., Sayre, K., Bowden, J.W., Howden, S.M., 2004. Simulated wheat growth affected by rising temperature, increased water deficit and elevated atmospheric CO2. F. Crop. Res. 85, 85–102. https://doi.org/10.1016/S0378-4290(03)00154-0

Asseng, S., Keating, B.A., Fillery, I.R.P., Gregory, P.J., Bowden, J.W., Turner, N.C., Palta, J.A., Abrecht, D.G., 1998b. Performance of the APSIM-wheat model in Western Australia. F. Crop. Res. 57, 163–179.

Asseng, S., Turner, N.C., Keating, B.A., 2001. Analysis of water-and nitrogen-use efficiency of wheat in a Mediterranean climate. Plant Soil 233, 127–143.

Asseng, S., Van Keulen, H., Stol, W., 2000. Performance and application of the APSIM Nwheat model in the Netherlands. Eur. J. Agron. 12, 37–54.

Aubert, D., Loumagne, C., Oudin, L., 2003. Sequential assimilation of soil moisture and streamflow data in a conceptual rainfall--runoff model. J. Hydrol. 280, 145–161.

Bach, H., Mauser, W., 2003. Methods and examples for remote sensing data assimilation in land surface process modeling. IEEE Trans. Geosci. Remote Sens. 41, 1629–1637. https://doi.org/10.1109/TGRS.2003.813270

Bahri, H., Annabi, M., M'Hamed, H.C., Frija, A., 2019. Assessing the long-term impact of conservation agriculture on wheat-based systems in Tunisia using APSIM simulations under a climate change context. Sci. Total Environ. 692, 1223–1233.

Bai, H., Wang, J., Fang, Q., Huang, B., 2020. Does a trade-off between yield and efficiency reduce water and nitrogen inputs of winter wheat in the North China Plain? Agric. Water Manag. 233, 106095.

Bai, H., Xiao, D., Wang, B., Liu, D.L., Tang, J., 2022. Simulation of wheat response to future climate change based on coupled model inter-comparison project phase 6 multi-model ensemble projections in the North China Plain. Front. Plant Sci. 13, 829580.

Balwinder-Singh, Gaydon, D.S., Humphreys, E., Eberbach, P.L., 2011. The effects of mulch and irrigation management on wheat in Punjab, India—Evaluation of the APSIM model. F. Crop. Res. 124, 1–13.

Ban, H.-Y., Ahn, J.-B., Lee, B.-W., 2019. Assimilating MODIS data-derived minimum input data set and water stress factors into CERES-Maize model improves regional corn yield predictions. PLoS One 14, e0211874.

Baret, F., Houlès, V., Guérif, M., 2007. Quantification of plant stress using remote sensing observations and crop models: The case of nitrogen management. J. Exp. Bot. 58, 869–880. https://doi.org/10.1093/jxb/erl231

Barlow, K.M., Christy, B.P., O'leary, G.J., Riffkin, P.A., Nuttall, J.G., 2015. Simulating the impact of extreme heat and frost events on wheat crop production: A review. F.

Crop. Res. 171, 109–119.

Basso, B., Cammarano, D., Carfagna, E., 2013. Review of crop yield forecasting methods and early warning systems, in: Proceedings of the First Meeting of the Scientific Advisory Committee of the Global Strategy to Improve Agricultural and Rural Statistics, FAO Headquarters, Rome, Italy. p. 19.

Basso, B., Liu, L., 2019. Seasonal crop yield forecast: Methods, applications, and accuracies. Adv. Agron. 154, 201–255.

Bastiaanssen, W.G.M., Ali, S., 2003. A new crop yield forecasting model based on satellite measurements applied across the Indus Basin, Pakistan. Agric. Ecosyst. Environ. 94, 321–340.

Bell, L.W., Hargreaves, J.N.G., Lawes, R.A., Robertson, M.J., 2009. Sacrificial grazing of wheat crops: identifying tactics and opportunities in Western Australia's grainbelt using simulation approaches. Anim. Prod. Sci. 49, 797–806.

Bell, L.W., Lilley, J.M., Hunt, J.R., Kirkegaard, J.A., 2015. Optimising grain yield and grazing potential of crops across Australia's high-rainfall zone: a simulation analysis. 1. Wheat. Crop Pasture Sci. 66, 332–348.

Bernard, R., Vauclin, M., Vidal-Madjar, D., 1981. Possible use of active microwave remote sensing data for prediction of regional evaporation by numerical simulation of soil water movement in the unsaturated zone. Water Resour. Res. 17, 1603–1610.

Boas, T., Bogena, H., Grünwald, T., Heinesch, B., Ryu, D., Schmidt, M., Vereecken, H., Western, A., Hendricks Franssen, H.-J., 2021. Improving the representation of cropland sites in the Community Land Model (CLM) version 5.0. Geosci. Model Dev. 14, 573–601.

Boegh, E., Houborg, R., Bienkowski, J., Braban, C.F., Dalgaard, T., Van Dijk, N., Dragosits, U., Holmes, E., Magliulo, V., Schelde, K., others, 2013. Remote sensing of LAI, chlorophyll and leaf nitrogen pools of crop-and grasslands in five European landscapes. Biogeosciences 10, 6279–6307.

Bosi, C., Sentelhas, P.C., Huth, N.I., Pezzopane, J.R.M., Andreucci, M.P., Santos, P.M., 2020. APSIM-Tropical Pasture: A model for simulating perennial tropical grass growth and its parameterisation for palisade grass (Brachiaria brizantha). Agric.

Syst. 184, 102917.

Bouman, B. a. M., 1995. Crop modelling and remote sensing for yield prediction. NJAS wageningen J. life Sci. 43, 143–161.

Bouman, B.A.M., 2001. ORYZA2000: modeling lowland rice. IRRI.

Brission, N., Ruget, F., Gate, P., Lorgeou, J., Nicoullaud, B., Tayot, X., Plenet, D., Jeuffroy, M.H., Bouthier, A., Ripoche, D., Mary, B., Justes, E., 2002. STICS: a generic model for simulating crops and their water and nitrogen balances. II. Model validation for wheat and maize. Agronomie 22, 69–92.

Brisson, N., Gary, C., Justes, E., Roche, R., Mary, B., Ripoche, D., Zimmer, D., Sierra, J., Bertuzzi, P., Burger, P., Bussière, F., Cabidoche, Y.M., Cellier, P., Debaeke, P., Gaudillère, J.P., Hénault, C., Maraux, F., Seguin, B., Sinoquet, H., 2003. An overview of the crop model STICS. Eur. J. Agron. 18, 309–332. https://doi.org/10.1016/S1161-0301(02)00110-7

Brisson, Nadine, Gary, C., Justes, E., Roche, R., Mary, B., Ripoche, D., Zimmer, D., Sierra, J., Bertuzzi, P., Burger, P., others, 2003. An overview of the crop model STICS. Eur. J. Agron. 18, 309–332.

Brisson, N., Mary, B., Ripoche, D., Jeuffroy, M.H., Ruget, F., Nicoullaud, B., Gate, P., Devienne-Barret, F., Antonioletti, R., Durr, C., others, 1998a. STICS: a generic model for the simulation of crops and their water and nitrogen balances. I. Theory and parameterization applied to wheat and corn.

Brisson, N., Mary, B., Ripoche, D., Jeuffroy, M.H., Ruget, F., Nicoullaud, B., Gate, P., Devienne-Barret, F., Antonioletti, R., Durr, C., Richard, G., Beaudoin, N., Recous, S., Tayot, X., Plenet, D., Cellier, P., Machet, J.-M., Meynard, J.M., Delécolle, R., 1998b. STICS: a generic model for the simulation of crops and their water and nitrogen balances. I. Theory and parameterization applied to wheat and corn. Agronomie 18, 311–346. https://doi.org/10.1051/agro:19980501

Brisson, N., Ruget, F., Gate, P., Lorgeou, J., Nicoullaud, B., Tayot, X., Plenet, D., Jeuffroy, M.-H., Bouthier, A., Ripoche, D., others, 2002. STICS: a generic model for simulating crops and their water and nitrogen balances. II. Model validation for wheat and maize. Agronomie 22, 69–92.

Brown, H., Huth, N., Holzworth, D., 2018. Crop model improvement in APSIM: Using wheat as a case study. Eur. J. Agron. 0–1. https://doi.org/10.1016/j.eja.2018.02.002

Brown, H.E., Huth, N.I., Holzworth, D.P., Teixeira, E.I., Wang, E., Zyskowski, R.F., Zheng, B., 2019. A generic approach to modelling, allocation and redistribution of biomass to and from plant organs. in silico Plants 1, diy004.

Brown, H.E., Huth, N.I., Holzworth, D.P., Teixeira, E.I., Zyskowski, R.F., Hargreaves, J.N.G., Moot, D.J., 2014. Plant modelling framework: software for building and running crop models on the APSIM platform. Environ. Model. Softw. 62, 385–398.

Bryan, B.A., King, D., Zhao, G., 2014. Influence of management and environment on Australian wheat: information for sustainable intensification and closing yield gaps. Environ. Res. Lett. 9, 44005.

Bureau of Meteorology, 2020. Climate Data Online [WWW Document]. URL http://www.bom.gov.au/climate/data/index.shtml (accessed 6.6.22).

Bürgi, P.M., Lohman, R.B., 2021. High-Resolution Soil Moisture Evolution in Hyper-Arid Regions: A Comparison of InSAR, SAR, Microwave, Optical, and Data Assimilation Systems in the Southern Arabian Peninsula. J. Geophys. Res. Earth Surf. 126, e2021JF006158.

Bustos-Korts, D., Boer, M.P., Malosetti, M., Chapman, S., Chenu, K., Zheng, B., Van Eeuwijk, F.A., 2019. Combining crop growth modeling and statistical genetic modeling to evaluate phenotyping strategies. Front. Plant Sci. 10, 1491.

Carberry, P.S., Abrecht, D.G., 1991. Tailoring crop models to the semiarid tropics.

Carberry, P.S., Hochman, Z., Hunt, J.R., Dalgliesh, N.P., McCown, R.L., Whish, J.P.M., Robertson, M.J., Foale, M.A., Poulton, P.L., Van Rees, H., 2009. Re-inventing model-based decision support with Australian dryland farmers. 3. Relevance of APSIM to commercial crops. Crop Pasture Sci. 60, 1044–1056.

Carberry, P.S., Liang, W., Twomlow, S., Holzworth, D.P., Dimes, J.P., McClelland, T., Huth, N.I., Chen, F., Hochman, Z., Keating, B.A., 2013. Scope for improved eco-efficiency varies among diverse cropping systems. Proc. Natl. Acad. Sci. 110, 8381–8386.

Carrassi, A., Bocquet, M., Bertino, L., Evensen, G., 2018. Data assimilation in the

geosciences: An overview of methods, issues, and perspectives. Wiley Interdiscip. Rev. Clim. Chang. 9, e535.

Casadebaig, P., Zheng, B., Chapman, S., Huth, N., Faivre, R., Chenu, K., 2016. Assessment of the potential impacts of wheat plant traits across environments by combining crop modeling and global sensitivity analysis. PLoS One 11, e0146385.

Chakrabarti, S., Bongiovanni, T., Judge, J., Zotarelli, L., Bayer, C., 2014. Assimilation of SMOS soil moisture for quantifying drought impacts on crop yield in agricultural regions. IEEE J. Sel. Top. Appl. Earth Obs. Remote Sens. 7, 3867–3879. https://doi.org/10.1109/JSTARS.2014.2315999

Challinor, A.J., Wheeler, T.R., 2008. Crop yield reduction in the tropics under climate change: processes and uncertainties. Agric. For. Meteorol. 148, 343–356.

Chapagain, R., Remenyi, T.A., Harris, R.M.B., Mohammed, C.L., Huth, N., Wallach, D., Rezaei, E.E., Ojeda, J.J., 2022. Decomposing crop model uncertainty: A systematic review. F. Crop. Res. 279, 108448.

Chapman, S., Cooper, M., Podlich, D., Hammer, G., 2003. Evaluating plant breeding strategies by simulating gene action and dryland environment effects. Agron. J. 95, 99–113.

Chauhan, Y.S., Ryan, M., Chandra, S., Sadras, V.O., 2019. Accounting for soil moisture improves prediction of flowering time in chickpea and wheat. Sci. Rep. 9, 1–11.

Chen, C., Wang, E., Yu, Q., 2010a. Modeling wheat and maize productivity as affected by climate variation and irrigation supply in North China Plain. Agron. J. 102, 1037–1049.

Chen, C., Wang, E., Yu, Q., 2010b. Modelling the effects of climate variability and water management on crop water productivity and water balance in the North China Plain. Agric. Water Manag. 97, 1175–1184. https://doi.org/10.1016/j.agwat.2008.11.012

Chen, C., Wang, E., Yu, Q., Zhang, Y., 2010c. Quantifying the effects of climate trends in the past 43 years (1961--2003) on crop growth and water demand in the North China Plain. Clim. Change 100, 559–578.

Chen, Y., Zhang, Z., Tao, F., 2018. Improving regional winter wheat yield estimation through assimilation of phenology and leaf area index from remote sensing data.

Eur. J. Agron. 101, 163–173.

Clark, M.P., Rupp, D.E., Woods, R.A., Zheng, X., Ibbitt, R.P., Slater, A.G., Schmidt, J., Uddstrom, M.J., 2008. Hydrological data assimilation with the ensemble Kalman filter: Use of streamflow observations to update states in a distributed hydrological model. Adv. Water Resour. 31, 1309–1324.

Claverie, M., Demarez, V., Duchemin, B., Hagolle, O., Keravec, P., Marciel, B., Ceschia, E., Dejoux, J.-F., Dedieu, G., 2009. Spatialization of crop leaf area index and biomass by combining a simple crop model SAFY and high spatial and temporal resolutions remote sensing data, in: Geoscience and Remote Sensing Symposium, 2009 IEEE International, IGARSS 2009. pp. III--478.

Clevers, J., Büker, C., Van Leeuwen, H.J.C., Bouman, B.A.M., 1994. A framework for monitoring crop growth by combining directional and spectral remote sensing information. Remote Sens. Environ. 50, 161–170.

Clevers, J.G.P.., 1997. A simplified approach for yield prediction of sugar beet based on optical remote sensing data. Remote Sens. Environ. 61, 221–228. https://doi.org/10.1016/S0034-4257(97)00004-7

Collins, B., Najeeb, U., Luo, Q., Tan, D.K.Y., 2021. Contribution of climate models and APSIM phenological parameters to uncertainties in spring wheat simulations: Application of SUFI-2 algorithm in northeast Australia. J. Agron. Crop Sci.

Confalonieri, R., Bregaglio, S., Acutis, M., 2016. Quantifying uncertainty in crop model predictions due to the uncertainty in the observations used for calibration. Ecol. Modell. 328, 72–77.

Connolly, R.D., Bell, M., Huth, N., Freebairn, D.M., Thomas, G., 2002. Simulating infiltration and the water balance in cropping systems with APSIM-SWIM. Soil Res. 40, 221–242.

Čorňák, A., Delina, R., 2022. Application of Remote Sensing Data in Crop Yield and Quality: Systematic Literature Review. Qual. Innov. Prosper. 26, 22–36.

Courtier, P., Thépaut, J.-N., Hollingsworth, A., 1994. A strategy for operational implementation of 4D-Var, using an incremental approach. Q. J. R. Meteorol. Soc. 120, 1367–1387.

Crow, W.T., den Berg, M.J., 2010. An improved approach for estimating observation and model error parameters in soil moisture data assimilation. Water Resour. Res. 46.

Crow, W.T., Reichle, R.H., 2008. Comparison of adaptive filtering techniques for land surface data assimilation. Water Resour. Res. 44.

Crow, W.T., Ryu, D., 2009. A new data assimilation approach for improving runoff prediction using remotely-sensed soil moisture retrievals. Hydrol. Earth Syst. Sci. 13, 1–16.

Crow, W.T., Van Loon, E., 2006. Impact of incorrect model error assumptions on the sequential assimilation of remotely sensed surface soil moisture. J. Hydrometeorol. 7, 421–432.

Curnel, Y., de Wit, A.J.W., Duveiller, G., Defourny, P., 2011. Potential performances of remotely sensed LAI assimilation in WOFOST model based on an OSS Experiment. Agric. For. Meteorol. 151, 1843–1855. https://doi.org/10.1016/j.agrformet.2011.08.002

Dalgliesh, N., Cocks, B., Horan, H., others, 2012. APSoil-providing soils information to consultants, farmers and researchers, in: 16th Australian Agronomy Conference, Armidale, NSW.

Dalgliesh, N.P., Foale, M.A., McCown, R.L., 2009. Re-inventing model-based decision support with Australian dryland farmers. 2. Pragmatic provision of soil information for paddock-specific simulation and farmer decision making. Crop Pasture Sci. 60, 1031–1043.

Dalgliesh, N.P., Hochman, Z., Huth, N.I., Holzworth, D.P., 2016. Field Protocol to APSoil characterisations.

de Wit, A.J.W., van Diepen, C.A., 2007. Crop model data assimilation with the Ensemble Kalman filter for improving regional crop yield forecasts. Agric. For. Meteorol. 146, 38–56. https://doi.org/10.1016/j.agrformet.2007.05.004

Deihimfard, R., Eyni-Nargeseh, H., Mokhtassi-Bidgoli, A., 2018. Effect of future climate change on wheat yield and water use efficiency under semi-arid conditions as predicted by APSIM-wheat model. Int. J. Plant Prod. 12, 115–125.

Deihimfard, R., Mahallati, M.N., Koocheki, A., 2015. Yield gap analysis in major wheat growing areas of Khorasan province, Iran, through crop modelling. F. Crop. Res. 184, 28–38.

Del Moral, P., 1997. Nonlinear filtering: Interacting particle resolution. Comptes Rendus l'Académie des Sci. I-Mathematics 325, 653–658.

Dente, L., Satalino, G., Mattia, F., Rinaldi, M., 2008. Assimilation of leaf area index derived from ASAR and MERIS data into CERES-Wheat model to map wheat yield. Remote Sens. Environ. 112, 1395–1407. https://doi.org/10.1016/j.rse.2007.05.023

Dokoohaki, H., Kivi, M.S., Martinez-Feria, R., Miguez, F.E., Hoogenboom, G., 2021. A comprehensive uncertainty quantification of large-scale process-based crop modeling frameworks. Environ. Res. Lett. 16, 84010.

Dokoohaki, H., Miguez, F.E., Archontoulis, S., Laird, D., 2018. Use of inverse modelling and Bayesian optimization for investigating the effect of biochar on soil hydrological properties. Agric. Water Manag. 208, 268–274.

Dong, Y., Zhao, C., Yang, G., Chen, L., Wang, J., Feng, H., 2013. Integrating a very fast simulated annealing optimization algorithm for crop leaf area index variational assimilation. Math. Comput. Model. 58, 871–879. https://doi.org/10.1016/j.mcm.2012.12.013

Donohue, R.J., Lawes, R.A., Mata, G., Gobbett, D., Ouzman, J., 2018. Towards a national, remote-sensing-based model for predicting field-scale crop yield. F. Crop. Res. 227, 79–90.

Dorigo, W.A., Zurita-Milla, R., de Wit, A.J.W., Brazile, J., Singh, R., Schaepman, M.E., 2007. A review on reflective remote sensing and data assimilation techniques for enhanced agroecosystem modeling. Int. J. Appl. Earth Obs. Geoinf. 9, 165–193. https://doi.org/10.1016/j.jag.2006.05.003

Draper, C., Reichle, R., 2015. The impact of near-surface soil moisture assimilation at subseasonal, seasonal, and inter-annual timescales. Hydrol. Earth Syst. Sci. 19, 4831–4844.

Dzotsi, K.A., Basso, B., Jones, J.W., 2015. Parameter and uncertainty estimation for maize, peanut and cotton using the SALUS crop model. Agric. Syst. 135, 31–47.

Eicker, A., Schumacher, M., Kusche, J., Döll, P., Schmied, H.M., 2014. Calibration/data assimilation approach for integrating GRACE data into the WaterGAP Global Hydrology Model (WGHM) using an ensemble Kalman filter: First results. Surv. Geophys. 35, 1285–1309.

Elbern, H., Schmidt, H., Ebel, A., 1997. Variational data assimilation for tropospheric chemistry modeling. J. Geophys. Res. Atmos. 102, 15967–15985.

Evensen, G., 2003. The ensemble Kalman filter: Theoretical formulation and practical implementation. Ocean Dyn. 53, 343–367.

Evensen, G., 1994. Sequential data assimilation with a nonlinear quasi-geostrophic model using Monte Carlo methods to forecast error statistics. J. Geophys. Res. Ocean. 99, 10143–10162.

Fang, H., Liang, S., Hoogenboom, G., 2011. Integration of MODIS LAI and vegetation index products with the CSM-CERES-Maize model for corn yield estimation. Int. J. Remote Sens. 32, 1039–1065. https://doi.org/10.1080/01431160903505310

Fang, H., Liang, S., Hoogenboom, G., Teasdale, J., Cavigelli, M., 2008. Corn-yield estimation through assimilation of remotely sensed data into the CSM-CERES-Maize model. Int. J. Remote Sens. 29, 3011–3032. https://doi.org/10.1080/01431160701408386

FAO, 2020. World Food and Agriculture - Statistical Yearbook 2020. Rome.

FAOSTAT Statistical Database, 2017. International wheat production statistics [WWW Document]. Food Agric. Organ. United Nations. URL http://www.fao.org/faostat/en/#data/QCL/visualize

Fisher, J.S., Asseng, S., Bowden, J.W., Robertson, M.J., others, 2001. Trial-years without tears: enhancing recommendations of flowering and yield in wheat, in: Proceedings of the 10th Australian Agronomy Conference, Hobart,(Australian Society of Agronomy). Http://Www. Regional. Org. Au/Au/Asa/2001/6/d/Fisher. Htm.

Fletcher, A.L., Chen, C., Ota, N., Lawes, R.A., Oliver, Y.M., 2020. Has historic climate change affected the spatial distribution of water-limited wheat yield across Western Australia? Clim. Change 1–18.

Foody, G.M., Atkinson, P.M., 2002. Current status of uncertainty issues in remote

sensing and GIS. Uncertain. Remote Sens. GIS 287–302.

Frederiks, T.M., Christopher, J.T., Harvey, G.L., Sutherland, M.W., Borrell, A.K., 2012. Current and emerging screening methods to identify post-head-emergence frost adaptation in wheat and barley. J. Exp. Bot. 63, 5405–5416.

French, R.J., Schultz, J.E., 1984. Water use efficiency of wheat in a Mediterranean-type environment. I. The relation between yield, water use and climate. Aust. J. Agric. Res. 35, 743–764.

Fritz, S., See, L., Bayas, J.C.L., Waldner, F., Jacques, D., Becker-Reshef, I., Whitcraft, A., Baruth, B., Bonifacio, R., Crutchfield, J., Rembold, F., Rojas, O., Schucknecht, A., Van der Velde, M., Verdin, J., Wu, B., Yan, N., You, L., Gilliams, S., Mücher, S., Tetrault, R., Moorthy, I., McCallum, I., 2019. A comparison of global agricultural monitoring systems and current gaps. Agric. Syst. 168, 258–272. https://doi.org/https://doi.org/10.1016/j.agsy.2018.05.010

Fuller, M.P., Fuller, A.M., Kaniouras, S., Christophers, J., Fredericks, T., 2007. The freezing characteristics of wheat at ear emergence. Eur. J. Agron. 26, 435–441.

Gaydon, D. S., Balwinder-Singh, Wang, E., Poulton, P.L., Ahmad, B., Ahmed, F., Akhter, S., Ali, I., Amarasingha, R., Chaki, A.K., Chen, C., Choudhury, B.U., Darai, R., Das, A., Hochman, Z., Horan, H., Hosang, E.Y., Kumar, P.V., Khan, A.S.M.M.R., Laing, A.M., Liu, L., Malaviachichi, M.A.P.W.K., Mohapatra, K.P., Muttaleb, M.A., Power, B., Radanielson, A.M., Rai, G.S., Rashid, M.H., Rathanayake, W.M.U.K., Sarker, M.M.R., Sena, D.R., Shamim, M., Subash, N., Suriadi, A., Suriyagoda, L.D.B., Wang, G., Wang, J., Yadav, R.K., Roth, C.H., 2017. Evaluation of the APSIM model in cropping systems of Asia. F. Crop. Res. 204, 52–75. https://doi.org/10.1016/j.fcr.2016.12.015

Gaydon, D.S., Lisson, S.N., Xevi, E., others, 2006. Application of APSIM 'multi-paddock'to estimate whole-of-farm water-use efficiency, system water balance and crop production for a rice-based operation in the Coleambally Irrigation District, NSW, in: Proceedings of the 13th Australian Society of Agronomy Conference. pp. 10–14.

Gaydon, D S, Wang, E., Poulton, P.L., Ahmad, B., Ahmed, F., Akhter, S., Ali, I., Amarasingha, R., Chaki, A.K., Chen, C., others, 2017. Evaluation of the APSIM

model in cropping systems of Asia. F. Crop. Res. 204, 52–75.

Gitelson, A., Merzlyak, M.N., 1994. Spectral reflectance changes associated with autumn senescence of Aesculus hippocastanum L. and Acer platanoides L. leaves. Spectral features and relation to chlorophyll estimation. J. Plant Physiol. 143, 286–292.

Gitelson, A.A., 2004. Wide dynamic range vegetation index for remote quantification of biophysical characteristics of vegetation. J. Plant Physiol. 161, 165–173.

Gitelson, A.A., Gritz, Y., Merzlyak, M.N., 2003a. Relationships between leaf chlorophyll content and spectral reflectance and algorithms for non-destructive chlorophyll assessment in higher plant leaves. J. Plant Physiol. 160, 271–282.

Gitelson, A.A., Viña, A., Arkebauer, T.J., Rundquist, D.C., Keydan, G., Leavitt, B., 2003b. Remote estimation of leaf area index and green leaf biomass in maize canopies. Geophys. Res. Lett. 30.

Gitelson, A.A., Viña, A., Ciganda, V., Rundquist, D.C., Arkebauer, T.J., 2005. Remote estimation of canopy chlorophyll content in crops. Geophys. Res. Lett. 32.

Glen, G., Isaacs, K., 2012. Estimating Sobol sensitivity indices using correlations. Environ. Model. & Softw. 37, 157–166.

Gobron, N., Pinty, B., Verstraete, M.M., Widlowski, J.-L., 2000. Advanced vegetation indices optimized for up-coming sensors: Design, performance, and applications. IEEE Trans. Geosci. Remote Sens. 38, 2489–2505.

Gorelick, N., Hancher, M., Dixon, M., Ilyushchenko, S., Thau, D., Moore, R., 2017. Google Earth Engine: Planetary-scale geospatial analysis for everyone. Remote Sens. Environ. https://doi.org/10.1016/j.rse.2017.06.031

Gruber, A., De Lannoy, G., Crow, W., 2019. A Monte Carlo based adaptive Kalman filtering framework for soil moisture data assimilation. Remote Sens. Environ. 228, 105–114.

Guérif, M., Duke, C.L., 2000. Adjustment procedures of a crop model to the site specific characteristics of soil and crop using remote sensing data assimilation. Agric. Ecosyst. Environ. 81, 57–69. https://doi.org/10.1016/S0167-8809(00)00168-7

Guo, C., Zhang, L., Zhou, X., Zhu, Y., Cao, W., Qiu, X., Cheng, T., Tian, Y., 2018.

Integrating remote sensing information with crop model to monitor wheat growth and yield based on simulation zone partitioning. Precis. Agric. 19, 55–78.

Hadria, R., Duchemin, B., Lahrouni, A., Khabba, S., Er-Raki, S., Dedieu, G., Chehbouni, A.G., Olioso, A., 2006. Monitoring of irrigated wheat in a semi-arid climate using crop modelling and remote sensing data: Impact of satellite revisit time frequency. Int. J. Remote Sens. 27, 1093–1117. https://doi.org/10.1080/01431160500382980

Hain, C.R., Crow, W.T., Anderson, M.C., Mecikalski, J.R., 2012. An ensemble Kalman filter dual assimilation of thermal infrared and microwave satellite observations of soil moisture into the Noah land surface model. Water Resour. Res. 48.

Hammer, G.L., Muchow, R.C., 1991. Quantifying climatic risk to sorghum in Australia's semiarid tropics and subtropics: model development and simulation.

Hammer, G.L., van Oosterom, E., McLean, G., Chapman, S.C., Broad, I., Harland, P., Muchow, R.C., 2010. Adapting APSIM to model the physiology and genetics of complex adaptive traits in field crops. J. Exp. Bot. 61, 2185–2202.

Hansen, J.W., Mishra, A., Rao, K.P.C., Indeje, M., Ngugi, R.K., 2009. Potential value of GCM-based seasonal rainfall forecasts for maize management in semi-arid Kenya. Agric. Syst. 101, 80–90.

Hao, S., Ryu, D., Western, A., Perry, E., Bogena, H., Franssen, H.J.H., 2021. Performance of a wheat yield prediction model and factors influencing the performance: A review and meta-analysis. Agric. Syst. 194, 103278.

Hartig, F., Calabrese, J.M., Reineking, B., Wiegand, T., Huth, A., 2011. Statistical inference for stochastic simulation models--theory and application. Ecol. Lett. 14, 816–827.

He, L., Cleverly, J., Chen, C., Yang, X., Li, J., Liu, W., Yu, Q., 2014. Diverse responses of winter wheat yield and water use to climate change and variability on the semiarid Loess Plateau in China. Agron. J. 106, 1169–1178.

He, L., Zhao, G., Jin, N., Zhuang, W., Yu, Q., 2015. Global sensitivity analysis of APSIM-Wheat parameters in different climate zones and yield levels. Trans. Chinese Soc. Agric. Eng. 31, 148–157.

Hearn, A.B., 1994. OZCOT: a simulation model for cotton crop management. Agric.

Syst. 44, 257–299.

Helmert, J., Şensoy Şorman, A., Alvarado Montero, R., De Michele, C., De Rosnay, P., Dumont, M., Finger, D.C., Lange, M., Picard, G., Potopová, V., others, 2018. Review of snow data assimilation methods for hydrological, land surface, meteorological and climate models: Results from a cost harmosnow survey. Geosciences 8, 489.

Hochman, Z., Dang, Y.P., Schwenke, G.D., Dalgliesh, N.P., Routley, R., McDonald, M., Daniells, I.G., Manning, W., Poulton, P.L., 2007. Simulating the effects of saline and sodic subsoils on wheat crops growing on Vertosols. Aust. J. Agric. Res. 58, 802–810.

Hochman, Z., Gobbett, D., Holzworth, D., McClelland, T., van Rees, H., Marinoni, O., Garcia, J.N., Horan, H., 2013. Reprint of "Quantifying yield gaps in rainfed cropping systems: A case study of wheat in Australia." F. Crop. Res. 143, 65–75.

Hochman, Z., Holzworth, D., Hunt, J.R., 2009a. Potential to improve on-farm wheat yield and WUE in Australia. Crop Pasture Sci. 60, 708–716.

Hochman, Z., Van Rees, H., Carberry, P.S., Hunt, J.R., McCown, R.L., Gartmann, A., Holzworth, D., Van Rees, S., Dalgliesh, N.P., Long, W., others, 2009b. Re-inventing model-based decision support with Australian dryland farmers. 4. Yield Prophet®helps farmers monitor and manage crops in a variable climate. Crop Pasture Sci. 60, 1057–1070.

Holzworth, D., Huth, N.I., Fainges, J., Brown, H., Zurcher, E., Cichota, R., Verrall, S., Herrmann, N.I., Zheng, B., Snow, V., 2018. APSIM Next Generation: Overcoming challenges in modernising a farming systems model. Environ. Model. Softw. 103, 43–51.

Holzworth, D., Meinke, H., DeVoil, P., Wegener, M., Huth, N., Hammer, G., Howden, M., Robertson, M., Carberry, P., Freebairn, D., Murphy, C., 2006. The development of a farming systems model (APSIM) – a disciplined approach. Int. Environ. Model. Softw. Soc. 1–13. https://doi.org/10.1111/j.1439-0434.2010.01768.x

Holzworth, D.P., Huth, N.I., deVoil, P.G., 2011. Simple software processes and tests improve the reliability and usefulness of a model. Environ. Model. Softw. 26, 510–

516.

Holzworth, D.P., Huth, N.I., deVoil, P.G., Zurcher, E.J., Herrmann, N.I., McLean, G., Chenu, K., van Oosterom, E.J., Snow, V., Murphy, C., Moore, A.D., Brown, H., Whish, J.P.M., Verrall, S., Fainges, J., Bell, L.W., Peake, A.S., Poulton, P.L., Hochman, Z., Thorburn, P.J., Gaydon, D.S., Dalgliesh, N.P., Rodriguez, D., Cox, H., Chapman, S., Doherty, A., Teixeira, E., Sharp, J., Cichota, R., Vogeler, I., Li, F.Y., Wang, E., Hammer, G.L., Robertson, M.J., Dimes, J.P., Whitbread, A.M., Hunt, J., van Rees, H., McClelland, T., Carberry, P.S., Hargreaves, J.N.G., MacLeod, N., McDonald, C., Harsdorf, J., Wedgwood, S., Keating, B.A., 2014a. APSIM - Evolution towards a new generation of agricultural systems simulation. Environ. Model. Softw. 62, 327–350. https://doi.org/10.1016/j.envsoft.2014.07.009

Holzworth, D.P., Huth, N.I., DeVoil, P.G., Zurcher, E.J., Herrmann, N.I., McLean, G., Chenu, K., van Oosterom, E.J., Snow, V., Murphy, C., others, 2014b. APSIM--evolution towards a new generation of agricultural systems simulation. Environ. Model. Softw. 62, 327–350.

Horie, T., Yajima, M., Nakagawa, H., 1992a. Yield forecasting. Agric. Syst. 40, 211–236.

Horie, T., Yajima, M., Nakagawa, H., 1992b. Yield Forecasting. Agric. Syst. 40, 211–236. https://doi.org/10.1007/s10964-015-0332-y

Houser, P.R., Shuttleworth, W.J., Famiglietti, J.S., Gupta, H. V, Syed, K.H., Goodrich, D.C., 1998. Integration of soil moisture remote sensing and hydrologic modeling using data assimilation. Water Resour. Res. 34, 3405–3420.

Hsiao, Theodore C., Heng, L., Steduto, P., Rojas-Lara, B., Raes, D., Fereres, E., 2009. Aquacrop-The FAO crop model to simulate yield response to water: III. Parameterization and testing for maize. Agron. J. 101, 448–459. https://doi.org/10.2134/agronj2008.0218s

Hsiao, Theodore C, Heng, L., Steduto, P., Rojas-Lara, B., Raes, D., Fereres, E., 2009. AquaCrop—The FAO crop model to simulate yield response to water: III. Parameterization and testing for maize. Agron. J. 101, 448–459.

Huang, H., Huang, J., Wu, Y., Zhuo, W., Song, J., Li, X., Li, L., Su, W., Ma, H., Liang,

S., 2023. The improved winter wheat yield estimation by assimilating GLASS LAI into a crop growth model with the proposed Bayesian posterior-based ensemble Kalman filter. IEEE Trans. Geosci. Remote Sens. 61, 1–18.

Huang, J., Gómez-Dans, J.L., Huang, H., Ma, H., Wu, Q., Lewis, P.E., Liang, S., Chen, Z., Xue, J.-H., Wu, Y., others, 2019a. Assimilation of remote sensing into crop growth models: Current status and perspectives. Agric. For. Meteorol. 276, 107609.

Huang, J., Ma, H., Sedano, F., Lewis, P., Liang, S., Wu, Q., Su, W., Zhang, X., Zhu, D., 2019b. Evaluation of regional estimates of winter wheat yield by assimilating three remotely sensed reflectance datasets into the coupled WOFOST--PROSAIL model. Eur. J. Agron. 102, 1–13.

Huang, J., Ma, H., Su, W., Zhang, X., Huang, Y., Fan, J., Wu, W., 2015a. Jointly Assimilating MODIS LAI and ET Products into the SWAP Model for Winter Wheat Yield Estimation. IEEE J. Sel. Top. Appl. Earth Obs. Remote Sens. 8, 4060–4071. https://doi.org/10.1109/JSTARS.2015.2403135

Huang, J., Sedano, F., Huang, Y., Ma, H., Li, X., Liang, S., Tian, L., Zhang, X., Fan, J., Wu, W., 2016. Assimilating a synthetic Kalman filter leaf area index series into the WOFOST model to improve regional winter wheat yield estimation. Agric. For. Meteorol. 216, 188–202.

Huang, J., Tian, L., Liang, S., Ma, H., Becker-Reshef, I., Huang, Y., Su, W., Zhang, X., Zhu, D., Wu, W., 2015b. Improving winter wheat yield estimation by assimilation of the leaf area index from Landsat TM and MODIS data into the WOFOST model. Agric. For. Meteorol. 204, 106–121. https://doi.org/10.1016/j.agrformet.2015.02.001

Huete, A., Didan, K., Miura, T., Rodriguez, E.P., Gao, X., Ferreira, L.G., 2002. Overview of the radiometric and biophysical performance of the MODIS vegetation indices. Remote Sens. Environ. 83, 195–213.

Hunt, J., van Rees, H., Hochman, Z., Carberry, P., Holzworth, D., Dalgliesh, N., Brennan, L., Poulton, P., van Rees, S., Huth, N.I., others, 2006. Yield Prophet®: An online crop simulation service, in: Proceedings of the 13th Australian Agronomy Conference. pp. 10–14.

Hunt, W., Birch, C., Vanclay, F., Coutts, J., 2014. Recommendations arising from an analysis of changes to the Australian agricultural research, development and extension system. Food Policy 44, 129–141.

Hurtado, E., Artigao, M.M., Caselles, V., 1994. Estimating Maize (Zea mays) cvapotranspiration from NOAA-AVHRR thermal data in the Albacete area, Spain. Int. J. Remote Sens. 15, 2023–2037.

Hussain, J., Khaliq, T., Ahmad, A., Akhtar, J., 2018. Performance of four crop model for simulations of wheat phenology, leaf growth, biomass and yield across planting dates. PLoS One 13, e0197546.

Hussain, J., Khaliq, T., Asseng, S., Saeed, U., Ahmad, A., Ahmad, B., Ahmad, I., Fahad, M., Awais, M., Ullah, A., others, 2020. Climate change impacts and adaptations for wheat employing multiple climate and crop modelsin Pakistan. Clim. Change 163, 253–266.

Iizumi, T., Shin, Y., Kim, W., Kim, M., Choi, J., 2018. Global crop yield forecasting using seasonal climate information from a multi-model ensemble. Clim. Serv. 11, 13–23.

Iizumi, T., Yokozawa, M., Nishimori, M., 2009. Parameter estimation and uncertainty analysis of a large-scale crop model for paddy rice: Application of a Bayesian approach. Agric. For. Meteorol. 149, 333–348. https://doi.org/10.1016/j.agrformet.2008.08.015

Ines, A.V.M., Das, N.N., Hansen, J.W., Njoku, E.G., 2013. Assimilation of remotely sensed soil moisture and vegetation with a crop simulation model for maize yield prediction. Remote Sens. Environ. 138, 149–164.

Ines, A.V.M., Honda, K., Gupta, A. Das, Droogers, P., Clemente, R.S., 2006. Combining remote sensing-simulation modeling and genetic algorithm optimization to explore water management options in irrigated agriculture. Agric. water Manag. 83, 221–232.

Innes, P.J., Tan, D.K.Y., Van Ogtrop, F., Amthor, J.S., 2015. Effects of high-temperature episodes on wheat yields in New South Wales, Australia. Agric. For. Meteorol. 208, 95–107.

Jackson, T.J., Schugge, T.J., Nicks, A.D., Coleman, G.A., Engman, E.T., 1981. Soil moisture updating and microwave remote sensing for hydrological simulation/La remise à jour de l'état d'humidité des sols en vue de la simulation hydrologique. Hydrol. Sci. J. 26, 305–319.

Jain, S.K., Singh, V.P., 2003. Water resources systems planning and management. Elsevier.

Jazwinski, A.H., 2007. Stochastic processes and filtering theory. Courier Corporation.

Jégo, G., Pattey, E., Liu, J., 2012. Using Leaf Area Index, retrieved from optical imagery, in the STICS crop model for predicting yield and biomass of field crops. F. Crop. Res. 131, 63–74.

Jiang, Z., Chen, Z., Chen, J., Liu, J., Ren, J., Li, Z., Sun, L., Li, H., 2014a. Application of crop model data assimilation with a particle filter for estimating regional winter wheat yields. IEEE J. Sel. Top. Appl. Earth Obs. Remote Sens. 7, 4422–4431.

Jiang, Z., Chen, Z., Chen, J., Ren, J., Li, Z., Sun, L., 2014b. The estimation of regional crop yield using ensemble-based four-dimensional variational data assimilation. Remote Sens. 6, 2664–2681. https://doi.org/10.3390/rs6042664

Jin, H., Li, A., Wang, J., Bo, Y., 2016. Improvement of spatially and temporally continuous crop leaf area index by integration of CERES-Maize model and MODIS data. Eur. J. Agron. 78, 1–12.

Jin, M., Liu, X., Wu, L., Liu, M., 2015. An improved assimilation method with stress factors incorporated in the WOFOST model for the efficient assessment of heavy metal stress levels in rice. Int. J. Appl. Earth Obs. Geoinf. 41, 118–129.

Jin, N., Tao, B., Ren, W., He, L., Zhang, D., Wang, D., Yu, Q., 2022. Assimilating remote sensing data into a crop model improves winter wheat yield estimation based on regional irrigation data. Agric. Water Manag. 266, 107583.

Jin, X., Kumar, L., Li, Z., Feng, H., Xu, X., Yang, G., Wang, J., 2018. A review of data assimilation of remote sensing and crop models. Eur. J. Agron. 92, 141–152. https://doi.org/10.1016/j.eja.2017.11.002

Jin, X., Li, Z., Feng, H., Ren, Z., Li, S., 2020. Estimation of maize yield by assimilating biomass and canopy cover derived from hyperspectral data into the AquaCrop

model. Agric. Water Manag. 227, 105846.

Jin, X., Li, Z., Yang, G., Yang, H., Feng, H., Xu, X., Wang, J., Li, X., Luo, J., 2017. Winter wheat yield estimation based on multi-source medium resolution optical and radar imaging data and the AquaCrop model using the particle swarm optimization algorithm. ISPRS J. Photogramm. Remote Sens. 126, 24–37.

Johansen, K., Ziliani, M.G., Houborg, R., Franz, T.E., McCabe, M.F., 2022. CubeSat constellations provide enhanced crop phenology and digital agricultural insights using daily leaf area index retrievals. Sci. Rep. 12, 1–12.

Jones, C.A., Kiniry, J.R., 1986. CERES-Maize; a simulation model of maize growth and development.

Jones, J W, Hoogenboom, G., Porter, C., Boote, K., Batchelor, W., Hunt, L., Ritchie, J., 2003. The DSSAT cropping system model European Journal of Agronomy.

Jones, James W, Hoogenboom, G., Porter, C.H., Boote, K.J., Batchelor, W.D., Hunt, L.A., Wilkens, P.W., Singh, U., Gijsman, A.J., Ritchie, J.T., 2003. The DSSAT cropping system model. Eur. J. Agron. 18, 235–265.

Jongschaap, R.E.E., 2006. Run-time calibration of simulation models by integrating remote sensing estimates of leaf area index and canopy nitrogen. Eur. J. Agron. 24, 316–324.

Jongschaap, R.E.E., Schouten, L.S.M., 2005. Predicting wheat production at regional scale by integration of remote sensing data with a simulation model. Agron. Sustain. Dev. 25, 481–489.

Julier, S.J., Uhlmann, J.K., 2004. Unscented filtering and nonlinear estimation. Proc. IEEE 92, 401–422.

Kalman, R.E., 1960. A new approach to linear filtering and prediction problems. J. basic Eng. 82, 35–45.

Kang, Y., Özdoğan, M., 2019. Field-level crop yield mapping with Landsat using a hierarchical data assimilation approach. Remote Sens. Environ. 228, 144–163.

Kawakita, S., Takahashi, H., Moriya, K., 2020. Prediction and parameter uncertainty for winter wheat phenology models depend on model and parameterization method

differences. Agric. For. Meteorol. 290, 107998.

Keating, B.A., Carberry, P.S., Hammer, G.L., Probert, M.E., Robertson, M.J., Holzworth, D., Huth, N.I., Hargreaves, J.N.., Meinke, H., Hochman, Z., McLean, G., Verburg, K., Snow, V., Dimes, J.P., Silburn, M., Wang, E., Brown, S., Bristow, K.L., Asseng, S., Chapman, S., McCown, R.L., Freebairn, D.M., Smith, C.J., 2003. An overview of the crop model. Eur. J. Agron. 18, 267–288. https://doi.org/10.1016/S0223-5234(03)00100-4

Keating, B A, Carberry, P.S., Hammer, G.L., Probert, M.E., Robertson, M.J., Holzworth, D., Huth, N.I., Hargreaves, J.N.G., Meinke, H., Hochman, Z., McLean, G., Verburg, K., Snow, V., Dimes, J.P., Silburn, M., Wang, E., Brown, S., Bristow, K.L., Asseng, S., Chapman, S., McCown, R.L., Freebairn, D.M., Smith, C.J., 2003. An overview of the crop model. Eur. J. Agron. 18, 267–288. https://doi.org/10.1016/S0223-5234(03)00100-4

Keating, B.A., Gaydon, D., Huth, N.I., Probert, M.E., Verburg, K., Smith, C.J., Bond, W., 2002. Use of modelling to explore the water balance of dryland farming systems in the Murray-Darling Basin, Australia. Eur. J. Agron. 18, 159–169.

Keating, B.S., Meinke, H., Probert, M.E., Huth, N.I., Hills, I.G., others, 2001. NWheat: documentation and performance of a wheat module for APSIM.

Kersebaum, K.C., Boote, K.J., Jorgenson, J.S., Nendel, C., Bindi, M., Frühauf, C., Gaiser, T., Hoogenboom, G., Kollas, C., Olesen, J.E., others, 2015. Analysis and classification of data sets for calibration and validation of agro-ecosystem models. Environ. Model. & Softw. 72, 402–417.

Kivi, M.S., Blakely, B., Masters, M., Bernacchi, C.J., Miguez, F.E., Dokoohaki, H., 2022. Development of a data-assimilation system to forecast agricultural systems: A case study of constraining soil water and soil nitrogen dynamics in the APSIM model. Sci. Total Environ. 820, 153192.

Kumar, S. V, Reichle, R.H., Peters-Lidard, C.D., Koster, R.D., Zhan, X., Crow, W.T., Eylander, J.B., Houser, P.R., 2008. A land surface data assimilation framework using the land information system: Description and applications. Adv. Water Resour. 31, 1419–1432.

Kundzewicz, Z.W., Kanae, S., Seneviratne, S.I., Handmer, J., Nicholls, N., Peduzzi, P., Mechler, R., Bouwer, L.M., Arnell, N., Mach, K., others, 2014. Flood risk and climate change: global and regional perspectives. Hydrol. Sci. J. 59, 1–28.

Lahoz, W.A., Schneider, P., 2014. Data assimilation: making sense of Earth Observation. Front. Environ. Sci. 2, 16.

Laluet, P., Olivera-Guerra, L., Rivalland, V., Simonneaux, V., Inglada, J., Bellvert, J., Er-raki, S., Merlin, O., 2023. A sensitivity analysis of a FAO-56 dual crop coefficient-based model under various field conditions. Environ. Model. & Softw. 160, 105608.

Launay, M., Guérif, M., 2005. Assimilating remote sensing data into a crop model to improve predictive performance for spatial applications. Agric. Ecosyst. Environ. 111, 321–339. https://doi.org/10.1016/j.agee.2005.06.005

Lawes, R.A., Oliver, Y.M., Robertson, M.J., 2009. Integrating the effects of climate and plant available soil water holding capacity on wheat yield. F. Crop. Res. 113, 297–305.

Le Dimet, F.-X., Talagrand, O., 1986. Variational algorithms for analysis and assimilation of meteorological observations: theoretical aspects. Tellus A Dyn. Meteorol. Oceanogr. 38, 97–110.

Lei, F., Crow, W.T., Kustas, W.P., Dong, J., Yang, Y., Knipper, K.R., Anderson, M.C., Gao, F., Notarnicola, C., Greifeneder, F., others, 2020. Data assimilation of high-resolution thermal and radar remote sensing retrievals for soil moisture monitoring in a drip-irrigated vineyard. Remote Sens. Environ. 239, 111622.

Li, J., Wang, E., Wang, Y., Xing, H., Wang, D., Wang, L., Gao, C., 2016. Reducing greenhouse gas emissions from a wheat--maize rotation system while still maintaining productivity. Agric. Syst. 145, 90–98.

Li, K., Yang, X., Liu, Z., Zhang, T., Lu, S., Liu, Y., 2014. Low yield gap of winter wheat in the North China Plain. Eur. J. Agron. 59, 1–12.

Li, Ryu, D., Western, A.W., Wang, Q.J., 2015. Assimilation of stream discharge for flood forecasting: Updating a semidistributed model with an integrated data assimilation scheme. Water Resour. Res. 51, 3238–3258.

Li, T., Angeles, O., Marcaida III, M., Manalo, E., Manalili, M.P., Radanielson, A., Mohanty, S., 2017. From ORYZA2000 to ORYZA (v3): An improved simulation model for rice in drought and nitrogen-deficient environments. Agric. For. Meteorol. 237, 246–256.

Li, Y., Ryu, D., Western, A.W., Wang, Q.J., 2013. Assimilation of stream discharge for flood forecasting: The benefits of accounting for routing time lags. Water Resour. Res. 49, 1887–1900.

Li, Y., Ryu, D., Western, A.W., Wang, Q.J., Robertson, D.E., Crow, W.T., 2014. An integrated error parameter estimation and lag-aware data assimilation scheme for real-time flood forecasting. J. Hydrol. 519, 2722–2736.

Li, Z., Jin, X., Zhao, C., Wang, J., Xu, X., Yang, G., Li, C., Shen, J., 2015a. Estimating wheat yield and quality by coupling the DSSAT-CERES model and proximal remote sensing. Eur. J. Agron. 71, 53–62.

Li, Z., Wang, J., Xu, X., Zhao, C., Jin, X., Yang, G., Feng, H., 2015b. Assimilation of two variables derived from hyperspectral data into the DSSAT-CERES model for grain yield and quality estimation. Remote Sens. 7, 12400–12418.

Li, Zhou, Q., Zhou, J., Zhang, G., Chen, C., Wang, J., 2014. Assimilating remote sensing information into a coupled hydrology-crop growth model to estimate regional maize yield in arid regions. Ecol. Modell. 291, 15–27. https://doi.org/10.1016/j.ecolmodel.2014.07.013

Liang, H., Qi, Z., DeJonge, K.C., Hu, K., Li, B., 2017. Global sensitivity and uncertainty analysis of nitrate leaching and crop yield simulation under different water and nitrogen management practices. Comput. Electron. Agric. 142, 201–210.

Lilley, J.M., Kirkegaard, J.A., 2008. Seasonal variation in the value of subsoil water to wheat: simulation studies in southern New South Wales. Aust. J. Agric. Res. 58, 1115–1128.

Lilley, J.M., Kirkegaard, J.A., Robertson, M.J., Probert, M.E., Angus, J.F., Howe, G., 2003. Simulating crop and soil processes in crop sequences in southern NSW, in: Proceedings of the 11th Australian Agronomy Conference'. Geelong.

Littleboy, M., Silburn, D.M., Freebairn, D.M., Woodruff, D.R., Hammer, G.L., Leslie,

J.K., 1992. Impact of soil erosion on production in cropping systems. I. Development and validation of a simulation model. Soil Res. 30, 757–774.

Liu, B., Asseng, S., Liu, L., Tang, L., Cao, W., Zhu, Y., 2016a. Testing the responses of four wheat crop models to heat stress at anthesis and grain filling. Glob. Chang. Biol. 22, 1890–1903.

Liu, B., Asseng, S., Müller, C., Ewert, F., Elliott, J., Lobell, D.B., Martre, P., Ruane, A.C., Wallach, D., Jones, J.W., Rosenzweig, C., Aggarwal, P.K., Alderman, P.D., Anothai, J., Basso, B., Biernath, C., Cammarano, D., Challinor, A., Deryng, D., De Sanctis, G., Doltra, J., Fereres, E., Folberth, C., Garcia-Vila, M., Gayler, S., Hoogenboom, G., Hunt, L.A., Izaurralde, R.C., Jabloun, M., Jones, C.D., Kersebaum, K.C., Kimball, B.A., Koehler, A.K., Kumar, S.N., Nendel, C., O'Leary, G.J., Olesen, J.E., Ottman, M.J., Palosuo, T., Prasad, P.V.V., Priesack, E., Pugh, T.A.M., Reynolds, M., Rezaei, E.E., Rötter, R.P., Schmid, E., Semenov, M.A., Shcherbak, I., Stehfest, E., Stöckle, C.O., Stratonovitch, P., Streck, T., Supit, I., Tao, F., Thorburn, P., Waha, K., Wall, G.W., Wang, E., White, J.W., Wolf, J., Zhao, Z., Zhu, Y., 2016b. Similar estimates of temperature impacts on global wheat yield by three independent methods. Nat. Clim. Chang. 6, 1130–1136. https://doi.org/10.1038/nclimate3115

Liu, F., Liu, X., Ding, C., Wu, L., 2015. The dynamic simulation of rice growth parameters under cadmium stress with the assimilation of multi-period spectral indices and crop model. F. Crop. Res. 183, 225–234.

Liu, F., Liu, X., Zhao, L., Ding, C., Jiang, J., Wu, L., 2014. The dynamic assessment model for monitoring cadmium stress levels in rice based on the assimilation of remote sensing and the WOFOST model. IEEE J. Sel. Top. Appl. Earth Obs. Remote Sens. 8, 1330–1338.

Liu, J.S., Chen, R., 1998. Sequential Monte Carlo methods for dynamic systems. J. Am. Stat. Assoc. 93, 1032–1044.

Liu, K., Harrison, M.T., Yan, H., Liu, D.L., Meinke, H., Hoogenboom, G., Wang, B., Peng, B., Guan, K., Jaegermeyr, J., others, 2023. Silver lining to a climate crisis in multiple prospects for alleviating crop waterlogging under future climates. Nat. Commun. 14, 765.

Lobell, D.B., 2013a. The use of satellite data for crop yield gap analysis. F. Crop. Res. 143, 56–64.

Lobell, D.B., 2013b. Errors in climate datasets and their effects on statistical crop models. Agric. For. Meteorol. 170, 58–66.

Lobell, D.B., Sibley, A., Ivan Ortiz-Monasterio, J., 2012. Extreme heat effects on wheat senescence in India. Nat. Clim. Chang. 2, 186–189. https://doi.org/10.1038/nclimate1356

Lobell, Sibley, A., Ortiz-Monasterio, J.I., 2012. Extreme heat effects on wheat senescence in India. Nat. Clim. Chang. 2, 186–189. https://doi.org/10.1038/nclimate1356

Lorenc, A.C., 1986. Analysis methods for numerical weather prediction. Q. J. R. Meteorol. Soc. 112, 1177–1194.

Lorenc, A.C., Ballard, S.P., Bell, R.S., Ingleby, N.B., Andrews, P.L.F., Barker, D.M., Bray, J.R., Clayton, A.M., Dalby, T., Li, D., others, 2000. The Met. Office global three-dimensional variational data assimilation scheme. Q. J. R. Meteorol. Soc. 126, 2991–3012.

Lu, Y., Chibarabada, T.P., McCabe, M.F., De Lannoy, G.J.M., Sheffield, J., 2021a. Global sensitivity analysis of crop yield and transpiration from the FAO-AquaCrop model for dryland environments. F. Crop. Res. 269, 108182.

Lu, Y., Chibarabada, T.P., Ziliani, M.G., Onema, J.-M.K., McCabe, M.F., Sheffield, J., 2021b. Assimilation of soil moisture and canopy cover data improves maize simulation using an under-calibrated crop model. Agric. Water Manag. 252, 106884.

Luck, J., Spackman, M., Freeman, A., Tre¸ bicki, P., Griffiths, W., Finlay, K., Chakraborty, S., 2011. Climate change and diseases of food crops. Plant Pathol. 60, 113–121.

Ludwig, F., Asseng, S., 2006. Climate change impacts on wheat production in a Mediterranean environment in Western Australia. Agric. Syst. 90, 159–179.

Luo, L., Sun, S., Xue, J., Gao, Z., Zhao, J., Yin, Y., Gao, F., Luan, X., 2023. Crop yield estimation based on assimilation of crop models and remote sensing data: A systematic evaluation. Agric. Syst. 210, 103711.

Luo, Q., Bellotti, W., Williams, M., Bryan, B., 2005. Potential impact of climate change on wheat yield in South Australia. Agric. For. Meteorol. 132, 273–285.

Luo, Q., Bellotti, W., Williams, M., Wang, E., 2009. Adaptation to climate change of wheat growing in South Australia: analysis of management and breeding strategies. Agric. Ecosyst. & Environ. 129, 261–267.

Luo, Q., Kathuria, A., 2013. Modelling the response of wheat grain yield to climate change: a sensitivity analysis. Theor. Appl. Climatol. 111, 173–182.

Ma, G., Huang, J., Wu, W., Fan, J., Zou, J., Wu, S., 2013. Assimilation of MODIS-LAI into the WOFOST model for forecasting regional winter wheat yield. Math. Comput. Model. 58, 634–643. https://doi.org/10.1016/j.mcm.2011.10.038

Ma, H., Wang, J., Liu, T., Guo, Y., Zhou, Y., Yang, T., Zhang, W., Sun, C., 2023. Time series global sensitivity analysis of genetic parameters of CERES-maize model under water stresses at different growth stages. Agric. Water Manag. 275, 108027.

Machwitz, M., Giustarini, L., Bossung, C., Frantz, D., Schlerf, M., Lilienthal, H., Wandera, L., Matgen, P., Hoffmann, L., Udelhoven, T., 2014. Enhanced biomass prediction by assimilating satellite data into a crop growth model. Environ. Model. Softw. 62, 437–453.

Maiorano, A., Martre, P., Asseng, S., Ewert, F., Müller, C., Rötter, R.P., Ruane, A.C., Semenov, M.A., Wallach, D., Wang, E., Alderman, P.D., Kassie, B.T., Biernath, C., Basso, B., Cammarano, D., Challinor, A.J., Doltra, J., Dumont, B., Rezaei, E.E., Gayler, S., Kersebaum, K.C., Kimball, B.A., Koehler, A.K., Liu, B., O'Leary, G.J., Olesen, J.E., Ottman, M.J., Priesack, E., Reynolds, M., Stratonovitch, P., Streck, T., Thorburn, P.J., Waha, K., Wall, G.W., White, J.W., Zhao, Z., Zhu, Y., 2017a. Crop model improvement reduces the uncertainty of the response to temperature of multi-model ensembles. F. Crop. Res. 202, 5–20. https://doi.org/10.1016/j.fcr.2016.05.001

Maiorano, A., Martre, P., Asseng, S., Ewert, F., Müller, C., Rötter, R.P., Ruane, A.C., Semenov, M.A., Wallach, D., Wang, E., Alderman, P.D., Kassie, B.T., Biernath, C., Basso, B., Cammarano, D., Challinor, A.J., Doltra, J., Dumont, B., Rezaei, E.E., Gayler, S., Kersebaum, K.C., Kimball, B.A., Koehler, A.K., Liu, B., O'Leary, G.J., Olesen, J.E., Ottman, M.J., Priesack, E., Reynolds, M., Stratonovitch, P., Streck, T.,

Thorburn, P.J., Waha, K., Wall, G.W., White, J.W., Zhao, Z., Zhu, Y., 2017b. Crop model improvement reduces the uncertainty of the response to temperature of multi-model ensembles. F. Crop. Res. 202, 5–20. https://doi.org/10.1016/j.fcr.2016.05.001

Makowski, D., Naud, C., Jeuffroy, M.-H., Barbottin, A., Monod, H., 2006. Global sensitivity analysis for calculating the contribution of genetic parameters to the variance of crop model prediction. Reliab. Eng. & Syst. Saf. 91, 1142–1147.

Manivasagam, V.S., Sadeh, Y., Kaplan, G., Bonfil, D.J., Rozenstein, O., 2021. Studying the feasibility of assimilating Sentinel-2 and PlanetScope imagery into the SAFY crop model to predict within-field wheat yield. Remote Sens. 13, 2395.

Manschadi, A.M., Christopher, J., deVoil, P., Hammer, G.L., 2006. The role of root architectural traits in adaptation of wheat to water-limited environments. Funct. plant Biol. 33, 823–837.

Martre, P., Quilot-Turion, B., Luquet, D., Memmah, M.-M.O.-S., Chenu, K., Debaeke, P., 2015a. Model-assisted phenotyping and ideotype design, in: Crop Physiology. Elsevier, pp. 349–373.

Martre, P., Wallach, D., Asseng, S., Ewert, F., Jones, J.W., Rötter, R.P., Boote, K.J., Ruane, A.C., Thorburn, P.J., Cammarano, D., others, 2015b. Multimodel ensembles of wheat growth: many models are better than one. Glob. Chang. Biol. 21, 911–925.

Massari, C., Brocca, L., Barbetta, S., Papathanasiou, C., Mimikou, M., Moramarco, T., 2014. Using globally available soil moisture indicators for flood modelling in Mediterranean catchments. Hydrol. Earth Syst. Sci. 18, 839–853.

McCown, R.L., Hammer, G.L., Hargreaves, J.N.G., Holzworth, D., Huth, N.I., 1995. APSIM: an agricultural production system simulation model for operational research. Math. Comput. Simul. 39, 225–231. https://doi.org/10.1016/0378-4754(95)00063-2

McCown, R.L., Hammer, G.L., Hargreaves, J.N.G., Holzworth, D.P., Freebairn, D.M., 1996. APSIM- A novel software system for model development.pdf. Agric. Syst. 50, 255–271.

Meehl, G.A., Zwiers, F., Evans, J., Knutson, T., Mearns, L., Whetton, P., 2000. Trends

in extreme weather and climate events: issues related to modeling extremes in projections of future climate change. Bull. Am. Meteorol. Soc. 81, 427–436.

Mielenz, H., Thorburn, P.J., Scheer, C., Migliorati, M.D.A., Grace, P.R., Bell, M.J., 2016. Opportunities for mitigating nitrous oxide emissions in subtropical cereal and fiber cropping systems: A simulation study. Agric. Ecosyst. Environ. 218, 11–27.

Mishra, V., Cruise, J.F., Mecikalski, J.R., 2021. Assimilation of coupled microwave/thermal infrared soil moisture profiles into a crop model for robust maize yield estimates over Southeast United States. Eur. J. Agron. 123, 126208.

Moeller, C., Pala, M., Manschadi, A.M., Meinke, H., Sauerborn, J., 2007. Assessing the sustainability of wheat-based cropping systems using APSIM: model parameterisation and evaluation. Aust. J. Agric. Res. 58, 75–86.

Mohanty, M., Probert, M.E., Reddy, K.S., Dalal, R.C., Mishra, A.K., Subba Rao, A., Singh, M., Menzies, N.W., 2012. Simulating soybean-wheat cropping system: APSIM model parameterization and validation. Agric. Ecosyst. Environ. 152, 68–78. https://doi.org/10.1016/j.agee.2012.02.013

Moradkhani, H., Sorooshian, S., 2009. General review of rainfall-runoff modeling: model calibration, data assimilation, and uncertainty analysis. Hydrol. Model. water cycle 1–24.

Morel, J., Bégué, A., Todoroff, P., Martiné, J.F., Lebourgeois, V., Petit, M., 2014. Coupling a sugarcane crop model with the remotely sensed time series of fIPAR to optimise the yield estimation. Eur. J. Agron. 61, 60–68. https://doi.org/10.1016/j.eja.2014.08.004

Moulin, S., Bondeau, A., Delecolle, R., 1998. Combining agricultural crop models and satellite observations: From field to regional scales. Int. J. Remote Sens. 19, 1021–1036. https://doi.org/10.1080/014311698215586

Muruganantham, P., Wibowo, S., Grandhi, S., Samrat, N.H., Islam, N., 2022. A systematic literature review on crop yield prediction with deep learning and remote sensing. Remote Sens. 14, 1990.

Nearing, G.S., Crow, W.T., Thorp, K.R., Moran, M.S., Reichle, R.H., Gupta, H. V, 2012. Assimilating remote sensing observations of leaf area index and soil moisture for

wheat yield estimates: An observing system simulation experiment. Water Resour. Res. 48.

Neitsch, S.L., Arnold, J.G., Kiniry, J.R., Williams, J.R., 2011. Soil and water assessment tool theoretical documentation version 2009.

Nguy-Robertson, A., Gitelson, A., Peng, Y., Viña, A., Arkebauer, T., Rundquist, D., 2012. Green leaf area index estimation in maize and soybean: Combining vegetation indices to achieve maximal sensitivity. Agron. J. 104, 1336–1347.

Nguy-Robertson, A.L., Peng, Y., Gitelson, A.A., Arkebauer, T.J., Pimstein, A., Herrmann, I., Karnieli, A., Rundquist, D.C., Bonfil, D.J., 2014. Estimating green LAI in four crops: Potential of determining optimal spectral bands for a universal algorithm. Agric. For. Meteorol. 192, 140–148.

Nonhebel, S., 1994. Inaccuracies in weather data and their effects on crop growth simulation results. I. Potential production. Clim. Res. 4, 47–60.

Nuttall, J., Wallace, A., Price, D., Armstrong, R., Sounness, C., others, 2010. Fast-tracking the adaptation of grain production systems to a changing climate using a participatory action research, development and extension (PARD&E) process, in: Food Security from Sustainable Agriculture-Proceedings of 15th Agronomy Conference.

O'Leary, G.J., Christy, B., Nuttall, J., Huth, N., Cammarano, D., Stöckle, C., Basso, B., Shcherbak, I., Fitzgerald, G., Luo, Q., others, 2015. Response of wheat growth, grain yield and water use to elevated CO 2 under a Free-Air CO 2 Enrichment (FACE) experiment and modelling in a semi-arid environment. Glob. Chang. Biol. 21, 2670–2686.

O'Leary, G.J., Li Liu, D., Ma, Y., Li, F.Y., McCaskill, M., Conyers, M., Dalal, R., Reeves, S., Page, K., Dang, Y.P., others, 2016. Modelling soil organic carbon 1. Performance of APSIM crop and pasture modules against long-term experimental data. Geoderma 264, 227–237.

Ojeda, J.J., Rezaei, E.E., Kamali, B., McPhee, J., Meinke, H., Siebert, S., Webb, M.A., Ara, I., Mulcahy, F., Ewert, F., 2021. Impact of crop management and environment on the spatio-temporal variance of potato yield at regional scale. F. Crop. Res. 270,

108213.

Oliver, Y., Wong, M., Robertson, M., Wittwer, K., others, 2006. PAWC determines spatial variability in grain yield and nitrogen requirement by interacting with rainfall on northern WA sandplain, in: Proceedings of the 13th Australian Agronomy Conference. pp. 10–14.

Oliver, Y.M., Robertson, M.J., 2009. Quantifying the benefits of accounting for yield potential in spatially and seasonally responsive nutrient management in a Mediterranean climate. Soil Res. 47, 114–126.

Oliver, Y.M., Robertson, M.J., Stone, P.J., Whitbread, A., 2009. Improving estimates of water-limited yield of wheat by accounting for soil type and within-season rainfall. Crop pasture Sci. 60, 1137–1146.

Osman, R., Ata-Ul-Karim, S.T., Tahir, M.N., Ishaque, W., Xu, M., 2022. Multi-model ensembles for assessing the impact of future climate change on rainfed wheat productivity under various cultivars and nitrogen levels. Eur. J. Agron. 139, 126554.

Pagani, V., Guarneri, T., Busetto, L., Ranghetti, L., Boschetti, M., Movedi, E., Campos-Taberner, M., Garcia-Haro, F.J., Katsantonis, D., Stavrakoudis, D., Ricciardelli, E., Romano, F., Holecz, F., Collivignarelli, F., Granell, C., Casteleyn, S., Confalonieri, R., 2018. A high-resolution, integrated system for rice yield forecasting at district level. Agric. Syst. 0–1. https://doi.org/10.1016/j.agsy.2018.05.007

Palosuo, T., Kersebaum, K.C., Angulo, C., Hlavinka, P., Moriondo, M., Olesen, J.E., Patil, R.H., Ruget, F., Rumbaur, C., Takáč, J., Trnka, M., Bindi, M., Çaldağ, B., Ewert, F., Ferrise, R., Mirschel, W., Şaylan, L., Šiška, B., Rötter, R., 2011. Simulation of winter wheat yield and its variability in different climates of Europe: A comparison of eight crop growth models. Eur. J. Agron. 35, 103–114. https://doi.org/10.1016/j.eja.2011.05.001

Paniconi, C., Marrocu, M., Putti, M., Verbunt, M., 2003. Newtonian nudging for a Richards equation-based distributed hydrological model. Adv. Water Resour. 26, 161–178.

Pardon, L., Huth, N.I., Nelson, P.N., Banabas, M., Gabrielle, B., Bessou, C., 2017. Yield and nitrogen losses in oil palm plantations: Main drivers and management trade-

offs determined using simulation. F. Crop. Res. 210, 20–32.

Pauwels, V.R.N., Verhoest, N.E.C., De Lannoy, G.J.M., Guissard, V., Lucau, C., Defourny, P., 2007. Optimization of a coupled hydrology--crop growth model through the assimilation of observed soil moisture and leaf area index values using an ensemble Kalman filter. Water Resour. Res. 43.

Paydar, Z., Huth, N., Ringrose-Voase, A., Young, R., Bernardi, T., Keating, B., Cresswell, H., 2005. Deep drainage and land use systems. Model verification and systems comparison. Aust. J. Agric. Res. 56, 995–1007.

Peake, A.S., Huth, N.I., Carberry, P.S., Raine, S.R., Smith, R.J., 2014. Quantifying potential yield and lodging-related yield gaps for irrigated spring wheat in sub-tropical Australia. F. Crop. Res. 158, 1–14.

Peel, M.C., Finlayson, B.L., McMahon, T.A., 2007. Updated world map of the Köppen-Geiger climate classification. Hydrol. earth Syst. Sci. 11, 1633–1644.

Peel, M.C., McMahon, T.A., Finlayson, B.L., 2002. Variability of annual precipitation and its relationship to the El Niño--Southern Oscillation. J. Clim. 15, 545–551.

Peng, Y., Gitelson, A.A., 2011. Application of chlorophyll-related vegetation indices for remote estimation of maize productivity. Agric. For. Meteorol. 151, 1267–1276.

Perkins, S.E., Alexander, L. V, Nairn, J.R., 2012. Increasing frequency, intensity and duration of observed global heatwaves and warm spells. Geophys. Res. Lett. 39.

Perry, E.M., Morse-Mcnabb, E.M., Nuttall, J.G., O'Leary, G.J., Clark, R., 2014. Managing wheat from space: Linking MODIS NDVI and crop models for predicting australian dryland wheat biomass. IEEE J. Sel. Top. Appl. Earth Obs. Remote Sens. 7, 3724–3731. https://doi.org/10.1109/JSTARS.2014.2323705

Phelan, D.C., Harrison, M.T., McLean, G., Cox, H., Pembleton, K.G., Dean, G.J., Parsons, D., do Amaral Richter, M.E., Pengilley, G., Hinton, S.J., others, 2018. Advancing a farmer decision support tool for agronomic decisions on rainfed and irrigated wheat cropping in Tasmania. Agric. Syst. 167, 113–124.

Pianosi, F., Beven, K., Freer, J., Hall, J.W., Rougier, J., Stephenson, D.B., Wagener, T., 2016. Sensitivity analysis of environmental models: A systematic review with practical workflow. Environ. Model. & Softw. 79, 214–232.

Pipunic, R.C., Walker, J.P., Western, A., 2008. Assimilation of remotely sensed data for improved latent and sensible heat flux prediction: A comparative synthetic study. Remote Sens. Environ. 112, 1295–1305.

Planet Labs Inc, 2021. Planet Imagery [WWW Document]. URL https://www.planet.com/products/planet-imagery/ (accessed 12.14.21).

Post, J., Hattermann, F.F., Krysanova, V., Suckow, F., 2008. Parameter and input data uncertainty estimation for the assessment of long-term soil organic carbon dynamics. Environ. Model. & Softw. 23, 125–138.

Povey, A.C., Grainger, R.G., 2015. Known and unknown unknowns: uncertainty estimation in satellite remote sensing. Atmos. Meas. Tech. 8, 4699–4718.

Prévot, L., Chauki, H., Troufleau, D., Weiss, M., Baret, F., Brission, N., 2003. Assimilating optical and radar data into the STICS crop model for wheat. Agronomie 23, 297–303. https://doi.org/10.1051/agro

Probert, M E, Carberry, P.S., McCown, R.L., Turpin, J.E., 1998. Simulation of legume-cereal systems using APSIM. Aust. J. Agric. Res. 49, 317–328.

Probert, M.E., Dimes, J.P., 2004. Modelling release of nutrients from organic resources using APSIM, in: ACIAR PROCEEDINGS. pp. 25–31.

Probert, M. E., Dimes, J.P., Keating, B.A., Dalal, R.C., Strong, W.M., 1998. APSIM's water and nitrogen modules and simulation of the dynamics of water and nitrogen in fallow systems. Agric. Syst. 56, 1–28. https://doi.org/10.1016/S0308-521X(97)00028-0

Probert, M.E., Keating, B.A., Thompson, J.P., Parton, W.J., 1995. Modelling water, nitrogen, and crop yield for a long-term fallow management experiment. Aust. J. Exp. Agric. 35, 941–950.

Raes, D., Steduto, P., Hsiao, T.C., Fereres, E., 2009a. Aquacrop-The FAO crop model to simulate yield response to water: II. main algorithms and software description. Agron. J. 101, 438–447. https://doi.org/10.2134/agronj2008.0140s

Raes, D., Steduto, P., Hsiao, T.C., Fereres, E., 2009b. AquaCrop—the FAO crop model to simulate yield response to water: II. Main algorithms and software description. Agron. J. 101, 438–447.

Ramirez-Villegas, J., Koehler, A.K., Challinor, A.J., 2017. Assessing uncertainty and complexity in regional-scale crop model simulations. Eur. J. Agron. 88, 84–95. https://doi.org/10.1016/j.eja.2015.11.021

Ramos, T.B., Simionesei, L., Oliveira, A.R., Darouich, H., Neves, R., 2018. Assessing the impact of LAI data assimilation on simulations of the soil water balance and maize development using MOHID-Land. Water 10, 1367.

Ran, H., Kang, S., Hu, X., Yao, N., Li, S., Wang, W., Galdos, M. V, Challinor, A.J., 2022. A framework to quantify uncertainty of crop model parameters and its application in arid Northwest China. Agric. For. Meteorol. 316, 108844.

RapidEye, 2016. RapidEye Satellite Imagery - Product Specifications.

Ratliff, L.F., Ritchie, J.T., Cassel, D.K., 1983. Field-measured limits of soil water availability as related to laboratory-measured properties. Soil Sci. Soc. Am. J. 47, 770–775.

Reichle, R.H., Koster, R.D., 2005. Global assimilation of satellite surface soil moisture retrievals into the NASA Catchment land surface model. Geophys. Res. Lett. 32.

Reichle, R.H., Koster, R.D., Liu, P., Mahanama, S.P.P., Njoku, E.G., Owe, M., 2007. Comparison and assimilation of global soil moisture retrievals from the Advanced Microwave Scanning Radiometer for the Earth Observing System (AMSR-E) and the Scanning Multichannel Microwave Radiometer (SMMR). J. Geophys. Res. Atmos. 112.

Reichle, R.H., Kumar, S. V, Mahanama, S.P.P., Koster, R.D., Liu, Q., 2010. Assimilation of satellite-derived skin temperature observations into land surface models. J. Hydrometeorol. 11, 1103–1122.

Reichle, R.H., Walker, J.P., Koster, R.D., Houser, P.R., 2002. Extended versus Ensemble Kalman Filtering for Land Data Assimilation. J. Hydrometeorol. 3, 728–740. https://doi.org/10.1175/1525-7541(2002)003<0728:EVEKFF>2.0.CO;2

Ren, J., Yu, F., Du, Y., Qin, J., Chen, Z., 2009. Assimilation of field measured LAI into crop growth model based on SCE-UA optimization algorithm. Int. Geosci. Remote Sens. Symp. 3, 573–576. https://doi.org/10.1109/IGARSS.2009.5417822

Ren, J., Yu, F., Qin, J., Chen, Z., 2010. INTEGRATING REMOTELY SENSED LAI

WITH EPIC MODEL BASED ON GLOBAL OPTIMIZATION ALGORITHM FOR REGIONAL CROP YIELD ASSESSMENT Key Laboratory of Resources Remote-Sensing & Digital Agriculture , Ministry of Agriculture , Beijing 100081 , China ; 2 Institute of 2147–2150. https://doi.org/10.1109/IGARSS.2010.5654060

Resnick, D., 2020. Political economy of food system reform. Nat. Food 1, 154.

Rettie, F.M., Gayler, S., KD Weber, T., Tesfaye, K., Streck, T., 2022. Climate change impact on wheat and maize growth in Ethiopia: A multi-model uncertainty analysis. PLoS One 17, e0262951.

Richter, G.M., Acutis, M., Trevisiol, P., Latiri, K., Confalonieri, R., 2010. Sensitivity analysis for a complex crop model applied to Durum wheat in the Mediterranean. Eur. J. Agron. 32, 127–136.

Rigby, J.R., Porporato, A., 2008. Spring frost risk in a changing climate. Geophys. Res. Lett. 35.

Roberts, M.J., Braun, N.O., Sinclair, T.R., Lobell, D.B., Schlenker, W., 2017. Comparing and combining process-based crop models and statistical models with some implications for climate change. Environ. Res. Lett. 12, 95010.

Robertson, M.J., Carberry, P.S., Huth, N.I., Turpin, J.E., Probert, M.E., Poulton, P.L., Bell, M., Wright, G.C., Yeates, S.J., Brinsmead, R.B., 2002. Simulation of growth and development of diverse legume species in APSIM. Aust. J. Agric. Res. 53, 429–446.

Robertson, M.J., Lilley, J.M., 2016. Simulation of growth, development and yield of canola (Brassica napus) in APSIM. Crop Pasture Sci. 67, 332–344.

Robinson, A.R., Lermusiaux, P.F.J., 2000. Overview of data assimilation. Harvard reports Phys. Ocean Sci. 62, 1–13.

Rosenzweig, C., Jones, J.W., Hatfield, J.L., Ruane, A.C., Boote, K.J., Thorburn, P., Antle, J.M., Nelson, G.C., Porter, C., Janssen, S., Asseng, S., Basso, B., Ewert, F., Wallach, D., Baigorria, G., Winter, J.M., 2013. The Agricultural Model Intercomparison and Improvement Project (AgMIP): Protocols and pilot studies. Agric. For. Meteorol. 170, 166–182. https://doi.org/10.1016/j.agrformet.2012.09.011

Rötter, R.P., Carter, T.R., Olesen, J.E., Porter, J.R., 2011. Crop-climate models need an

overhaul. Nat. Clim. Chang. 1, 175–177. https://doi.org/10.1038/nclimate1152

Rötter, R.P., Palosuo, T., Kersebaum, K.C., Angulo, C., Bindi, M., Ewert, F., Ferrise, R., Hlavinka, P., Moriondo, M., Nendel, C., Others, 2012. Simulation of spring barley yield in different climatic zones of Northern and Central Europe: a comparison of nine crop models. F. Crop. Res. 133, 23–36.

Rötter, R.P., Tao, F., Höhn, J.G., Palosuo, T., 2015. Use of crop simulation modelling to aid ideotype design of future cereal cultivars. J. Exp. Bot. 66, 3463–3476.

Rouse, J.W., Haas, R.H., Schell, J.A., Deering, D.W., 1973. Monitoring vegetation systems in the Great Plains with ERTS, in: Third Earth Resources Technology Satellite-1 Symposium: Section AB. Technical Presentations. p. 309.

Ryu, D., Crow, W.T., Zhan, X., Jackson, T.J., 2009. Correcting unintended perturbation biases in hydrologic data assimilation. J. Hydrometeorol. 10, 734–750.

Sadeh, Y., Zhu, X., Dunkerley, D., Walker, J.P., Zhang, Y., Rozenstein, O., Manivasagam, V.S., Chenu, K., 2021. Fusion of Sentinel-2 and PlanetScope time-series data into daily 3 m surface reflectance and wheat LAI monitoring. Int. J. Appl. Earth Obs. Geoinf. 96, 102260.

Sadras, V., Baldock, J., Roget, D., Rodriguez, D., 2003. Measuring and modelling yield and water budget components of wheat crops in coarse-textured soils with chemical constraints. F. Crop. Res. 84, 241–260.

Saltelli, A., 2002. Making best use of model evaluations to compute sensitivity indices. Comput. Phys. Commun. 145, 280–297.

Sasaki, Y., 1970. Some basic formalisms in numerical variational analysis. Mon. Weather Rev. 98, 875–883.

Schneider, K., 2003. Assimilating remote sensing data into a land-surface process model. Int. J. Remote Sens. 24, 2959–2980.

Seidel, S.J., Palosuo, T., Thorburn, P., Wallach, D., 2018. Towards improved calibration of crop models--Where are we now and where should we go? Eur. J. Agron. 94, 25–35.

Sexton, J., Everingham, Y.L., Inman-Bamber, G., 2017. A global sensitivity analysis of

cultivar trait parameters in a sugarcane growth model for contrasting production environments in Queensland, Australia. Eur. J. Agron. 88, 96–105.

Shamudzarira, Z., Robertson, M.J., 2002. Simulating response of maize to nitrogen fertilizer in semi-arid Zimbabwe. Exp. Agric. 38, 79–96.

Shiferaw, B., Smale, M., Braun, H.-J., Duveiller, E., Reynolds, M., Muricho, G., 2013. Crops that feed the world 10. Past successes and future challenges to the role played by wheat in global food security. Food Secur. 5, 291–317.

Shokri, A., Walker, J.P., van Dijk, A.I.J.M., Pauwels, V.R.N., 2019. On the use of adaptive ensemble Kalman filtering to mitigate error misspecifications in GRACE data assimilation. Water Resour. Res. 55, 7622–7637.

Shroyer, J.P., Mikesell, M.E., Paulsen, G.M., 1995. Spring freeze injury to Kansas wheat. Cooperative Extension Service, Kansas State University.

Silvestro, P.C., Casa, R., Hanuš, J., Koetz, B., Rascher, U., Schuettemeyer, D., Siegmann, B., Skokovic, D., Sobrino, J., Tudoroiu, M., 2021. Synergistic Use of Multispectral Data and Crop Growth Modelling for Spatial and Temporal Evapotranspiration Estimations. Remote Sens. 13, 2138.

Silvestro, P.C., Pignatti, S., Pascucci, S., Yang, H., Li, Z., Yang, G., Huang, W., Casa, R., 2017. Estimating wheat yield in China at the field and district scale from the assimilation of satellite data into the Aquacrop and simple algorithm for yield (SAFY) models. Remote Sens. 9, 509.

Smith, K.A., McTaggart, I.P., Tsuruta, H., 1997. Emissions of N2O and NO associated with nitrogen fertilization in intensive agriculture, and the potential for mitigation. Soil use Manag. 13, 296–304.

Sobol', I.M., 1990. On sensitivity estimation for nonlinear mathematical models. Mat. Model. 2, 112–118.

Soltani, A., Sinclair, T.R., 2015. A comparison of four wheat models with respect to robustness and transparency: Simulation in a temperate, sub-humid environment. F. Crop. Res. 175, 37–46.

Steduto, P., Hsiao, T.C., Raes, D., Fereres, E., 2009a. Aquacrop-the FAO crop model to simulate yield response to water: I. concepts and underlying principles. Agron. J.

101, 426–437. https://doi.org/10.2134/agronj2008.0139s

Steduto, P., Hsiao, T.C., Raes, D., Fereres, E., 2009b. AquaCrop—The FAO crop model to simulate yield response to water: I. Concepts and underlying principles. Agron. J. 101, 426–437.

Stone, P.J., Nicolas, M.E., 1995. A survey of the effects of high temperature during grain filling on yield and quality of 75 wheat cultivars. Aust. J. Agric. Res. 46, 475–492.

Sun, H., Zhang, X., Wang, E., Chen, S., Shao, L., 2015. Quantifying the impact of irrigation on groundwater reserve and crop production--a case study in the North China Plain. Eur. J. Agron. 70, 48–56.

Sun, L., Seidou, O., Nistor, I., Liu, K., 2016. Review of the Kalman-type hydrological data assimilation. Hydrol. Sci. J. 61, 2348–2366.

Supit, I., Hooyer, A.A., Van Diepen, C.A., 1994. System description of the WOFOST 6.0 crop simulation model implemented in the CGMS Vol. 1: Theory and algorithms. Agric. Ser. Luxemb.

Talagrand, O., Courtier, P., 1987. Variational assimilation of meteorological observations with the adjoint vorticity equation. I: Theory. Q. J. R. Meteorol. Soc. 113, 1311–1328.

Tandeo, P., Ailliot, P., Bocquet, M., Carrassi, A., Miyoshi, T., Pulido, M., Zhen, Y., 2020. A review of innovation-based methods to jointly estimate model and observation error covariance matrices in ensemble data assimilation. Mon. Weather Rev. 148, 3973–3994.

Tao, F., Rötter, R.P., Palosuo, T., Gregorio Hernández Díaz-Ambrona, C., Mínguez, M.I., Semenov, M.A., Kersebaum, K.C., Nendel, C., Specka, X., Hoffmann, H., others, 2018. Contribution of crop model structure, parameters and climate projections to uncertainty in climate change impact assessments. Glob. Chang. Biol. 24, 1291–1307.

Tao, F., Zhang, Z., 2013. Climate change, high-temperature stress, rice productivity, and water use in Eastern China: a new superensemble-based probabilistic projection. J. Appl. Meteorol. Climatol. 52, 531–551.

Thorburn, P.J., Probert, M.E., Robertson, F.A., 2001. Modelling decomposition of sugar

cane surface residues with APSIM--Residue. F. Crop. Res. 70, 223–232.

Thorp, K.R., Hunsaker, D.J., French, A.N., 2010. Assimilating leaf area index estimates from remote sensing into the simulations of a cropping systems model. Trans. ASABE 53, 251–262.

Thorp, K.R., Wang, G., West, A.L., Moran, M.S., Bronson, K.F., White, J.W., Mon, J., 2012. Estimating crop biophysical properties from remote sensing data by inverting linked radiative transfer and ecophysiological models. Remote Sens. Environ. 124, 224–233.

Tian, L.., Li, Z.., Huang, J.., Wang, L.., Su, W.., Zhang, C.., Liu, J.., 2013. Comparison of two optimization algorithms for estimating regional winter wheat yield by integrating MODIS leaf area index and world food studies model. Sens. Lett. 11, 1261–1268. https://doi.org/10.1166/sl.2013.2871

Togliatti, K., Archontoulis, S. V, Dietzel, R., Puntel, L., VanLoocke, A., 2017. How does inclusion of weather forecasting impact in-season crop model predictions? F. Crop. Res. 214, 261–272.

Trenberth, K.E., 2011. Changes in precipitation with climate change. Clim. Res. 47, 123–138.

Tripathy, R., Chaudhari, K.N., Mukherjee, J., Ray, S.S., Patel, N.K., Panigrahy, S., Parihar, J.S., 2013. Forecasting wheat yield in Punjab state of India by combining crop simulation model WOFOST and remotely sensed inputs. Remote Sens. Lett. 4, 19–28.

Van Dam, J.C., Huygen, J., Wesseling, J.G., Feddes, R.A., Kabat, P., Van Walsum, P.E. V, Groenendijk, P., Van Diepen, C.A., 1997. Theory of SWAP version 2.0 Simulation of water flow, solute transport and plant growth in the soil-water-atmosphere-plant environment.

Van Diepen, C.A. van, Wolf, J., Van Keulen, H., Rappoldt, C., 1989. WOFOST: a simulation model of crop production. Soil use Manag. 5, 16–24.

van Ittersum, M.K., Leffelaar, P.A., Van Keulen, H., Kropff, M.J., Bastiaans, L., Goudriaan, J., 2003. On approaches and applications of the Wageningen crop models. Eur. J. Agron. 18, 201–234.

Van Oort, P.A.J., Wang, G., Vos, J., Meinke, H., Li, B.G., Huang, J.K., van der Werf, W., 2016. Towards groundwater neutral cropping systems in the Alluvial Fans of the North China Plain. Agric. Water Manag. 165, 131–140.

Van Wijk, M.T., Rufino, M.C., Enahoro, D., Parsons, D., Silvestri, S., Valdivia, R.O., Herrero, M., 2014. Farm household models to analyse food security in a changing climate: A review. Glob. Food Sec. 3, 77–84.

Varella, H., Guérif, M., Buis, S., 2010. Global sensitivity analysis measures the quality of parameter estimation: The case of soil parameters and a crop model. Environ. Model. & Softw. 25, 310–319.

Vogeler, I., Sharp, J., Cichota, R., Lilburne, L., 2022. Sensitivity analysis of soil parameters in the Agricultural Production Systems sIMulator (APSIM). Soil Res.

Vrugt, J.A., Gupta, H. V, Nualláin, B., Bouten, W., 2006. Real-time data assimilation for operational ensemble streamflow forecasting. J. Hydrometeorol. 7, 548–565.

Vrugt, J.A., Ter Braak, C.J.F., Clark, M.P., Hyman, J.M., Robinson, B.A., 2008. Treatment of input uncertainty in hydrologic modeling: Doing hydrology backward with Markov chain Monte Carlo simulation. Water Resour. Res. 44.

Wagner, M.P., Slawig, T., Taravat, A., Oppelt, N., 2020. Remote sensing data assimilation in dynamic crop models using particle swarm optimization. ISPRS Int. J. Geo-Information 9, 105.

Walker, J.P., Houser, P.R., 2005. Hydrologic data assimilation, in: Advances in Water Science Methodologies. CRC Press, pp. 25–48.

Wallach, D., Goffinet, B., Bergez, J.-E., Debaeke, P., Leenhardt, D., Aubertot, J.-N., 2002. The effect of parameter uncertainty on a model with adjusted parameters. Agronomie 22, 159–170.

Wallach, D., Nissanka, S.P., Karunaratne, A.S., Weerakoon, W.M.W., Thorburn, P.J., Boote, K.J., Jones, J.W., 2017. Accounting for both parameter and model structure uncertainty in crop model predictions of phenology: A case study on rice. Eur. J. Agron. 88, 53–62. https://doi.org/10.1016/j.eja.2016.05.013

Wallach, D., Thorburn, P.J., 2017. Estimating uncertainty in crop model predictions: Current situation and future prospects. Eur. J. Agron. 88, A1–A7.

https://doi.org/10.1016/j.eja.2017.06.001

Wang, B., Feng, P., Liu, D.L., O'Leary, G.J., Macadam, I., Waters, C., Asseng, S., Cowie, A., Jiang, T., Xiao, D., others, 2020. Sources of uncertainty for wheat yield projections under future climate are site-specific. Nat. Food 1, 720–728.

Wang, E., Chen, C., Yu, Q., 2009. Modeling the response of wheat and maize productivity to climate variability and irrigation in the North China Plain, in: 18th World IMACS/MODSIM Congress. pp. 2742–2748.

Wang, E., Martre, P., Zhao, Z., Ewert, F., Maiorano, A., Rötter, R.P., Kimball, B.A., Ottman, M.J., Wall, G.W., White, J.W., others, 2017. The uncertainty of crop yield projections is reduced by improved temperature response functions. Nat. Plants 3, 17102.

Wang, E., Van Oosterom, E., Meinke, H., Asseng, S., Robertson, M.J., Huth, N., Keating, B., Probert, M., 2003. The new APSIM-Wheat Model—performance and future improvements, in: Proceedings of the 11th Australian Agronomy Conference.

Wang, G.-C., Wang, E.-L., Yao, H., Xu, J.-J., 2014. Soil carbon sequestration potential as affected by management practices in northern China: a simulation study. Pedosphere 24, 529–543.

Wang, J., Li, X., Lu, L., Fang, F., 2013a. Parameter sensitivity analysis of crop growth models based on the extended Fourier Amplitude Sensitivity Test method. Environ. Model. Softw. 48, 171–182.

Wang, J., Li, X., Lu, L., Fang, F., 2013b. Estimating near future regional corn yields by integrating multi-source observations into a crop growth model. Eur. J. Agron. 49, 126–140.

Wang, J., Wang, E., Feng, L., Yin, H., Yu, W., 2013c. Phenological trends of winter wheat in response to varietal and temperature changes in the North China Plain. F. Crop. Res. 144, 135–144.

Welch, G., Bishop, G., others, 1995. An introduction to the Kalman filter.

Williams, J. R., Jones, C.A., Kiniry, J.R., Spanel, D.A., 1989. The EPIC Crop Growth Model. Trans. ASAE 32, 0497–0511. https://doi.org/10.1177/001088047601700202

Williams, J R, Jones, C.A., Kiniry, J.R., Spanel, D.A., 1989. The EPIC crop growth model. Trans. ASAE 32, 497–511.

Wisiol, K., 1987. Choosing a basis for yield forecasts and estimates.

Wong, M.T.F., Asseng, S., 2006. Determining the causes of spatial and temporal variability of wheat yields at sub-field scale using a new method of upscaling a crop model. Plant Soil 283, 203–215.

Wu, L., Liu, X., Wang, P., Zhou, B., Liu, M., Li, X., 2013. The assimilation of spectral sensing and the WOFOST model for the dynamic simulation of cadmium accumulation in rice tissues. Int. J. Appl. Earth Obs. Geoinf. 25, 66–75. https://doi.org/10.1016/j.jag.2013.04.002

Wu, R., Lawes, R., Oliver, Y., Fletcher, A., Chen, C., 2019. How well do we need to estimate plant-available water capacity to simulate water-limited yield potential? Agric. Water Manag. 212, 441–447.

Xiao, D., Tao, F., 2014. Contributions of cultivars, management and climate change to winter wheat yield in the North China Plain in the past three decades. Eur. J. Agron. 52, 112–122.

Xing, H., Xu, X., Li, Z., Chen, Y., Feng, H., Yang, G., Chen, Z., 2017. Global sensitivity analysis of the AquaCrop model for winter wheat under different water treatments based on the extended Fourier amplitude sensitivity test. J. Integr. Agric. 16, 2444–2458.

Xu, T., Chen, F., He, Xinlei, Barlage, M., Zhang, Z., Liu, S., He, Xiangping, 2021. Improve the Performance of the Noah-MP-Crop Model by Jointly Assimilating Soil Moisture and Vegetation Phenology Data. J. Adv. Model. Earth Syst. 13, e2020MS002394.

Yan, Z., Zhang, X., Rashid, M.A., Li, H., Jing, H., Hochman, Z., 2020. Assessment of the sustainability of different cropping systems under three irrigation strategies in the North China Plain under climate change. Agric. Syst. 178, 102745.

Yang, Q., Shi, L., Han, J., Zha, Y., Yu, J., Wu, W., Huang, K., 2023. Regulating the time of the crop model clock: A data assimilation framework for regions with high phenological heterogeneity. F. Crop. Res. 293, 108847.

Yang, Yanmin, Li Liu, D., Anwar, M.R., Zuo, H., Yang, Yonghui, 2014. Impact of future climate change on wheat production in relation to plant-available water capacity in a semiaridenvironment. Theor. Appl. Climatol. 115, 391–410.

Yao, F., Tang, Y., Wang, P., Zhang, J., 2015. Estimation of maize yield by using a process-based model and remote sensing data in the Northeast China Plain. Phys. Chem. Earth, Parts A/B/C 87, 142–152.

Yu, Q., Cui, Y., Liu, L., 2023. Assessment of the parameter sensitivity for the ORYZA model at the regional scale-A case study in the Yangtze River Basin. Environ. Model. & Softw. 159, 105575.

Yunusa, I.A.M., Bellotti, W.D., Moore, A.D., Probert, M.E., Baldock, J.A., Miyan, S.M., 2004. An exploratory evaluation of APSIM to simulate growth and yield processes for winter cereals in rotation systems in South Australia. Aust. J. Exp. Agric. 44, 787–800.

Zadoks, J.C., Chang, T.T., Konzak, C.F., 1974. A decimal code for the growth stages of cereals. Weed Res. 14, 415–421.

Zeleke, K.T., Nendel, C., 2016. Analysis of options for increasing wheat (Triticum aestivum L.) yield in south-eastern Australia: The role of irrigation, cultivar choice and time of sowing. Agric. Water Manag. 166, 139–148.

Zeppel, M.J.B., Wilks, J. V, Lewis, J.D., 2014. Impacts of extreme precipitation and seasonal changes in precipitation on plants. Biogeosciences 11, 3083–3093.

Zhang, C., Liu, J., Shang, J., Dong, T., Tang, M., Feng, S., Cai, H., 2021. Improving winter wheat biomass and evapotranspiration simulation by assimilating leaf area index from spectral information into a crop growth model. Agric. Water Manag. 255, 107057.

Zhang, Y., Feng, L., Wang, E., Wang, J., Li, B., 2012. Evaluation of the APSIM-Wheat model in terms of different cultivars, management regimes and environmental conditions. Can. J. Plant Sci. 92, 937–949.

Zhang, Y., Feng, L.P., Wang, J., Wang, E.L., Xu, Y.L., 2013. Using APSIM to explore wheat yield response to climate change in the North China Plain: the predicted adaptation of wheat cultivar types to vernalization. J. Agric. Sci. 151, 836–848.

Zhang, Y., Walker, J.P., Pauwels, V.R.N., 2022. Assimilation of wheat and soil states for improved yield prediction: The APSIM-EnKF framework. Agric. Syst. 201, 103456.

Zhang, Y., Walker, J.P., Pauwels, V.R.N., Sadeh, Y., 2021. Assimilation of Wheat and Soil States into the APSIM-Wheat Crop Model: A Case Study. Remote Sens. 14, 65.

Zhao, G., Bryan, B.A., Song, X., 2014. Sensitivity and uncertainty analysis of the APSIM-wheat model: Interactions between cultivar, environmental, and management parameters. Ecol. Modell. 279, 1–11. https://doi.org/10.1016/j.ecolmodel.2014.02.003

Zhao, G., Hoffmann, H., van Bussel, L.G.J., Enders, A., Specka, X., Sosa, C., Yeluripati, J., Tao, F., Constantin, J., Raynal, H., others, 2015. Effect of weather data aggregation on regional crop simulation for different crops, production conditions, and response variables. Clim. Res. 65, 141–157.

Zhao, J., Pu, F., Li, Y., Xu, J., Li, N., Zhang, Y., Guo, J., Pan, Z., 2017. Assessing the combined effects of climatic factors on spring wheat phenophase and grain yield in Inner Mongolia, China. PLoS One 12.

Zhao, Y., Chen, S., Shen, S., 2013. Assimilating remote sensing information with crop model using Ensemble Kalman Filter for improving LAI monitoring and yield estimation. Ecol. Modell. 270, 30–42.

Zhao, Z., Qin, X., Wang, E., Carberry, P., Zhang, Y., Zhou, S., Zhang, X., Hu, C., Wang, Z., 2015. Modelling to increase the eco-efficiency of a wheat--maize double cropping system. Agric. Ecosyst. Environ. 210, 36–46.

Zhao, Z., Wang, E., Wang, Z., Zang, H., Liu, Y., Angus, J.F., 2014a. A reappraisal of the critical nitrogen concentration of wheat and its implications on crop modeling. F. Crop. Res. 164, 65–73.

Zhao, Z., Wang, E., Xue, L., Wu, Y., Zang, H., Qin, X., Zhang, J., Wang, Z., 2014b. Accuracy of root modelling and its impact on simulated wheat yield and carbon cycling in soil. F. Crop. Res. 165, 99–110.

Zheng, B., Chapman, S.C., Christopher, J.T., Frederiks, T.M., Chenu, K., 2015. Frost

trends and their estimated impact on yield in the Australian wheatbelt. J. Exp. Bot. 66, 3611–3623.

Zheng, B., Chenu, K., Doherty, A., Chapman, S., 2014. The APSIM-wheat module (7.5 R3008). Agric. Prod. Syst. Simulator Initiat. 615, 1--42.

Zhou, S., Zhang, Y., Williams, A.P., Gentine, P., 2019. Projected increases in intensity, frequency, and terrestrial carbon costs of compound drought and aridity events. Sci. Adv. 5, eaau5740.

Zhuo, W., Huang, J., Xiao, X., Huang, H., Bajgain, R., Wu, X., Gao, X., Wang, J., Li, X., Wagle, P., 2022. Assimilating remote sensing-based VPM GPP into the WOFOST model for improving regional winter wheat yield estimation. Eur. J. Agron. 139, 126556.

Ziliani, M.G., Altaf, M.U., Aragon, B., Houborg, R., Franz, T.E., Lu, Y., Sheffield, J., Hoteit, I., McCabe, M.F., 2022. Early season prediction of within-field crop yield variability by assimilating CubeSat data into a crop model. Agric. For. Meteorol. 313, 108736.

Appendix A Supplementary material for Chapter 1

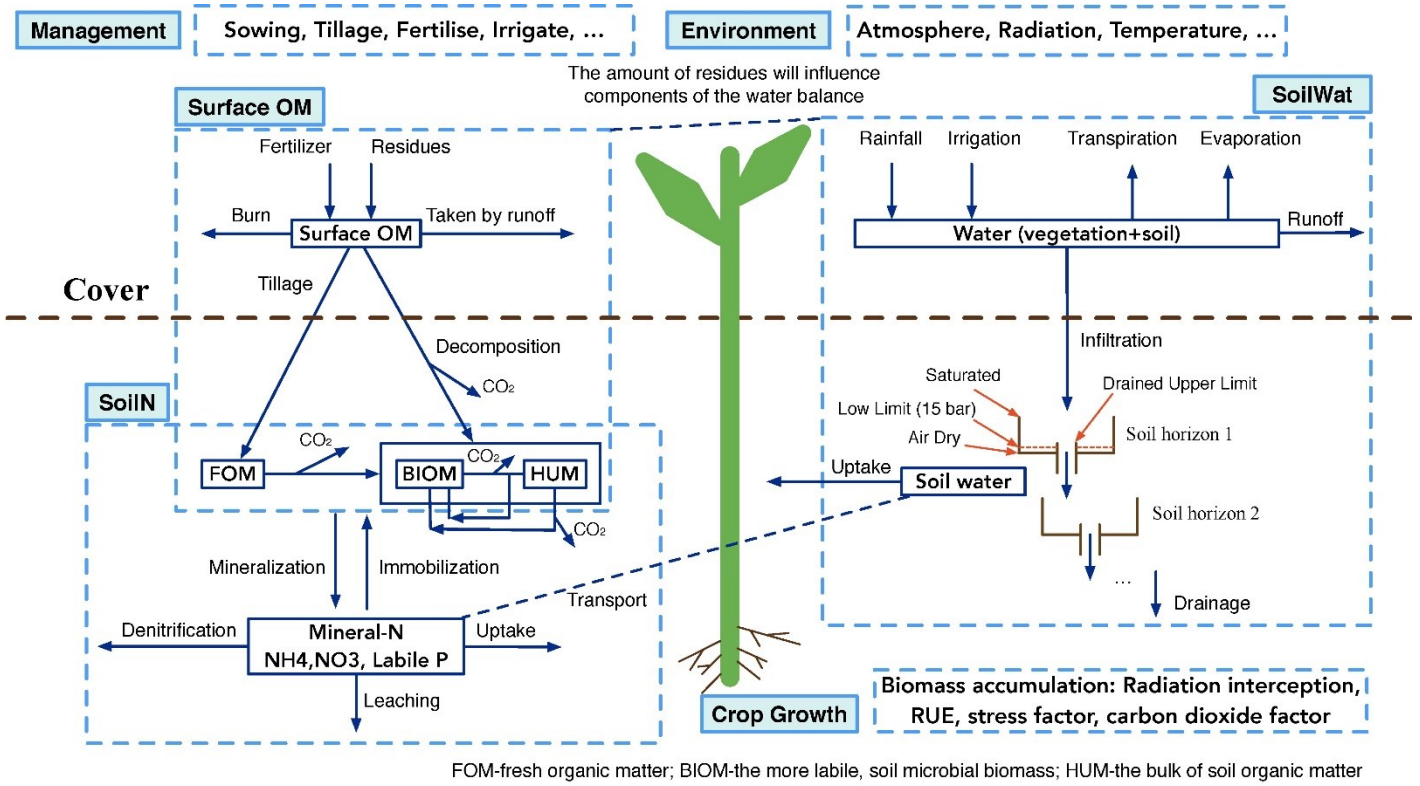

Figure A. 1. Schematic of the APSIM model's main processes used in this study

Appendix B Supplementary material for Chapter 2

Table B. 1. Calibrated cultivar parameters of APSIM-Wheat

Reference	Cultivar	Location	tt_end_of_juverile	tt_floral_initiation	tt_start_grain_fill	tt_startgf_to_mat	potential_grain_filling_rate	grain_per_gram_stem	max_grain_size	vern_sens	photop_sens	phyllochron
(Wang et al., 2009; Chen et al., 2010b; Chen et al., 2010c)	Gaoyou 503	NCP, China	/	/	/	500	0.0023	23	/	1.7	2.3	85
(Wang et al., 2009; Chen et al., 2010c)	Xifeng 24	NCP, China	/	/	/	500	0.0025	22	/	1.5	2	85
(Wang et al., 2009; Chen et al., 2010c)	Keyu 13	NCP, China	/	/	/	420	0.0023	22	/	1.5	2	85
(Wang et al., 2009; Chen et al., 2010c)	Zhengmai 9023	NCP, China	/	/	/	420	0.0025	26	/	1.8	2	85
(Chen et al., 2010d)	Not specified	Not specified	/	/	/	/	/	/	/	/	/	/
Balwinder-Singh et al., 2011)	PBW343	Punjab, India	/	/	/	750	/	/	/	1.7	3.8	95
(Zhang et al., 2012; 2013)	Nongda211	NCP, China	/	/	/	540	0.0028	27	/	3.4	3.2	/
(Zhang et al., 2012; 2013)	Han6172	NCP, China	/	/	/	560	0.0025	33	/	3.1	3.3	/
(Zhang et al., 2012; 2013)	Yanzhan4110	NCP, China	/	/	/	550	0.0028	33	/	2.9	3.3	/
(Wang et al., 2013)	Not specified	Not specified	/	Calibrated, value was not specified.	/	/	/	/	/	Calibrated, value was not specified.	Calibrated, value was not specified.	/
(He et al., 2014)	Changwu89134	Loess Plateau, China	/	/	/	650	0.0025	25	/	2	3	/
(Wang et al., 2014)	Not specified	Not specified	/	/	/	/	/	/	/	/	/	/
(Zhao et al., 2014a)	SJZ15	NCP, China	/	/	/	530	/	/	/	2.3	3.5	/
(Zhao et al., 2014b, 2015)	SJZ15	NCP, China	/	/	/	530	0.003	/	0.05	2.3	3.5	/

(Zhao et al., 2014b, 2015)	SJZ8	NCP, China	/	/	/	540	0.003	/	0.046	2.3	3.3	/
(Xiao et al., 2014)	Fengkang7, Jingdong8	Tangshan, China	680, 660	/	/	590, 630	0.0020, 0.0025	21.0, 26.0	0.041, 0.045	1.8, 1.6	2	85
(Xiao et al., 2014)	Hengshui741, Shimai12	Nangong, China	620, 590	/	/	600, 650	0.0021, 0.0025	20.0, 25.0	0.038, 0.042	1.7, 1.6	2	85
(Xiao et al., 2014)	Boai7422, Zhengmai9023	Zhumadian, China	620, 600	/	/	580, 600	0.0020, 0.0025	24.0, 27.0	0.039, 0.046	1.7, 1.6	2	85
(Xiao et al., 2014)	Fu63, Lumai23	Huimin, China	620, 620	/	/	570, 590	0.0022, 0.0025	24.0, 28.0	0.042, 0.046	1.8, 1.7	2	85
(Li et al., 2014)	Nine local varisties	NCP, China	/	/	/	420-610	0.0022-0.0032	22.0-30.0	/	1.0-3.0	1.8-3.3	/
(Soltani et al., 2015)	Local varieties	Grogan, Iran	/	/	707	580	0.00129	28	/	1.5	4.7	95
(Sun et al., 2015)	Jimai7, Jimai36, Shi733	NCP, China	/	/	/	550	0.0025	28.5, 29.5	/	1.3, 1.4	2	/
(Deihimfard et al., 2015)	Chamran (early maturing)	North-eastern Iran	380	500	545	/	/	22	0.044	2.5	3.5	/

Table B. 2. Detailed Information of validation datasets

	APSIM version	Study area	Validation datasets year	Cultivar (cv.)	Environmental condition	Management condition	PAWC	APSIM performance	Model main application
(Probert et al., 1995)	APSIM 1.X	Warwick, Queensland, Australia	1969-1992	Timgalen (1969-1974, 1978-1981), Cook (1983-1984), Kite (1985-1987), Hartog (1990), QT4118 (1992)	In some seasons, crops suffered from diseases like root-lesion nematodes and crown rot.	Two tillage managements: conventional and no tillage. Two residue managements: stubble burned, and stubble retained. Three rates of N application: 0, 23, 69 kg N/ha.	N/A	R2=0.30, RMSE=0.937 t/ha	Model development and validation
(Probert et al., 1998)	APSIM 1.X	Gatton, Queensland, Australia	1992-1995	N/A	N/A	A range of nitrogen inputs and irrigation regimes.	N/A	Predicted yield = 1.03 * observed yield - 0.27 (t/ha), R^2=0.78	Model evaluation
(Asseng et al., 1998b)	APSIM NWheat	Beverley, Merredin, Moora, and Wongan Hills, Western Australia, Australia	Beverley (1990-1993), Merredin (1973, 1986), Moora (1994-1995), Wongan Hills (1983, 1994)	Dagger, Gamenya, Gutha, Kulin, Spear	Beverley: average annual rainfall=421 mm, growing season rainfall=352 mm, soil type: duplex. Merredin: average annual rainfall=310 mm, growing season rainfall=234 mm, soil type: duplex. Moora: average annual rainfall=458 mm, growing season rainfall=388 mm, soil type: deep sand. Wongan Hills: average annual rainfall=386 mm, growing season	Different nitrogen supply, irrigation, sowing date, sowing density, and deep ripping.	N/A	Observed yield range=1.0 - 4.0 t/ha, R2=0.77, RMSD=0.4 t/ha. Observed biomass range=0.1 - 11.0 t/ha, R2=0.90, RMSD=0.8 t/ha. Observed LAI range=0 - 3.8 m2/m2, R2=0.59, RMSD=0.6 m2/m2.	Model evaluation

					rainfall=318 mm, soil type: loamy sand.				
(Asseng et al., 1998a)	APSIM NWheat	Moora, Western Australia, Australia	1994-1995	Spear	Deep sand, average annual rainfall=459 mm, ranged from 203 to 790 mm.	Nitrogen fertiliser applied of 0, 50, and 90 kg N/ha.	N/A	Discrepancies between observed and predicted yields are less than 0.4 t/ha.	Establish the probability of yield
(Asseng et al., 2000)	APSIM NWheat	The Eest, PAGV, The Bouwing, The Netherland	1983-1984	Arminda	The Eest and PAGV: Soil type: silty loam, average annual rainfall=646 mm. The Bouwing: soil type: silty clay loam, average annual rainfall=763 mm.	Nitrogen fertiliser applications: The Eest: 0, 60, 110, 150, 160 kg N/ha. PAGV: 80, 140, 180, 240 kg N/ha. The Bouwing: 0, 60, 70, 160, 170, 230 kg N/ha.	N/A	Observed yield range=0.4-8.3 t/ha, R2=0.90, RMSD=0.8 t/ha. Observed biomass range=0.03-20 t/ha, R2=0.97, RMSD=1.2 t/ha. Observed LAI range=0-5.5 m2/m2, R2=0.65, RMSD=1.2 m2/m2.	Explore the relationship between yield and N-fertiliser application
(Fisher et al., 2001)	APSIM Nwheat (1.55)	Balla, Wongan Hills, Merredin, East Beverley, Katanning, Newdegate, Esperance, and Salmon Gums, Western Australia, Australia	1989-1992	Spear, Kulin	Wongan Hills: based on 1900-1999 historical weather data, the weather was dominated by summer rainfall<=45 mm, annual rainfall<=390 mm, early season (April to May)<=140 (n=46) and summer rainfall>45 mm, annual rainfall>390 mm, early season>140 (n=47).	Fertiliser application: 90 kg at sowing, 60 kg 4 weeks after sowing. Total of 111 sowing dates between 9th April and 19th July.	N/A	Spear: dates of anthesis-RMSD=12.1days, R2=0.76, bias=-1.0%. Kulin: dates of anthesis-RMSD=9.5days, R2=0.86, bias=1.4%.	Provide information on choice of cultivar and sowing date
(Asseng et al., 2001)	APSIM NWheat	Moora, Wongan Hills, Merredin, Western Australia, Australia	Up to 87 continuoud years.	Spear, Amery	Sand, clay soil. Average annual rainfall: Moora: 461 mm, Wongan Hills: 386 mm, Merredin: 310 mm. Growing season rainfall: Moora: 392 mm (mean), 165 - 648 mm (range), Wongan Hills: 322 mm (mean), 112 - 535 mm (range), Merredin: 235 mm (mean), 102 - 418 mm (range).	Fertiliser N was aaplied: 0, 30, 60, 90, 150, 210 kg N/ha. Three sowing dates: DOY 135 (15 May), DOY 155 (4 June), DOY 175 (24 June).	Sand PAWC= 55 mm, clay soil PAWC= 109 mm.	The yield in the Mediterranean climatic region of Western Australia depends on soil water-holding capacity, nitrogen management, rainfall amount and especially, seasonal rainfall distribution.	Explore the water- and nitrogen-use efficiency
(Asseng et al., 2002)	APSIM NWheat	New South Wales, Australia; Wongan Hills and Cunderdin, Western Australia, Australia	1997 (Western Australia)	Spear, Amery	Average annual rainfall: Wongan Hills=391 mm, Cunderdin=367 mm, New South Wales=436, 536 mm. Soil Type: Wongan Hills: sand (PAWC=55 mm), Cunderdin: Clay (PAWC=109 mm), New South Wales: loam (PAWC=159 mm).	Fertiliser N was applied: 0, 30, 60, 90 kg N/ha at Wongan Hills experiment.	Sand PAWC= 55 mm, clay soil PAWC= 109 mm, loam PAWC= 159 mm.	Western Australia: grain protein-RMSD=1.9 - 2.0%. New South Wales: the slight overestimation of grain protein by the model was primarily a result of overestimating available nitrogen.	Model development and validation
(Lilley et al., 2003)	APSIM 2.1	Near Harden, NSW, Australia	1989-2000	Janz	Soil: red brown earth with total carbon in the surface of 1.3%. C:N ratio = 10. Growing season rainfall=179-539mm (April to mid-November). Mean annual temperature=14.7°C and the difference between the highest and lowest mean monthly teperatures=16°C.	Fertiliser N application in 1993, 1994, 1996, 1998, 1999 and 2000 at rates of 97, 23, 22, 114, 130, and 110 kgN/ha, respectively.	PAWC= 169 mm	Corresponded well in dynamics.	Model evaluation
(Lilley et al., 2003)	APSIM 2.1	Near Condobolin, NSW, Australia	1991-1993	Rosella (1991-1992),	Soil: red brown earth with total carbon in the surface of 1.3%. C:N ratio = 13. During the three years, growing	In 1991 and 1993, 25 kg N/ha was applied at sowing, while in	PAWC= 145mm	In 1991, the model failed to simulate the effects of environmental stresses. The	Model evaluation

				Dollarbird (1993)	season rainfall = 234, 341 and 324 mm respectively. Mean annual temperature=17.5 °C.	1992, 10 kg N/ha was applied at sowing.		simulation of yield and biomass doubled the observed values.	
(Sadras et al., 2003)*	N/A	Mallee region of Southeastern Australia	1998-2002	Hartog	Soil: sandy regolithic, hypocalcic, calcarosols. Sand, 29.7–95.5%; clay, 1.5–21.4%; pH 7.6–10.2; Na concentration: 11-2439 mg/kg; B concentration: 0.56-29.0mg/kg; EC: 0.05-1.31 dS/m. Growing season rainfall=218-351mm, maximum temperature =18-19.5 °C	Fertilised (no nitrogen stress)	N/A	RMSE of yield is from 0.31t/ha to 0.19 t/ha, R2 is from 0.60 to 0.74. R2 of soil water content simulation is from 0.47 cm3/cm3 to 0.72 cm3/cm3, RMSE is from 2.1-3 to 9.3-4). Both yield and SWC simulations improved while field-measured soil water properties were used instead of estimates based on soil texture.	Quantify the effect of environmental factors
(Wang et al., 2003)*	N/A	Queensland (QLD) and Western Australia (WA)	1987-1995	Five cultivars	Soil types: duplex, deep sand, loamy sand.	Four experiments with fertilised (4 N treatments), some with water treatments or residue treatments	N/A	Simulation of biomass (RMSD=1.62 t/ha) and yield (RMSD=0.74 t/ha) with R2>0.80 and nitrogen uptake (R2>0.75, RMSD=0.02 t/ha). Could explain >80% of the total biomass/yield/maximum LAI variations.	Model evaluation
(Asseng et al., 2004)	APSIM Nwheat	Obregon, Mexico; Maricopa, USA; Lincoln, New Zealand; Wongan Hills and Cunderdin, Western Australia, Australia	1989-1990 and 1994-1995 (Obregon); 1991 (Lincoln); 1997 (Western Australia); 1992-1994, 1995-1997 (Maricopa)	Yecora70, Batten, Amery, Wilgoyne, Spear	Clay loam, sandy loam, sand, and clay	Rising temperature (Obregon), increased levels of water deficit (Lincoln), late water deficit (Western Australia), elevated atmospheric CO2 (Maricopa).	N/A	Obregon: yield-RMSD=1.0 t/ha, biomass-RMSD=2.8 t/ha; Lincoln: yield-RMSD=1.2 t/ha, biomass-RMSD=1.9 t/ha, R2=0.90, LAI-RMSD=1.3 m2/m2, LAI-R2=0.53; Western Australia: yield-RMSD=0.5 t/ha, yield-R2=0.77, biomass-RMSD=1.1 t/ha, R2=0.86; Maricopa: yield-RMSD=1.1 t/ha, yield-R2=0.72, biomass-RMSD=1.6 t/ha, R2=0.94, LAI-RMSD=0.9 m2/m2, LAI-R2=0.73.	Assess the effects of climate change on crop yield.
(Yunusa et al., 2004)	APSIM 1.4 Patch 2	Roseworthy, Minnipa, and Wunkar, South Australia, Australia	1995-1996 (Roseworthy), 1997 (Minnipa, Wunkar)	Janz (Roseworthy, Minnipa, Wunkar), Excalibur (Roseworthy)	Roseworthy: average annual rainfall=420 mm, growing season rainfall=320 mm, minimum and maximum temperatures=8.2 and 18.8°C. Soil: red brown earth. Minnipa: growing season rainfall=230 mm, minimum and maximum temperatures=7.9 and 19.1°C. Soil: sandy loam topsoil underlayed by calcareous subsoil. Wunkar: growing season rainfall=170 mm, minimum and maximum temperatures=5.5 and 18.8°C. Soil: loamy sand, grading into calcareous sandy clay and heavy clay.	Roseworthy: nitrogen fertiliser applied of 0, 50, 75, 100 kg N/ha.	N/A	Yield-R2=0.69, RMSD=0.447 t/ha; grain weight-R2=0.31, RMSD=7.0 mg; grain protein-R2=0.03, RMSD=5.7%.	Evaluate yield response to environmental factors
(Luo et al., 2005)	APSIM 2.0	Cummins, Keith, Lameroo, Minnipa,	Continuous 100 years	Janz, Excalibur	Cummins, Keith, Naracoorte, and Roseworthy: wetter climates with an average annual rainfall=430 - 580 mm.	Fertilised to ensure no nitrogen stress. Changing rainfall,	PAWC= 76 - 157 mm	Rainfall is by far the most influential factor on change in	Assess the effects of climate change on crop yield.

		Naracoorte, Orroroo, Roseworthy, and Wanbi, South Australia, Australia			Growing season rainfall=292 - 397 mm. The other four sites: drier with an average annual rainfall=304 - 388 mm, growing season rainfall=186 - 251 mm. Cummins: clay loam, PAWC=140 mm, Keith: loamy sand, PAWC=76 mm, Lameroo: fine sandy loam, PAWC=111 mm, Minnipa: sandy loam, PAWC=157 mm, Naracoorte: sandy clay loam, PAWC=125 mm, Orroroo: sandy loam, PAWC=134 mm, Roseworthy: loam, PAWC=122 mm, Wanbi: sandy loam, PAWC=132 mm.	temperature, and CO2 concentration conditions.		median grain yield in the medium to low rainfall areas.	
(Paydar et al., 2005)*	N/A	APSIM was validated using a field experiment carried out in the southern area of the Liverpool Plains catchment, located in northern New South Wales, Australia.	1995-1998	N/A	Black vertosol, average annual rainfall=684mm	Nitrogen fertiliser was applied at a rate of 100 kg N/ha.	The soil moisture holding capacity is 505 mm for a 3 m depth.	In general, the model provides a satisfactory representation of the key biological and hydrological processes. Yield estimations are typically accurate for wheat, barley, and sorghum, but less accurate for legumes.	Assess the impacts of various crop management techniques on the water equilibrium.
(Oliver et al., 2006)*	N/A	Two paddocks in Buntine, on the northern sandplain of the Western Australia wheatbelt.	1997, 1999, 2002-2005	N/A	Annual cumulative rainfall less than 400mm	The crops received fertilisation, with N applied at sowing ranging from 0 to 150 kg/ha, and an additional 50 kg/ha N present in the soil profile.	PAWC= 32-110mm	RMSD=0.518 t/ha	Explore the importance of PAWC as a driver of yield variation
(Hunt et al., 2006)*	Yield Prophet	338 paddocks of 236 growers in Australia	2005	N/A	N/A	N/A	N/A	Paddocks with appropriate measured soil characterisation and soil profile samples: R^2=0.68, 68% of simulated results were found to fall within 0.5 t/ha. or fields lacking sufficient soil data: R^2=0.54, 49% of the model outputs were within 0.5 t/ha.	Explore the importance of PAWC as a driver of yield variation
(Wong and Asseng, 2006)	APSIM NWheat	70 ha field near Three Springs, Western Australia, Australia	1998-2002	Blade, Brookton, Carnamah	The annual average rainfall in this region was 445 mm, with 370 mm occurring during the growing season from May to October.	In the simulations, the nitrogen application rates were set at 0, 60, 150, and 210 kg N/ha.	PAWC= 140-162mm	RMSE=1.0 t/ha	Develop an method to use APSIM spatially
(Moeller et al., 2007)	APSIM 4.2	Dry Areas at Tel Hadya, north-western Syria	1998-2000	Cham3	Continental Mediterranean climate that is semi-arid, with cool and wet winters and hot and dry summers. Average annual rainfall = 340 mm, average annual temperature = 17.6 °C. Growing season: early/mid November - early/late May. Soil: vertisol and Inceptisol. pH is around 8. The soil organic matter content is mostly lower than 1% in the top 0.20 m layer.	Nitrogen fertiliser applied of 0, 60 and 100 kg N/ha. Irrigation: 0 and 342 mm	N/A	For all treatments, APSIM overestimated leaf area growth, crop N uptake, and biomass accumulation during pre-anthesis growth at 90-130 days after sowing. The overestimation of leaf area could be a contributing factor to the slight over-prediction of pre-anthesis biomass growth. Additionally, the	Model parameterisation and validation

								more rapid biomass growth could result in overestimation of crop N uptake.	
(Hochman et al., 2007)	APSIM 5.0	A total of 33 paddocks, consisting of grey, brown, and red cracking clays. 6 sites in southern Queensland, 13 sites in northern New South Wales in 2003, and 14 sites in southern Queensland in 2004.	2003-2004	Baxter, H45, Wollaroi, Yallaroi, Babbler, Hybrid Meteor, Strzelecki, and Sunbrook	N/A	No significant weeds, pests, diseases, or nutrient stresses.	PAWC= 93-120mm	When measured PAWC data are used. The simulated results accounted for 82% of observed variation in grain yield, R2=0.82, RMSD=0.5 t/ha. When CLL (PAWC=DUL-CLL) were calculated instead of measured, the model account for 70% of the observed variability in grain yield with R2=0.69 and a RMSD of 0.78 t/ha. When CLL were calculated and kl is adjusted using Cl, the model accounted for 84% of the observed wariability in grain yield with R2=0.84 and a RMSD of 0.53 t/ha.	Evaluate yield response to environmental factors
(Lilley and Kirkegaard, 2008)*	APSIM 5.0	Gundibindyal, NSW, Australia. PAWC=175mm	2000-2004	Rosella, Janz	In-crop rainfall=440 mm	Nitrogen fertiliser applied of 178 kg N/ha	PAWC= 175mm	R2=0.90, RMSD=0.4 t/ha	Evaluate yield response to environmental factors
(Lawes et al., 2009)	APSIM 5.2	Two fields situated near Buntine, Western Australia.	1997-2005	Calingiri, Brown manured, Westonia, Wyalkatchem	Average annual rainfall = 300 - 400 mm	Sowing dates ranged from 15th May to 2nd June. Nitrogen fertiliser applied from 20 to 60 kg N/ha.	PAWC= 52-131mm	R2=0.86, RMSE=0.31 t/ha	Explore the yield-PAWC relationship
(Oliver et al., 2009) (assembled datasets)	APSIM 5.2	146 wheat crops collected from Northern wheatbelt of WA, the eastern wheatbelt of WA, the south coast WA region, and the upper Eyre Peninsula of SA, Australia.	1996-2006	Various varieties	Average annual rainfall=300 - 500mm, growing-season rainfall 243mm ± 88mm.	Not nitrogen limited	PAWC= 33-434 mm	The model showed wheat yield overestimation: RMSE=0.455 t/ha, slope of 0.92, intercept 226, R^2=0.78. Simulated yields matched the observed yield within 10% in 48% of cases. Yield was overestimated by more than 10% in 29% of cases, while in 23% of cases, the yield was underestimated by more than 10%.	As a predictive tool benchmark
(Wang et al., 2009)*	APSIM 5.3	North China Plain (NCP)	1998-2001 at Luancheng, 1997-2001 and 2002-2005 at Yucheng, 2004-2006 at Fengqiu	Gaoyou 503, Zhixuan 1, Keyu 13, Zhengmai 9023	Luancheng: AAR=481 mm. PAWC=335 mm. Yucheng: PAWC=341 mm. Fengqiu: PAWC=204 mm.	Luancheng: Irri of 202 – 404 mm. Yucheng: N treatments: 182 – 215 kg N/ha, irri of 110, 152, 230, 400 mm.	Luancheng: 335mm, Yucheng: 341 mm, Fengqiu: 204 mm	R^2=0.66, RMSD=0.8 t/ha	Evaluate yield response to environmental factors
(Anwar et al., 2009)	APSIM 5.3	The area of interest is a 90 ha section of a 167-	2004 (wheat), 2005 (barley), and additional	Yitpi	The region receives an annual average rainfall of 354 mm, of which 239 mm occurs during the growing season	Nitrogen treatments: 0, 14, 26, 50 kg/ha (2004), 0, 25, 33, 50 kg/ha (2005)	PAWC= 219-294mm	R2=0.96, RMSE=0.31 t/ha	Evaluate yield response to

		ha paddock located in Birchip, Victorian Mallee, Australia. Additional data from Lubeck, southern Wimmera of Victoria	validation data in 2004-2006.		(April-October). The surface soil texture ranges from loamy sand to sandy clay loam, while the subsoil texture varies from sandy loam to sandy clay.				environmental factors
(Bell et al., 2009)* (assembled datasets)	APSIM 5.4	Western Australia includes experimental data of different soil types, nitrogen rates, sowing dates and growing seasons. And crops in Queensland and New Zealand.	2002-2005, 1980s-1990s	Wyalkatchem	Average anuual rainfall ranged from 300 to 595 mm. Soil types: red loam, deep sand and shallow gravel.	rainfed, Nitrogen fertiliser treatment of 100 kg N/ha.	PAWC= 0-75mm	The standing biomass variation was explained by the model with an accuracy of 95%, while for the grain yield, the variation was explained with an accuracy of 89%. The model had a slight tendency to underestimate yield and biomass in high-yield sites. The RMSD was 0.537 t/ha for yield and 1.27 t/ha for biomass, representing 18% and 17%, respectively, of the mean observed values.	Compare the profits of yield harvesting and sacrificing the crop to grazing
(Oliver and Robertson, 2009)	N/A	31 fields across two catchments (Mingenew-Irwin region and Wallatin-O'Brien region) in Western Australia wheatbelt	2004-2006	Wyalkatchem, Carnamah, Bonnie Rock, Westonia, Yitpi, Calingiri	Average annual rainfall=308 - 446 mm (growing season 75% - 86%) (check Table 1-1)	N applied from 10 to 74 kg N/ha.	PAWC= 59-208mm	R2=0.80, RMSE=0.538 t/ha	Evaluate yield response to environmental factors
(Hochman et al., 2009a) (assembled datasets)	Yield Prophet (based on APSIM 6.1)	A total of 344 winter wheat sites in Australia. Victoria (176 sites), South Australia (75 sites), New South Wales (43 sites), Western Australia (38 sites) and Queensland (4 sites)	2004-2007	Various varieties	A variety of soil types were present, including shallow sands with a PAWC of 22 mm, as well as deep Vertosols with a PAWC of 279 mm.	Soil N was between 32 and 588 kg N/ha, with a mean of 124 kg N/ha). 11 crops were irrigated.	PAWC= 22–279mm	R2=0.71, RMSD=0.8 t/ha (n=334)	Model evaluation based on a large dataset from on-farm crops
(Carberry et al., 2009) (assemble datasets)	Yield Prophet	There are more than 700 commercially grown crops, including barley, canola, maize, wheat, and others in Australia. Wheat n=495.	1992-2007	Various varieties	Different sowing dates, soil types	N/A	N/A	R2=0.52 - 0.89, RMSD=0.19 - 0.80 t/ha	Model evaluation

(Chen et al., 2010b)*	APSIM 5.1	Luancheng, North China Plain (NCP), wheat-maize double cropping system	2000-2001	Gaoyou503	The soil at the Luancheng site is composed of loam, with the texture ranging from sandy loam in the top layers to light/medium loam between 40-80 cm depth, and light clay below 80 cm.	Irrigated (80-118 mm) and fertilised (urea 150 kg N/ha)	N/A	The model demonstrated an ability to account for over 90% of the variability in crop biomass and yield, as well as over 84% of the variability in soil water content.	Explore optimal water management strategies
(Chen et al., 2010a)*	APSIM 5.3	APAIM was calibrated and tested using field data from three experimental stations in the wheat-maize double cropping system in the North China Plain (NCP): Luancheng (1998-2001), Yucheng (1997-2002), Fengqiu (2004-2006))	1997-2002, 2004-2006 (calibration: Luancheng)	Gaoyou503, Zhixuan1, Keyu13, Zhengmai9023	Average annual rainfall=481-615 mm	Rainfed/Irrigated (0-420 mm at critical stages) and fertilised (No nitrogen stress)	Luancheng=350 mm, Yucheng=263 mm, and Fengqiu=204 mm	Although the model tended to overestimate maximum LAI, it did not necessarily result in overestimation of biomass as biomass production is not highly sensitive to LAI beyond a value of three. The RMSE for biomass and yield simulations were 1.40 t/ha and 0.83 t/ha, respectively.	Evaluate yield response to environmental factors
(Chen et al., 2010c)*	APSIM 5.3	North China Plain (NCP). Three stations: Luancheng (1998-2001), Yucheng (1997-2001, 2002-2005) and Fengqiu (2004-2006).	1997-2006	Zhixuan1	Average annual rainfall=481-615 mm	Rainfed/Irrigated and fertilised (lacked accurate irrigation and fertilisation records)	Luancheng=350 mm, Yucheng=263 mm, and Fengqiu=204 mm	No significant systematic over- or under-estimations was found when predicting LAI, biomass and yield. LAI-d index=0.85, biomass-d=0.92, yield-d=0.96. LAI-R2=0.61, biomass-R2=0.62, yield-R2=0.88.	Evaluate yield response to environmental factors
(Holzworth et al., 2014b) (assembled datasets)	N/A	Assembled datasets	N/A	Various varieties	Range of soil types, locations, sowing dates.	N/A	N/A	R2=0.93, RMSE=0.46 t/ha	Model development and validation
(Balwinder-Singh et al., 2011)*	APSIM 5.1	Punjab, India	2006-2008	PBW343	Clay loam soil. Growing season rainfall=88, 159 mm.	Nitrogen fertiliser applied to ensure no nitrogen stress. With and without mulch. Six irrigation scheduling treatments, including 75, 150, 225 mm.	N/A	The simulated and observed yields showed good consistency for the treatment that did not experience significant water deficit stress during the grain filling stage. Mulch: yield-RMSE=0.443 t/ha, NRMSE=12.4%, R2=0.91. Biomass-RMSE=0.3 t/ha, NRMSE=3.6%, R2=0.99. Non-mulch: yield-RMSE=0.55 t/ha, NRMSE=16.5%, R2=0.86. Biomass-RMSE=0.8 t/ha, NRMSE=10.8%, R2=0.92.	Model calibration and evaluation
(Lobell et al., 2012)	N/A	A dataset on wheat phenology and daily	2000-2009	Zippy	March and April have averaged 20-30 days of daily temperature exceeded 34°C (grain filling period of wheat).	Irrigated, average fertiliser rates = 145 kg N/ha.	N/A	The datasets showed that a 2°C increase in temperature in the region would lead to a reduction	Evaluate yield response to

		temperatures in the Indo-Gangetic Plains (IGP) in India was developed by researchers using satellite data.						of approximately nine days in the photosynthetically active part of the growing season. APSIM simulated less significant shortening of the growing season, especially for later sowing dates.	environmental factors
(Mohanty et al., 2012)	APSIM 6.0	Bhopal, India	2002-2006	Sujata	Annual rainfall: 2002: 763 mm; 2003: 1113 mm; 2004: 863 mm; 2005: 917 mm	Three N treatments: (1) cotrol: no nutrient added, (2) inorganic: 100 kg/ha N, 22 kg/ha P, 17 kg/ha K, (3) organic: 16 t/ha farmyard manure. Irrigated for 80 or 240 mm.	N/A	Soil water content: R^2=0.71-0.88, the performance was better for 0-15 cm soil layer than 60-90 cm depth. Overall EF = 0.26 – 0.58, RMSE = 0.036 – 0.044. The model provided realistic predictions of wheat grain yield and N uptake.	Model calibration and evaluation
(Zhang et al., 2012)	APSIM 6.1	North China Plain (NCP)	2009-2010	Nongdan211, Han6172, Yanzhan4110	Shangzhuang: AAR=104, 114 mm, AAT=8.0, 5.9°C. Quzhou: AAR=260, 128 mm, AAT=9.8, 7.7°C. Huangfanqu: AAR=307, 313 mm, AAT=10.4, 9.6°C.	N applied of 240 kg N/ha and irrigated of 120 mm. Delayed sowing dates.	N/A	Increased errors of simulated phenology and yield, with the average absolute RMSE of 2d, 3d and 3-4d in phenology, and the normalised RMSE of 7-12% (0.29 – 0.57 t/ha), 11-16% (0.65 – 1.09 t/ha) and 16-22% (0.56 – 0.97 t/ha) in yield.	Model evaluation
(Zhang et al., 2012)	APSIM 6.1	North China Plain (NCP)	2009-2010	Nongda211, Han6172, Yanzhan4110	Shangzhuang: AAR=104, 114 mm, AAT=8.0, 5.9°C. Quzhou: AAR=260, 128 mm, AAT=9.8, 7.7°C. Huangfanqu: AAR=307, 313 mm, AAT=10.4, 9.6°C.	N applied of 240 kg N/ha and irrigated of 120 mm. Decreased Planting density.	N/A	With average normalised RMSE of 9-12% (0.54 – 0.56 t/ha), 11-12% (0.72 – 0.90 t/ha) and 16-19% (0.77 – 1.26 t/ha). The simulation of green leaf biomass and LAI were relatively poor.	Model evaluation
(Hochman et al., 2013)	N/A	Wimmera, Victoria, Australia	Continuous 26 years	Yitpi	45 stations with 5 soil types	If the soil N in the root zone dropped below 50 kg N/ha, a nitrogen fertiliser application of 50 kg N/ha was carried out.	N/A	The estimated annual yield gaps are between 0.66 and 4.12 t/ha, with an average of 2.0 t/ha.	Quantify yield gaps
(Wang et al., 2013c)	APSIM 5.3	Six sites in North China Plain	1980-2009	Multiple local varieties	Average annual temperatures at six sites were 13.0, 12.9, 13.0, 14.1, 14.5 and 15.1°C, while annual rainfall totals were 515, 538, 535, 588, 550 and 995 mm, respectively.	The winter wheat received three to four flood irrigations, with a total of 250-300 mm of water applied.	N/A	The model made a slight overestimation of the days to jointing and flowering and a slight underestimation of the days to emergence and maturity dates.	Explore the phenological trends
(Zhang et al., 2013)*	APSIM 6.1	North China Plain (NCP)	2009-2010	Nongda211, Han6172, Yanzhan4110	mean minimum temperature of −8·8 - −3.8°C in January	The crops were irrigated and fertilised using basin irrigation in the 2008/09 and 2009/10 seasons. In the 2008/09 season, 60 mm of basin irrigation was applied before winter (GS20) and at the jointing (GS30) stage, while in the 2009/10 season, basin irrigation was applied at the jointing and flowering (GS60) stages. Nitrogen fertilisers were applied twice at the planting and	N/A	Underestimate yield of 0.4-0.6 t/ha, RMSE=0.5-0.9 t/ha	Assess the effects of climate change on crop yield.

						jointing stages in both seasons, at a rate of 120 kg N/ha each time.			
(Carberry et al., 2013) (assembled datasets)	Yield Prophet	849 commercial wheat crops in Australia	2004-2011, 849 commercial wheat crops - Yield Prophet	Various varieties	Average annual rainfall=182 mm	Rainfed (Australia)	N/A	APSIM was able to closely simulate commercial wheat yield.	Quantify yield gaps
(Brown et al., 2014) (assembled datasets)	N/A	28 cropping sites in Australia, USA, New Zealand, and NCP, China	N/A	Various varieties	Average anuual rainfall ranged from 227 to 839 mm.	N Fertiliser application ranged from 0 to 325 kg N/ha. Irrigated or rainfed.	N/A	Biomass-R2=0.93, grain yield-R2=0.92, biomass nitrogen-R2=0.87, grain nitrogen-R2=0.87	Model development and validation
(Bryan et al., 2014)*	APSIM 7.3	Northern NSW region, Western Australia, South Australia Victoria region	2006	N/A	N/A	N fertiliser applied of 225 kg N/ha.	N/A	The means of the simulated yields did not differ significantly from the means of the yields reported by the census. Census-reported yield=0.54 - 2.31 t/ha (median=1.26 t/ha), simulated yield=0.639 - 2.906 t/ha (median=1.553 t/ha).	Evaluate yield response to environmental factors
(Peake et al., 2014)*	APSIM 7.4	2008 (13 fields in Queensland and NSW); 2009 (3 fields in Central Queensland and 4 fields at South-East Queensland)	2008-2009	EGA Gregory, Kennedy, Ventura, Strezelecki, Baxter	Crops experienced lodging, water stress, high temperature, hail damage in 2008. In 2009, lodging, water stress, moderate to severe nitrogen stress were also observed.	2008 crops were fertilised. All crops were irrigated.	N/A	APSIM accounted for 72% of the non-lodged wheat yield variation and a RMSD=1.08 t/ha. While overestimated lodged crop yield and underestimated crop in the low-nitrogen field.	Quantify yield gaps and yield response to environmental factors
(He et al., 2014)	APSIM 7.4	Loess Plateau, China	2007-2008	Changwu89134	Average max temperature=15.2 - 17.1°C. Average min temperature=2.4 - 6.4°C. Average annual precipitation=320.8 - 479.8 mm.	Urea applied of 300 kg/ha. Rainfed.	N/A	Simulated LAI, AGB, extractable SW (the 100cm depth), ET agreed well with observed values. LAI-d index=0.91, R2=0.89. Biomass-d=0.96, R2=0.91. ESW-d=0.94, R2=0.78. ET-d=0.95, R2=0.85.	Evaluate yield response to environmental factors
(Wang et al., 2014)*	APSIM 7.5	Four sites from Northern China	1961-2060 (repeat the weather data, without climate change); 1989-2003 (from 2017_Gaydon_FCR)	N/A	Annual rainfall=262, 608, 630, 848	Irrigated and fertilised. Three scenarios. (1) Fertiliser; (2) stubble managed and fertilised; (3) control (rainfed and irrigated, without fertiliser and stubble)	N/A	Reasonably simulate 50% - 90% of the variation in the grain yield.	Evaluate yield response to environmental factors
(Zhao et al., 2014a)	APSIM 7.5	Wuqiao, North China Plain (NCP)	2009-2011	SJZ15	The average annual rainfall at the site was 550 mm (1961–2010). The average annual temperature is 12.9 oC.	Irrigation ranged from 75 mm to 375 mm. Nitrogen fertiliser applied from 0 to 330 kg N/ha. Weeds, insect pests, and diseases were effectively managed, and the crops did not experience any nutrient-related constraints.	PAWC= 452mm down to depth of 2m	Simulated more biomass and grain than observed. The adjustment of the new N concentrations improved the simulation of wheat biomass and N uptake, especially under low N input.	Evaluate the threshold nitrogen concentration used in the model
(Zhao et al., 2014b)*	APSIM 7.5	Eight field experiments at Wuqiao, North China Plain (NCP)	2003-2011	Calibration: Exp 4 (2005) and Exp 8 (N330), SJZ8	The region experiences a summer monsoon and has an average annual temperature of 12.9 ˚C. The annual rainfall from 1961 to 2010 is 550 mm.	Winter wheat (mid-October to early June) and summer maize rotation. Irrigated (3 × 75 mm). 0, 123, 158, 192, 261, 330 kg N/ha	N/A	The APSIM model had the capability to simulate more than 85% of the variability in aboveground biomass, RMSE =	Evaluate the root modelling

				and SJZ15. Other experiments data in Exp 1-8 used for validation, SJZ8, SJZ15, ND09-1, JM22, YN15, W62036.	During the months of July to September, which are considered the summer season, 64% of the annual rainfall occurred. Calcaric Fluvisol with a sandy clay loam texture.	nitrogen fertiliser applied. No water, nutrients, weeds and pest stresses.		1.10, and over 80% of the variation in final yield, RMSE = 0.73. The adjustments made to root parameters had little effect on the model's ability to simulate wheat shoot biomass and grain yield in the majority of experiments.	
(Xiao and Tao, 2014)*	N/A	Northern China	2005-2009	Fengkang7, Jingdong8, Hengshui741, Shimai12, Boai7422, Zhengmai9023, Fu63, Lumai23	Average annual temperature from 12.8 to 15.7 for all four locations.	Irrigated (4 times * 50 mm) and fertilised (TS-Fengkang7, NG-Hengshui741, ZM-Boai7422, HM-Fu63: 90 kg N/ha used as base fertiliser and 60 kg N/ha added at jointing stage; TS-Jingdong8, NG-Shimai12, Zhengmai9023, Lumai23: 120 kg N/ha used as base fertiliser and 75 kg N/ha added at jointing stage)	N/A	R^2=0.85, The average residual between modelled and observed yield was smaller than 0.5 t/ha	Evaluate yield response to environmental factors
(Li et al., 2014)	N/A	Sixteen sites in NCP, China	1981-2010 (The model was calibrated and validated using 16 sites). Calibration data and validation data were separated.	Jinfeng1, Jiamai26, Gaoyou503, Bainong3217, Yumai18, Zhengmai9023, Jinan13, Lumai15, Lumai21	N/A	Local traditional practices: irrigation was not conducted every year, but fertiliser was used several times every year.	N/A	RMSE=0.3205-0.8291 t/ha, NRMSE(%)=5.7-14.1, D-value=0.90-0.97, R2=0.71-0.89	Identify the change pattern of yields
(Soltani and Sinclair, 2015) (assembled datasets)	APSIM 7.X	35 experimental datasets at Grogan, Iran	2005-2008	Several local varieties	Silty clay. Average rainfall during the growing season (December - June)=340mm, average maximum temperature during pre-anthesis=17.2˚C, average minimum temperature=7.3˚C.	Nitrogen fertiliser was applied from 0 to 122 kg N/ha. Part of crops were irrigated. Multiple sowing dates (8-12 sowing dates). Multiple sowing densities (6-7 densities ranged from 50-800 plant/m2).	N/A	LAI at anthesis: RMSE=0.74, r=0.53, CV=18.3; dry mass at anthesis: RMSE=149.69 g/m2, r=0.51, CV=22.34; dry mass at maturity: RMSE=244.30 g/m2, r=0.72, CV=25.7; yield: RMSE=61.82 g/m2, r=0.81, CV=14.57	Model intercomparison and evaluation
(Sun et al., 2015)	APSIM 7.0	Two experiments at Luancheng station, NCP, China (used for calibration and validation)	2006-2012 (first experiment), 1984-2012 (second experiment)	Jimai7, Jimai36, Jimai733	The water loss due to evaporation and plant transpiration during the crop growth period ranges from 400-450 mm. The soil type is loam, with an average water holding capacity of 38% and a wilting point of 13%.	Nitrogen application rates were 100-125 kg N/ha (1984-1990), 220 kg N/ha (in the 1990s), and 250 kg N/ha (after 2000). Phosphorus application rates were 100 kg/ha (in the 1980s), 150 kg/ha in the 1990s, and 180 kg/ha recently. In the first experiment, four irrigation treatments were tested: full irrigation (irrigated to avoid water stress), critical stage irrigation (one additional irrigation at jointing stage),	N/A	APSIM showed an ability to explain over 83% of the variability in the measured grain yields of wheat across the four irrigation treatments tested in the first experiment. The RMSE values for winter wheat yields were 0.330, 0.567, 0.923, and 0.762 t/ha for the FI, CI, MI, and RF treatments, respectively. In the second experiment, the model simulated winter wheat grain yields with an RMSE of 0.590 t/ha. This experiment	Evaluate yield response to environmental factors

						minimum irrigation (irrigated before sowing if the top 50cm soil layer had less than 70% field capacity), and rain-fed. In the second experiment, irrigation was managed similarly to the full irrigation scenario.		involved managing water supply similarly to the full irrigation treatment from the first experiment.	
(Acuña et al., 2015)	APSIM 7.1	Cambridge, Campbell Town, Epping Forest, Hagley, Forthside, Longford, Sassafras, Symmons Plains, Westbury, Tasmania, Australia	1980s, 2000s	Brennan, Isis, Machellar, Revenue, Tennant (winter wheat) and Kellalac (spring wheat)	Average annual rainfall=499-965 mm, average MaxT=16.1-17.6˚C, average MinT=4.6-8.2˚C.	Nitrogen fertiliser applications: 24 - 245 kg N/ha.	N/A	R2=0.84, RMSE=1 t/ha.	Explore the potential management strategies to close the yield gap
(Deihimfard et al., 2015)*	APSIM 7.2	North-eastern Iran	2009-2011	Late maturing: Sionz, Gascozhen; early maturing: Chamran	Growing season rainfall=137-298 mm, average MaxT=9.7-14˚C, average MinT=6.9-10.1˚C, average mean temperature=8.8-12.3˚C.	N applied at four levels: 0, 55, 110, 172 kg N/ha. All treatments involved splitting the nitrogen fertiliser (urea) in half, with 50% being applied at the time of planting and the other 50% being applied at anthesis. Irrigated 5 to 9 times with 50 mm each time.	N/A	n=15, R2=0.83, RMSE=0.71 t/ha	Quantify yield gaps
(O'Leary et al., 2015)	APSIM 7.4	A Free-Air CO2 Enrichment (FACE) experiment was conducted in Horsham, Australia.	2007-2009	Yitpi	Under elevated CO2 conditions	Two water regimes (rainfed and irrigation), two nitrogen fertilisation regimes (0 and 53-138 kg/ha) and two sowing dates (normal and late) for both daytime ambient (365 umol mol-1) and elevated (550 umol mol-1) CO_2 atmospheric conditions.	N/A	APSIM tended to over-simulate LAI at DC65 (R2=0.24, RMSE=0.70 m2/m2), biomass at DC31 (R2=0, RMSE=1.592 t/ha), biomass at DC65 (R2=0.56, RMSE=1.542 t/ha) and yield (R2=0.20, RMSE=1.294 t/ha).	Assess the effects of climate change on crop yield.
(Innes et al., 2015)	APSIM 7.5	Datasets Statistical Division 150 (SD150), six shires were selected: Carrathool, Coolamon. Narrandera, Wagga Wagga, Lockhart, and Temora. (ABARE)	1982-2008	Hartog	Growing season rainfall=250 - 400mm, recurrent drought, high temperature and low rainfall	Fertilised with 150 kg/ha urea (equivalent to 69 kg N/ha nitrogen).	N/A	Yield variation (%): R2=0.69, RMSE=18.9%	Evaluate model under high-temperature episodes
(Zhao et al., 2015)*	APSIM 7.5	Wuqiao, North China Plain (NCP)	2009-2010	SJZ8, SJZ15	The region experiences a summer monsoon and has an average annual temperature of 12.9 ˚C. The annual rainfall from 1961 to 2010 is 550 mm. During the months of July to September, which are considered the	Winter wheat (mid-October to early June) and summer maize rotation. 1st experiment: 3 × 75 mm irrigations. 0, 123, 192, 261, 330 kg N/ha N applied. 2nd experiment: 1/2/3/5 × 75 mm	N/A	RMSE=0.33 t/ha, R2=0.97. The simulated grain yield remained similar with modified parameters.	Analyse the resource use efficiency

					summer season, 64% of the annual rainfall occurred. Calcaric Fluvisol with a sandy clay loam texture.	irrigations. 158 kg N/ha N applied.			
(Ahmed et al., 2016)	N/A	Islamabad, Pakistan	2009-2011	Tatara, NARC-2009, Sehar-2006, SKD-1, F-Sarhad	The region experiences abundant rainfall with an average annual precipitation exceeding 1000mm, while the average annual temperature is 21.3°C. The annual potential evapotranspiration in the area is estimated to be approximately 1600 mm.	N/A	N/A	Phenology, maximum LAI, accumulated biomass and yield, with RMSE within range 2.03 – 5.09 day, 0.14 – 0.32 m2/m2, 0.15 – 0.40 t/ha, 0.12 – 0.31 t/ha, and R2 larger than 0.8, 0.83, 0.92 and 0.82 respectively.	Model calibration and evaluation
(Van Oort et al., 2016)	APSIM 7.4	Water shortage area in NCP, China	2006 and 2007 (two-year data)	Shimai12 (winter wheat)	Continental monsoon: cold and dry winters. Average annual rainfall=533 mm, only 2% occurs in winter.	Three levels of irrigation: (1) zero irrigation during wheat growing season, (2) 75 mm water at stem extension (75 mm total) and (3) 75 mm at stem extension plus 75 mm water at booting (150 mm total). Enough irrigation was applied to before sowing to ensure the emergence of wheat. Enough N was applied to ensure no nutrient limitation.	N/A	The model was able to account for 95% of the variation in biomass for both wheat and maize, 90% of the variation in LAI, 84% of the variation in soil water content throughout the year, and 82% of the variation in crop grain yields under various irrigation practices. The model's RMSE for biomass, LAI, available soil water content, and grain yield was 0.88 t/ha, 0.72, 27 mm, and 0.64 t/ha, respectively.	Construct groundwater neutral cropping systems
(Li et al., 2016)	APSIM 7.5	Huantai site in NCP, China	2008-2010	Jimai22	The region experienced a temperate monsoon climate during the period of 1990-2010, with an average annual temperature of 13.9°C and average annual rainfall of 547 mm.	Four N treatments were applied: no N (CK), farmer conventional N (234 kg/ha urea applied), reduced N (144 kg/ha urea applied) and reduced N with manure (54 kg/ha chicken manure + 90 kg/ha urea applied).	N/A	The final biomass and grain yield variations simulated by APSIM matched 94% and 88% with the truth, respectively, and the corresponding RMSE values were 1.28 t/ha and 0.82 t/ha.	Explore possibility of resources usage reduction while maintaining the yield
(Mielenz et al., 2016)*	APSIM 7.5	Kingaroy and Kingsthorpe, both situated in South Eastern Queensland, Australia	2009 (Kingsthorpe), 2011 (Kingaroy)	Hartog (Kingaroy), Lang (Kingsthorpe)	Humid subtropical. Average annual temperature of 18.2 °C at both sites. Annual average precipitations are 776 mm and 630 mm.	**Kingaroy**: In a sprinkler-irrigated experiment, four fertilisation treatments were examined, including a control group where no N fertiliser was applied, a group with the conventional N fertiliser rate adjusted based on the estimated residual soil N (urea applied at a rate of 20 kg/ha), a group with the conventional fertiliser rate (urea applied at a rate of 80 kg/ha), and a group with the conventional fertiliser rate using urea coated with DMPP nitrification inhibitor (urea applied at a rate of 80 kg/ha, with DMPP urea only applied at top dressing 60 kg/ha). **Kingsthorpe**: fertilised, three irrigation treatments and three replications. High irrigation	N/A	Overall yield prediction (four crop types): R^2=0.92 Three cases were within the range of the measured values' standard deviation.	Identify strategies for mitigating crop N2O emissions

						(when 50% of the PAWC was depleted), medium irrigation (when 60% of the PAWC was depleted), low irrigation (when 85% of the PAWC was depleted)			
(Zeleke and Nendel, 2016)*	APSIM 7.6	Wagga Wagga, NSW Australia	2013-2014	EGA Gregory, Livingston	Sandy clay loam Red Kandosol. For 2013 and 2014: number of frosts=40 days, 48 days; AR=263 mm, 326 mm.	irrigation (mm)=247 (in 2013), 229 (in 2014).	N/A	R2=0.92, RMSE=0.65 t/ha	Evaluate yield response to environmental factors
(O'Leary et al., 2016)*	APSIM 7.6	Eastern Australia (Wagga Wagga in New South Wales, Warwick in Queensland)	1979-2003 (Wagga Wagga), 1968-2012 (Warwick)	N/A	In some seasons, crops suffered from diseases like root-lesion nematodes and crown rot.	Different stubble, tillage and nitrogen application managements applied.	N/A	At both Wagga Wagga and Warwick the simulated yield are considered typical with RMSE of 1.08 t/ha and 1.39 t/ha.	Evaluate yield response to environmental factors
(Liu et al., 2016a)*	APSIM 7.7	Environment-controlled chamber experiments were conducted at Nanjing in growing season 2010-2013 and at Rugao in growing season 2013-2014.	2010-2014 (four-year with two cultivars)	Yangmai16, Xumai30	Environment-controlled phytotron experimental datasets under heat stress at anthesis and grain filling stages. A plant density of 10 plants per pot was maintained, with a pot diameter of 0.28m.	N and irrigation were applied to ensure no water or nitrogen stress.	N/A	When heat stress occurred at anthesis, APSIM overestimated grain filling durations and the effects of heat stress on total aboveground biomass at maturity. On the other hand, it underestimated grain size with heat stress at anthesis but overpredicted the effects of heat stress on LAI. The model underestimated the observed decline in grain filling rates with heat stress. The simulated yield by APSIM showed an R^2 of 0.73 with the observed yield when heat occurred at anthesis, and an R^2 of 0.46 with the observed yield when heat occurred during grain filling.	Evaluate the model ability of simulating heat impacts
(Araya et al., 2017)	APSIM 7.4	Ethiopia	2011-2012	HAR-2501	N/A	Two levels of nitrogen fertiliser applied: (1) 0, (2) 64 kg N/ha. Rainfed.	N/A	Simulated phenology R2 over 0.8, 6.0 day, yield R2=0.63, 0.14t/ha	Assess the effects of climate change on crop yield.
(Gaydon et al., 2017)* (assembled datasets)	N/A	12 Asian countries, total of 43 experimental datasets, 966 crops (326 wheat)	Various years	Various varieties	Different weather conditions (temperature, rainfall, CO2 level).	Different sowing dates, dates of transplanting, varieties, CO2, nitrogen and surface residue treatments, rainfed or irrigation conditions	N/A	R^2=0.79, RMSE=0.845 t/ha, standard deviation=1.794 t/ha (n=326). The validation dataset showed a strong correlation (R^2 > 0.99) and low error in simulating phenology. However, in India's high-temperature conditions, APSIM overestimated the length of the crop growth period. In the North China Plain, simulations of winter wheat growth indicated that APSIM significantly underestimated the leaf area index (LAI), biomass, and yield of the crop. The incorrect temperature response of	Model evaluation

								physiological processes in the wheat model was the main reason for the underestimation.	
(Zhao et al., 2017)*	N/A	There are ten agricultural meteorological experimental stations in Inner Mongolia, China that are representative of the region.	2011-2014	Spring wheat	The average annual temperature was between -1˚C and 10˚C. The average annual precipitation is between 50 mm and 450 mm.	N/A	N/A	The yield's RMSE varied between 28.95 kg/ha and 208.35 kg/ha, while the NRMSE of the yield was controlled within 10%, ranging from 0.92% to 6.4%. The D index ranged from 0.85 to 0.95, and the MAE value ranged from 41.1 to 410.85. Simulated phenology during the emergence and maturity stages had RMSEs of 1.22d-5.49d and 1.13d-3.00d, respectively, with smaller errors. The NRMSEs were also controlled within 10%, ranging from 1.06% to 5.09% and 0.65% to 1.45%. The D indices were close to 1, with fluctuations of 0.49–0.99 and 0.69–1.	Assess the effects of climate change on crop yield.
(Holzworth et al., 2018)	APSIM Next Generation	Various locations	Wheat model: 650 simulation years	Various varieties	N/A	N/A	N/A	Included in the model files.	Model development and validation
(Hussain et al., 2018)	APSIM 7.8	Two climate regions: Faisalabad (semi-arid), Layyah (arid) in Punjab-Pakistan	2013-2015	Lasani-2008, Punjab-2011, Galaxy-2013	Growing season temperature was btween -0.1 and 43˚C.	The study involved three cultivars and eleven planting dates, with intervals of 15-16 days between October 16th and March 16th. The crop received irrigation without water stress, and nitrogen, phosphorus, and potassium were applied at rates of 120, 85, and 60 kg/ha.	N/A	At Faisalabad, APSIM had a large NRMSE of 65.5% for yield estimation. In Layyah during 2013-14 and 2014-15, it over-simulated the grain yield for planting dates after December 1st. Furthermore, with the exception of the October 15th planting, it highly over-simulated the grain yield for all planting dates at Layyah during 2014-15.	Model intercomparison and evaluation
(Phelan et al., 2018)*	APSIM 7.8	Cressy, Symmons Plains, Epping Forest, Burnie, Tasmania, Australia	2005-2010	Mackellar_Tas, Revenue, Tennant	Cressy, Epping forest, Symmons plains: average annual rainfall=628 mm, average annual maximum temperature=17.2, average annual minimum temperature=5.1. Soil: fine sandy loam (PAWC=217 mm), clay loam (96 mm), loam (PAWC=221 mm).	Rainfed and fertilised (A rate of 25 kg N/ha was generally used to apply nitrogen fertiliser during sowing, along with an additional top-dressed application of 50 kg N/ha in early spring.).	PAWC= 96-221 mm	R2=0.83, MPE (mean prediction error)=11%, MEF (modelling efficiency)=0.82, v (ratio of variance in measured to simulated values)=1.09.	Produce data for further incorporation into another model
(Brown et al., 2018) (assembled datasets)	APSIM 7.9	Australia, Belgium, China, Ethiopia, Iran, New Zealand, Turkey, USA. In this paper, a collection of criteria that a	N/A	Various varieties	48 experiments, 655 treatments, different planting years.	Different time of sowing, N fertiliser, irrigation, residue additions, population, cultivar, tillage.	N/A	All variables: $R^2 \geq 0.84$ and NSE ≥ 0.81. Yield: $R^2 = 0.84$, RMSE=1.005 t/ha and NSE = 0.81. Grain protein: $R^2 = 0.42$ and a NSE of 0.36. Flag leaf: R^2=0.98. Anthesis: R^2=0.98.	Model development and validation

		contemporary crop model ought to satisfy is presented, along with a discussion on the methods and software employed by the APSIM development community to construct and uphold models that fulfill these criteria.							
(Bahri et al., 2019)	N/A	Nabeul, Cherfech, Hendi Zitoun, Boulifa, Oued Mliz, and Mornag, Tunisia	1989-1992, 1996-1998, 1999-2000, 2003-2006	Karim	Nabeul: growing season rainfall=232 mm, soil: sandy; Cherfech: GSR=345, 516 mm, soil: silty clay loam; Hendi Zitoun: GSR=299, 139, 105 mm, soil: silty clay; Boulifa: GSR=424, 499, 520 mm, soil: silt-clay sandy; Oued Mliz: GSR=240 mm, soil: clay loam; Mornag: GSR=125 mm, soil: clay loam.	Nabeul: irrigation=228 mm, N fertiliser=132 kg N/ha; Cherfech: irrigation=255, 163 mm, N fertiliser=198, 132 kg N/ha; Hendi Zitoun: irrigation=290, 300, 250 mm, N fertiliser=60, 150 kg N/ha; Boulifa: irrigation=0, N fertiliser=76, 150 kg N/ha; Oued Mliz: irrigation=100 mm, N fertiliser=150 kg N/ha; Mornag: irrigation=252 mm, N fertiliser=150 kg N/ha.	N/A	RMSE=1.647 t/ha, agreement index=0.83	Evaluate yield response to environmental factors
(Bai et al., 2020)	APSIM 7.7	North China Plain (NCP), China	1981-2015	Jimai22, Jining142, Zhengzhou761	Growing season rainfall=100 - 300 mm	On-farm: N fertiliser were applied at sowing and jointing. Three to four times irrigation. High-yield: Four irrigation scenarios were tested, which included (1) no irrigation, (2) one irrigation with an interval of 5 mm for 0-140 mm, (3) two irrigations with an interval of 5 mm for each 0-140 mm, and (4) three irrigations with an interval of 5 mm for each 0-140 mm. Two nitrogen fertilization scenarios were also assessed, namely (1) a single N application of 0-300 kg N/ha at sowing stage with an interval of 5 kg N/ha, and (2) split N application (sowing and jointing stages) of 0-300 kg N/ha with an interval of 5 kg N/ha.	N/A	In 24 cities of NCP from 2007 to 2015, the simulated potential yields and observed high yield records had an RMSE of 1.15 t/ha and an NRMSE of 12%. In 36 cities of NCP from 2009 to 2014, the simulated on-farm wheat yield and surveyed yield had an RMSE of 0.576 t/ha and an NRMSE of 8.8%.	Quantify yield gaps and seek for options to increase yield
(Araya et al., 2020)*	APSIM 7.7	Kulumsa, Oromia; Hagereselam, Tigray region; Ilala; Wukro,	2006-2008, 2012 (KARC), 2014 (HS),	early, medium and late maturing cultivars	For Site 1, the mean annual rainfall and cropping season rainfall (June - November) were approximately 820 mm and 503 mm, respectively. The	To evaluate the potential impacts of climate change, rainfed conditions, optimal planting dates, and density as determined	N/A	Yield-NRMSE (normalised RMSE) =22.8%, days of flowering-RMSE=4.3%, days of maturity-NRMSE=8.3%.	Assess the effects of climate change on crop yield.

		Tigray region, Ethiopia	2014 (HS, IL, WU)		site's mean annual maximum and minimum temperature were 23.1˚C and 10˚C, and the soil type was black vertisol. Site 2 had a mean annual rainfall and cropping season rainfall of 669 mm and 542 mm, respectively. The mean annual maximum and minimum temperatures were 22.5˚C and 11.1˚C. At Site 3, the soil type was black vertisol, and the mean annual rainfall and cropping season rainfall were 583 mm and 491 mm, respectively. The mean annual maximum and minimum temperatures were 23.6˚C and 12.1˚C. Site 4 had clay soils, with mean annual rainfall and cropping season rainfall of 565.6 mm and 335.4 mm, respectively. The mean annual maximum and minimum temperatures were 28.0˚C and 11.1˚C.	by the model were used, along with two different fertiliser rates. The regional agronomists recommended one rate at 64 kg N/ha, and the other at 128 kg N/ha.			
(Yan et al., 2020)*	APSIM 7.9	Luancheng Agro-Eco-Experimental station, NCP, China.	2007-2016 (validation 2011-2016)	KN199	Loamy soil. Growing season rainfall=50-230mm. Average annual temperature=12.7˚C.	Three irrigation treatments: (1) full irrigation (225 – 375 mm), (2) critical stage irrigation (75 mm at jointing stage in addition to minimum irrigation), (3) minimum irrigation (keep the top 50 cm soil layer above 75% of field capacity).	N/A	The model was capable of elucidating around 90% of the winter wheat's phenology, biomass accumulation, grain yield, and seasonal evapotranspiration. The RMSE values for winter wheat yield were 0.263 t/ha, 0.598 t/ha, and 0.453 t/ha for the MI, CI, and FI treatments, respectively.	Explore possibility of resources usage reduction while maintaining the yield
(Fletcher et al., 2020)*	APSIM 7.8	Western Australia. ABARES obersed datasets at the scale of the statistical area level 2	2010, 2015	N/A	Rainfed (water limited condition)	N/A	N/A	RMSE=0.77 t/ha, R2=0.69	The climate change impacts on the distribution of Australian wheat belt

Appendix C Supplementary material for Chapter 3

Table C. 1. The selected weather scenarios

	Mean Tmax (°C)	Mean Tmin (°C)	Precipitation (mm)	Growing period precipitation (mm)
Wet year (1964)	20.5	7.4	546.2	453.1
Normal year (1989)	21.4	8.7	395.2	311.8
Dry year (2015)	22.7	8.6	253.4	140.2

Table C. 2. The historic weather data of Nhill, Victoria, Australia (Station 078040 for precipitation and Station 078031 for temperatures, Tmax: maximum temperature, Tmin: minimum temperature)

	Mean Tmax (°C)	Mean Tmin (°C)	Precipitation (mm)
lowest	20.2	4.0	163.5
10^{th} %ile	20.8	7.1	260.8
mean	21.6	8.0	400.8
median	21.6	8.1	399.8
90^{th} %ile	22.5	8.8	526.7
highest	24.6	9.5	738.8

Table C. 3. The selected soil textures and the proportion of sand, silt, and clay sized particles

	Sandy soil (layer 1/layer 2 - 6)	Loamy soil (layer 1/layer 2 - 6)	Clayey soil (layer 1/layer 2 - 6)
Clay %	5/15	25/35	40/70
Silt %	15/10	25/25	30/15
Sand %	80/75	50/40	30/15
Soil textures	Loamy sand/Sandy loam	Loam/Clay loam	Silty clay/Clay

Table C. 4. Mean and standard deviation values of the soil textures used for the soil layers of the three soil types used in this study

Soil layer texture	Porosity (PO) (m^3/m^3)		Drained upper limit (DUL) (m^3/m^3)		Lower limit of 15 bar (LL15) (m^3/m^3)	
	Mean	Standard deviation	Mean	Standard deviation	Mean	Standard deviation
Loamy sand	0.437	0.069	0.160	0.053	0.044	0.023
Sandy loam	0.453	0.102	0.214	0.055	0.099	0.020
Loam	0.463	0.088	0.233	0.047	0.118	0.030
Clay loam	0.464	0.055	0.263	0.048	0.150	0.027
Silty clay	0.470	0.052	0.328	0.039	0.211	0.029
Clay	0.475	0.048	0.393	0.030	0.272	0.030

Table C. 5. The first order and total index variability with changing sample size for all parameters

	Standard deviation for indices when the sample size is between 30 and 3000		Standard deviation for indices when the sample size is between 30 and 6000		Standard deviation for indices when the sample size is between 30 and 9000		Standard deviation for indices when the sample size is between 30 and 10000	
	S_i	S_{Ti}	S_i	S_{Ti}	S_i	S_{Ti}	S_i	S_{Ti}
Precipitation	0.046	0.087	0.040	0.076	0.036	0.068	0.035	0.066
Tmax	0.044	0.088	0.038	0.075	0.034	0.067	0.032	0.065
Tmin	0.023	0.044	0.019	0.038	0.017	0.034	0.017	0.033
Fertilisation Amount	0.035	0.015	0.031	0.013	0.028	0.012	0.027	0.011
Initial Nitrogen Content	0.063	0.048	0.054	0.041	0.048	0.037	0.047	0.036
Soil Parameters	0.055	0.145	0.048	0.125	0.043	0.112	0.041	0.108

Table C. 6. First order and total sensitivity index with bootstrap confidence intervals for Scenario Norm _Lm_100

Scenario Norm _Lm_100: normal weather, nitrogen fertilisation 100 kg N/ha, loamy soil								
	S_i	Bootstrap average of S_i	95% CI of S_i		S_{Ti}	Bootstrap average of S_{Ti}	95% CI of S_{Ti}	
Precipitation	0.2813	0.2814	0.2811	0.2817	0.4211	0.4211	0.4205	0.4217
Tmax	0.0648	0.0647	0.0646	0.0648	0.1625	0.1626	0.1622	0.1631
Tmin	0.0279	0.0279	0.0278	0.0280	0.1045	0.1045	0.1041	0.1049
Fertilisation amount	0.0378	0.0378	0.0377	0.0379	0.0543	0.0543	0.0542	0.0544

Initial nitrogen content	0.1949	0.1951	0.1949	0.1953	0.2237	0.2238	0.2236	0.2240
Soil parameters	0.2305	0.2307	0.2304	0.2310	0.4080	0.4082	0.4074	0.4091

Table C. 7. First order and total indices of uncertain factors at 50 kg N/ha nitrogen fertilisation amount

Nitrogen fertilisation 50 kg N/ha										
		Sandy soil			Loamy soil			Clayey soil		
		S_i value	S_{Ti} value	(S_{Ti}-S_i)	S_i value	S_{Ti} value	(S_{Ti}-S_i)	S_i value	S_{Ti} value	(S_{Ti}-S_i)
Wet year	Precipitation	0.0086	0.2047	0.1961	0.1011	0.5303	0.4292	0.0064	0.0120	0.0056
	Tmax	0.0037	0.0269	0.0232	0.0082	0.1089	0.1007	0.0061	0.0153	0.0092
	Tmin	0.0024	0.0154	0.0130	0.0012	0.0760	0.0748	0.0037	0.0110	0.0073
	Fertilisation amount	0.1581	0.1589	0.0008	0.0745	0.0773	0.0028	0.1974	0.2019	0.0045
	Initial nitrogen content	0.5511	0.5660	0.0149	0.2843	0.2913	0.0070	0.7525	0.7534	0.0009
	Soil parameters	0.0724	0.2612	0.1888	0.1171	0.5734	0.4563	0.0214	0.0307	0.0093
	SUM	0.7963	1.2331	-	0.5864	1.6572	-	0.9875	1.0243	-
Normal year	Precipitation	0.1682	0.2468	0.0786	0.0804	0.1658	0.0854	0.0049	0.0157	0.0108
	Tmax	0.0290	0.0846	0.0556	0.0152	0.0734	0.0582	0.0032	0.0130	0.0098
	Tmin	0.0162	0.0601	0.0439	0.0205	0.0568	0.0363	0.0035	0.0094	0.0059
	Fertilisation amount	0.0801	0.1003	0.0202	0.1218	0.1424	0.0206	0.1744	0.1764	0.0020
	Initial nitrogen content	0.3652	0.4044	0.0392	0.5555	0.6095	0.0540	0.7861	0.7893	0.0032
	Soil parameters	0.2339	0.3285	0.0946	0.1188	0.2149	0.0961	0.0250	0.0315	0.0065
	SUM	0.8926	1.2247	-	0.9122	1.2628	-	0.9971	1.0353	-
	Precipitation	0.2104	0.3519	0.1415	0.1394	0.3254	0.1860	0.0876	0.1039	0.0163

Dry year	Tmax	0.0704	0.1157	0.0453	0.0419	0.1128	0.0709	0.0347	0.0567	0.0220
	Tmin	0.0215	0.0569	0.0354	0.0074	0.0683	0.0609	0.0176	0.0325	0.0149
	Fertilisation amount	0.0125	0.0300	0.0175	0.0367	0.0767	0.0400	0.1337	0.1503	0.0166
	Initial nitrogen content	0.0790	0.1111	0.0321	0.2169	0.2813	0.0644	0.6179	0.6539	0.0360
	Soil parameters	0.4024	0.5568	0.1544	0.2776	0.4860	0.2084	0.0685	0.0843	0.0158
	SUM	0.7962	1.2224	-	0.7199	1.3505	-	0.9600	1.0816	-

Table C. 8. First order and total indices of uncertain factors at 100 kg N/ha nitrogen fertilisation amount

Nitrogen fertilisation 100 kg N/ha										
		Sandy soil			Loamy soil			Clayey soil		
		S_i value	S_{Ti} value	(S_{Ti}-S_i)	S_i value	S_{Ti} value	(S_{Ti}-S_i)	S_i value	S_{Ti} value	(S_{Ti}-S_i)
Wet year	Precipitation	0.0446	0.4297	0.3851	0.1395	0.6703	0.5308	0.0049	0.0121	0.0072
	Tmax	0.0046	0.0539	0.0493	0.0047	0.1276	0.1229	0.0080	0.0216	0.0136
	Tmin	0.0032	0.0306	0.0274	0.0001	0.0909	0.0908	0.0044	0.0181	0.0137
	Fertilisation amount	0.0879	0.0994	0.0115	0.0330	0.0379	0.0049	0.1868	0.1911	0.0043
	Initial nitrogen content	0.2850	0.3309	0.0459	0.1269	0.1392	0.0123	0.7309	0.7363	0.0054
	Soil parameters	0.1558	0.5533	0.3975	0.1633	0.7275	0.5642	0.0387	0.0489	0.0102

	SUM	0.5811	1.4978	-	0.4675	1.7934	-	0.9737	1.0281	-
Normal year	Precipitation	0.3391	0.4421	0.1030	0.2813	0.4211	0.1398	0.0785	0.1203	0.0418
	Tmax	0.0718	0.1425	0.0707	0.0648	0.1625	0.0977	0.0278	0.0657	0.0379
	Tmin	0.0179	0.0770	0.0591	0.0279	0.1045	0.0766	0.0084	0.0382	0.0298
	Fertilisation amount	0.0209	0.0311	0.0102	0.0378	0.0543	0.0165	0.1448	0.1734	0.0286
	Initial nitrogen content	0.0997	0.1203	0.0206	0.1949	0.2237	0.0288	0.6136	0.6820	0.0684
	Soil parameters	0.3297	0.4561	0.1264	0.2305	0.4080	0.1775	0.0293	0.0509	0.0216
	SUM	0.8791	1.2691	-	0.8372	1.3741	-	0.9024	1.1305	-
Dry year	Precipitation	0.2582	0.4098	0.1516	0.2202	0.4531	0.2329	0.3285	0.3467	0.0182
	Tmax	0.0724	0.1175	0.0451	0.0742	0.1558	0.0816	0.1674	0.2296	0.0622
	Tmin	0.0276	0.0655	0.0379	0.0209	0.0982	0.0773	0.0686	0.1279	0.0593
	Fertilisation amount	0.0078	0.0094	0.0016	0.0100	0.0110	0.0010	0.0403	0.0500	0.0097
	Initial nitrogen content	0.0291	0.0387	0.0096	0.0382	0.0463	0.0081	0.1367	0.1658	0.0291
	Soil parameters	0.4093	0.5700	0.1607	0.3405	0.5921	0.2516	0.1723	0.1955	0.0232
	SUM	0.8044	1.2109	-	0.7040	1.3565	-	0.9138	1.1155	-

Table C. 9. The ensemble yield mean and standard deviation (kg/ha)

	Sandy soil		Loamy soil		Clayey soil	
	N Fert 50	N Fert 100	N Fert 50	N Fert 100	N Fert 50	N Fert 100
Wet year	Mean=3349.76 Std=586.16	Mean=4517.19 Std=532.56	Mean=3206.18 Std=815.92	Mean=4404.24 Std=973.49	Mean=3311.64 Std=497.68	Mean=4522.99 Std=457.16
Normal year	Mean=3087.74 Std=418.89	Mean=3571.28 Std=379.91	Mean=3194.19 Std=487.58	Mean=3872.09 Std=399.31	Mean=3300.16 Std=582.69	Mean=4568.14 Std=429.20
Dry year	Mean=1873.97 Std=188.32	Mean=1982.29 Std=187.61	Mean=2064.52 Std=233.65	Mean=2222.48 Std=221.05	Mean=2596.89 Std=290.56	Mean=3002.13 Std=206.75

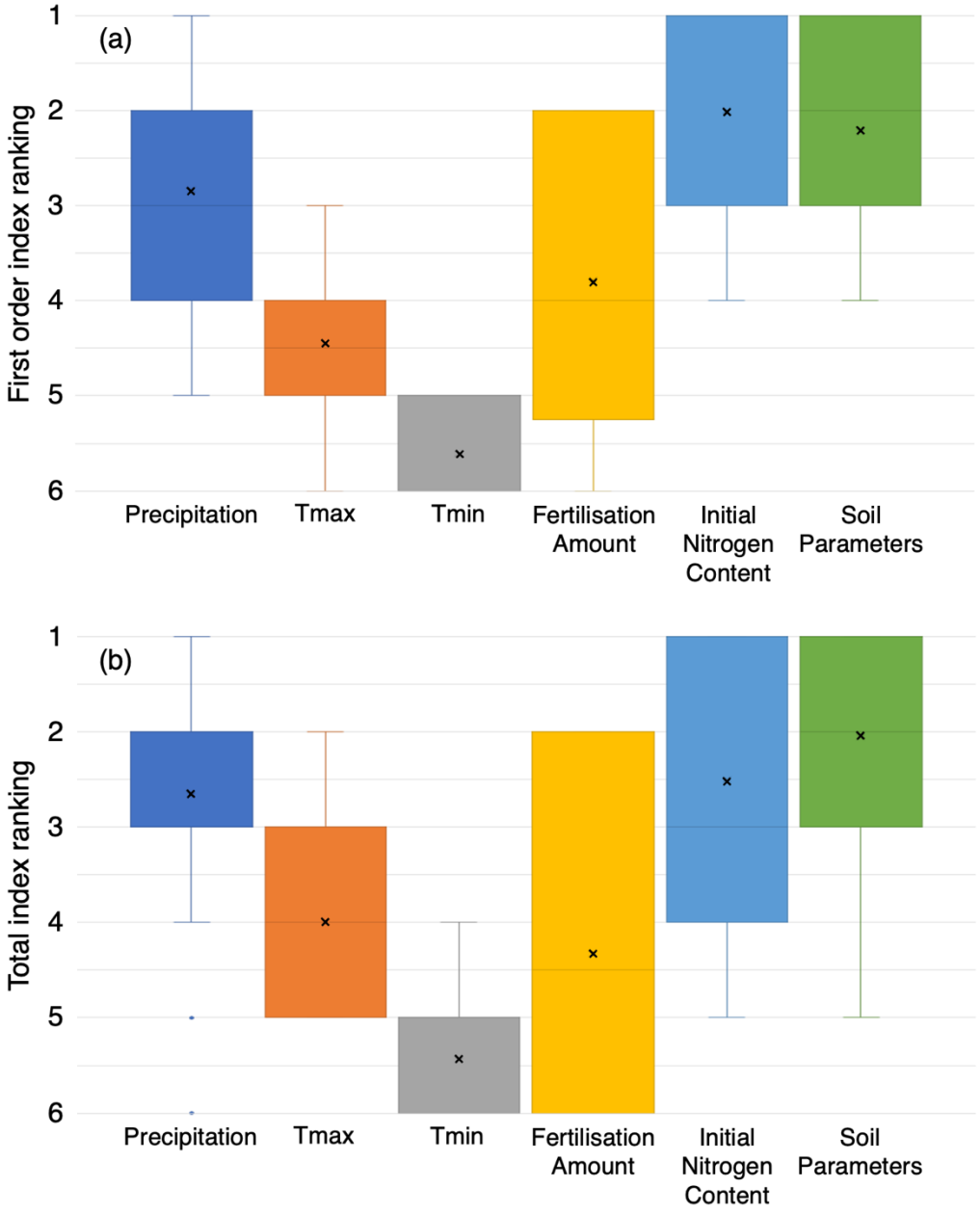

Figure C. 1. The distribution of (a) first order index and (b) total index ranks for each parameter under all eighteen scenarios. The six parameters are listed on the horizontal axis; the ranks are

ordered along the vertical axis. The cross mark represents the median value, the box denotes the interquartile range, the whisker shows the maximum and minimum ranks.

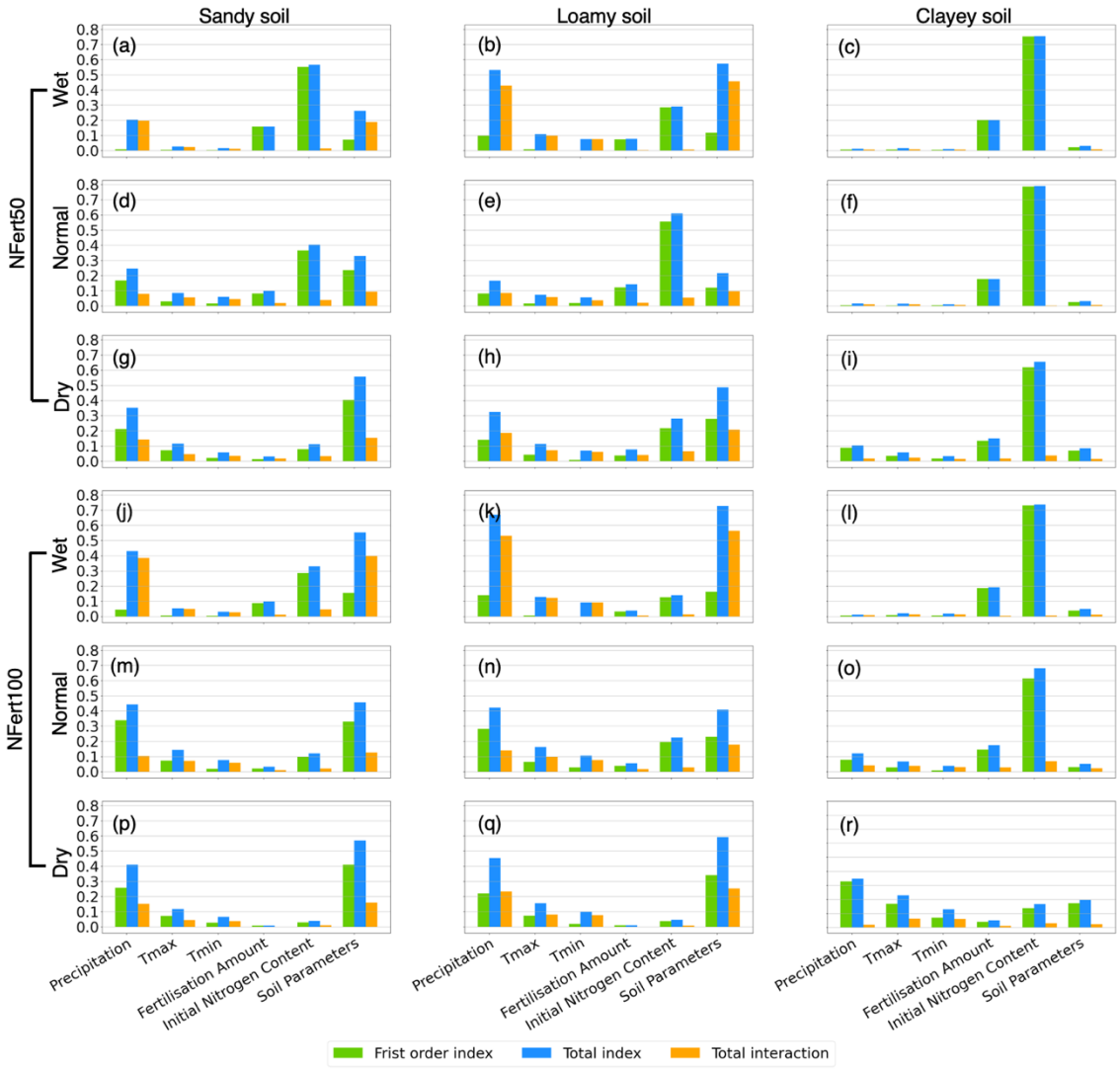

Figure C. 2. The first order sensitivity index, total sensitivity index, and total interaction of each of the six factors for all scenarios. The different columns of plots are results for different soil types; the upper three rows are for the 50 kg N/ha fertilisation level under wet, normal, and dry weather scenarios, the lower three rows are for the 100 kg N/ha; The first order sensitivity index, total sensitivity index, and total interaction for each of the six parameters are indicated in the legend.

Appendix D Supplementary material for Chapter 5

Table D. 1. The mean and standard deviation (std) of the lower limit of 15 bar (LL15), drained upper limit (DUL), saturation (SAT), crop lower limit (CLL), and plant available water capacity (PAWC) for the selected soil profile.

Layer	Depth (cm)	LL15 (mm/mm)		DUL (mm/mm)		SAT (mm/mm)		CLL (mm/mm)		PAWC (mm)
		Mean	Std	Mean	Std	Mean	Std	Mean	Std	
0-10	10	0.134	0.020	0.305	0.047	0.355	0.069	0.130	0.0235	17.5
10-20	10	0.234	0.030	0.290	0.047	0.340	0.069	0.200	0.0235	9.0
20-30	10	0.234	0.027	0.290	0.048	0.340	0.069	0.230	0.0240	6.0
30-40	10	0.270	0.027	0.364	0.048	0.414	0.069	0.260	0.0288	10.4
40-50	10	0.270	0.027	0.395	0.039	0.445	0.048	0.257	0.0273	13.8
50-90	40	0.257	0.028	0.395	0.039	0.445	0.048	0.257	0.0273	13.8
90-130	40	0.257	0.028	0.395	0.039	0.445	0.048	0.257	0.0295	13.8

Appendix E Supplementary material for Chapter 6

Table E. 1. The mean and standard deviation (std) of the lower limit of 15 bar (LL15), drained upper limit (DUL), saturation (SAT), crop lower limit (CLL), and plant available water capacity (PAWC) for the low-yield open loop selected soil profile. Soil information was obtained by selecting a suitable soil profile from the APSoil database (Oliver and Robertson, 2009).

Layer	Depth (cm)	LL15 (mm/mm)		DUL (mm/mm)		SAT (mm/mm)		CLL (mm/mm)		PAWC (mm)
		Mean	Std	Mean	Std	Mean	Std	Mean	Std	
0-10	10	0.134	0.020	0.305	0.047	0.355	0.069	0.130	0.0235	17.5
10-20	10	0.234	0.030	0.290	0.047	0.340	0.069	0.200	0.0235	9.0
20-30	10	0.234	0.027	0.290	0.048	0.340	0.069	0.230	0.024	6.0
30-40	10	0.270	0.027	0.364	0.048	0.414	0.069	0.260	0.0288	10.4
40-50	10	0.270	0.027	0.395	0.039	0.445	0.048	0.257	0.0273	13.8
50-90	40	0.257	0.028	0.395	0.039	0.445	0.048	0.257	0.0273	13.8
90-130	40	0.257	0.028	0.395	0.039	0.445	0.048	0.257	0.0295	13.8

Table E. 2. The mean and standard deviation (std) of the lower limit of 15 bar (LL15), drained upper limit (DUL), saturation (SAT), crop lower limit (CLL), and plant available water capacity (PAWC) for the high-yield open loop selected soil profile. Soil information was obtained by selecting a suitable soil profile from the APSoil database (Oliver and Robertson, 2009).

Layer	Depth	LL15 (mm/mm)		DUL (mm/mm)		SAT (mm/mm)		CLL (mm/mm)		PAWC
	(cm)	Mean	Std	Mean	Std	Mean	Std	Mean	Std	(mm)
0-10	10	0.200	0.030	0.342	0.047	0.398	0.082	0.181	0.0246	16.1
10-20	10	0.267	0.030	0.399	0.047	0.496	0.082	0.212	0.0240	18.7
20-30	10	0.265	0.027	0.422	0.048	0.496	0.082	0.242	0.0249	18.0
30-40	10	0.234	0.027	0.457	0.048	0.512	0.082	0.251	0.0283	20.6
40-50	10	0.252	0.027	0.410	0.041	0.465	0.051	0.212	0.0312	19.8
50-90	40	0.257	0.028	0.410	0.041	0.465	0.051	0.212	0.0312	19.8
90-130	40	0.257	0.028	0.410	0.041	0.465	0.051	0.212	0.0312	19.8

Table E. 3. The specific dates for the 15 cloud-free Sentinel-2 and 13 cloud-free PlanetScope images.

Sentinel-2 (15 images)	PlanetScope (13 images)
	2019-05-26
2019-05-29	
	2019-06-03
2019-06-08	
2019-06-13	
	2019-06-17
	2019-06-23
2019-06-28	
2019-07-03	
	2019-07-06
2019-07-13	
2019-07-18	
2019-07-23	
2019-08-12	
2019-08-17	
	2019-08-23
	2019-08-29
	2019-09-03
2019-09-11	
	2019-09-17
	2019-09-18
2019-10-01	
	2019-10-15
2019-10-21	
	2019-10-25
2019-10-31	
2019-11-05	
	2019-11-11

Table E. 4. The performance of low-yield and high-yield open loop cases with different observation errors (DA: data assimilation, A: additive, M: multiplicative).

Open loop case	Ground truth yield (t/ha)	Observation uncertainty type	Observation uncertainty magnitude	DA ensemble mean (t/ha)	Increment from open loop by DA (t/ha)	Innovations variance
Low-yield open loop (4.45 t/ha)	4.67	A	0.2	3.73	-0.72	4.03
			0.5	3.86	-0.59	0.71
			0.8	4.04	-0.41	0.50
			1.1	4.22	-0.23	0.37
		M	10%	4.47	0.02	3.00
			20%	4.59	0.14	1.45
			30%	4.46	0.01	0.98
	5.20	A	0.2	4.21	-0.24	1.93
			0.5	4.20	-0.25	0.51
			0.8	4.26	-0.19	0.28
			1.1	4.34	-0.11	0.19
		M	10%	4.68	0.23	2.79
			20%	4.66	0.21	1.19
			30%	4.57	0.12	0.84
	5.87	A	0.2	4.24	-0.21	2.31
			0.5	4.16	-0.29	0.69
			0.8	4.28	-0.17	0.41
			1.1	4.34	-0.11	0.29
		M	10%	4.78	0.33	2.83
			20%	4.82	0.37	1.53
			30%	4.67	0.22	1.06
	6.47	A	0.2	4.40	0.36	3.83
			0.5	4.39	-0.06	0.82
			0.8	4.38	-0.07	0.40
			1.1	4.42	-0.03	0.26
		M	10%	4.97	0.52	3.07
			20%	4.90	0.45	1.56
			30%	4.73	0.28	1.05
High-yield open loop (6.85 t/ha)	4.67	M	10%	5.87	-0.98	1.80
			20%	5.91	-0.94	0.82
			30%	6.01	-0.84	0.62
	5.20	M	10%	5.89	-0.96	2.48
			20%	5.96	-0.89	1.19
			30%	6.10	-0.75	0.71
	5.87	M	10%	6.11	-0.74	1.82
			20%	6.14	-0.71	0.79
			30%	6.23	-0.62	0.55
	6.47	M	10%	6.63	-0.22	2.56
			20%	6.46	-0.39	1.12
			30%	6.44	-0.41	0.71

Table E. 5. The performance data assimilation for all 58 patches with the low-yield open loop case using 20% multiplicative observation error (DA: data assimilation)

Open loop case (t/ha)	Patch number	Ground truth yield (t/ha)	DA ensemble mean (t/ha)	Increment from open loop by DA (t/ha)	Residual between DA mean and truth (t/ha)	Efficiency	Standard deviation after DA
Yield estimates: 4.45	L-1	6.33	4.85	0.4	-1.48	0.21	0.34
	L-2	6.2	4.78	0.33	-1.42	0.19	0.32
	L-3	6.05	4.8	0.35	-1.25	0.22	0.35
	L-4	6.14	4.78	0.33	-1.36	0.20	0.35
	L-5	6.28	4.87	0.42	-1.41	0.23	0.37

Ensemble standard deviation before DA: 0.76	L-6	6.33	4.96	0.51	-1.37	0.27	0.30
	L-7	5.74	4.86	0.41	-0.88	0.32	0.30
	L-8	6.22	4.85	0.4	-1.37	0.23	0.35
	L-9	5.92	4.86	0.41	-1.06	0.28	0.37
	L-10	5.67	4.87	0.42	-0.80	0.35	0.37
	L-11	6.53	5.03	0.58	-1.50	0.28	0.33
	L-12	6.15	4.8	0.35	-1.35	0.21	0.32
	L-13	6.38	4.86	0.41	-1.52	0.21	0.35
	L-14	6.28	4.99	0.54	-1.29	0.30	0.37
	L-15	5.78	4.92	0.47	-0.86	0.35	0.36
	L-16	6.07	4.87	0.42	-1.20	0.26	0.37
	L-17	5.87	4.82	0.37	-1.05	0.26	0.38
	L-18	5.71	4.83	0.38	-0.88	0.30	0.40
	L-19	6.05	4.78	0.33	-1.27	0.21	0.34
	L-20	6.47	4.9	0.45	-1.57	0.22	0.36
	L-21	6.31	4.88	0.43	-1.43	0.23	0.38
	L-22	5.65	4.85	0.4	-0.80	0.33	0.30
	L-23	5.2	4.66	0.21	-0.54	0.28	0.31
	L-24	5.65	4.78	0.33	-0.87	0.28	0.34
	L-25	6.11	4.79	0.34	-1.32	0.20	0.34
	L-26	5.43	4.69	0.24	-0.74	0.24	0.32
	L-27	4.67	4.59	0.14	-0.08	0.64	0.35
	L-28	4.99	4.75	0.3	-0.24	0.56	0.40
	L-29	6.02	4.89	0.44	-1.13	0.28	0.34
	L-30	6.44	4.9	0.45	-1.54	0.23	0.37
	L-31	6.41	4.93	0.48	-1.48	0.24	0.39
	R-1	6.44	4.94	0.49	-1.5	0.25	0.37
	R-2	6.22	4.79	0.34	-1.43	0.19	0.36
	R-3	6.13	4.78	0.33	-1.35	0.20	0.32
	R-4	6.31	4.78	0.33	-1.53	0.18	0.38
	R-5	6.41	4.8	0.35	-1.61	0.18	0.36
	R-6	6.02	4.76	0.31	-1.26	0.20	0.35
	R-7	6.44	5.01	0.56	-1.43	0.28	0.38
	R-8	6.16	4.82	0.37	-1.34	0.22	0.37
	R-9	6.22	4.89	0.44	-1.33	0.25	0.33
	R-10	6.01	4.77	0.32	-1.24	0.21	0.38
	R-11	6.23	4.81	0.36	-1.42	0.20	0.37
	R-12	6.22	4.83	0.38	-1.39	0.21	0.37
	R-13	6.03	4.89	0.44	-1.14	0.28	0.37
	R-14	5.94	4.76	0.31	-1.18	0.21	0.33
	R-15	6.6	4.97	0.52	-1.63	0.24	0.33
	R-16	6.27	4.85	0.4	-1.42	0.22	0.34
	R-17	5.35	4.65	0.2	-0.70	0.22	0.33
	R-18	5.78	4.8	0.35	-0.98	0.26	0.31
	R-19	5.06	4.62	0.17	-0.44	0.28	0.29
	R-20	6.45	4.84	0.39	-1.61	0.20	0.38
	R-21	6.02	4.76	0.31	-1.26	0.21	0.37
	R-22	5.6	4.75	0.3	-0.85	0.26	0.32
	R-23	4.79	4.68	0.23	-0.11	0.68	0.30
	R-24	6.04	4.9	0.45	-1.14	0.28	0.34
	R-25	5.99	4.78	0.33	-1.21	0.21	0.32
	R-26	5.78	4.69	0.24	-1.09	0.18	0.30
	R-27	4.8	4.78	0.33	-0.02	0.94	0.30

Table E. 6. The performance data assimilation for all 58 patches with the high-yield open loop case using 20% multiplicative observation error (DA: data assimilation)

Open loop case (t/ha)	Patch number	Ground truth yield (t/ha)	DA ensemble mean (t/ha)	Increment from open loop by DA (t/ha)	Residual between DA mean and truth (t/ha)	Efficiency	Standard deviation after DA
Yield estimates: 6.85 Ensemble standard deviation before DA: 0.71	L-1	6.33	6.53	-0.32	0.20	0.62	0.59
	L-2	6.2	6.43	-0.42	0.23	0.65	0.59
	L-3	6.05	6.26	-0.59	0.21	0.74	0.57
	L-4	6.14	6.11	-0.74	-0.03	0.96	0.56
	L-5	6.28	6.08	-0.77	-0.20	0.65	0.54
	L-6	6.33	6.41	-0.44	0.08	0.85	0.60
	L-7	5.74	6.22	-0.63	0.48	0.57	0.60
	L-8	6.22	6.27	-0.58	0.05	0.92	0.56
	L-9	5.92	6.08	-0.77	0.16	0.83	0.54
	L-10	5.67	6	-0.85	0.33	0.72	0.52
	L-11	6.53	6.54	-0.31	0.01	0.97	0.58
	L-12	6.15	6.18	-0.67	0.03	0.96	0.58
	L-13	6.38	6.18	-0.67	-0.20	0.57	0.56
	L-14	6.28	6.11	-0.74	-0.17	0.70	0.53
	L-15	5.78	5.92	-0.93	0.14	0.87	0.52
	L-16	6.07	6.42	-0.43	0.35	0.55	0.56
	L-17	5.87	6.14	-0.71	0.27	0.72	0.54
	L-18	5.71	6.01	-0.84	0.30	0.74	0.53
	L-19	6.05	6.15	-0.7	0.10	0.87	0.57
	L-20	6.47	6.46	-0.39	-0.01	0.97	0.56
	L-21	6.31	6.34	-0.51	0.03	0.94	0.56
	L-22	5.65	6.12	-0.73	0.47	0.61	0.60
	L-23	5.2	5.96	-0.89	0.76	0.54	0.59
	L-24	5.65	6.23	-0.62	0.58	0.52	0.58
	L-25	6.11	6.18	-0.67	0.07	0.91	0.57
	L-26	5.43	5.81	-1.04	0.38	0.73	0.58
	L-27	4.67	5.91	-0.94	1.24	0.43	0.54
	L-28	4.99	6.04	-0.81	1.05	0.44	0.53
	L-29	6.02	6.36	-0.49	0.34	0.59	0.60
	L-30	6.44	6.63	-0.22	0.19	0.54	0.57
	L-31	6.41	6.6	-0.25	0.19	0.57	0.54
	R-1	6.44	6.18	-0.67	-0.26	0.37	0.54
	R-2	6.22	5.94	-0.91	-0.28	0.56	0.55
	R-3	6.13	6.1	-0.75	-0.03	0.96	0.53
	R-4	6.31	6.4	-0.45	0.09	0.83	0.53
	R-5	6.41	6.3	-0.55	-0.11	0.75	0.57
	R-6	6.02	5.89	-0.96	-0.13	0.84	0.55
	R-7	6.44	6.5	-0.35	0.06	0.85	0.53
	R-8	6.16	6.05	-0.8	-0.11	0.84	0.56
	R-9	6.22	5.99	-0.86	-0.23	0.63	0.57
	R-10	6.01	5.96	-0.89	-0.05	0.94	0.53
	R-11	6.23	6.26	-0.59	0.03	0.95	0.56
	R-12	6.22	6.17	-0.68	-0.05	0.92	0.56
	R-13	6.03	6.24	-0.61	0.21	0.74	0.56
	R-14	5.94	6.12	-0.73	0.18	0.80	0.58
	R-15	6.6	6.5	-0.35	-0.10	0.60	0.59
	R-16	6.27	6.34	-0.51	0.07	0.88	0.58
	R-17	5.35	5.98	-0.87	0.63	0.58	0.59
	R-18	5.78	5.83	-1.02	0.05	0.95	0.58
	R-19	5.06	5.89	-0.96	0.83	0.54	0.59

	R-20	6.45	6.23	-0.62	-0.22	0.45	0.55
	R-21	6.02	5.94	-0.91	-0.08	0.90	0.55
	R-22	5.6	5.65	-1.2	0.05	0.96	0.57
	R-23	4.79	5.79	-1.06	1.00	0.51	0.60
	R-24	6.04	6.37	-0.48	0.33	0.59	0.59
	R-25	5.99	6.33	-0.52	0.34	0.60	0.59
	R-26	5.78	6.15	-0.7	0.37	0.65	0.59
	R-27	4.8	5.63	-1.22	0.83	0.60	0.59